Volume 69A
Number 5
Sept.–Oct. 1965

Physics and Chemistry

U.S. DEPARTMENT OF COMMERCE

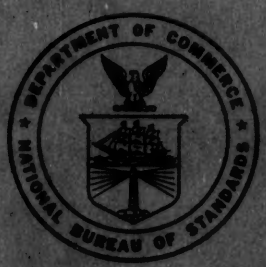

SECTION A

JOURNAL OF RESEARCH

NATIONAL BUREAU OF STANDARDS

Journal of Research

of the

National Bureau of Standards

A. Physics and Chemistry

Sept.–Oct. • 1965

VOLUME • 69A

NUMBER • 5

Editor: C. W. Beckett

Associate Editors: D. D. Wagman
J. M. Richardson

Publication dates:
Feb. 1, Apr. 1, June 1, Aug. 1, Oct. 1, Dec. 1, 1965

JOURNAL OF RESEARCH

The National Bureau of Standards Journal of Research reports research and development in the fields of activity shown at right. Also included from time to time are survey articles on topics closely related to the Bureau's scientific and technical program.

The Journal is published in four separate sections as follows:

A. Physics and Chemistry

Contains papers of interest primarily to scientists working in these fields. Issued six times a year. Annual subscription: domestic, $4.00; foreign, $4.75. Single copy, 70c.

B. Mathematics and Mathematical Physics

Presents studies and compilations designed mainly for the mathematician and the theoretical physicist. Issued quarterly. Annual subscription: domestic, $2.25; foreign, $2.75. Single copy, 75c.

C. Engineering and Instrumentation

Reports research and development results of interest chiefly to the engineer and the applied scientist. Issued quarterly. Annual subscription: domestic, $2.25; foreign, $2.75. Single copy, 75c.

D. Radio Science (formerly Radio Propagation)

Published in cooperation with U.S. National Committee of URSI. Presents papers in radio propagation, communications, and radio science generally. Issued monthly. Annual subscription: domestic, $9.00; foreign, $11.50. Single copy, $1.00.

The National Bureau of Standards is a principal focal point in the Federal Government for assuring maximum application of the physical and engineering sciences to the advancement of technology in industry and commerce. Its responsibilities include development and maintenance of the national standards of measurement, and the provision of means for making measurements consistent with those standards; determination of physical constants and properties of materials; development of methods for testing materials, mechanisms, and structures, and making such tests as may be necessary, particularly for government agencies; cooperation in the establishment of standard practices for incorporation in codes and specifications; advisory service to government agencies on scientific and technical problems; invention and development of devices to serve special needs of the Government; assistance to industry, business and consumers in the development and acceptance of commercial standards and simplified trade practice recommendations; administration of programs in cooperation with United States business groups and standards organizations for the development of international standards of practice; and maintenance of a clearinghouse for the collection and dissemination of scientific, technical and engineering information.

Institute for Basic Standards. Applied Mathematics. Electricity. Metrology. Mechanics. Heat. Atomic Physics. Physical Chemistry. Laboratory Astrophysics.* Radiation Physics. Radio Standards Laboratory.* Radio Standards Physics & Radio Standards Engineering. Office of Standard Reference Data.

Institute for Materials Research. Analytical Chemistry. Polymers. Metallurgy. Inorganic Materials. Reactor Radiations. Cryogenics.* Materials Evaluation Laboratory. Office of Standard Reference Materials.

Institute for Applied Technology. Building Research. Information Technology. Performance Test Development. Electronic Instrumentation. Textile and Apparel Technology Center. Technical Analysis. Office of Weights and Measures. Office of Engineering Standards. Office of Invention and Innovation. Office of Technical Resources. Clearinghouse for Federal Scientific and Technical Information.**

Central Radio Propagation Laboratory.* Ionospheric Telecommunications. Tropospheric Telecommunications. Space Environment Forecasting. Aeronomy.

*Located at Boulder, Colo., 80301.
**Located at 5285 Port Royal Road, Springfield, Va. 22171.

U.S. DEPARTMENT OF COMMERCE
John T. Connor, Secretary
NATIONAL BUREAU OF STANDARDS
A. V. Astin, Director

Order all publications from the Superintendent of Documents
U.S. Government Printing Office, Washington, D.C., 20402
Use of funds for printing this publication approved by the Director of the Bureau of the Budget (June 19, 1961).

JOURNAL OF RESEARCH of the National Bureau of Standards—A. Physics and Chemistry
Vol. 69A, No. 5, September–October 1965

Current Research on Preservation of Archival Records on Silver-Gelatin Type Microfilm in Roll Form

C. S. McCamy and C. I. Pope

(June 9, 1965)

This is a progress report on a study of aging blemishes on microfilm and measures to prevent their formation. Recommendations, based on current information, include: avoiding excessive densities, avoiding physical damage to the film, the use of potassium iodide in the fixer, thorough washing, uniform drying, storage at low temperature and humidity in sealed containers, avoidance of airborne reactants, increased archival use of positive copies, and periodic inspection.

1. Introduction

One method of preserving records for archival purposes is to photograph the records, producing images of reduced size made up of silver dispersed in a gelatin film, and to keep the film under conditions suitable for its preservation. This method has been in use on a commercial scale for more than a third of a century. In recent years it has been found that blemishes not previously noted developed on some such microfilms years after the films were processed and placed in storage [1].[1] Some of these blemishes were described in detail by Henn and Wiest and others by McCamy [1,2]. Reference 2 gave recommended procedures for sampling and inspecting film and reporting blemishes. Large numbers of rolls of microfilm in use in the Government have been inspected, utilizing these techniques, and the results of those inspections are being analyzed. The mechanisms of formation of aging blemishes and methods of preventing their formation are being studied at the National Bureau of Standards and in laboratories of the photographic industry. The mechanisms are being elucidated and promising methods of prevention have been proposed. The purpose of this publication is to provide guidance based on the findings to date.

If a document is intrinsically valuable, an archivist may elect to preserve the original as long as he can. Methods of preserving documents have been developed at this Bureau [3,4,5]. By preserving a photograph of the document, in a separate place, the preservation of at least the appearance of the document is further assured.

There are a number of other reasons that photography is employed for the preservation of records. Perhaps one of the most obvious is that a camera can reduce the area occupied by the record. Systems commonly used today produce images having areas $1/100$ to $1/1000$ of the areas of the originals. The high costs of buildings, maintenance, filing equipment, and heating and air conditioning prohibit the retention of many original records, but it is feasible to retain the images on microfilm.

Perhaps one of the less obvious reasons for microfilming is that the microphotograph is quite often more stable than the original document. A high grade of paper is not always used in anticipation of the archival value of the document. In the Federal records there are many letters from private citizens or foreign sources. The Government cannot control the quality of paper and ink used in the correspondence it receives.

The classical Government research pertinent to microfilm stability is the paper on the stability of motion picture films published by Hill and Weber in 1936 [6, 7]. Since there were at that time some rather old copies of photographs made on silver and gelatin emulsions and the major difficulties had been with the nitrate base, the primary interest was in the base materials. These workers noted that ordinary oven-aging in dry air had no effect on the gelatin emulsion of acetate films as far as could be observed. They tested the stability of cellulose acetate by a number of laboratory procedures and concluded, "While it is not possible to predict the life of acetate film from these results, the data show that the chemical stability of the film, with respect to oven aging, is greater than that of papers of maximum purity for permanent records. On the basis of this comparison, cellulose-acetate motion picture film appears to be very promising for permanent records." NBS Miscellaneous Publication M–158, published the following year by the same authors, gave recommended properties of film for permanent records [8]. By Act of Congress, in 1940, the National Bureau of Standards was assigned the responsibility for the maintenance of standards for the reproduction of permanent Government records by microphotographic processes [9]. Subsequent legislation assigned this responsibility to the National Archives in 1943 and to the Administrator, General Services Administration, in 1949 [10, 11]. However, as a service, the actual maintenance of the standards

[1] Figures in brackets indicate the literature references at the end of this paper.

was continued from 1940 until 1957 by the Photographic Research Section of the National Bureau of Standards. In 1945, the American Standards Association adopted a standard Specification for Photographic Films for Permanent Records based upon the NBS standard [12]. This standard was revised in 1957 [13]. In that year the NBS standard was rescinded and an interim Federal standard was issued, followed by Federal Standard 125a, which simply referenced the American Standards Association standard [14]. Since that time, our research on the stability of photographs has resulted in papers on the chemical mechanisms of fixing, fading, and sulfiding, and chemical analytical techniques for determining residual thiosulfate [15,16,17].

Large numbers of rolls of microfilm processed and preserved at the National Archives are in good condition after many years and have no aging blemishes. This demonstrates that under the right conditions microfilm can be sufficiently stable. It is important to know what conditions of film processing and storage are necessary and sufficient to achieve this stability consistently. These conditions can be stated with confidence only when the mechanism of formation of aging blemishes is fully understood.

2. Classification of Aging Blemishes

To promote consistent reporting, the various kinds of aging blemishes have been classified according to six types, as illustrated in the photomicrographs, figures 1 through 6, and as described below.

Type 1

Type 1 are circular spots, usually 50 to 150 μ in diameter, with sharp boundaries. Concentric light and dark rings are common. Spots normally occur as reduced density in high-density "background" areas, but may make incursions into low-density lines or characters. They are usually brown, orange, reddish, or yellow in color. It is common to find many spots about the same size on a sample. The spots are often seen centered on scratches in the emulsion, sometimes closely packed, like beads on a string. They sometimes occur in higher concentration at steep density gradients, sometimes giving the appearance of a continuous band. By reflected light, the spots may display a silvery sheen.

Type 2

Type 2 are defects in the light lines forming the characters themselves, rather than in the high-density "background." The lines making up the characters become lighter, yellowish, and broader. The boundaries of the defect are sharp.

Type 3

Type 3 are about 10 to 15 μ across. When they occur, there is usually a large number per unit of area. They usually range from pale yellow to orange in color. Their boundaries are sharp. By reflected light, the spots may display a silvery sheen.

Type 4

Type 4 are spots of less regular shape than type 1 but a little larger, usually lighter in color, and less sharply bounded. A circular central "nucleus" is common. These spots occur in high-density "background" areas. They do *not* make incursions on low-density characters; on the contrary, their shapes may be very distorted to accommodate to the spaces between characters or parts of characters.

Type 5

Type 5 is a reddening of the dark background in the immediate neighborhood of lighter characters. The boundaries of the discoloration are very diffuse. The shape is not regular, being determined by the shape of the characters or line of characters with which the discoloration is associated.

Type 6

Type 6 is a reddish, orange, or yellow spot of reduced density, lightest at the center and gradually blending into the surrounding background. An irregular opaque or crystalline particle is commonly observed on the surface of the film at the center of the spot. The sizes of the spots may vary considerably, even within a small region.

3. Film Inspections

Large numbers of rolls of Federal record film were inspected, but it would have been impossible for us to inspect a sizable fraction of federally held microfilm in a reasonable time. Therefore, in cooperation with the National Archives, about 100 employees of other Government agencies were trained to inspect films and report their findings. The procedures followed were those given in reference 2. To date over 7,000 rolls of film, representing a sampling of about 10 million rolls, have been inspected and reported. The information is being encoded for a detailed statistical study by means of a digital computer. This study will quantitatively evaluate the interrelationship of all variables considered to be of importance at the time the inspection program was begun. Though this analysis may reveal trends not now known, the reports have shown no obvious indications of conditions greatly different from those encountered in the initial NBS inspections, upon which the following observations are based.

Aging blemishes were observed on microfilm in roll form but not on other films, with the following exceptions. Two instances involved film on nitrate base, a type of base which has not been in use in this country for many years. One was 9-in. aerial film about 25 years old, the other was 35 mm motion picture film about 50 years old. The spots on the aerial film looked like Type 1 blemishes but the others resembled general fading more than aging blemishes. A collection of 2½-in. square (No. 120) pictorial negatives on a fine-grain roll-film manufactured, exposed, processed, and stored in Europe was very badly affected. No blemishes have been reported on such pictorial negatives in this country. Blemishes have been reported on some microfilm

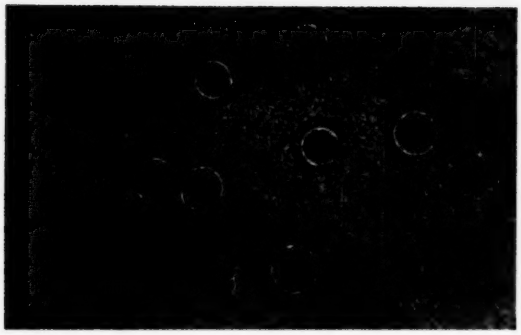

1

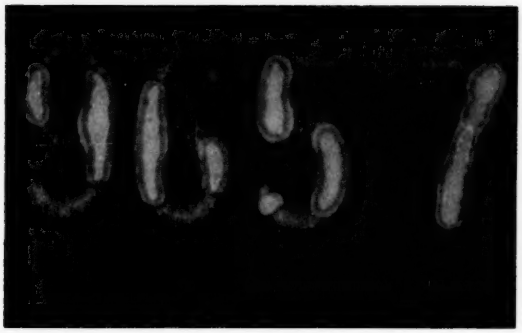

2

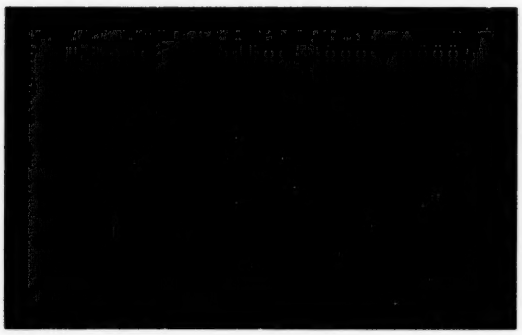

3

4

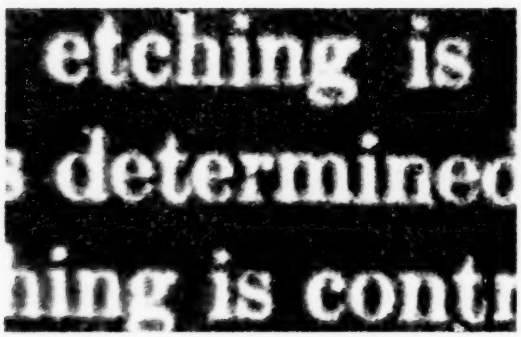

5

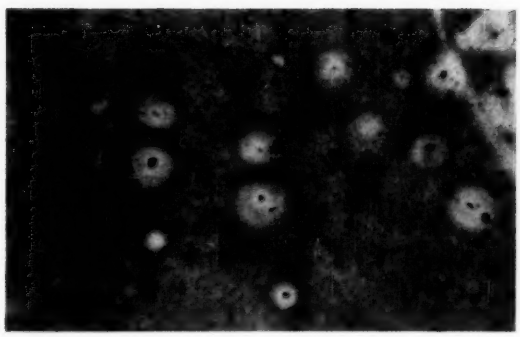

6

FIGURE 1. *Type 1*. On the record film, the spots shown range from 120 to 170 microns in diameter.
FIGURE 2. *Type 2*. On the record film, the height of the numbers is 180 microns.
FIGURE 3. *Type 3*. On the record film, the spots are about 15 microns across.
FIGURE 4. *Type 4*. On the record film, the height of the numbers is 240 microns.
FIGURE 5. *Type 5*. On the record film, the height of the lower case letters is 120 microns.
FIGURE 6. *Type 6*. On the record film, these spots range from 30 to 110 microns in diameter.

chips mounted on aperture cards. About 35,000 positive microfilm chips mounted on aperture cards were accumulated in our office between 1953 and 1957. This collection has been exposed to ordinary office conditions, with air conditioning during the summer months. The collection was recently inspected and no aging blemishes were found. Further studies of films on aperture cards have been initiated.

Aging blemishes were not observed on the information areas of positive copies having dark characters on a light background, although aging blemishes have been observed on the high-density borders of such films.

Microfilm was found stored on reels made of plastic, painted steel, anodized aluminum, and fiberboard. Some was stored on cores, without flanges, made of plastic or wood.

The film was stored in cardboard boxes, one reel to a box. Most boxes were those generally supplied commercially, but some agencies, such as the National Archives, had boxes specially made for their use. The boxes of film were usually stored in shallow drawers in painted steel cabinets, or on painted steel shelves.

With a few exceptions, blemishes were not observed on the outer convolution of film. The pattern of blemishes began, often abruptly, at the beginning of the second convolution. The most frequent exception was the observation of a pattern of blemishes beneath a rubber band, string, or adhesive tape, used to bind the roll.

On a given small area on a film, the spots of Types 1 and 3 very often displayed a remarkable uniformity of size. The general features of the outer rings of ringed spots also tended to display similarity over a small spatial range.

Given the conditions for blemish formation, blemishes appeared to form more readily at higher densities. Several instances were found in which a number of frames in a row had numerous blemishes, while a frame in their midst having a lower density was free of blemishes. Conversely, a denser frame with blemishes has been observed among lower density frames without blemishes. A series of consecutive frames had blemishes concentrated within a rough arc centered at one side of the frame (not a side at the edge of the film). Apparently the illuminance had been higher on one side of the original documents, because there was a consistent pattern of higher density within a rough arc on that side. When the leaders were fogged they were the densest parts of the films and typically had many more blemishes than other areas on the film.

Even the types of aging blemishes not regarded as character associated, such as Type 1, were often concentrated at places corresponding to high gradients of density. The straight boundary between the dense background of a filmed document and the clear space between frames was sometimes marked by a nearly solid line of blemishes.

Type 1 and Type 3 blemishes were often observed in a nearly continuous string along scratches in the emulsion.

In a series of frames of copies of reports or other documents on identical forms, Type 2 blemishes were observed on the corresponding characters of as many as 25 consecutive frames.

In one file of film about 30 years old, of which there was no processing or early storage history, there was a consistent high incidence of Type 1 blemishes, except on a few rolls that had no blemishes. The only known storage difference between the unblemished films and the others was that each reel of unblemished film was surrounded by a strawboard band, dark grayish yellow in color. A typical band measured 1.25 mm thick, 303 mm long, and 22.6 mm wide—too wide to fit between the flanges of the 16 mm reel. The band was wrapped around the outer edge of the reel. Such bands have not been observed elsewhere. The strawboard was quite alkaline, having a *p*H of about 9, whereas the cardboard in the storage boxes tested was acid, having a *p*H of 4 to 6. The strawboard had a lower concentration of rosin than any of the box stock tested. The strawboard was so brittle that it broke when bent 45 deg over a support with a 4–mm radius of curvature.

In the course of inspections, it was discovered that in a number of instances on one roll, blemishes were arrayed in closed or nearly closed rings. Such formations were called "atolls." On the same roll, barely perceptible water spots were observed. The faint water spots on the back of the film were coincident with atolls of the same size and shape on the emulsion side of the next convolution. An example of this phenomenon was sent to John Calhoun at Eastman Kodak Company, who had an analysis made of the residue at the edge of the water spot. The analysis revealed nothing more than a minute residue of the minerals commonly found in water and a trace of sulfate ion.

One of the most significant findings was a collection of about 37,500 rolls of 35 mm microfilm without blemishes. This film was exposed, processed, and stored at the National Archives. It was manufactured by two different American manufacturers since 1940.

Two aspects of the processing at the National Archives are considered notable: the presence of an exceptional amount of iodide ion in the fixing bath and an exceptionally high rate of wash water consumption per unit of film area. The iodide in the fixing bath presumably resulted from the processing of considerable amounts of positive film along with negative film.

The blemishes had a lower visual optical density than the normal background, and a spectral transmittance higher at long wavelengths than at short wavelengths in the visible spectrum. Because of this spectral transmittance and the ultraviolet and blue sensitivity of photographic copying materials, the printing density was much higher than the visual density. As a consequence, the blemishes were often not noticed on photographic prints of films having

blemishes and the legibility of the prints appeared better than that of the blemished film. This effect can be observed directly by placing a deep blue filter, such as Wratten No. 47, over the light souce and examining the film with a microscope. The legibility of films badly damaged by Type 2 blemishes has been greatly improved by this technique.

A certain roll of negative film was manufactured in 1936 and processed in 1936 or 1937. A copy of the film was made between 1936 and 1944, one in 1958, and another in 1963. Albert H. Leisinger, Jr., of the National Archives obtained the original and the copies and photographed corresponding frames of each, with a magnification of about 20. The pre-1944 copy showed no noticeable blemishes. The 1958 copy revealed about 300 Type 1 blemishes on the negative. The 1963 copy exhibited no increase in the number of spots but some growth in the diameter of spots. The ratio of diameters ranged from 1.5 to 2.

One of the objectives of the initial film inspections was to find the extent to which Government films were affected by blemishes and to ascertain whether or not any information had been lost. Of the total number of collections of microfilms, a large fraction had some blemishes. In those collections having blemishes, a fraction of the rolls were involved. On a roll, blemishes sometimes were and sometimes were not on the information frames. When blemishes occurred on information frames, only a fraction of the frames were affected. On a blemished frame, only a fraction of the blemishes were on or around characters. Of the six types, only the infrequently occurring Type 2 formed in the characters, although Type 1 sometimes crossed over parts of characters. Other types showed a natural aversion to attacking characters. As a result of the redundancy of the records, the statistical distribution of blemishes, and the characteristics of the mode of formation of blemishes in the vicinity of characters, the amount of loss of information in Federal records appeared to be extremely small. Nonetheless, one agency reported some such loss in the only existing copies of certain reports having tabulated numerical data. The only observed cases of actual loss of information resulted from Type 2 blemishes.

P. R. Achenbach and C. W. Phillips (of the Building Research Division), who are experienced in heating and air conditioning engineering, examined a few Government microfilm storage facilities. They found that the buildings were not always well designed for the purpose, air conditioning was not always adequate, and the practice of monitoring temperature and humidity at a central location in a room did not always assure proper control of these variables at the perimeter of the room where some of the films were stored. There were indications in some cases that moisture had condensed on the inner surfaces of outside walls where storage cabinets had been placed against the walls, preventing free circulation of air. The humidity obviously becomes too high for good microfilm storage at the back of a cabinet under such conditions.

In every major respect, the reports of inspections described by Henn and Wiest [1] were verified. Their inspections included privately held microfilms while ours were limited to Government records. There was some duplication of the collections inspected but the inspections were entirely independent. The Eastman Kodak Company called the discovery of blemishes to our attention and we adopted classification terminology consistent with theirs, extending it somewhat, so that our reports could be readily compared.

4. Experimental Research

4.1. Structure of Blemishes

The structure and chemical nature of typical blemishes have been described by Henn and Wiest [1]. The irregular granular pattern characteristic of normal photographic image silver is absent in the light colored areas of the blemishes. The whole thickness of the image layer is generally involved.

Samples of microfilm having Type 1 blemishes 20μ to 50μ in diameter were redeveloped in a metol-hydroquinone developer and washed. The color of the spots changed from light yellow to a deeper yellow, orange, or reddish orange. A still deeper color was obtained when the samples were treated in a 0.1 percent solution of either potassium bromide or potassium iodide. These results suggest that silver ions, silver gelatinate, or both are present in the spots and that they may be reduced to silver.

When samples of blemishes were fixed in sodium thiosulfate, they became lighter in color but the grainy dark rings remained. This result indicates that some ionic silver may be removed from the colored areas but that much of the color is attributable to colloidal silver.

When a normal microfilm image is bleached to a yellow color by gaseous hydrogen peroxide, the yellow color cannot be entirely removed by bathing in sodium thiosulfate. This implies that much of the color is attributable to colloidal silver, since silver ions would presumably be removed.

Film samples with Type 1 blemishes were treated in a solution of 2.5 percent mercuric chloride and 2.5 percent potassium bromide, washed in a very dilute hydrochloric acid solution, and then developed. The dark concentric rings and dark rims of the spots were greatly intensified, indicating that these rings are largely made up of silver grains.

Samples were bleached in a solution of 5 g of potassium dichromate and 5 ml of concentrated sulfuric acid per liter, cleared in a solution of 50 g of sodium sulfite and 1.0 g of sodium hydroxide per liter, fixed in a solution of 240 g of sodium thiosulfate per liter, and washed. The light brownish silver sulfide image normally remaining after a dichromate bleach was observed in the normal image areas. The spots were a darker brown in the center, in the dark concentric rings, and in the dark outer rims, indicating concentrations of silver sulfide in these areas. A permanganate bleach made the spots colorless and

difficult to observe in the gelatin, removing all granular silver, colloidal silver, and silver sulfide.

Type 1 blemishes were scanned with an electron probe and the characteristic x-radiation of silver was monitored. The scans revealed silver in the light areas but much more in the dark concentric rings and dark rims of spots.

4.2. General Mechanism

The currently favored hypothesis is that blemish formation is a chemical reaction in which the normal silver grains are corroded away, the silver ions migrate, and are in large part redeposited as colloidal silver or as mirrorlike deposits of silver and silver sulfide at the upper or lower surface of the gelatin layer. Considerable evidence obtained here and elsewhere supports this hypothesis [1]. An oxidation reaction of some kind is required to ionize the metallic silver and a reduction reaction is required to redeposit the silver. Peroxides can bring about oxidation-reduction reactions with silver so it is natural to suspect that blemishes are formed by peroxides attacking the image silver [1]. Why the attack should be localized and why the blemishes should assume their typical forms are not entirely clear. The heavy concentration of blemishes along scratches in the gelatin may be attributed to the removal of the protective gelatin layer. Any weakness in the gelatin layer, in the sense of permeability to chemicals or concentration of reactive or catalytic species could determine the site of attack. In the normal image, the nature of the gelatin depends on the local density of image silver. The local concentrations of various chemicals, such as thiosulfates, retained in the image also depend on the local image density. For these reasons, the strong influence of the image upon the location and form of blemishes is consistent with the working hypothesis.

4.3. Liesegang Ring Phenomenon

The very concentric ring patterns in the Type 1 blemishes and less regular concentric ring patterns in Type 4 blemishes are strongly reminiscent of the phenomenon first described by R. E. Liesegang [18, 19] and known as Liesegang ring formation. K. H. Stern, of NBS who has had wide experience with this type of reaction, [20] considered the Type 1 blemish to have typical Liesegang ring structure, although Liesegang rings are generally produced on a larger scale.

The classic experiment of Liesegang was repeated using a microscopic droplet of silver nitrate solution on a gel layer containing potassium dichromate. The reaction proceeded as Liesegang reported, but in this case formed a concentric ring pattern in the size range of Type 1 aging blemishes, proving that the phenomenon is demonstrable on this scale. A gel layer containing silver sulfide formed 8 concentric rings in 30 days under the action of a single minute droplet of a metol-hydroquinone developer solution. The literature of Liesegang phenomena abounds in references to rings formed in reactions with silver salts in gelatin. Thus, the ring structure in aging blemishes is not fully explained but neither is it unprecedented in silver-gelatin systems. It is likely that the mechanism is the same as that producing Liesegang rings in general.

4.4. Experimental Control of Temperature and Humidity

To obtain various conditions of temperature and humidity for experimental purposes, various saturated salt solutions were placed in closed containers which were placed in ovens thermostatically controlled at various temperatures [21, 22, 23]. Because of the large numbers of containers involved in the current survey of a wide variety of effects, the usual technique of stirring the atmosphere in the containers was dispensed with. Inaccuracy in humidity determination is known to result from failure to stir the solution and from contamination of the solution, but for the purpose of the present study the relative humidities produced by various saturated salt solutions were taken to be those given in table 1 and, accordingly, the relative humidities given elsewhere in this report must be considered approximate. Temperatures above room temperature were controlled within a range of 2 °C.

TABLE 1. *Percent relative humidity over saturated salt solutions, for various temperatures*

Salt	Temperature				
	Room temp (20-28 °C)	40 °C	50 °C	60 °C	70 °C
Magnesium nitrate	53	49	46	[a] 43	.....
Sodium bromide	58	52	50	50	[a] 50
Sodium chloride	76	75	75	75	[a] 75
Potassium chloride	85	82	81	81	.....
Barium chloride [b]	90	89	88	88	.....
Lithium chloride	12	12	11	.....	.....
Potassium sulfate	97	96	96	.....	.....

[a] By extrapolation.
[b] Humidities calculated from vapor pressure data for barium chloride solutions in International Critical Tables, Vol. III, (1928), p. 368.

4.5. Effect of Imbibed Chemicals on Film Exposed to Hydrogen Peroxide

Processed and dried microfilm samples were treated 3 min in 0.1 percent solutions of various compounds, some of which might be found in processing solutions or wash water. It is estimated that the concentration of the compounds was about 8 $\mu g/cm^2$ on the films. The excess solution was shaken from the samples, which were then placed in a 16-oz jar and stored at 60 °C and a relative humidity of 43 percent over a solution of 40 g of magnesium nitrate ($Mg(NO_3)_2 \cdot 6H_2O$) and 5 ml of 30 percent hydrogen peroxide in 10 ml of water. Spots ranging from pinholes to the size of natural aging blemishes formed. The results are given in table 2. Corresponding control samples without this treatment formed no blemishes under the same storage conditions.

4.6. Experiments With Dry Chemical Contaminants

Various dry salts were ground to a powder and the emulsion sides of dry microfilm samples were pressed against the powder and tapped gently to

remove loose powder. The films were stored in 16-oz jars at 60 °C and 43 percent rh. Irregular but generally round spots formed. The results are given in table 3. Corresponding control samples without this treatment formed no blemishes under the same conditions of temperature and humidity.

TABLE 2. *Effect of various imbibed chemicals on microfilm stored in the presence of hydrogen peroxide*

Compound	Time	Effect
	hr	
Aluminum potassium sulfate	17	Light yellow spots.
Boric acid	18	Light yellow spots.
Calcium carbonate	72	Yellow spots.
Cupric acetate	17	Image bleached.
Cupric carbonate	72	Image nearly bleached.
Magnesium sulfate	17	Light yellow spots.
Mono-methyl-para-aminophenol sulfate	18	Yellow spots.
Potassium bromide	72	Yellow spots.
Sodium chloride	18	Yellow spots.
Sodium nitrate	17	Light yellow spots.
Sodium silicate	72	White and yellow spots.
Sodium sulfite	17	Light yellow spots.

TABLE 3. *Effect of various powdered chemicals on microfilm*

Chemical	Temp.	Relative humidity	Time	Effect
	°C	%	*Days*	
Ferric sulfate	60	88	11	Yellow spots.
Potassium bromide	60	88	4	None.
Potassium iodide	60	88	4	Gray spots.
Sodium chloride	60	88	4	None.
Sodium thiosulfate	60	43	6	Yellow spots.
Sulfur	50	88	4	Yellow spots with diffuse edges.

4.7. Biological Studies

Several samples of various kinds of blemishes were studied by E. H. Zeitler at the Armed Forces Institute of Pathology. Employing a variety of staining techniques and methods of microscopic examination, he found no remains of microorganisms or evidence of attack by microorganisms. Henn and Wiest reported that no bacteria or fungi were present in their samples [1].

In our laboratories, dried spores were obtained from cultures of fungi grown in a gelatin solution.

Samples of microfilm were contaminated by brushing dry spores onto the surface and by bathing them in water containing spores. They were stored at 46 percent and 75 percent rh at room temperature and at 50 °C, in desiccator jars. Some fungal growth was observed at 75 percent rh at room temperature but no blemishes appeared during a storage period of 9 months.

Contaminated film was treated with the fungicide, sodium pentachlorophenol (2%), and stored at 46 percent rh and 50 °C. A few spots formed on the control sample after 29 days exposed to peroxide.

Contaminated films stored at 90 percent rh and 97 percent rh and room temperature were so badly attacked by fungal growth that the gelatin was consumed, but at no time did spots form.

In no case were spots formed by the spores. Although spore incubation might weaken the gelatin and invite attack, this effect has not been observed. Bacterial action by a few organisms on the gelatin surface, perhaps during drying, seemed a possible precursor of attack. Evidence of such activity has not been observed, though it should be detectable if present.

4.8. Experiments With Peroxides

During the biological experiments, one control sample unexpectedly developed spots. The desiccator jars stored at 50 °C had a small amount of a stop-cock grease on the rim to secure a vapor-tight seal, while those stored at room temperature had petrolatum on the rims. It soon became apparent that spots formed in the presence of the stop-cock grease. A few spots had developed in 79 days on the control sample stored at 46 percent rh and 50 °C. With more grease around the top of the jar in other experiments, spots developed in 2 to 4 weeks at 46 percent rh and 50 °C.

This grease had a very faint odor of rancid vegetable oil. The mass spectrograph detected nothing more than water in the vapor. Infrared spectra of the grease itself and the iodine number were used to identify it as castor oil hydrogenated about 30 percent. The double bond compounds of the kinds found in castor oil form peroxides with the oxygen in the air and polymerization bonding of a molecule with another double bond molecule releases hydrogen peroxide which may react with the image silver.

The interior of some desiccator jars was coated about ⅛ in. thick with this grease, from the top to the porcelain plate near the bottom. Microfilm samples were stored at various temperatures and humidities. The results are given in table 4. In all of these tests, it was noted that the areas of the samples closest to the grease surface were affected first. The spots formed in the presence of this grease were visually indistinguishable from naturally occurring spots.

TABLE 4. *Effect of fumes of hydrogenated castor oil on microfilm*

Temp.	Relative humidity	Time	Effect
°C	%	*Days*	
25	58	60	Many spots.
25	76	60	No spots.
40	52	21	Many spots.
40	75	29	Many spots.
50	11	90	No spots but appreciable general bleaching.
50	50	10–15	Many spots, general bleaching.
50	75	15–20	Many spots, general bleaching.
60	50	7–10	Many spots.
60	75	7–10	Many spots.
60	88	7–10	Many spots.

The unsaturated compounds in linseed oil and castor oil and oleic and linoleic acids were tested for their ability to form spots on film. Linseed oil and linoleic acid caused numerous spots in 25 days at 50 percent rh and 50 °C on samples close to the oils. These experiments were done in 16 oz jars having small openings to permit the influx of air. In large unvented desiccator jars the reaction was less severe. The results are given in table 5.

TABLE 5. *Effect of fumes of several oils and acids on microfilm in closed desiccator jars*

Test substance	Temp.	Relative humidity	Time	Effect
	°C	%	*Days*	
Linseed oil	50	50	24	Few spots.
	50	50	70	Slightly more spots.
	60	75	28	No spots.
Linoleic acid	50	50	63	No spots, slight yellowing
Castor oil	60	50	55	A few spots.
Oleic acid	50	50	63	Very few spots.

Corresponding control samples formed no blemishes under the same storage conditions.

Films were exposed to turpentine in large vented desiccator jars at room temperature with the following results: 58 percent rh, general bleaching in 35 days; 76 percent rh, general bleaching and spots in 9 days; 90 percent rh, heavy yellow and red coloration, general bleaching, and yellow spot formation in 4 to 5 days; 97 percent rh, considerable general image bleaching but no spot formation in 4 days.

The effects of dipentene, pinene, and turpentine were compared in separate closed desiccator jars at room temperature and 90 percent rh. At 9 days the attack was about the same, with turpentine showing slightly stronger attack.

Varsol, acetaldehyde, gasoline, and formaldehyde caused no spots in 28 days at 90 percent rh and room temperature. Benzaldehyde produced a slight yellowing of the image in 9 days at 85 percent rh and room temperature.

Films were exposed to powdered rosin placed in culture dishes in closed desiccator jars. At 85 percent rh and room temperature, heavy image bleaching and a few spots were observed at 6 days and an increase in bleaching and formation of reddish spots at 15 days. At 58 percent rh and room temperature, weak general bleaching was found at 2 days and considerable yellowing and many spots, including Type 3, at 5 days. A sample given the gold treatment of Henn and Wiest [1] showed slight yellowing at 5 days. Abietic acid, the chief constituent of rosin, is known to form peroxide under certain conditions of temperature and humidity.

Similar tests with cinnamaldehyde at room temperature and 85 percent rh caused almost complete general bleaching of the image and formation of an orange color in 7 days (in a 16 oz jar) and at 58 percent rh heavy bleaching and the formation of large bright yellow spots after 13 days (in a large desiccator jar).

A solution of titanium sulfate turns yellow in the presence of a very small concentration of hydrogen peroxide in the atmosphere. A 10-ml beaker of this test solution was placed in a desiccator jar coated with the stop-cock grease and stored at 58 percent rh and room temperature. The yellow color was appreciable after 24 hr. Turpentine, pinene, and dipentene triturated with water gave a strong indication of peroxide after 30 to 60 min. Powdered rosin from one of the aging tests was dissolved in a sodium hydroxide solution and acidified with acetic acid. The solution contained peroxide according to the iodide-starch test. (The solution of rosin is too yellow to permit use of the titanium method.) Tests with known concentrations of hydrogen peroxide showed that the titanium method detected about 15 μg of hydrogen peroxide in 25 ml of water and the iodide-starch test detected about 20 μg per 25 ml of water. Nitrites and compounds of chlorine may also give a positive indication with the iodide-starch test.

4.9. Experiments With Cardboard

Rosin is widely used in paper making although the concentration may be only a few percent. Cardboard may contain natural resins. Alum is often added to papers, creating an acid condition favoring peroxide formation. Furthermore, Marraccini and Kleinert report that measurable amounts of peroxide form in the natural aging of commercial paper pulps and that the peroxide formation rate is related to fiber length [25]. They have described a method of measuring the minute amounts of peroxide [24] and have found peroxide formation to increase with humidity and the total amount of peroxide to increase linearly with time of aging [25]. Peroxide formation follows one mechanism in the presence of air and various others in the absence of air [26]. All of these facts strongly suggest that minute amounts of peroxides generated in the aging degradation of the boxes in which the film is stored can cause aging blemishes under some conditions.

To obtain further evidence on this point, microfilm was aged in contact with cardboard from microfilm storage cartons. Cartons marketed by five major American suppliers and one foreign supplier were used. Both old and new cartons were used. Some films were clamped between two pieces of cardboard. Others were stapled to the carton to hold the emulsion against the cardboard. Some were stored in the presence of acetic acid vapor; others were stored without acid.

Films were clamped between pieces of cardboard and stored under various conditions. The results are given in table 6. Corresponding control samples formed no blemishes under the same storage conditions. In the test at 50 percent rh and 70 °C, one spot was evident at 28 days; when the humidity was changed to 75 percent, many spots, some quite large, formed in 6 days.

TABLE 6. *Effect of cardboard strips on microfilm*

Temp.	Relative humidity	Time	Effect
°C	%	*Days*	
50	75	28	Few faint spots.
50	81	14	Very few yellow spots.
50	81	28	Few yellow spots.
50	96	28	No spots.
70	50 then 75	28 then 6	One spot; then many spots.

Films were clamped between pieces of cardboard from film storage boxes, and were placed in desiccator jars with acetic acid in the humidistat solution. The results are given in table 7. Corresponding control samples formed no blemishes under the same storage conditions.

TABLE 7. *The effect of cardboard on microfilm in the presence of acetic acid vapor*

Acetic acid	Temp.	Relative humidity	Time	Effect
%	°C	%	*Days*	
3	50	50	34	No spots.
3	50	75	3	Many spots, near white to pale pink.
2	50	75	31	Many spots resembling natural ones.
2	60	50	12	None.
2	60	75	12	Several yellowish spots.
2	60	81	12	Several yellowish spots.
2	60	50	26	Few spots.
2	60	75	26	More spots.
2	60	81	26	More spots, paper clips and staples severely attacked.

Samples were placed in cartons so the emulsion lay against the sides and other short samples were laid emulsion down on the bottom of cartons in large desiccators. No acid was used. The results are given in table 8. Corresponding control samples formed no blemishes under the same storage conditions. The tendency toward spot formation increased with humidity, as would be predicted on the basis of the paper degradation hypothesis and the results published by Marraccini and Kleinert. The effect of temperature was not as important as the effect of humidity.

TABLE 8. *The effect of storage boxes on microfilm*

Temp.	Relative humidity	Time	Effect
°C	%	*Days*	
50	50	40	No spots.
60	50	55	No spots.
70	50 then 75	28 then 6	None; then many spots.
50	75	38	Few white spots.
60	75	23	Few yellow spots.
60	75	41	Few yellow and white spots.
60	81	23	Several very similar to natural spots.
60	81	41	Large increase in yellow spot formation; many spots similar to natural ones.

4.10. Effect of Optical Density

In the laboratory, the dependence of the tendency to blemish formation on density could be readily observed. The results confirm the field observation. For example, on a density step tablet exposed to the very active stop-cock grease, there were no spots on the density steps 0.16 to 0.43 but spots on density steps 0.58 and above. The small density difference of 0.15 made the difference between spots and no spots. The degree of attack increased with density at densities above 0.58.

4.11. Effect of Gold Protective Treatment

Henn and Wiest proposed a gold protective treatment for microfilms [1]. The chemistry of their proposal appears theoretically sound. Microfilms processed and given the gold protective treatment both during processing and after processing, in a commercial microfilm laboratory, have been studied. In all tests to date, the gold treated film has been consistently more resistant than untreated film to general attack by mild peroxides and has been virtually free of spot formation. The inertness of the gold treated image is demonstrated by its resistance to a short exposure to strong nitric acid. With severe and prolonged exposure to a peroxide atmosphere, the gold treated material is affected and, under these conditions, can even exhibit a resistance inferior to the untreated material, but it is questionable whether tests of this severity are pertinent to practice. Since this process has just recently been introduced commercially, there is little background of experience in practice.

5. Recommendations

Though our research on these blemishes has not been completed, those now engaged in microfilming and those planning records systems for the future have an immediate need for current information. Decisions with regard to expenditures of resources for the preservation of private and public records require value judgments based upon various considerations. However, since some technical judgments are involved, we offer the following suggestions and recommendations based upon our recent findings, past experience, and consultations with many people responsible for microfilming and preservation of records in Government and industry. The recommendations should be viewed in that perspective.

The blemish formation process, like all chemical processes, requires a combination of conditions. The elimination of one contributory factor may prevent the formation of blemishes under a given set of conditions, but we recommend, as a conservative policy, that all contributory factors be avoided, insofar as it is practical to do so. The following recommendations and suggestions are based upon this principle.

We recommend the use of film having a safety cellulose-ester base meeting applicable raw stock requirements, the viscosity retention requirement, and flexibility requirements of the American Standard Specifications for Photographic Films for Permanent Records [13] until that standard is revised.

The observation that the incidence and severity of blemishes tend to be greater on high-density areas suggests that for archival purposes it would be desirable to use no higher density than is required to serve the intended purpose, rather than strive for a high density for the sake of appearance.

Throughout the exposing and processing operations it is important to avoid scratching film, not only because scratches are undesirable in themselves but because blemishes form along scratches.

Since the processing conditions establish the conditions of the image and the gelatin, they play a role in establishing the probability of attack. The con-

tributions of all the various processing conditions are not yet sufficiently well understood to warrant detailed recommendations with respect to all aspects of processing. Pope has reported that the presence of the iodide ion prevents most of the sulfiding of the image during fixing and aids in the elimination of residual chemicals during washing [15]. Henn, Wiest, and Mack [29] report that the presence of iodide in fixing baths was associated with a reduction or complete elimination of aging blemish formation in a number of private and Government processing plants. A private communication from Robert O. Bieling of Bell and Howell reported an increase in general fading on accelerated aging after such iodide treatment. This report has been confirmed at NBS. Since general fading has not, as of this time, been associated with the presence of iodide in the fixer in actual practice, the accelerated test may be too severe. On the other hand, the test may be predicting actual future performance. We have received no reports that general fading has ever been a problem to users of archival microfilm which was properly washed, while aging blemishes have actually destroyed small amounts of information in a few known cases. Since most microfilm images have rather high contrast, a considerable amount of general fading could be tolerated without loss of information. On the basis of these considerations, the addition of 0.2 g of potassium iodide per liter of fixing solution, to fixing solutions not otherwise containing an equivalent amount of iodide ion, appears desirable if the films are stored according to the recommendations given below.

Long experience as well as the results reported here of the effects of imbibed chemicals on microfilm support the conclusion that for archival purposes, film should be thoroughly washed to remove chemicals remaining after processing. Failure to do so invites general fading reactions and spot formation.

Efficient removal of water droplets before drying aids in preventing deposition of chemicals and promotes uniform drying, therefore, greater uniformity in image and gelatin characteristics. The nature of the drying process plays an important role in establishing the characteristics of the gelatin layer. The effects of time, temperature, humidity, and air velocity are not sufficiently well known to allow us to make detailed recommendations. Great care should be taken to avoid dust, fumes of any kind, and gases other than those in normal clean air.

We recommend that the American Standard Method for Determining the Thiosulfate Content of Processed Black-and-White Photographic Film and Plates be used until it is revised [28]. We suggest the method of Pope as an improvement for a revised standard [17].

The provisions of the American Standard Practice for Storage of Microfilm, [27] with the few variations noted in this paper, should be carefully observed.

The use of paper, string, adhesive tape, or rubber bands to bind the roll introduces chemical and physical variables which should be evaluated for each material. Such study may be justified if there is a real need for the use of such materials.

Chemicals or materials employed in splicing operations should be scrutinized carefully in light of the present findings. The use of such "foreign" materials can be avoided by the use of a thermally welded joint. This method is in satisfactory use in a Government agency which is one of the larger users of microfilm.

To avoid the peroxide generated in paper cartons and protect film from gases and vapors originating elsewhere, it is suggested that rolls of film be stored in sealed containers as defined in American Standard Practice for Storage of Microfilm [27]. Unpainted anodized aluminum appears to be a desirable material for containers. Hundreds of thousands of aluminum cans and reels have been used by one Government agency and they have been found practical and not too expensive. The reels were made of 0.051-in. thick anodized 2024 aluminum alloy and the cans were made of 0.032-in. thick anodized 3003 aluminum alloy. The 2024 aluminum alloy provides the elasticity required for a reel to maintain its shape. Other materials should be scrutinized carefully, in the light of our findings. It should be borne in mind that spots were formed readily by amounts of material too small to be detected by a mass spectrograph which could detect concentrations corresponding to 10^{-7} to 10^{-9} moles per liter of the atmosphere sampled.

Low temperature and humidity appear to be desirable storage conditions. It is recommended that film to be in inactive storage be placed in the container in equilibrium with air at a relative humidity of 15 to 20 percent at 50 to 60 °F, and that film for active files be placed in the container in equilibrium with air at a relative humidity of 30 to 35 percent at 50 to 60 °F. It is recommended that the storage temperature not be permitted to exceed 70 °F and that it be maintained between 50 and 60 °F where practical. Films may be stored at a lower temperature if they are warmed sufficiently before opening the container to avoid condensation of moisture on the film when the container is opened.

Archival films should not be exposed to sulfur dioxide, hydrogen sulfide, peroxides, volatile bases such as ammonia, volatile acids such as acetic acid, engine exhaust gases, or gaseous industrial wastes. The fumes from turpentine, linseed oil, or drying paints containing such materials should also be avoided. To prevent fingerprints, clean cloth gloves, available from dealers in photographic supplies, should be used whenever film is handled. The film should be handled by the edges, rather than the surfaces to avoid scratching the surfaces or depositing dust. Film handling equipment must be kept clean at all times and should be inspected periodically for cleanliness and any condition likely to scratch or otherwise damage film. Areas in which film is han-

dled must be kept as clean and dust free as practical operations permit. Special air filtration and air washing may be required to avoid objectionable air-borne contaminants. Since the gaseous decomposition products evolved by nitrate-base films are very corrosive, such films should be removed from any building housing permanent records.

No aging blemishes have been observed on the information areas of positive prints having dark characters on a nearly clear background, although aging blemishes have been observed on the high-density borders of one such film and others have been reported to us. For this reason the retention of such positive films is a recommended procedure when additional security is desired. A positive copy appears to be the best choice when only one film is to be retained in a permanent file and a positive copy will serve the intended purpose.

The probability of loss of information can be very greatly reduced by making more than one microfilm copy and preserving the copies in separate places.

The only positive assurance that records are being preserved is obtained by a regular program of inspection. This principle was recognized in the American Standard Practice for Storage of Microfilm adopted in 1957 [27]. Detailed sampling and inspection procedures are outlined in NBS Handbook 96 [2]. Experience has amply demonstrated that the routine satisfactory use of microfilms does not constitute adequate inspection. The attention of the user is on the information rather than the condition of the film and the optical nature of the blemishes makes them difficult to detect in the routine use of film. Undoubtedly there will now be a keener awareness of the condition of the film on the part of professional microfilm users, but systematic and well designed sampling and inspection are still necessary parts of record preservation. The sampling procedure should be regulated so that inspectors obtain a different sample each time. Careful inspection of each stratum every two years should reveal unsatisfactory conditions in time to allow appropriate action to be taken. After a number of years, if no problems have been encountered, this inspection period could be reasonably extended.

We recommend that existing collections of archival microfilm be stored under the same conditions recommended here for new archival microcopies. If the films have aging blemishes which appear to threaten legibility, the information on the films can be preserved by copying the films on permanent record materials and preserving the copies.

Nothing in these recommendations should be construed to mean that silver-gelatin type microfilm is the only possible material for archival record storage or that the roll form is necessarily preferred. There are, indeed, other possible materials but we have not conducted sufficient studies of their properties to make recommendations with respect to their use for the storage of records of permanent value.

This research was sponsored in part by the National Archives and Records Service, the Library of Congress, the Social Security Administration, the Navy Bureau of Weapons, and The Adjutant General's Office of the Department of the Army. In addition, the National Microfilm Association solicited and secured financial support from the Bell and Howell Company, E. I. DuPont de Nemours and Company, Dynacolor Corporation, International Business Machines, Minnesota Mining and Manufacturing Company, Recordak Corporation, University Microfilms, and Xerox Corporation.

The authors appreciate the cooperation of the sponsors and many other Government agencies that permitted access to records, supplied old films for research, permitted inspections and measurements to be made, and gave advice and helpful leads. A most cooperative spirit was found in the laboratories of the film manufacturers.

The photomicrographs were made by Myron Berkovitz. Miss Anna-Mary Bush assisted in the preliminary inspections and carried out the research on the Liesegang phenomenon.

6. References

[1] R. W. Henn and D. G. Wiest, Microscopic spots in processed microfilm: their nature and prevention, Phot. Sci. Eng. **7,** 253 (1963).

[2] C. S. McCamy, Inspection of processed photographic record films for aging blemishes, National Bureau of Standards Handbook 96, (1964), U.S. Government Printing Office, Washington, D.C. 20402.

[3] B. W. Scribner, The protection of documents with cellulose acetate sheeting, NBS Misc. Publ. 168 (1940).

[4] Preservation of the Declaration of Independence and the Constitution of the United States, NBS Circular 505 (1951).

[5] W. K. Wilson and B. W. Forshee, Preservation of documents by lamination, NBS Mono. 5 (1959).

[6] J. R. Hill and C. G. Weber, Stability of motion-picture films as determined by accelerated aging, J. Res. NBS **17,** 871 (1936).

[7] B. W. Scribner, Summary report of research at the National Bureau of Standards on the stability and preservation of records on photographic film, NBS Misc. Publ. 162 (1939).

[8] J. R. Hill and C. G. Weber, Evaluation of motion-picture film for permanent records, NBS Misc. Publ. 158 (1937).

[9] Public Law No. 788, 76th Congress, Chap. 727—3d Session, (H.R. 10026). Approved September 24, 1940.

[10] Public Law No. 115, 78th Congress, chap. 192—1st Session, (H.R. 2943). Approved July 7, 1943.

[11] Federal Records Act of 1950. United States Code, Title 44, Sec. 399(a).

[12] American Standard Specifications for Photographic Films for Permanent Records. Z38.3.2–1945. (American Standards Association, New York).

[13] American Standard Specifications for Photographic Films for Permanent Records. PH1.28–1957. (American Standards Association, New York).

[14] Federal Standard 125a, Federal Standard Film, Photographic and Film, Photographic, Processed; (For Permanent Record Use) April 24, 1958.

[15] C. I. Pope, Formation of silver sulfide in the photographic image during fixation, J. Res. NBS **64C** (Engr. and Instr.) No. 1, 65 (1960).

[16] C. I. Pope, Stability of residual thiosulfate in processed microfilm, J. Res. NBS **67C** (Engr. and Instr.) No. 1, 15 (1963).
[17] C. I. Pope, Determination of residual thiosulfate in processed film, J. Res. NBS **67C** (Engr. and Instr.) No. 3, 237 (1963).
[18] R. E. Liesegang, Naturw. Wichschr. **11,** 353 (1896).
[19] R. E. Liesegang, Phot. Archiv. **21,** 221 (1896).
[20] K. H. Stern, The Liesegang phenomenon, Chem. Rev. **54** (1954).
[21] A. Wexler and S. Hasegawa, Humidity-temperature relationships of some saturated salt solutions in the temperature range 0 to 50 °C, J. Res. NBS **53,** 19 (1954) RP2512.
[22] D. S. Carr and L. B. Harris, Solutions for maintaining constant relative humidity, Ind. and Eng. Chem. p. 2015 (Sept. 1949).
[23] F. E. M. O'Brien, The control of humidity by saturated salt solutions, J. Sci. Inst. and Phys. in Ind. **25,** 73 (1948).
[24] L. M. Marraccini and T. N. Kleinert, Spectrophotometric estimation of peroxide in cellulosic materials, pp. 78–80, Svensk Papperstidning **65,** (Jan–June 1962).
[25] L. M. Marraccini and T. N. Kleinert, Aging and colour reversion of bleached pulps, ibid. p. 126–131.
[26] T. N. Kleinert and L. M. Marraccini, Aging and colour revision of bleached pulps, ibid. **66,** (Jan–June 1963), p. 189–195.
[27] American Standard Practice for Storage of Microfilm. PH5.4–1957. (American Standards Association, New York).
[28] American Standard Method for Determining the Thiosulfate Content of Processed Black-and-White Photographic Film and Plates. PH4.8–1958. (American Standards Association, New York).
[29] R. W. Henn, D. G. Wiest, and Bernadette D. Mack, Microscopic spots in processed microfilm: the effect of iodide, Phot. Sci. Eng. *9,* 167(1965).

(Paper 69A5–359)

JOURNAL OF RESEARCH of the National Bureau of Standards—A. Physics and Chemistry
Vol. 69A, No. 5, September–October 1965

Franck-Condon Factors to High Quantum Numbers VI: C_2 Band Systems

R. W. Nicholls [1]

(May 10, 1965)

Franck-Condon factor arrays have been computed numerically and are displayed to highest known vibrational quantum numbers for the following C_2 band systems:

Freymark	: $(e^1\Sigma_u^+ - b^1\Pi_u)$
Mulliken	: $(d^1\Sigma_u^+ - x^1\Sigma_g^+)$
Fox-Herzberg	: $(B^3\Pi_g - X'^3\Pi_u)$
Deslandres-d'Azambuja	: $(c^1\Pi_g - b^1\Pi_u)$
Swan	: $(A^3\Pi_g - X'^3\Pi_u)$
Phillips	: $(b^1\Pi_u - x^1\Sigma_g^+)$
Ballik-Ramsay	: $(A'^3\Sigma_g^- - X'^3\Pi_u)$

1. Introduction

In each of a number of previous papers, Franck-Condon factor arrays have been presented, molecule by molecule, for each of its common and important band systems: N_2, N_2^+ [Nicholls 1961, 1962a]; CO^+ [Nicholls 1962b]; CN [Nicholls 1964a]; NO [Nicholls 1964b]; O_2 [Nicholls 1965]. In this paper Franck-Condon factor arrays are displayed for all important band systems of C_2.

The C_2 molecule has important applications to astrophysics in the emission spectra from comets and in the absorption spectra from cool stars. It also has important applications to hydrocarbon combustion [Gaydon 1957]. There is thus a continuing demand for reliable transition probability data for various C_2 band systems. To this end, for example, Hagan [1963] has recently made measurements on the absolute oscillator strength of the (0,0) band of the Swan system. (See Mentall and Nicholls [1965].)

The band systems of C_2 are listed with descriptive comments in table 1, and the transitions from which they arise are indicated on the simplified energy-level diagram of figure 1.

The discovery by Ballik and Ramsay [1959, 1960] that the true ground state of gaseous C_2 was $x^1\Sigma_g^+$ (the lowest state of the Phillips and Mulliken systems), rather than $X^3\Pi_u$ (the lowest state of the Swan system now designated $X'^3\Pi_u$) as had previously been assumed, has clarified our picture of the disposition of levels. The situation has been discussed in great detail by Ballik and Ramsay [1963a, b] and their designations of states are employed in this paper. Perturbations in the $A'^3\Sigma_g^-$ state led them to locate $x^1\Sigma_g^+$ 610 cm^{-1} below $X'^3\Pi$. Perturbations in the $b^1\Pi_u$ state suggest the presence of the $A''^3\Sigma_u^+$ state from which no radiative transitions have yet been found.

TABLE 1. *Band systems of* C_2

Band system	Wavelength range (A)	Reference
Freymark $(e^1\Sigma_g^+ - b^1\Pi_u)$	2072–2217	[1]
Mulliken $(d^1\Sigma_u^+ - x^1\Sigma_g^+)$	2313–2415	[2]
Fox-Herzberg $(B^3\Pi_g - X'^3\Pi_u)$	2378–3283	[3]
Deslandres-d'Azambuja $(c^1\Pi_g - b^1\Pi_u)$	3398–4102	[4]
Swann $(A^3\Pi_g - X'^3\Pi_u)$	4365–7853	[5, 6, 7]
Phillips $(b^1\Pi_u - x^1\Sigma_g^+)$	7715–12091	[8, 9]
Ballik-Ramsay $(A'^3\Sigma_g^- - X'^3\Pi_u)$	11726–24745	[10]

References
[1] Freymark (1951).
[2] Landsverk (1939).
[3] Phillips (1949).
[4] Herzberg and Sutton (1940).
[5] Johnson (1927).
[6] Phillips (1948b).
[7] Herzberg (1946).
[8] Phillips (1948a).
[9] Ballik and Ramsay (1963b).
[10] Ballik and Ramsay (1963a).

2. Method

The straightforward method of computer calculation described in the first paper of this series [Nicholls 1961] was used to evaluate the arrays, and the calculations were performed at the Computation Center of The National Bureau of Standards.

[1] Visiting Professor, Department of Aeronautics and Astronautics, Stanford University, on leave from the University of Western Ontario, now in Department of Physics, York University, Toronto.

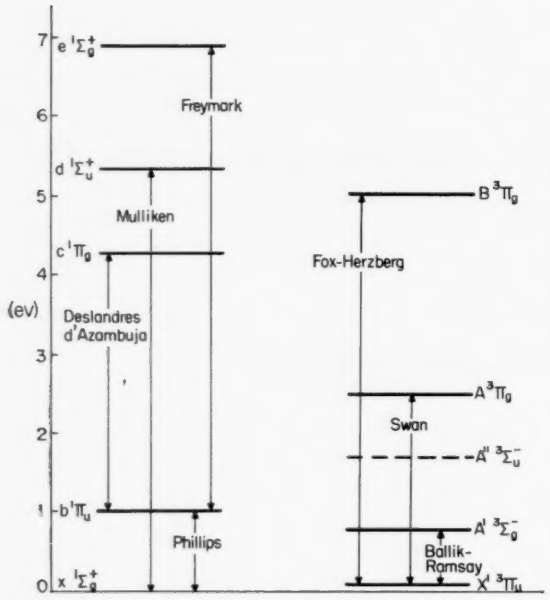

FIGURE 1. *Partial energy level diagram for* C_2.

TABLE 2. *Basic data*

State	ω_e(cm^{-1})	$\omega_e x_e$(cm^{-1})	r_e(A)	v_{max}	Reference
$x^1\Sigma_g^+$	1854.71	13.34	1.24253	5	[1, 2]
$b^1\Pi$	1608.35	12.078	1.3184	8	[1, 2]
$c^1\Pi$	1809.1	15.81	1.2552	6	[1, 2]
$d^1\Sigma_u^+$	1829.57	13.97	1.2378	5	[1, 2]
$e^1\Sigma_g^+$	1671.5	40.02	1.2517	5	[1, 2]
$X'^3\Pi_u$	1641.35	11.69	1.3119	13	[1, 2]
$A'^3\Sigma_g^-$	1470.45	11.19	1.36928	4	[1, 2]
$A^3\Pi_g$	1788.22	16.44	1.2660	13	[1, 2]
$B^3\Pi_g$	1106.56	39.26	1.5350	4	[1, 2]

$\mu_A = 6.00194$

References
[1] Ballik and Ramsay (1963b).
[2] Wallace (1962).

Input data were ω_e, $\omega_e x_e$, r_e, v_{max} for both states and μ_A for the molecules. The notation is conventional [Herzberg 1950]. The Morse model was adopted for molecular potentials and the computer program provided for all needed vibrational wave functions and their overlap integral squares, the Franck-Condon factors. The Morse potential is admittedly an empirical expedient, but the range of vibrational quantum numbers involved in most of the systems is low enough to justify its use. (See sec. 4. discussion.) The input data used in the calculations are summarized in table 2. Ballik and Ramsay's summary [1963b] of C_2 data and Wallace's [1962] compilations were used.

3. Results

Franck-Condon factor arrays are displayed in tables 3 through 9 for the band systems listed in table 1. The Condon loci [Nicholls 1963, Murty 1964] are indicated on the tables by setting the entries for bands which lie on local maxima of the Franck-Condon factor surface in bold faced type. The negative number in each entry is the power of ten by which it is multiplied.

4. Discussion

The Condon loci of tables 3 through 9 agree well with the $v'-v''$ positions of the commonly excited bands of each system [Pearse and Gaydon 1963, Wallace 1962], which is some justification of the adequacy of the potential model employed. In view of the importance of C_2 spectra to combustion studies some preliminary, limited ($v'+v'' \leq 6$) tables of Franck-Condon factors for C_2 systems of combustion importance were computed some years ago (Nicholls, Fraser, and Jarmain [1959]) by the approximate method of Fraser and Jarmain [1953]. The Mulliken, Deslandres-d'Azambuja, Phillips, Fox-Herzberg, and Swan systems of C_2 were treated as well as 14 band systems of other molecules. Basic data for these calculations were taken from Herzberg's [1950] compilation. A comparison between the entries of the limited approximate tables and those of this paper indicates that for the C_2 band systems treated the Franck-Condon factors were acceptable.

TABLE 4. *Franck-Condon factors to high vibrational quantum numbers for the* C_2 *Mulliken* ($d^1\Sigma_u^+ - X^1\Sigma_g^+$) *system*

v' \ v''	0	1	2	3	4	5
0	**9.9659–1**	3.2059–3	1.9741–4	7.8375–6	4.0407–7	2.4151–8
1	3.3154–3	**9.9055–1**	5.5526–3	5.5311–4	2.8989–5	1.8715–6
2	9.7176–5	5.9451–3	**9.8573–1**	7.1390–3	1.0339–3	6.6972–5
3	3.6867–7	3.0045–4	7.9164–3	**9.8199–1**	8.0604–3	1.6118–3
4	2.5241–9	1.8533–6	6.1685–4	9.2616–3	**9.7925–1**	8.4085–3
5	6.2444–10	7.9781–9	5.7079–6	1.0510–3	1.0019–2	**9.7737–1**

TABLE 3. *Franck-Condon factors to high vibrational quantum numbers for the* C_2 *Freymark* ($e^1\Sigma_g^+ - b^1\Pi_u$) *system*

v' \ v''	0	1	2	2	3	4	5	7	8
0	**5.4103–1**	**2-8232-1**	1.1692–1	5.1251–2	1.3171-2	3.8774–3	1.0618–3	2.7011–4	6.3191–5
1	4.0076–1	1.1998–1	**2)0714–1**	**1.5170–1**	7.4629–2	3.0305–2	1.0731–2	**3.4182–3**	9-8891–4
2	5.7777–2	**4.9616–1**	2.6730–2	1.1897–1	**1.4131–1**	8.8599–2	4.3451–2	1.7778–2	6.3966–3
3	3.1770–5	9.9376–2	**5.3176–1**	1.0371–2	6.2267–2	**1.2076–1**	8.8321–2	5.0463–2	2.3012–2
4	3.9811–4	6.7389–4	1.0731–1	**5.6820–1**	1.3962–2	2.8781–2	**1.0542–1**	8.0092–2	5.2524–2
5	3.1007–6	1.3714–3	7.5584–3	7.9011–2	**6.0274–1**	3.5530–2	8.9253–3	**1.0131–1**	6.7123–2

TABLE 5. *Franck-Condon factors to high vibrational quantum numbers for the* C_2 *Fox-Herzberg* $B^3\Pi_g - X'^3\Pi_u$

v' \ v''	0	1	2	3	4	5	6	7	8
0	1.4369–3	1.2826–2	5.1012–2	1.2046–1	**1.9023–1**	**2.1504–1**	**1.8236–1**	**1.2034–1**	**6.3754–2**
1	4.9176–3	3.3567–2	9.2494–2	**1.2742–1**	8.1493–2	9.9149–3	1.6509–2	9.7844–2	**1.6238–1**
2	9.7331–3	5.1224–2	**9.5733–2**	6.5454–2	3.5013–3	3.0368–2	9.1015–2	6.3191–2	3.9953–3
3	1.4669–2	6.0055–2	7.3803–2	1.6848–2	1.1130–2	6.5229–2	3.9538–2	2.8033–4	5.0808–2
4	1.8718–2	**6.0202–2**	4.6500–2	4.6442–4	3.4636–2	4.5646–2	1.0560–3	3.4079–2	5.7214–2

v' \ v''	9	10	11	12	13
0	2.7861–2	1.0281–2	3.2669–3	9.0834–4	2.2386–4
1	**1.5926–1**	**1.1155–1**	6.0802–2	2.7111–2	1.0217–2
2	2.5140–8	1.0327–1	**1.4992–1**	**1.3578–1**	9.0583–2
3	8.1780–2	3.0748–2	8.0493–4	4.9589–2	**1.1695–1**
4	8.2749–3	1.7440–2	7.1192–2	5.6860–2	6.7070–3

TABLE 6. *Franck-Condon factors to high vibrational quantum numbers for the* C_2 *Deslandres-D'Azambuja* ($c^1\Pi_g - b^1\Pi_u$) *system*

v' \ v''	0	1	2	3	4	5	6	7	8
0	**5.5083–1**	**3.0217–1**	1.0619–1	3.0532–2	7.8455–3	1.8797–3	4.2980–4	9.5066–5	2.0502–5
1	3.5613–1	9.4332–2	**2.6413–1**	**1.7509–1**	7.4478–2	2.5412–2	7.6113–3	2.0945–3	5.4340–4
2	8.4095–2	**3.9457–1**	1.1158–4	1.5034–1	**1.8469–1**	1.1138–1	4.8806–2	1.7821–2	5.7893–3
3	8.6154–3	1.8062–1	**3.1377–1**	3.3201–2	5.8565–2	**1.5371–1**	**1.3025–1**	7.1957–2	3.1497–2
4	3.4244–4	2.6977–2	2.5951–1	2.0869–1	8.8989–2	1.0906–2	1.0660–1	**1.2967–1**	8.9610–2
5	2.6811–6	1.3440–3	5.3123–2	**3.1208–1**	1.1889–1	**1.2873–1**	1.8475–4	6.1353–2	**1.1405–1**
6	1.6219–8	1.0619–5	3.1685–3	8.4248–2	**3.3965–1**	5.6088–2	**1.4428–1**	1.1745–2	2.7417–2

TABLE 7. *Franck-Condon factors to high vibrational quantum numbers for the* C_2 *Swan* ($A^3\Pi_g - X^3\Pi_u$) *system*

v' \ v''	0	1	2	3	4	5	6	7	8
0	**7.3521–1**	2.1299–1	4.3116–2	7.3685–3	1.1290–3	1.5815–4	2.0200–5	2.2948–6	2.1734–7
1	2.3964–1	**3.6359–1**	**2.7839–1**	9.1572–2	2.1685–2	4.2612–3	7.3256–4	1.1190–4	1.5012–5
2	2.4459–2	3.6141–1	1.6196–1	**2.7071–1**	1.2956–1	3.9873–2	9.6382–3	1.9745–3	3.5267–4
3	6.0678–4	5.9842–2	**4.1392–1**	6.0271–2	**2.3192–1**	1.5271–1	5.8658–2	1.6942–2	4.0459–3
4	5.5115–7	2.1773–3	9.8472–2	**4.2756–1**	1.5311–2	**1.8441–1**	**1.6203–1**	7.5545–2	2.5514–2
5	2.1740–7	3.8862–7	4.1610–3	1.3623–1	**4.2108–1**	9.1898–4	1.3917–1	**1.6060–1**	8.9045–2
6	7.0147–11	1.2358–6	2.5079–7	6.2936–3	1.7109–1	**4.0579–1**	1.6223–3	1.0079–1	**1.5182–1**
7	1.7848–10	2.5007–10	3.9227–6	8.2977–6	8.2031–3	2.0219–1	**3.8838–1**	8.5489–3	7.0408–2
8	1.7883–12	1.2537–9	1.0832–8	9.0464–6	4.4554–5	9.5676–3	2.2925–1	**3.7272–1**	1.6832–2
9	7.9470–14	2.9973–11	4.4814–9	8.8068–8	1.6657–5	1.4280–4	1.0150–2	2.5226–1	**3.6094–1**
10	1.5722–14	3.0887–13	2.2908–10	1.0365–8	4.0284–7	2.5451–5	3.4883–4	9.8199–3	2.7118–1
11	9.7273–16	1.6637–13	7.7563–14	1.1066–9	1.5973–8	1.3269–6	3.2488–5	7.1409–4	8.5784–3
12	3.7499–17	6.1945–15	8.8470–13	2.8168–12	3.8682–9	1.4030–8	3.4847–6	3.3780–5	1.2845–3
13	6.4868–17	1.0561–17	7.1793–14	3.0065–12	5.3820–11	1.0471–8	2.1434–9	7.6779–6	2.6234–5

v' \ v''	9	10	11	12	13
0	1.4327–8	2.7418–10	6.1829–11	9.5247–11	4.7276–11
1	1.6850–6	1.3762–7	4.6135–9	2.1048–10	7.1365–10
2	5.4844–5	7.1641–6	7.0484–7	3.5017–8	1.3613–10
3	8.3043–4	1.4746–4	2.2083–5	2.5601–6	1.7185–7
4	6.9828–3	1.6239–3	3.2521–4	5.5135–5	7.3985–6
5	3.4578–2	1.0697–2	2.7859–3	6.2263–4	1.1823–4
6	9.8547–2	4.3405–2	1.5005–2	4.3333–3	1.0711–3
7	**1.3872–1**	1.0408–1	5.1409–2	1.9666–2	6.2441–3
8	4.7539–2	**1.2363–1**	1.0609–1	5.8187–2	2.4423–2
9	2.3983–2	3.0999–2	**1.0821–1**	**1.0519–1**	6.3516–2
10	**3.5422–1**	2.8884–2	1.9451–2	9.3517–2	**1.0208–1**
11	2.8592–1	**3.5316–1**	3.1186–2	1.1656–2	8.0171–2
12	6.5773–3	2.9617–1	**3.5807–1**	3.0960–2	6.5757–3
13	2.0843–3	4.1424–3	3.0144–1	**3.6907–1**	2.8503–2

TABLE 8. *Franck-Condon factors to high vibrational quantum numbers for the C_2 Phillips ($b^1\Pi_u - X^1\Sigma_g^+$) System*

v' \ v''	0	1	2	3	4	5
0	**4.1236–1**	**3.9817–1**	1.5473–1	3.1090–2	3.4503–3	2.0875–4
1	3.3170–1	5.6587–3	**2.8886–1**	**2.7069–1**	8.8395–2	1.3623–2
2	1.6205–1	1.7295–1	5.7561–2	1.1534–1	**3.0149–1**	1.5525–1
3	6.2841–2	**2.0003–1**	3.2573–2	**1.4270–1**	1.7246–2	**2.6322–1**
4	2.1419–2	1.2565–1	1.3937–1	1.0154–3	**1.5715–1**	2.5365–3
5	6.7559–3	5.9704–2	**1.4573–1**	5.9413–2	3.5622–2	**1.5915–1**
6	2.0320–3	2.4250–2	9.5558–2	**1.2165–1**	9.7757–3	8.0346–2
7	5.9395–4	8.9460–3	4.9267–2	1.1252–1	7.5289–2	1.2709–3
8	1.7089–4	3.1039–3	2.1997–2	7.3567–2	**1.0548–1**	3.1284–2

TABLE 9. *Franck-Condon factors to high vibrational quantum numbers for the C_2 Balik-Ramsay ($A'^3\Sigma_g^- - X'^3\Pi_u$) system*

v' \ v''	0	1	2	3	4	5	6	7	8
0	**6.3264–1**	**3.0651–1**	5.5850–2	4.8034–3	2.0018–4	3.6882–6	2.2459–8	1.3197–11	2.6323–14
1	2.7082–1	1.8572–1	**3.9354–1**	1.3231–1	1.6697–2	9.1714–4	2.9873–5	1.4930–7	9.2627–11
2	7.4773–2	**2.9573–1**	2.2032–2	**3.6188–1**	2.0686–1	3.6164–2	2.5187–3	6.8891–5	5.6689–7
3	1.7212–2	1.4558–1	**2.2056–1**	4.0121–3	**2.7815–1**	**2.6652–1**	6.2457–2	5.3743–3	1.7319–4
4	3.6280–3	4.8567–2	1.8220–1	**1.2646–1**	4.6055–2	1.8372–1	**3.0517–1**	9.4055–2	9.8190–3

v' \ v''	9	10	11	12	13
0	1.1545–16	2.0194–18	1.4300–16	9.3339–17	6.8311–18
1	2.7707–13	1.8307–16	4.8804–17	1.1030–16	4.1606–16
2	3.6613–10	1.3992–12	4.2312–15	1.0989–16	6.1078–17
3	1.6139–6	1.0667–9	5.3184–12	1.9904–14	5.7532–16
4	3.6727–4	3.8274–6	2.5420–9	1.5550–11	1.0865–13

The Morse model for potentials implies that $\omega_e y_e$ is zero. Ballik and Ramsay [1963b] report very small $\omega_e y_e$ values for most states. For only two cases is $\omega_e y_e$ greater than unity: $c^1\Pi_g$ (−4.02) and $B^3\Pi_g$ (2.805). For both of these v_{max} is low enough that the divergence from Morse behavior is small. Some comments were made in the preceding paper of this series [Nicholls 1965] on the relative unimportance of the adequacy of the model of potential used when the Franck-Condon factors are used twice compensatingly as a smoothing parameter in the determination of transition probability parameters form band intensity measurements.

Most of the data of this paper was presented orally at the AGARD Combustion and Propulsion symposium in London, April 1963. Only the Franck-Condon factor surface for the C_2 Swan bands was incorporated in the proceedings of the meeting [Nicholls 1964c].

The great assistance of Miss Ruth Zucker of the NBS Computation Laboratory to this work is gratefully acknowledged. The author is most grateful to Dr. A. A. Ramsay for making prepublication copies of his paper with Dr. Ballik available, and to Dr. Hagan for making a prepublication copy of her thesis available.

The work has been supported largely through research grants from National Aeronautics and Space Administration (NsG–349) and The Air Force Office of Scientific Research (AF–AFOSR–62–236). Some support from contracts with the Air Force Cambridge Research Center (AF19(628)–2820) and the Defence Research Board of Canada, and grants from the National Research Council of Canada are also gratefully acknowledged.

5. References

E. A. Ballik and D. A. Ramsay (1959), J. Chem. Phys. **31,** 1128.
E. A. Ballik and D. A. Ramsay (1960), Astrophys. J. **132,** 898.
E. A. Ballik and D. A. Ramsay (1963a), Astrophys. J. **137,** 61.
E. A. Ballik and D. A. Ramsay (1963b), Astrophys. J. **137,** 84.
H. Freymark (1951), Ann. Phys. Leipz. (Ser. 6) **8,** 221.
P. A. Fraser and W. R. Jarmain (1953), Proc. Phys. Soc. **A66,** 1145.
A. G. Gaydon (1957), The Spectroscopy of Flames (Chapman and Hall, London).
Lucy G. Hagan (1963), Ph. D. Thesis, University of California, The Absolute Intensity of C_2 Swan Bands, UCRL report 10620.
G. Herzberg (1946), Phys. Rev. **70,** 762.
G. Herzberg (1950), Spectra of Diatomic Molecules (D. Van Nostrand, New York).
G. Herzberg and R. B. Sutton (1940), Can. J. Res. **18A,** 74.
R. C. Johnson (1927), Phil. Trans. Roy. Soc. **A226,** 157.
O. G. Landsverk (1939), Phys. Rev. **56,** 769.
J. E. Mentall and R. W. Nicholls (1965), Proc. Phys. Soc. (in press).
Mary F. Murty (1964), M.Sc. Thesis, University of Western Ontario, Condon Loci of Diatomic Molecular Spectra
R. W. Nicholls (1961), J. Res. NBS **65A** (Phys. and Chem.) No. 5, 451.
R. W. Nicholls (1962a), J. Quant. Spectr. Radiative Transfer **2,** 433.
R. W. Nicholls (1962b), Can. J. Phys. **40,** 1772.
R. W. Nicholls (1963), Nature **199,** 794.
R. W. Nicholls (1964a), J. Res. NBS **68A** (Phys. and Chem.) No. 1, 75.
R. W. Nicholls (1964b), J. Res. NBS **68A** (Phys. and Chem.) No. 5, 535.
R. W. Nicholls (1964c), Laboratory Astrophysics and Combustion Spectroscopy, p. 413, Supersonic Flow, Chemical Processes and Radiative Transfer, ed. D. B. Olfe and V. Zackkay (Pergamon, New York).
R. W. Nicholls (1965), J. Res. NBS **69A** (Phys. and Chem.) No. 4, 369.
R. W. Nicholls, P. A. Fraser, and W. R. Jarmain (1959), Combustion and flame, **3,** 13.
R. W. B. Pearse and A. G. Gaydon (1963), The Identification of Molecular Spectra 3d ed. (Chapman and Hall, London).
J. G. Phillips (1948a), Astrophys. J. **107,** 389.
J. G. Phillips (1948b), Astrophys. J. **108,** 434.
J. G. Phillips (1949), Astrophys. J. **110,** 73.
L. V. Wallace (1962), Astrophys. J. Suppl. **7,** No. 68, 165.

Paper 69A5–360

JOURNAL OF RESEARCH of the National Bureau of Standards—A. Physics and Chemistry
Vol. 69A, No. 5, September–October 1965

Matrices of Spin-Orbit Interaction in the Electron Configurations $p^2\,d$ and $p^4\,d$

Jack L. Tech [1] and Roy H. Garstang [2]

(May 27, 1965)

The matrices of spin-orbit interaction in the $p^2\,d$ and $p^4\,d$ electron configurations have been calculated in the LS representation. The matrices have been checked by showing that their eigenvalues, calculated by use of an IBM 7090, agree with the correct eigenvalues known from the theory of jj-coupling. For the sake of completeness, the energies of electrostatic interaction for these configurations are also given.

1. Introduction

In a previous paper [1] [3] one of us reported the complete energy matrices in the LS representation for the $p^2\,p$ and $p^4\,p$ electron configurations, in the approximation that includes both electrostatic and spin-orbit interactions. Each of the present authors had calculated independently, and for different purposes, the corresponding energy matrices for spin-orbit interaction in the $p^2\,d$ and $p^4\,d$ configurations. After intercomparing our results, we formed a final check of the matrices by using an IBM 7090 to determine their eigenvalues and showing them to agree with the correct eigenvalues easily calculated from the theory of jj-coupling [cf. 2, ch. 10]. In this paper we report the $n'\,d$ matrices in a form identical to that used earlier in the $n'\,p$ case (n' is the principal quantum number of the electron that is outside the p^2 or p^4 core).

The primary use of such interaction matrices is to obtain approximate predicted values for the energy levels of atomic systems as an aid in interpreting and understanding their spectra. The eigenvalues of the matrices represent the discrete energy levels of the atomic system. The eigenvectors of the matrices are useful in obtaining approximate wave functions of the actual levels in terms of the LS eigenfunctions. The eigenvectors also give directly the transformation matrices needed for the calculation of line strengths in intermediate coupling from the strengths in LS coupling, as done for example by one of us earlier for lines of astrophysical importance [3].

2. Spin-Orbit Interaction

The matrices of spin-orbit interaction for the configuration $p^2\,d$ are given in table 3. Since the energy matrix is diagonal in J, the nondiagonal elements occur only between levels having the same J value. There is thus one matrix for each possible value of J. The rows and columns of the matrices are specified by the name of the term in the notation of LS-coupling, the terms in parentheses denoting the parent terms in p^2. The elements of these matrices are linear combinations of the spin-orbit integrals ζ and ζ', where ζ stands for ζ_p of the core and ζ' stands for ζ_d of the external electron. Both these integrals are positive. Their coefficients were hand-calculated by well-known methods [cf. ref. 2, ch. 11, and ref. 4]. Although these coefficients have been thoroughly checked, it will be appropriate to write a simplified expression, in the notation of reference [4], by which any given matrix element may easily be recalculated if occasion arises. For this purpose, it can be shown that, in the configuration $p^2\,l$, the element

$$(\mathrm{S_1L_1\tfrac{1}{2}}l\mathrm{SJ}||\zeta_p(\mathbf{S}_1\cdot\mathbf{L}_1)+\zeta_l(\mathbf{s}_l\cdot\mathbf{l})||\mathrm{S_1'L_1'\tfrac{1}{2}}l\mathrm{S'L'J})$$

[1] Present address: Harvard College Observatory, Cambridge, Mass. 02138.
[2] The National Bureau of Standards, Boulder, Colo.
[3] Figures in brackets indicate the literature references at the end of this paper.

is given by

$$\sqrt{(2S+1)(2L+1)(2S'+1)(2L'+1)}\begin{Bmatrix} SS'1 \\ L'LJ \end{Bmatrix}\Big[(-1)^{S_1+S'_1+L_1+L'_1+L+L'+J+l+\frac{1}{2}}$$

$$\times\sqrt{(2S_1+1)(2L_1+1)(2S'_1+1)(2L'_1+1)}\begin{Bmatrix} L_1L'_1 1 \\ 1\ 1\ 1 \end{Bmatrix}\begin{Bmatrix} S_1S'_1 1 \\ \frac{1}{2}\ \frac{1}{2}\ \frac{1}{2} \end{Bmatrix}\begin{Bmatrix} SS'1 \\ S'_1S_1\frac{1}{2} \end{Bmatrix}\begin{Bmatrix} LL'1 \\ L'_1L_1 l \end{Bmatrix}6\zeta_p$$

$$+(-1)^{S+S'+J+l+\frac{1}{2}}\sqrt{l(l+1)(2l+1)}\begin{Bmatrix} SS'1 \\ \frac{1}{2}\frac{1}{2}S_1 \end{Bmatrix}\begin{Bmatrix} LL'1 \\ l\ lL_1 \end{Bmatrix}\sqrt{\frac{3}{2}}\zeta_l\Big],$$

where the subscript 1 indicates quantum numbers associated with the parent term of the core, and the $6-j$ symbols are equivalent to Racah's W coefficients. We have kept this expression literal in l since it holds for all l. It may thus be used also to recalculate any p^2 p element given in reference [1]. The values of the $6-j$ symbols can be found in reference [9].

The matrices for the p^4 d configuration are identical to the above except that in this case the sign of the spin-orbit coupling parameter ζ_p is reversed [2, p. 299].

TABLE 1. *Electrostatic energies for* p^2 d

Parent	Term	Energy
(^{3}P)	^{4}F	$E-3F_2-2F'_2-4G'_1+3G'_3$
	^{4}D	$E-3F_2+7F'_2-4G'_1-42G'_3$
	^{4}P	$E-3F_2-7F'_2+6G'_1-42G'_3$
(^{1}D)	^{2}G	$E+3F_2+4F'_2-4G'_1+18G'_3$
	^{2}S	$E+3F_2+14F'_2+G'_1-42G'_3$

	(^{3}P) ^{2}F	(^{1}D) ^{2}F
(^{3}P) ^{2}F	$E-3F_2-2F'_2+5G'_1+30G'_3$	$-3\sqrt{6}G'_1+6\sqrt{6}G'_3$
(^{1}D) ^{2}F	$-3\sqrt{6}G'_1+6\sqrt{6}G'_2$	$E+3F_2-8F'_2+2G'_1+6G'_3$

	(^{3}P) ^{2}D	(^{1}D) ^{2}D	(^{1}S) ^{2}D
(^{3}P) ^{2}D	$E-3F_2+7F'_2+5G'_1+\frac{105}{2}G'_3$	$+\frac{15\sqrt{21}}{2}G'_3$	$-3\sqrt{3}G'_1+21\sqrt{3}G'_3$
(^{1}D) ^{2}D	$+\frac{15\sqrt{21}}{2}G'_3$	$E+3F_2-3F'_2+3G'_1-\frac{27}{2}G'_3$	$+4\sqrt{7}F'_2-\sqrt{7}G'_1-3\sqrt{7}G'_3$
(^{1}S) ^{2}D	$-3\sqrt{3}G'_1+21\sqrt{3}G'_3$	$+4\sqrt{7}F'_2-\sqrt{7}G'_1-3\sqrt{7}G'_3$	$E+12F_2$

	(^{3}P) ^{2}P	(^{1}D) ^{2}P
(^{3}P) ^{2}P	$E-3F_2-7F'_2+\frac{105}{2}G'_3$	$+3G'_1+\frac{63}{2}G'_3$
(^{1}D) ^{2}P	$+3G'_1+\frac{63}{2}G'_3$	$E+3F_2+7F'_2+2G'_1-\frac{63}{2}G'_3$

3. Electrostatic Interaction

To obtain the complete energy matrices in intermediate coupling, the electrostatic matrices must be added to the spin-orbit matrices of table 3. The matrices of electrostatic interaction in Russell-Saunders coupling are well-known for the $p^2\,d$ and $p^4\,d$ configurations, and we give them here in tables 1 and 2 for the sake of completeness. The elements of the matrices are expressed as linear combinations of the usual Slater parameters F_k and G_k, which are defined as certain integrals over radial wave functions [2, p. 177.] We calculated the coefficients of these parameters from the general tables [4] given by Slater [5, vol. II, appendix 21]. We have checked them in the manner outlined by Racah [6].

Following Slater, the energies are stated in terms of the average energy, $E_{av}=E$, which represents the center of gravity of the terms of the configuration, each term being assigned the weight $(2S+1)(2L+1)$. The energy expressions can easily be converted, if desired, so as to

[4] A typographical error exists in Slater's tables. The nondiagonal matrix element for $p^4\,l$ $((^3P)\,^2(l+1)|H|(^1D)\,^2(l+1))$ should read: $-3(2l+1)\sqrt{3l(l+2)}$. This quantity multiplies $G^{l+1}(pl)/2(2l+1)(2l+3)^2$.

TABLE 2. *Electrostatic energies for* p^4 d

Parent	Term	Energy
(^3P)	^4F	$E-3F_2+2F_2'-2G_1'-21G_3'$
	^4D	$E-3F_2-7F_2'-2G_1'-21G_3'$
	^4P	$E-3F_2+7F_2'-2G_1'-21G_3'$
(^1D)	^2G	$E+3F_2-4F_2'-2G_1'+24G_3'$
	^2S	$E+3F_2-14F_2'+8G_1'-21G_3'$

	$(^3P)\,^2F$	$(^1D)\,^2F$
$(^3P)\,^2F$	$E-3F_2+2F_2'-2G_1'+69G_3'$	$-15\sqrt{6}G_3'$
$(^1D)\,^2F$	$-15\sqrt{6}G_3'$	$E+3F_2+8F_2'-2G_1'-6G_3'$

	$(^3P)\,^2D$	$(^1D)\,^2D$	$(^1S)\,^2D$
$(^3P)\,^2D$	$E-3F_2-7F_2'+\frac{23}{2}G_1'+42G_3'$	$+\frac{3}{2}\sqrt{21}G_1'-3\sqrt{21}G_3'$	$+3\sqrt{3}G_1'-21\sqrt{3}G_3'$
$(^1D)\,^2D$	$+\frac{3}{2}\sqrt{21}G_1'-3\sqrt{21}G_3'$	$E+3F_2+3F_2'+\frac{3}{2}G_1'-18G_3'$	$-4\sqrt{7}F_2'+\sqrt{7}G_1'+3\sqrt{7}G_3'$
$(^1S)\,^2D$	$+3\sqrt{3}G_1'-21\sqrt{3}G_3'$	$-4\sqrt{7}F_2'+\sqrt{7}G_1'+3\sqrt{7}G_3'$	$E+12F_2$

	$(^3P)\,^2P$	$(^1D)\,^2P$
$(^3P)\,^2P$	$E-3F_2+7F_2'+\frac{11}{2}G_1'-21G_3'$	$+\frac{15}{2}G_1'$
$(^1D)\,^2P$	$+\frac{15}{2}G_1'$	$E+3F_2-7F_2'+\frac{11}{2}G_1'-21G_3'$

conform to the usage of Condon and Shortley. In this case, E is replaced in the energy expressions by the following quantities:

Configuration	E
$p^2\,d$	$(F_0+2F_0')-2F_2-2G_1'-21G_3'$
$p^4\,d$	$(6F_0+4F_0')-12F_2-4G_1'-42G_3'$

Here as in tables 1 and 2 the parameters without primes refer to the (p, p) interactions while those with primes refer to the (p, d) interactions. In accordance with Condon and Shortley, the subscripted parameters are defined in terms of the superscripted parameters as follows:

$$F_2(p, p)=(1/25)F^2(p, p), \qquad F_2(p, d)=(1/35)F^2(p, d),$$
$$G_1(p, d)=(1/15)G^2(p, d), \qquad G_3(p, d)=(1/245)G^3(p, d).$$

4. Conclusion

The complete energy matrices in the approximation that includes electrostatic and spin-orbit interactions are now available, in several coupling schemes, for most electron configurations of the types $p^2\,l$ and $p^4\,l$. The $p^2\,s$ and $p^4\,s$ cases are treated by Condon and Shortley [2, pp. 198 and 268] in the LS scheme. Our $n'\,p$ and $n'\,d$ results are also built in the LS scheme. Möller [7] calculated the matrices of $p^4\,l$ electrostatic interaction in the $J_c\,l$ repre-

TABLE 3. *Matrices of spin-orbit interaction for the configuration* $p^2\,d$

$J=\frac{9}{2}$	$(^1D)\ ^2G$	$(^3P)\ ^4F$
$(^1D)\ ^2G$	$+\zeta'$	$+\frac{\sqrt{2}}{2}\zeta$
$(^3P)\ ^4F$	$+\frac{\sqrt{2}}{2}\zeta$	$+\frac{1}{2}(\zeta+2\zeta')$

$J=\frac{7}{2}$	$(^1D)\ ^2G$	$(^3P)\ ^4F$	$(^3P)\ ^2F$	$(^1D)\ ^2F$	$(^3P)\ ^4D$
$(^1D)\ ^2G$	$-\frac{5}{4}\zeta'$	$+\frac{\sqrt{2}}{4}\zeta$	$-\frac{\sqrt{6}}{4}\zeta$	$-\frac{3}{4}\zeta'$	0
$(^3P)\ ^4F$	$+\frac{\sqrt{2}}{4}\zeta$	0	$-\frac{\sqrt{3}}{6}(\zeta-4\zeta')$	$+\frac{\sqrt{2}}{4}\zeta$	$+\frac{\sqrt{6}}{6}(\zeta-\zeta')$
$(^3P)\ ^2F$	$-\frac{\sqrt{6}}{4}\zeta$	$-\frac{\sqrt{3}}{6}(\zeta-4\zeta')$	$+\frac{1}{3}(\zeta-\zeta')$	$+\frac{\sqrt{6}}{12}\zeta$	$+\frac{\sqrt{2}}{6}(\zeta+2\zeta')$
$(^1D)\ ^2F$	$-\frac{3}{4}\zeta'$	$+\frac{\sqrt{2}}{4}\zeta$	$+\frac{\sqrt{6}}{12}\zeta$	$+\frac{3}{4}\zeta'$	$+\frac{\sqrt{3}}{3}\zeta$
$(^3P)\ ^4D$	0	$+\frac{\sqrt{6}}{6}(\zeta-\zeta')$	$+\frac{\sqrt{2}}{6}(\zeta+2\zeta')$	$+\frac{\sqrt{3}}{3}\zeta$	$+\frac{1}{6}(\zeta+5\zeta')$

$J=\frac{5}{2}$	$(^3P)\ ^4F$	$(^3P)\ ^2F$	$(^1D)\ ^2F$	$(^3P)\ ^4D$	$(^3P)\ ^2D$	$(^1D)\ ^2D$	$(^1S)\ ^2D$	$(^3P)\ ^4P$
$(^3P)\ ^4F$	$-\frac{7}{18}(\zeta+2\zeta')$	$-\frac{\sqrt{5}}{9}(\zeta-4\zeta')$	$+\frac{\sqrt{30}}{18}\zeta$	$+\frac{8\sqrt{5}}{45}(\zeta-\zeta')$	$-\frac{\sqrt{70}}{45}(\zeta+2\zeta')$	$+\frac{\sqrt{30}}{45}\zeta$	$-\frac{2\sqrt{210}}{45}\zeta$	0
$(^3P)\ ^2F$	$-\frac{\sqrt{5}}{9}(\zeta-4\zeta')$	$-\frac{4}{9}(\zeta-\zeta')$	$-\frac{\sqrt{6}}{9}\zeta$	$+\frac{1}{9}(\zeta+2\zeta')$	$+\frac{\sqrt{14}}{18}(2\zeta+\zeta')$	$+\frac{\sqrt{6}}{18}\zeta$	$-\frac{\sqrt{42}}{9}\zeta$	0
$(^1D)\ ^2F$	$+\frac{\sqrt{30}}{18}\zeta$	$-\frac{\sqrt{6}}{9}\zeta$	$-\zeta'$	$+\frac{\sqrt{6}}{9}\zeta$	$-\frac{\sqrt{21}}{9}\zeta$	$-\zeta'$	0	0
$(^3P)\ ^4D$	$+\frac{8\sqrt{5}}{45}(\zeta-\zeta')$	$+\frac{1}{9}(\zeta+2\zeta')$	$+\frac{\sqrt{6}}{9}\zeta$	$-\frac{1}{36}(\zeta+5\zeta')$	$-\frac{\sqrt{14}}{36}(\zeta-10\zeta')$	$+\frac{7\sqrt{6}}{36}\zeta$	$+\frac{\sqrt{42}}{9}\zeta$	$+\frac{\sqrt{105}}{20}(\zeta-\zeta')$
$(^3P)\ ^2D$	$-\frac{\sqrt{70}}{45}(\zeta+2\zeta')$	$+\frac{\sqrt{14}}{18}(2\zeta+\zeta')$	$-\frac{\sqrt{21}}{9}\zeta$	$-\frac{\sqrt{14}}{36}(\zeta-10\zeta')$	$+\frac{1}{18}(2\zeta-5\zeta')$	$+\frac{\sqrt{21}}{18}\zeta$	$+\frac{2\sqrt{3}}{9}\zeta$	$+\frac{\sqrt{30}}{20}(\zeta+2\zeta')$
$(^1D)\ ^2D$	$+\frac{\sqrt{30}}{45}\zeta$	$+\frac{\sqrt{6}}{18}\zeta$	$-\zeta'$	$+\frac{7\sqrt{6}}{36}\zeta$	$+\frac{\sqrt{21}}{18}\zeta$	$+\frac{1}{2}\zeta'$	0	$+\frac{\sqrt{70}}{20}\zeta$
$(^1S)\ ^2D$	$-\frac{2\sqrt{210}}{45}\zeta$	$-\frac{\sqrt{42}}{9}\zeta$	0	$+\frac{\sqrt{42}}{9}\zeta$	$+\frac{2\sqrt{3}}{9}\zeta$	0	$+\zeta'$	$-\frac{\sqrt{10}}{5}\zeta$
$(^3P)\ ^4P$	0	0	0	$+\frac{\sqrt{105}}{20}(\zeta-\zeta')$	$+\frac{\sqrt{30}}{20}(\zeta+2\zeta')$	$+\frac{\sqrt{70}}{20}\zeta$	$-\frac{\sqrt{10}}{5}\zeta$	$-\frac{1}{4}(\zeta-3\zeta')$

$J=\frac{3}{2}$	$(^3P)\ ^4F$	$(^3P)\ ^4D$	$(^3P)\ ^2D$	$(^1D)\ ^2D$	$(^1S)\ ^2D$	$(^3P)\ ^4P$	$(^3P)\ ^2P$	$(^1D)\ ^2P$
$(^3P)\ ^4F$	$-\frac{2}{3}(\zeta+2\zeta')$	$+\frac{\sqrt{70}}{30}(\zeta-\zeta')$	$-\frac{\sqrt{70}}{30}(\zeta+2\zeta')$	$+\frac{\sqrt{30}}{30}\zeta$	$-\frac{\sqrt{210}}{15}\zeta$	0	0	0
$(^3P)\ ^4D$	$+\frac{\sqrt{70}}{30}(\zeta-\zeta')$	$-\frac{1}{6}(\zeta+5\zeta')$	$-\frac{1}{12}(\zeta-10\zeta')$	$+\frac{\sqrt{21}}{12}\zeta$	$+\frac{\sqrt{3}}{3}\zeta$	$+\frac{\sqrt{5}}{5}(\zeta-\zeta')$	$-\frac{1}{4}(\zeta+2\zeta')$	$+\frac{1}{4}\zeta$
$(^3P)\ ^2D$	$-\frac{\sqrt{70}}{30}(\zeta+2\zeta')$	$-\frac{1}{12}(\zeta-10\zeta')$	$-\frac{1}{12}(2\zeta-5\zeta')$	$-\frac{\sqrt{21}}{12}\zeta$	$-\frac{\sqrt{3}}{3}\zeta$	$+\frac{\sqrt{5}}{20}(\zeta+2\zeta')$	$+\frac{1}{4}(2\zeta+\zeta')$	$+\frac{1}{4}\zeta$
$(^1D)\ ^2D$	$+\frac{\sqrt{30}}{30}\zeta$	$+\frac{\sqrt{21}}{12}\zeta$	$-\frac{\sqrt{21}}{12}\zeta$	$-\frac{3}{4}\zeta'$	0	$+\frac{\sqrt{105}}{60}\zeta$	$-\frac{\sqrt{21}}{12}\zeta$	$-\frac{\sqrt{21}}{4}\zeta'$
$(^1S)\ ^2D$	$-\frac{\sqrt{210}}{15}\zeta$	$+\frac{\sqrt{3}}{3}\zeta$	$-\frac{\sqrt{3}}{3}\zeta$	0	$-\frac{3}{2}\zeta'$	$-\frac{\sqrt{15}}{15}\zeta$	$+\frac{\sqrt{3}}{3}\zeta$	0
$(^3P)\ ^4P$	0	$+\frac{\sqrt{5}}{5}(\zeta-\zeta')$	$+\frac{\sqrt{5}}{20}(\zeta+2\zeta')$	$+\frac{\sqrt{105}}{60}\zeta$	$-\frac{\sqrt{15}}{15}\zeta$	$+\frac{1}{6}(\zeta-3\zeta')$	$+\frac{\sqrt{5}}{12}(\zeta+6\zeta')$	$+\frac{\sqrt{5}}{4}\zeta$
$(^3P)\ ^2P$	0	$-\frac{1}{4}(\zeta+2\zeta')$	$+\frac{1}{4}(2\zeta+\zeta')$	$-\frac{\sqrt{21}}{12}\zeta$	$+\frac{\sqrt{3}}{3}\zeta$	$+\frac{\sqrt{5}}{12}(\zeta+6\zeta')$	$-\frac{1}{12}(2\zeta+3\zeta')$	$+\frac{1}{4}\zeta$
$(^1D)\ ^2P$	0	$+\frac{1}{4}\zeta$	$+\frac{1}{4}\zeta$	$-\frac{\sqrt{21}}{4}\zeta'$	0	$+\frac{\sqrt{5}}{4}\zeta$	$+\frac{1}{4}\zeta$	$+\frac{1}{4}\zeta'$

$J=\frac{1}{2}$	$(^3P)\ ^4D$	$(^3P)\ ^4P$	$(^3P)\ ^2P$	$(^1D)\ ^2P$	$(^1D)\ ^2S$
$(^3P)\ ^4D$	$-\frac{1}{4}(\zeta+5\zeta')$	$+\frac{1}{4}(\zeta-\zeta')$	$-\frac{\sqrt{2}}{4}(\zeta+2\zeta')$	$+\frac{\sqrt{2}}{4}\zeta$	0
$(^3P)\ ^4P$	$+\frac{1}{4}(\zeta-\zeta')$	$+\frac{5}{12}(\zeta-3\zeta')$	$+\frac{\sqrt{2}}{12}(\zeta+6\zeta')$	$+\frac{\sqrt{2}}{4}\zeta$	$+\frac{\sqrt{3}}{3}\zeta$
$(^3P)\ ^2P$	$-\frac{\sqrt{2}}{4}(\zeta+2\zeta')$	$+\frac{\sqrt{2}}{12}(\zeta+6\zeta')$	$+\frac{1}{6}(2\zeta+3\zeta')$	$-\frac{1}{2}\zeta$	$+\frac{\sqrt{6}}{6}\zeta$
$(^1D)\ ^2P$	$+\frac{\sqrt{2}}{4}\zeta$	$+\frac{\sqrt{2}}{4}\zeta$	$-\frac{1}{2}\zeta$	$-\frac{1}{2}\zeta'$	$-\frac{\sqrt{6}}{2}\zeta'$
$(^1D)\ ^2S$	0	$+\frac{\sqrt{3}}{3}\zeta$	$+\frac{\sqrt{6}}{6}\zeta$	$-\frac{\sqrt{6}}{2}\zeta'$	0

sentation. (Here J_c refers to the total angular momentum of the core.) These expressions are especially valuable in the analysis of configurations where the $J_c\, l$ coupling is very pure and hence the spin-orbit contribution can be neglected. To make the $J_c\, l$ matrices complete, however, Källén has calculated the spin-orbit elements and reports them in reference [8] together with the complete $p^4\ l$ matrices built in the $J_c\, j$ scheme.

5. References

[1] J. L. Tech, J. Res. NBS **67A** (Phys. and Chem.) No. 6, 555 (1963).
[2] E. U. Condon and G. H. Shortley, The Theory of Atomic Spectra (Cambridge University Press, London, 1951).
[3] R. H. Garstang, Monthly Notices of the RAS, **114,** 118 (1954).
[4] U. Fano and G. Racah, Irreducible Tensorial Sets (Academic Press, Inc. New York, N.Y. 1959).
[5] J. C. Slater, Quantum Theory of Atomic Structure, Vols. I and II (McGraw-Hill Book Co., New York, N.Y., 1960).
[6] G. Racah, Bull. Res. Counc. of Israel **8F,** 1 (1959).
[7] N. H. Möller, Ark. f. Fysik **18,** No. 9, 135 (1960).
[8] L. Minnhagen, Ark. f. Fysik **21,** No. 26, 415 (1962).
[9] M. Rotenberg, R. Bivins, N. Metropolis, and J. K. Wooten, Jr., The 3–j and 6–j Symbols (The Technology Press, MIT, Cambridge, Mass., 1959).

(Paper 69A5–361)

JOURNAL OF RESEARCH of the National Bureau of Standards—A. Physics and Chemistry
Vol. 69A, No. 5, September–October 1965

Heat of Formation of Calcium Aluminate Tricarbonate at 25 °C

H. A. Berman

(June 2, 1965)

The heat of formation at 25 °C, $\Delta H_f° = -16{,}228$ kJ/mole, of calcium aluminate tricarbonate, $3CaO \cdot Al_2O_3 \cdot 3CaCO_3 \cdot 30H_2O$ (c), was determined by the heat-of-solution method, with 2*N* HCl as the solvent, and $3CaO \cdot Al_2O_3 \cdot 6H_2O$ (c) and $CaCO_3$ (c) as the reactants. The heat of solution in 2*N* HCl is −501.0 kJ/mole, and the heat of the reaction $3CaO \cdot Al_2O_3 \cdot 6H_2O$ (c) + $3CaCO_3$ (c) + $24H_2O$ (l) → $3CaO \cdot Al_2O_3 \cdot 3CaCO_3 \cdot 30H_2O$ (c) is −186.6 kJ. The rate at which the heat of solution in 2*N* HCl changes with H_2O content at the $30H_2O$ level, $d(\Delta H)/dn$, is + 9.0 kJ/mole per mole H_2O. Heats of solution were determined for samples in the range of 6 to $31H_2O$, but decomposition appears to occur on drying to H_2O contents lower than $26H_2O$. The heats of stepwise reactions leading to the formation of calcium aluminate mono- and tricarbonate have also been calculated.

1. Introduction

Hydrated calcium aluminate tricarbonate, $3CaO \cdot Al_2O_3 \cdot 3CaCO_3 \cdot 30H_2O$, is a member of a series of complex salts represented by the general formula $3CaO \cdot Al_2O_3 \cdot 3CaX \cdot nH_2O$, in which *X* is a divalent anion or two units of a monovalent anion, and *n* is 30 to 32. This series is often referred to as the "high-form" series of complex calcium aluminates; its members generally crystallize as fine hexagonal or pseudohexagonal needles. The tricarbonate is related to calcium aluminate monocarbonate, $3CaO \cdot Al_2O_3 \cdot CaCO_3 \cdot 11H_2O$, which is the corresponding member of another series, known as the "low-form" series.

The tricarbonate was first made by Bessey, as reported by Jones [1] [1] and more recently described by Bessey [2], and was also prepared by Carlson and Berman [3]. Bessey reported a compound containing $27H_2O$; Carlson and Berman, $32H_2O$.

As part of a continuing investigation of the thermochemical properties of substances occurring in or related to hydraulic cements and their reaction products, the heat of formation of hydrated calcium aluminate tricarbonate was determined.

Measurements by the heat-of-solution method were made of the heat evolved at 25 °C in the reaction

$$3CaO \cdot Al_2O_3 \cdot 6H_2O(c) + 3CaCO_3(c) + 24H_2O(l) \xrightarrow{\Delta H_1} 3CaO \cdot Al_2O_3 \cdot 3CaCO_3 \cdot 30H_2O(c). \quad (1)$$

The heat of this reaction is the difference between the sum of the heats of solution of the reactants and the heat of solution of the product, in accordance with the following equations:

$$3CaO \cdot Al_2O_3 \cdot 6H_2O(c) + 1623.305(HCl \cdot 26.614H_2O)(aq) \xrightarrow{\Delta H_2} 3CaCl_2(aq) + 2AlCl_3(aq) + 1611.305(HCl \cdot 26.820H_2O)(aq) \quad (2)$$

$$3CaCO_3(c) + 3CaCl_2(aq) + 2AlCl_3(aq) + 1611.305(HCl \cdot 26.820H_2O)(aq) \xrightarrow{\Delta H_3} 6CaCl_2(aq) + 2AlCl_3(aq) + 3CO_2(aq) + 1605.305(HCl \cdot 26.922H_2O)(aq) \quad (3)$$

$$24H_2O(l) + 6CaCl_2(aq) + 2AlCl_3(aq) + 3CO_2(aq) + 1605.305(HCl \cdot 26.922H_2O)(aq) \xrightarrow{\Delta H_4} 6CaCl_2(aq) + 2AlCl_3(aq) + 3CO_2(aq) + 1605.305(HCl \cdot 26.937H_2O)(aq) \quad (4)$$

$$3CaO \cdot Al_2O_3 \cdot 3CaCO_3 \cdot 30H_2O(c) + 1623.305(HCl \cdot 26.614H_2O)(aq) \xrightarrow{\Delta H_5} 6CaCl_2(aq) + 2AlCl_3(aq) + 3CO_2(aq) + 1605.305(HCl \cdot 26.937H_2O)(aq). \quad (5)$$

[1] Figures in brackets indicate the literature references at the end of this paper.

The summation: equation 2 + equation 3 + equation 4 − equation 5 results in equation 1. Similar summation of the ΔH values results in ΔH_1.

The heat of solution of each of the reactants was measured in $HCl \cdot 26.61H_2O$(2.00N HCl at 25 °C). The heats of formation of the reactants were taken from Circular 500 [4] of the National Bureau of Standards.

All calculations in this paper are based on the 1961 atomic weights [5], and the results are expressed in absolute joules. Data reported in earlier work on the complex calcium aluminates [6, 7, 8], expressed in thermochemical calories, may be converted to joules by multiplying by 4.184. A summary of data so converted is included in this paper.

2. Preparation and Analysis of Samples

2.1. Preparation

Calcium aluminate tricarbonate was formed as a white precipitate by the addition of sodium carbonate solution to a mixture of calcium saccharate and either monocalcium aluminate or potassium aluminate solutions. Calcium saccharate is a solution of CaO in aqueous sucrose, which contains considerably more dissolved calcium than ordinary calcium hydroxide solution. A metastable solution of monocalcium aluminate, containing about 2 g of Al_2O_3 and 1 g of CaO per liter (approximately 0.02M), was prepared by shaking high-alumina cement with distilled H_2O about 3 hr and quickly filtering. Potassium aluminate solution was prepared by the method of Rabot and Mounier [9].

Four preparations of calcium aluminate tricarbonate were made, two of which provided useful thermochemical data. Details of the preparations are given in table 1.

Preparation 1 was made with calcium saccharate solution which was 0.307M with respect to CaO and contained 150 g of sucrose per liter. To 1750 ml of this solution 2500 ml of monocalcium aluminate solution was added, followed by 167 ml of 0.472M sodium carbonate solution. The CO_2/Al_2O_3 molar ratio was slightly more than 3:1. No precipitate formed at this point, but precipitation began after the addition of 2 liters of 0.02M $Ca(OH)_2$ and 100 ml of 0.44M NaOH. The crystals were filtered after standing 2 months.

Preparation 2 was made by adding 283 ml of potassium aluminate solution (0.204M Al_2O_3) to 2 liters of calcium saccharate solution (0.304M CaO), followed by 359 ml of 0.48M sodium carbonate solution (CO_2/Al_2O_3 molar ratio of 3:1). Precipitation began after further addition of 3 liters of CO_2-free distilled H_2O, which decreased the sucrose concentration to 50 g per liter. The crystals were filtered after 7 days.

Preparations 3 and 4 were made in the same manner as preparation 2 with slight differences in the concentrations and quantities of the potassium aluminate solutions, somewhat higher Al_2O_3/CaO ratios to obtain a larger quantity of precipitate, but the same CO_2/Al_2O_3 ratio as for preparations 1 and 2. In preparation 4 the calcium saccharate solution was diluted before, rather than after, the addition of the other solutions.

TABLE 1. *Properties of the preparations of calcium aluminate tricarbonate as originally dried at 79 percent relative humidity*

Preparation	1			2			3			4		
		No. of determinations	Std. error		No. of determinations	Std. error		No. of determinations	Std. error		No. of determinations	Std. error
Composition, weight percent:												
CaO [a]	29.09	6	[a] 0.03$_4$	28.05	4	[a] 0.02$_8$	27.73	5	[a] 0.04$_0$	27.00	8	[a] 0.02$_6$
Al_2O_3 [a]	8.94	4	[a] .02$_7$	8.45	2	[a] .02$_6$	8.11	6	[a] .00$_7$	7.91	8	[a] .01$_8$
Loss on ignition [a]	62.03	2	[a] .00$_6$	63.55	2	[a] .05$_0$	64.09	2	[a] .00$_8$	65.01	2	[a] .06$_9$
CO_2, by acid attack [a]	11.16	2	[a] .00$_5$	10.94	2	[a] .00$_2$	10.46	3	[a] .01$_0$	10.54	2	[a] .00$_2$
CO_2, by ignition [a]	21.38	2	[a] .52	21.96	3	[a] .27	24.87	4	[a] .73	29.70	3	[a] .67
Sucrose [b]	6.48	.....	[b] .34	7.13	.....	[b] .18	9.34	.....	[b] .47	12.42	.....	[b] .43
H_2O [b]	44.38	.....	[b] .34	45.48	.....	[b] .18	44.29	.....	[b] .47	42.05	.....	[b] .44
Molar ratios:												
$CaO:Al_2O_3$ [b]	5.92$_3$	.....	[b] .01$_9$	6.03$_6$	.....	[b] .02$_0$	6.21$_4$	.....	[b] .01$_1$	6.20$_3$	.....	[b] .01$_5$
$CO_2:Al_2O_3$ [b]	2.89$_4$	.....	[b] .00$_9$	3.00$_0$	.....	[b] .00$_9$	2.98$_7$	.....	[b] .00$_4$	3.08$_7$	.....	[b] .00$_7$
$H_2O:Al_2O_3$ [b]	28.11$_1$	.....	[b] .23	30.46$_7$	.....	[b] .15	30.89$_4$	.....	[b] .33	30.07$_7$	.....	[b] .32
Sucrose: Al_2O_3 [b]	0.21$_6$	.....	[b] .01$_1$	0.25$_1$	.....	[b] .00$_6$	0.34$_3$	.....	[b] .01$_7$	0.47$_8$	.....	[b] .01$_6$
Molar ratios of compounds present, to Al_2O_3:												
$3CaO \cdot Al_2O_3 \cdot 3CaCO_3 \cdot nH_2O$ [b]	.96$_5$	.....	[b] .00$_3$	1.000	.....	[b] .000	.99$_6$	.....	[b] .00$_1$	1.000	.....	[b] .000
where $n=$	28.68$_0$	.....	[b] .22	30.43$_1$	.....	[b] .15	30.76$_7$	.....	[b] .39	29.95$_9$	.....	[b] .32
$3CaO \cdot Al_2O_3 \cdot Ca(OH)_2 \cdot 12H_2O$ [b]	0.03$_4$	.....	[b] .00$_2$									
$Ca(OH)_2$ [b]				0.03$_6$	.....	[b] .00$_7$	0.24$_0$	.....	[b] .01$_1$	0.11$_8$	.....	[b] .00$_9$
$CaCO_3$ [b]										.08$_7$	.....	[b] .00$_7$
$Al_2O_3 \cdot 3H_2O$ [b]	.00$_{15}$	.....	[b] .00$_{35}$				.00$_4$	.....	[b] .00$_1$			
Sucrose [b]	.21$_6$	.....	[b] .01$_1$	.25$_1$	.....	[b] .00$_6$	.34$_3$	.....	[b] .01$_7$	.46$_8$	.....	[b] .01$_6$
Heat of solution of the preparation, ΔH J/g [a]	−430.3$_2$	4	[a] .5$_5$	−425.4$_7$	2	[a] .3$_6$	−414.1$_9$	3	[a] .3$_1$	−402.6$_8$	6	[a] 1.2
Corrected heat of solution of the $3CaO \cdot Al_2O_3 \cdot 3CaCO_3 \cdot nH_2O$ [b]												
ΔH J/g	−450.7$_4$	.....	.....	−456.7$_2$	.....	.....	−438.0$_7$	.....	.....	−453.7$_5$	.....	.....
kJ/mole	−490.0$_1$	.....	.....	−510.9$_3$	.....	.....	−492.8$_5$	.....	[b] 1.5	−503.7$_5$	.....	[b] 1.7

[a] Independently determined quantities. Standard errors calculated from replicate determinations.
[b] Derived quantities. Standard error of each derived quantity calculated directly from the standard errors of the applicable independently determined quantities. The independent quantities were used in these calculations to more places than shown in this table.

Preparations 3 and 4 were filtered after 7 and 8 months, respectively. Preparation 3 was washed on the filter with a 50-g/l sucrose solution to remove any excess CaO, and with absolute ethyl alcohol to remove the sucrose solution. Preparations 1, 2, and 4 were not washed, but were sucked "dry" on the filter.

The use of CaO-sucrose solutions appeared to be the only means of making the tricarbonate at room temperature, although Bessey made his early preparation without sucrose by adding ammonium carbonate solution slowly to calcium aluminate solution at low concentration with rapid stirring. It might be possible to prepare the compound at subfreezing temperatures without sucrose if an analogy with the calcium aluminate chlorides is valid; this possibility has not been investigated.

Preparation of the reagents, transfer of solutions, mixing, filtration, and other operations were performed in closed systems with precautions taken to exclude CO_2. All solutions were made with distilled water which had been boiled and then cooled in a current of CO_2-free air.

The filtered preparations were dried at 79 percent relative humidity in a desiccator over saturated NH_4Cl [10]. When the loss on ignition of a preparation had become constant, the material was ground and mixed in a sealed jar containing wood balls, and the ground material was returned to the desiccator for storage. Before placing the samples in the desiccators and after opening them at any time, the desiccators were evacuated to 2 to 4 cm Hg pressure and refilled with CO_2-free air which had been passed through a gas-washing bottle containing the same solution as in the desiccator. A detailed description of this technique may be found in reference [11].

The dried, ground samples were analyzed chemically to determine their composition. Heat-of-solution determinations were then made. The remaining portions of the preparations were subjected to further drying over the following desiccants: saturated $MgCl_2 \cdot 6H_2O$ (33% relative humidity) (which produced an insignificant loss of H_2O), saturated LiCl (12% relative humidity) [10], $20N$ H_2SO_4 (10% relative humidity), $23N$ H_2SO_4 (5% relative humidity) [12], and CaO (0% relative humidity). The heat of solution of these dried samples was determined at various stages of the drying process.

2.2. Chemical Analysis

Unlike other representatives of the complex calcium aluminate family prepared earlier [6, 7, 8], which had attained a maximum purity of 99 percent by weight, the preparations of calcium aluminate tricarbonate were only 87 to 92 percent pure. The major impurity was sucrose. This compound interferes with the usual method of determining H_2O content, which has been to ignite a sample at 1200 °C and subtract the separately determined CO_2 content from the loss on ignition. It interferes as well with the determination of Al_2O_3 and CaO by the classical precipitation methods.

The sucrose content was determined from the difference between the total CO_2 obtained by combustion of the sample in oxygen and the carbonate CO_2 obtained by dissolving the sample in dilute hydrochloric acid. This method was more accurate than attempts to determine sucrose by solubility in water or alcohol or by oxidimetric methods. Nevertheless, it proved to be the weakest link in the precision calculations. Inasmuch as the H_2O was determined as (ignition loss—carbonate CO_2—sucrose), the relatively poor precision of the sucrose determinations is reflected in the standard errors of the H_2O percentages and H_2O content of the preparations, table 1.[2] Fortunately, the sucrose had only a minor effect on the corrected heats of solution.

However, as shown in table 1, considerably better precision was obtained in the determination of CaO, Al_2O_3, and carbonate CO_2. The CaO and Al_2O_3 were determined by the referee methods of Federal Test Method Standard 158a [13], except that the dry sample was first ignited to destroy the sucrose, then dissolved in HCl. To conserve material, some determinations of Al_2O_3 and CaO were made from the solution remaining after a carbonate-CO_2 determination. In these instances the following technique was used to destroy the sucrose in the solution: The solution was evaporated on a steam bath to dryness, acidified with HCl, diluted with hot water, and filtered to remove any silica present (derived from decomposition of silicone grease used in the glass seals of the CO_2-evolution apparatus). The paper and precipitate were burned and ignited at about 600 °C, and any SiO_2 then volatilized with H_2SO_4 and HF. The filtrate was transferred by stages into the crucible containing the HF residue, and evaporated to dryness; the evaporation was completed in a 100° oven and the temperature then gradually raised in a furnace to 700 °C. The sucrose was thereby destroyed and the samples were ready for analysis after solution in HCl.

The oxide analyses and sucrose contents of the preparations are given in table 1. As pointed out in reference [8], the estimates of standard error for each determination were calculated separately for each preparation, rather than by pooling the standard error estimates for that particular determination for all preparations. This procedure is based on the assumption that, for a particular preparation, the precision of the analysis is dependent in part on the uniformity of the preparation and not simply on the degree to which an analytical method can be reproduced. The estimated uncertainty of the mole ratios of the compounds assumed to be present as impurities is an indication of the quantitative reliability of the impurity calculations. The method used for estimating this uncertainty is given in an appendix to this paper.

---

[2] $$\text{Standard error} = \sqrt{\frac{\Sigma x_i^2 - \frac{(\Sigma x_i)^2}{n}}{n(n-1)}}$$

where x_i is the result obtained for one measurement and n is the number o measurements.

TABLE 2. *X-ray diffraction patterns of calcium aluminate tricarbonate preparations*

Preparation 1		Preparation 2		Preparation 3		Preparation 4		C&B preparation [3]	
d, Å	Intensity [a]	*d*, Å	Intensity [a]	*d*, Å	Intensity [a]	*d*, Å	Intensity [a]	*d*, Å	Relative intensity
9.34	>100	9.40	>100	9.60	>100	9.71	>100	9.41	100
5.42	29	5.43	37	5.47	36	5.50	32	5.43	27
								5.31	4
4.82	28	4.84	35	4.87	24	4.90	20	4.83	20
4.62	35	4.62	34	4.65	24	4.68	21	4.62	26
		4.13	19						
3.79	52	3.79	42	3.81	52	3.83	38	3.80	42
3.52	27	3.52	22	3.53	25	3.56	13	3.52	20
3.37	35	3.37	40	3.39	38	3.41	28	3.37	27
3.13	7	3.14	8	3.15	8	3.17	7	3.13	4
3.036	9			3.06	34	3.06	5		
2.962	9	2.98	10	2.98	10	2.99	7	2.962	8
2.697	42	2.70	49	2.71	48	2.72	36	2.700	35
2.654	7	2.66	7	2.66	10	2.67	6	2.653	11
2.627	2	2.62	7	2.62	9	2.63	5		
2.603	3							2.605	5
2.527	[b] 22							2.529	7
2.505	84	2.51	77	2.520	88	2.52	65	2.507	67
								2.466	3
2.413	3	2.42	5	2.43	7	2.43	5	2.413	4
2.339	4	2.34	9	2.35	7	2.36	6	2.339	6
				2.32	6	2.32	4	2.310	4
2.255	3								
2.151	37	2.15	39	2.16	46	2.17	32	2.156	37
2.093	21	2.10	23	2.11	26	2.11	18	2.098	19
								2.049	3
1.997	6	2.00	9	2.00	9	2.01	6	1.996	5
1.976	3							1.977	3
1.912	8	1.916	11	1.92	8	1.93	8	1.913	7
1.878	13	1.883	18	1.89	18	1.89	12	1.879	12
1.823	5	1.826	10	1.83	12	1.83	9	1.822	9
[c] 1.786	5								
1.770	7	[c] 1.773	9	[c] 1.773	7	[c] 1.78	7	1.768	7
								1.758	2
								1.739	2
1.711	2					1.72	2	1.711	2
1.685	3	1.691	5	1.694	3	1.69	3	1.684	4
		1.674	3	1.677	3	1.68	3		
1.646	5	1.652	5	1.654	7	1.66	4	1.646	4
1.622	8	1.627	9	1.630	11	1.63	7	1.622	7
1.584	1	1.572	4					1.582	2
								1.568	2
								1.541	2
1.532	4	1.536	6					1.532	4
1.483	3	1.485	6					1.483	5
1.476	2							1.465	3

[a] Intensity for preparations 1, 2, 3, and 4 was measured from actual peak heights on the x-ray diffraction patterns, after subtracting the background level. The intensities for the first peak on each pattern were estimated to be 140 to 165.
[b] Shoulder on large peak; true intensity may be smaller.
[c] Broad peak, centering on *d*-spacing given.

2.3. Characterization

X-ray patterns of the preparations, summarized in table 2, were obtained by the powder method on a Geiger-counter diffractometer with copper Kα radiation. The *d*-spacings are essentially the same as those of the tricarbonate reported in reference [3], also shown in the table, except that a line at 3.035 Å, due possibly to free $CaCO_3$, is present in preparations 1, 3, and 4. Chemical analysis, however, suggests the presence of free $CaCO_3$ only in preparation 4; it is possible that calcium hydroxide or tetracalcium aluminate present in preparations 1 and 3 may have undergone partial carbonation while in the X-ray diffractometer. Other differences among the patterns probably represent small differences of diagram interpretation rather than real variation.

Microscopical examination showed the preparations to be almost entirely clumps of needlelike crystals of negative elongation with refractive indices ω=1.490, ϵ=1.480, both accurate to within 0.003 (ϵ slightly lower in some cases).

Differential thermal analysis (fig. 1) showed a large endothermic area peaking at 145 to 165 °C, due to H_2O loss; a large exothermic area with two peaks at 400 and 465°, presumably due to the oxidation of sucrose; a small exothermic peak at 730 to 800°; and a small endothermic area centering at 860 to 925°, presumably due to evolution of CO_2. The exothermic peak at 390° reported by Carlson and Berman [3], unexplained at that time, is probably an indication that sucrose was present in their preparation, considerably less sucrose, however, than in the preparations reported here. If the presence of sucrose in these preparations had been neglected and its weight included in the H_2O content, the formula reported would have been $3CaO{\cdot}Al_2O_3{\cdot}3CaCO_3{\cdot}38H_2O$ instead of $\ldots{\cdot}30H_2O$. Although quantitative analytical data cannot be deduced from DTA patterns made four years apart, it can be concluded roughly from the relative areas of the exotherms and endotherms in each pattern that a correction for the sucrose content of Carlson and Berman's preparation would have brought its H_2O content closer to $30H_2O$ than to the $32H_2O$

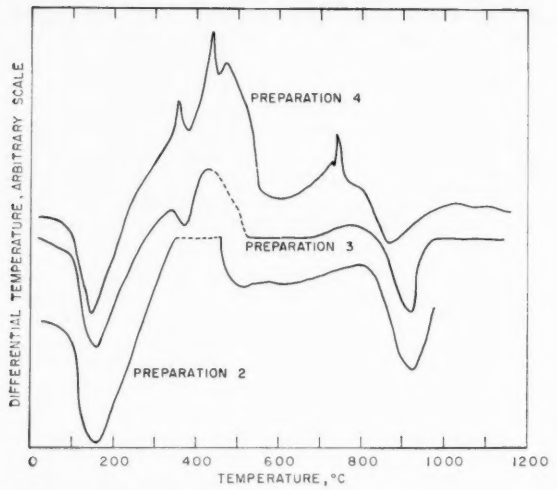

FIGURE 1. *Differential thermal analysis of preparations of calcium aluminate tricarbonate.*

Dashed lines indicate temperature differences which were off-scale (preparation 2) or estimated (preparation 3)

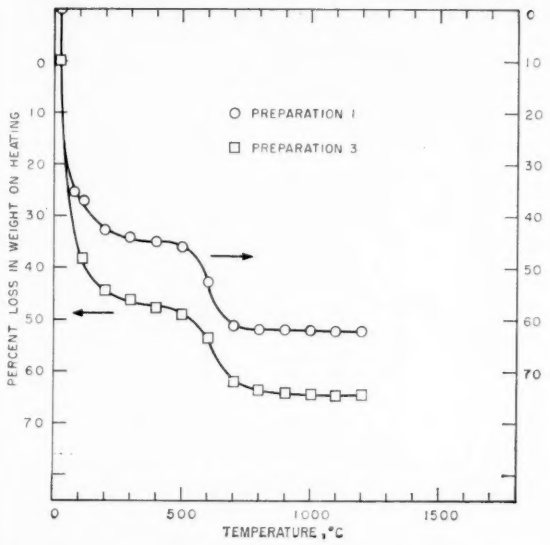

FIGURE 2. *Weight loss of preparations of calcium aluminate tricarbonate heated to constant weight at constant temperatures from 80 to 1200 °C.*

reported. The higher temperature found for the first endothermic peak in the current preparations (165°) than in the preparation of reference [3] can probably be attributed to their greater sucrose content.

Curves of weight loss versus temperature (fig. 2), determined by stepwise heating at a constant temperature to constant weight for each step, showed the greatest slope at low temperatures and leveled off to a minimum slope at about 350 °C. The slope then increased to another maximum between 600 and 700° and leveled off again at about 750° with small weight losses continuing up to 1200°. The first rapid weight loss below 350° represents evolution of water by a combination of dehydration of the tricarbonate and decomposition of the sucrose (a sample of pure sucrose was completely carbonized at 200°); the second, between 500 and 750°, represents loss of residual H_2O and CO_2. In this static thermogravimetric procedure, the changes took place at lower temperatures than in the dynamic DTA determination because the sample remained at a given temperature long enough to reach equilibrium.

3. Heat-of-Solution Measurements

Heats of solution were determined in $HCl \cdot 26.61_4 H_2O$ (2.00*N* HCl at 25 °C). The all-platinum calorimeter described in reference [7] was used, with some modifications to be described below.

As pointed out in the same reference, determination of the heat of solution of carbonates in acids introduces the problem of CO_2 evolution. On dissolving, the sample first releases a large quantity of heat and the temperature rises rapidly, but as CO_2 gas is released from solution endothermically, the temperature in the calorimeter falls (after correction for the temperature rise produced by stirring and leakage of heat from the water bath). This effect takes place even when the CO_2 available is not enough to saturate the acid, as reported in reference [7]. For this reason, it appears uncertain to the author whether the problem can really be solved by using HCl saturated with CO_2 at the start. The loss of heat due to gas evolution makes it difficult to obtain a final rating period in the calorimeter during which no reaction is taking place and the energy of stirring and heat leakage can be measured. If the escape of gas is too violent, it also removes heat from the area immediately around the sample before this heat can be transmitted to the rest of the calorimeter.

The problem was met in the case of $CaCO_3$ [7] by holding the sample under distilled H_2O in a glass bulb, breaking the bulb, and allowing the acid to rise through the sample as the sample fell into the acid. Rising bubbles gave up their sensible heat to the distilled H_2O. A heat-leakage constant obtained from calibration determinations was combined with an initial rating period (before breaking the bulb) to obtain the stirring energy effect for the particular run. It was then possible, for each 1 or 2-min period after breaking the bulb, to subtract the temperature rise due to heat leakage and to stirring energy from the observed temperature rise. This corrected temperature rise showed the rapid increase due to solution of the sample, followed by a gradual decrease due to CO_2 escape. By extrapolating the descending curve backwards to zero time (when the bulb had been broken), the temperature rise was obtained for solution of the entire sample with dissolved CO_2 as a product.

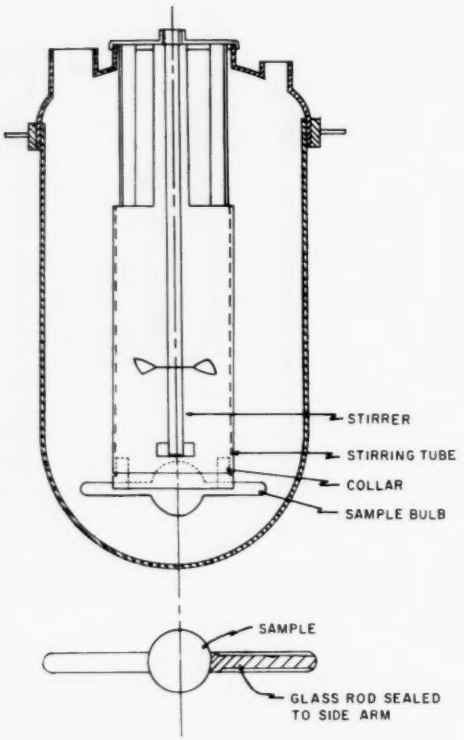

FIGURE 3. *Modifications in the calorimeter of reference* [7], *showing sealed glass sample bulb, plastic stirrer, and plastic collar on stirring tube.*

Enlarged view shows details of sample bulb.

This technique, used for $CaCO_3$, was not found necessary for calcium aluminate monocarbonate [7]. The tricarbonate samples, however, behaved more like $CaCO_3$, but the gradual decline in the corrected temperature rise was not as protracted. It was therefore possible in many determinations to obtain a final as well as an initial rating period, from which both the heat leakage and the stirring energy could be calculated.

Two methods of placing and breaking the bulb were used. For preparations 1 and 2, the "hanging-bulb" arrangement is shown in figure 1 of reference [7], where the bulb is drawn with dashed lines. The sample was released by dropping a 10-g weight onto the end of a glass rod, which in turn pierced the bottom of the bulb. Because of the uncertainty of defining how much of the mass of the bulb, rod, and connecting tubing was to be included within the calorimeter boundaries for the purpose of calculating heat capacity, an electrical calibration was first made, the entire assembly (calorimeter and jacket) cooled, and then the heat-of-solution determination performed, both determinations over approximately the same temperature range. A few determinations were made without calibrating; an average heat capacity was used, corrected for the differences in the masses of bulbs and samples within the calorimeter.

For preparations 3 and 4, and for the reported results of preparation 2, a sealed-bulb arrangement was used, as shown in figure 3. The bulb was centered between two side-arms, one closed at the bulb end to keep the sample from being trapped in that arm. A plastic collar was fitted to the bottom of the stirring tube, provided with grooves to hold the arms of the bulb. Some of the material was placed in the bulb through the open arm, the interior of the arm wiped clean, the sample weighed, and the open arm sealed at the tip. The bulb was centered on the bottom of the calorimeter and the stirring tube then inserted so that the grooves in the plastic ring were alined with the bulb arms. After assembly of calorimeter and jacket, acid was introduced gently to allow the bulb to float until the arms made contact with the plastic ring. To introduce the sample into the acid, the stirrer motor was stopped long enough to allow the stirrer to be pushed down against the bulb, a matter of 10 to 15 sec. A plastic stirrer replaced the normal platinum stirrer to provide the stiffness needed to break the bulb.

The sealed-bulb arrangement was adopted because the liquid placed over the sample in the hanging bulb is believed to have introduced errors in the thermochemical results. Water, used in preparation 1, although suitable for $CaCO_3$, may have further hydrated the samples and produced low heat-of-solution values. Dry *n*-propanol, completely miscible with water and possessing about the same vapor pressure at 25 °C, was used with preparation 2 to avoid the hydration effect, but it is probable that it dehydrated the samples to produce high heat-of-solution values.

Heats of solution for preparation 2 closer to those of preparations 3 and 4 were obtained when the sealed bulb was used in place of the hanging bulb. They were not considered reliable, however, because the preparation appeared to be slightly contaminated when the sealed-bulb determinations were made.

With the hanging bulb the acid charge was 740.00 g. It was not possible in the sealed-bulb technique to weigh the acid because of the conditions of assembly. The charge in this case was about 730 ml (755 g) and calibration was necessary for each determination. Calibration and heat of solution were not run over the same temperature range in preparations 3 and 4 because it was believed that cooling the jacket between the two runs upset the equilibrium of the initial rating period of the second (solution) run. The validity of calibrating at a lower temperature and dissolving the sample at a higher temperature was checked in one determination in which two calibrations were run, at both temperature levels. Several determinations were also made in which calibration and solution temperature levels were reversed.

Calorimeter samples were about 1 g for the samples dried at 79 percent relative humidity. The sample weights for material dried at lower humidities were smaller and contained the same molar quantity of calcium aluminate tricarbonate as the higher-humidity samples.

TABLE 3. *Properties of the preparations of calcium aluminate tricarbonate dried at relative humidities of 12 percent and less*

Desiccant	LiCl	$20N$ H_2SO_4	$23N$ H_2SO_4			CaO	
Relative humidity, percent	12	10	5			0	
Time exposed, days	17	[a] 9	[b] 1	[c] 20	[c] 28	49	49
Original preparation	4	4	4	3	3	3	4
Molar ratio, H_2O: Al_2O_3	27.51_7	25.89_5	24.32_2	15.16_1	12.56_8	5.89_4	5.84_0
Molar ratio of H_2O to $3CaO{\cdot}Al_2O_3{\cdot}3CaCO_3$, (n)	27.39_9	25.77_7	24.20_4	14.96_9	12.36_5	5.66_8	5.72_2
Heat of solution of sample, ΔH, J/g	-435.9_8	-466.6_1	-473.6_9	-706.7_3	-781.2_6	-1000.2_0	-937.3_7
Corrected heat of solution of the $3CaO{\cdot}Al_2O_3{\cdot}3CaCO_3{\cdot}nH_2O$ ΔH, J/g	-494.8_3	-532.3_9	-542.5_7	-786.1_7	-878.2_1	-1158.9_5	-1162.6_0
kJ/mole	-526.5_4	-550.9_4	-546.1_0	-660.4_9	-696.6_2	-779.4_2	-783.0_7

[a] Exposed 17 days to LiCl before exposure to $20N$ H_2SO_4
[b] Exposed 10 days to $20N$ H_2SO_4 and 17 days to LiCl before exposure to $23N$ H_2SO_4
[c] Exposed 34 days to LiCl before exposure to $23N$ H_2SO_4

To conform to eq (1), the corresponding sample weights for reactants $3CaO{\cdot}Al_2O_3{\cdot}6H_2O$ and $CaCO_3$ are 0.34 and 0.27 g, respectively, when dissolved in 740–760 g of calorimeter acid. This compares with sample weights ranging from 0.26 to 0.44 g of $3CaO{\cdot}Al_2O_3{\cdot}6H_2O$ actually used with 600 g of acid in earlier work [6, 7], which cover the desired sample-acid ratio. The heat of solution of 0.24 to 0.27 g of $CaCO_3$ in 740 g of acid was separately determined for this work because this sample-acid ratio had not been covered in reference [7].

The heat effect of adding the 24 moles of H_2O appearing in eqs (1) and (4) was estimated as the partial molal heat content of H_2O in 2N HCl [4], neglecting the contribution of the small amounts of other solutes present.

4. Results and Discussion

4.1. Heat of Solution of the Preparations

The heats of solution obtained with the original preparations (dried at 79 % relative humidity) are shown in table 1. Those obtained for the lower-humidity preparations are shown in table 3. Both tables also show heats of solution of the pure calcium aluminate tricarbonate, after correction for the impurities in the sample.

Detailed data of the heat-of-solution determinations for calcium carbonate, sucrose, and preparations 3 and 4, are shown in table 4.

4.2. Correction for Impurities

The calculation of the composition of a sample and of the heat of solution of the pure calcium aluminate tricarbonate present was performed as described in the appendices to references [6] and [7]. The nature of the impurities was suggested by the chemical analysis and its departures from the theoretical ratios for calcium aluminate tricarbonate. Inasmuch as departure from stoichiometry is often ascribed to analytical error, it is helpful to calculate what degree of uncertainty in the values obtained for impurities is attributable to the analysis; therefore, the precision of the impurity contents was calculated from the observed precision of the analyses. In general, the precision figures indicate that most of the values for the impurities are reliable to about 0.01 mole per mole of major component.

The nature of the sucrose impurity was not ascertained. X-ray patterns showed none of the lines of pure sucrose, and it was not possible to obtain a powder sample of calcium saccharate sufficiently free of H_2O to produce a crystalline diffraction pattern. The large variation of sucrose content from one preparation to another (between 6 and 12%) casts doubt on the hypothesis that the sucrose forms a part of the tricarbonate crystal structure. Microscopical examination showed some irregular crystals with positive elongation and refractive indices slightly greater and slightly less than 1.56, which may be attributed to sucrose, but they were less numerous than would be expected from the chemical analysis. DTA patterns and chemical analysis showed that the preparations contained organic matter that charred easily and was oxidized at about the same temperatures as pure sucrose. Consequently, for the purpose of correcting the observed heats of solution, the sucrose was treated as an impurity in its original form.

The following values were used for the heats of solution of the various impurities:

$CaCO_3$	$\Delta H = -354.00$ J/g (table 4)
$Ca(OH)_2$	-1763.95 J/g [14]
$Al_2O_3{\cdot}3H_2O$	-210.62 kJ/mole [7]
sucrose	$+23.0$ J/g (table 4).

Of the three determinations made of the heat of solution of sucrose, the one involving the largest sample was used (table 4, sucrose, run 2) because the greater temperature change could be measured more precisely. Note, however, that the values of the other two determinations agree quite well with that of the determination chosen.

TABLE 4. *Heat-of-solution determinations*

Preparation	Run	Calibration: Initial temp.	Time	Voltage	Current	Heater resistance	Electrical energy	Corrected temp. rise	Heat capacity	Solution: Initial temp.	Sample weight	Corrected temperature rise	Heat of solution ΔH	Standard error
		Ohm	*sec*	*Volt*	*A*	*Ohm*	*Joules*	*Ohm*	*J/ohm*	*Ohm*	*g*	*Ohm*	*J/g*	*J/g*
3	1	2.5413	479.993	9.16192	0.132471	69.021	583.750	0.020089	29,058.2	2.5702	0.9993	0.014240	−414.07	
	2	2.5401	599.993	9.17883	.132974	69.027	732.319	.025135	29,135.4	2.5726	1.0030	.014205	−413.74	
	3	2.5426	599.993	9.23737	.133831	69.023	741.739	.025455	29,139.2	2.5750	1.0236	.014570	−414.77	
		Mean, before correction for impurities											−414.19	0.30
4	1	2.5404	599.993	9.142048	.132442	69.027	726.466	.025049	29,001.8	2.5726	1.0286	.014360	−404.89	
	2	2.5501	599.993	6.40689	.092746	69.080	356.524	.012233	29,144.4	2.5705	1.1663	.015935	−398.20	
	3	2.5402	599.993	9.17778	.132966	69.024	732.191	.025146	29,177.6	2.5721	1.0393	.014364	−402.34	
	4	2.5403	599.993	9.17746	.132952	69.029	732.086	.025184	29,069.5	2.5741	0.9507	.013646	−400.41	
	5	2.5400	599.993	9.15160	.132580	69.027	727.984	.025042	29,070.5	2.5723	1.0299	.014378	−405.83	
	6	2.5399	599.993	9.16357	.132763	69.022	729.942	.025162	29,009.7	2.5722	1.0414	.014519	−404.39	
		Mean, before correction for impurities											−402.68	1.2
4(12 R.H.)	1	2.5399	599.993	9.07363	.131471	69.016	715.743	.024554	29,149.8	2.5711	0.8972	.013452	−437.07	
	2	2.5479	599.993	9.06777	.131376	69.021	714.764	.024635	29,014.2	2.5789	1.0510	.015753	−434.88	
		Mean, before correction for impurities											−435.98	1.1
4(10 RH)		2.5409	599.993	8.24040	.119386	69.023	590.266	.020348	29,008.3	2.5674	0.9352	.015043	−466.61	
4(5 RH)		2.5657	599.993	8.19526	.118737	69.020	583.842	.020051	29,117.8	2.5402	0.9003	.014646	−473.69	
3(5 RH)		2.5696	599.993	8.67179	.125633	69.025	653.670	.022520	29,026.8	2.5399	0.7774	.018928	−706.73	
3(5 RH)		2.5701	599.993	8.20185	.118819	69.028	584.714	.020138	29,035.4	2.5407	0.7147	.019231	−781.26	
3(0 RH)		2.5463	599.993	8.71194	.126235	69.014	659.843	.022483	29,348.0	2.5754	0.6610	.022483	−1000.20	
4(0 RH)		2.5721	599.993	8.72583	.126420	69.023	661.864	.022761	29,078.5	2.5408	0.6501	.020956	−937.37	
[a] $CaCO_3$ [b]	1								[d] 28,845.8		0.2492	.003930	[e] −354.37	
	2								[d] 28,770.2		0.2710	.003977	[e] −353.62	
		Mean											−354.00	0.38
Sucrose	[c] 1								[d] 28,590.1		0.4511	−.00032	+20.3	
	2								[d] 29,054.1	2.6057	1.1700	−.000928	+23.0	
	3	2.6095	239.993	8.99702	.130282	69.058	281.308	.009653	29,142.0	2.6092	0.1103	−.000085	+22.5	
Calibrations on the same charge at different initial temperature levels.														
	1	2.5398	599.993	9.18300	.133044	69.022	733.038	.025070	29,239.6					
	2	2.5828	419.993	9.18084	.133005	69.026	512.854	.017536	29,245.8					

[a] Hanging-bulb technique for $CaCO_3$ and sucrose, run 1. Sealed-bulb for all other determinations.
[b] Determined without the addition of tricalcium aluminate.
[c] Determined in acid to which 0.3268 g of tricalcium aluminate hexahydrate had been added.
[d] Heat capacity calculated from an average of previous runs and corrected for difference in weights of sample, bulb, and water in bulb.
[e] Total energy in each run corrected for energy of dilution of acid with water.
Run 1—7.6780 g H_2O, total energy 113.36 J, dilution energy 25.05 J, solution energy 88.31 J.
Run 2—5.6985 g H_2O, total energy 114.42 J, dilution energy 18.59 J, solution energy 95.83 J.

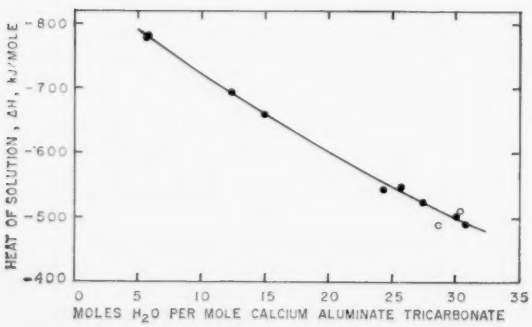

FIGURE 4. *Heat of solution of* $3CaO{\cdot}Al_2O_3{\cdot}3CaCO_3{\cdot}nH_2O$ (c).

Closed circles represent samples of preparations 3 and 4. Open circles represent samples of preparations 1 and 2. The solid curve was obtained from the closed circles.

The estimated standard error in the corrected heats of solution (calculated as described in the appendix) is about 2 kJ per mole. The poor precision of the sucrose analyses (which results from the poor precision of the determination of CO_2 by ignition) does not seriously affect the standard error of the corrected heats of solution because it enters only one of the minor terms in the calculation.

4.3. Heat of Solution of Calcium Aluminate Tricarbonate

Figure 4 is a plot of the corrected heats of solution against the calculated H_2O content of the pure compound. The points are derived from tables 1 and 3. The solid curve represents the following quadratic equation calculated by least squares

from the points:

$$\Delta H = -865.566 + 15.2184n - 0.10296n^2 \qquad (6)$$

where

ΔH = heat of solution in kJ/mole calcium aluminate tricarbonate.
n = moles H_2O/mole calcium aluminate tricarbonate.

The curve was obtained only from the closed circles, representing preparations 3 and 4. Open circles refer to the corrected heats of solution of preparations 1 and 2, which were not used in calculating the equation, for reasons discussed in section 3.

The crystal structure of some of the complex calcium aluminates remains intact as the H_2O content is decreased [8] although the interplanar spacings may change. However, the x-ray patterns of the tricarbonate samples dried at relative humidities of 12 percent and less showed no change in interplanar spacings, but did show a progressive loss of intensity with complete disappearance of the peaks at $6H_2O$ and little evidence of them at $14H_2O$. The microscope revealed increasing quantities of trapezoidal plates with positive elongation and refractive indices of 1.523 and 1.545, suggestive of calcium aluminate monocarbonate or tetracalcium aluminate ($3CaO \cdot Al_2O_3 \cdot Ca(OH)_2 \cdot 12H_2O$), but quite different in appearance from the crystals of these compounds usually observed. Evidently there was decomposition or loss of crystallinity accompanying the loss of H_2O and there is some indication in the x-ray patterns that much of this change took place between 26 and $24H_2O$. It is possible that the lower H_2O contents represent mixtures of $30H_2O$ material and decomposition products.

From eq (6), the heat of solution of $3CaO \cdot Al_2O_3 \cdot 3CaCO_3 \cdot 30H_2O$ in 2.00*N* HCl (at a sample-solution ratio of 1:755) is $\Delta H = -501.68$ kJ/mole. The change of heat of solution with H_2O content at this point, $d(\Delta H)/dn$, is 9.0$_4$ kJ/mole per mole H_2O.

4.4. Heat of Formation of the Product From the Reactants

The heat of the reaction represented by eq (1) is calculated from the heats of solution of the reactants and products. The heat effects of eqs (2), (3), (4), and (5) are added, as follows:

$\Delta H_2 = -580.36$ kJ/mole	eq (2)
$\Delta H_3 = -106.29$	eq (3)
$\Delta H_4 = -1.61$	eq (4)
$-\Delta H_5 = +501.68$	−eq (5)
$\Delta H_1 = -186.58$	eq (1)

The heat effect of eq (2) was obtained from the value of 1546.93 J/g for a sample of $3CaO \cdot Al_2O_3 \cdot 5.859H_2O$ [7], by correcting for its impurity content of 0.007 mole $CaCO_3$ per mole Al_2O_3 [6], and subtracting the correction of 0.46 kcal/mole (1.925 kJ/mole) discussed in reference [8].

4.5. Heat of Formation of Calcium Aluminate Tricarbonate From the Elements

The heat of formation of calcium aluminate tricarbonate is the sum of the heat effect of eq (1) and of the heats of formation of the reactants [3]:

ΔH_f°, $3CaO \cdot Al_2O_3 \cdot 6H_2O$ (c)	$= -5561.$
ΔH_f°, $3CaCO_3$ (c)	$= -3620.624$
ΔH_f°, $24H_2O$(l)	$= -6860.16$
ΔH, eq (1)	$= -186.58$
ΔH_f°, $3CaO \cdot Al_2O_3 \cdot 3CaCO_3 \cdot 30H_2O$ (c)	$= -16{,}228._{36}$ kJ/mole.

4.6. Summary of Heats of Formation and Heats of Reaction

The results of this paper and of references [6, 7, 8] may be combined and updated to produce the following thermochemical data on complex calcium aluminates:

Heats of Formation, ΔH_f°

$3CaO \cdot Al_2O_3 \cdot 3CaCO_3 \cdot 30H_2O$ (c)	$-16{,}228._{36}$ kJ/mole
$3CaO \cdot Al_2O_3 \cdot CaCO_3 \cdot 10.68H_2O$ (c)	$-8{,}188._{76}$
$3CaO \cdot Al_2O_3 \cdot 3CaSO_4 \cdot 32H_2O$ (c)	$-17{,}548._{38}$
$3CaO \cdot Al_2O_3 \cdot 3CaSO_4 \cdot 31H_2O$ (c)	$-17{,}252._{06}$
$3CaO \cdot Al_2O_3 \cdot CaSO_4 \cdot 12H_2O$ (c)	$-8{,}788._{19}$

Stepwise Heats of Reaction, ΔH

$3CaO \cdot Al_2O_3 \cdot 6H_2O$ (c) + $CaCO_3$ (c) + $4.68H_2O$ (l) → $3CaO \cdot Al_2O_3 \cdot CaCO_3 \cdot 10.68H_2O$ (c)
$\Delta H = -83.16$ kJ

$3CaO \cdot Al_2O_3 \cdot CaCO_3 \cdot 10.68H_2O$ (c) + $2CaCO_3$ (c) + $19.32H_2O$ (l) → $3CaO \cdot Al_2O_3 \cdot 3CaCO_3 \cdot 30H_2O$ (c)
$\Delta H = -103.42$ kJ

$3CaO \cdot Al_2O_3 \cdot 6H_2O$ (c) + $CaSO_4 \cdot 2H_2O$ (c) + $4H_2O$ (l) → $3CaO \cdot Al_2O_3 \cdot CaSO_4 \cdot 12H_2O$ (c)
$\Delta H = -62.71$ kJ

$3CaO \cdot Al_2O_3 \cdot CaSO_4 \cdot 12H_2O$ (c) + $2(CaSO_4 \cdot 2H_2O)$ + $15H_2O$ (l) → $3CaO \cdot Al_2O_3 \cdot 3CaSO_4 \cdot 31H_2O$ (c)
$\Delta H = -134.02$ kJ

$3CaO \cdot Al_2O_3 \cdot CaSO_4 \cdot 12H_2O$ (c) + $2(CaSO_4 \cdot 2H_2O)$ (c) + $16H_2O$ (l) → $3CaO \cdot Al_2O_3 \cdot 3CaSO_4 \cdot 32H_2O$ (c)
$\Delta H = -144.50$ kJ

5. Appendix

The standard errors of the mole ratios and the standard errors of the corrected heats of solution, arising from the estimated standard errors of the original analytical determinations and heat-of-solution determinations, were calculated directly from the original independently measured quantities by the general formula for propagation of error for independent variables

$$S_F = \sqrt{\left[\frac{\partial F}{\partial x}\right]^2 S_x^2 + \left[\frac{\partial F}{\partial y}\right]^2 S_y^2 + \left[\frac{\partial F}{\partial z}\right]^2 S_z^2 + \ldots}$$

where S_F is the standard error of the function $F(x, y, z, \ldots)$ and S_x, S_y, S_z, . . . are the standard errors of $x, y, z, \ldots$, respectively, and the partial derivatives are to be evaluated at the averages of the variables [15]. The independently measured quantities were: CaO, Al_2O_3, loss on ignition, CO_2 by acid attack, CO_2 by ignition, heat of solution of the preparation, and heat of solution of $CaCO_3$. Also treated as an independent quantity was the heat of solution of $Ca(OH)_2$, obtained from triplicate determinations in [14]. By making each standard error calculation directly from the original independent quantities, the effects of cross-correlation obtained in stepwise calculation were eliminated.

6. References

[1] F. E. Jones, The calcium aluminate complex salts, Proceedings of the Symposium on the Chemistry of Cements (Stockholm, 1938), 232. Ingeniorsvetenskapsakademien, Stockholm (1939).

[2] G. E. Bessey, private communication (1965).

[3] E. T. Carlson and H. A. Berman, Some observations on the calcium aluminate carbonate hydrates, J. Res. NBS, **64A** (Phys. and Chem.) No. 4, 333 (1960).

[4] F. D. Rossini, D. D. Wagman, W. H. Evans, S. Levine, and I. Jaffe, Selected values of chemical thermodynamic properties, NBS Circ. 500, U. S. Government Printing Office, Washington, D.C. 20402 (1952).

[5] Compt. Rend. of the 21st Conference of the International Union of Pure and Applied Chemistry, Montreal (1961), Report of the Committee on Atomic Weights, pp. 284–327.

[6] H. A. Berman and E. S. Newman, Heat of formation of calcium trisulfoaluminate at 25 °C, Proceedings of the Fourth International Symposium on the Chemistry of Cement (Washington, 1960); NBS Mono. 43, pp. 247–257.

[7] H. A. Berman and E. S. Newman, Heat of formation of calcium aluminate monocarbonate at 25 °C, J. Res. NBS, **65A** (Phys. and Chem.) No. 3, 197 (1961).

[8] H. A. Berman and E. S. Newman, Heat of formation of calcium aluminate monosulfate at 25 °C, J. Res. NBS, **67A** (Phys. and Chem.) No. 1, 1 (1963).

[9] R. Rabot and M. T. Mounier, On the existence of hexagonal tricalcium aluminate hydrate (in French), Revue des Matériaux de Construction et de Travaux Publics, No. 554, 449 (1961).

[10] A. Wexler and S. Hasegawa, Relative-humidity-temperature relationships of some saturated salt solutions in the temperature range 0 to 50 °C. J. Res. NBS **53,** 19 (1954) RP2512.

[11] H. A. Berman, Preparation of a carbonate-free complex calcium aluminate, J. Res. NBS, **69A** (Phys. and Chem.) No. 1, 45 (1965).

[12] R. H. Stokes and R. A. Robinson, Standard solutions for humidity control at 25 °C, Ind. Eng. Chem. **41,** 2013 (1949).

[13] Federal Test Method Standard 158a, Method 1101.1 (revised Sept. 23, 1960), General Services Administration Business Service Center, Washington, D.C. 20407.

[14] L. S. Wells and K. Taylor, Hydration of magnesia in dolomitic hydrated limes and putties. J. Res. NBS, **19,** 215 (1937), RP1022.

[15] J. Topping, Errors of observation and their treatment, The Institute of Physics, London, 1955, p. 20.

(Paper 69A5–362)

JOURNAL OF RESEARCH of the National Bureau of Standards—A. Physics and Chemistry
Vol. 69A, No. 5, September-October 1965

Vapor Pressure and Heat of Sublimation of Tungsten [1]

R. Szwarc,[2] E. R. Plante, and J. J. Diamond

(May 28, 1965)

The vapor pressure of tungsten was measured by the Langmuir method in the temperature range 2574 to 3183 °K using a vaccum microbalance. The least-squares line through the data, $\log P(\text{atm}) = 7.790 - 44680/T$, yields a second law $\Delta H_s^\circ(2850\ ^\circ\text{K}) = 204.4 \pm 2.7$ kcal/mol and $\Delta S_s^\circ(2850\ ^\circ\text{K}) = 35.64 \pm 0.97$ cal/mol deg. Our recommended equation for the vapor pressure is $\log P(\text{atm}) = 7.933 - 45087/T$ based on our experimentally determined mean third law $\Delta H_s^\circ(298\ ^\circ\text{K}) = 203.5$ kcal/mol and tabulated values for the entropies and enthalpies.

1. Introduction

This paper is the fourth in a series covering the vapor pressures of refractory metals. Three previous papers [1, 2, 3] [3] gave the vapor pressures and heats of sublimation of Pd, Pt, Ir, Rh, Ru, and Os.

The value of the heat of sublimation of tungsten listed in several reference works [4, 5] is based on the original data of Langmuir [6] which was revised in a later publication by Jones, Langmuir and Mackay [7]. Some reference works [5, 8] have also given weight to the data of Zwikker [9, 10] as reported by Jones, Langmuir, and Mackay [7]. We wish to make it clear here that references [9, 10] contain only smoothed data, and that reference [7] appears to be the only published source of Zwikker's original data.

Although the data from these two studies yield average third law heats of sublimation which are in excellent agreement, little attention has been paid to the ambiguous nature of the temperature scale [4] used by Jones et al. [7], or to the relatively large difference between the second and third law heats of sublimation obtained from the measurements of Zwikker.

The studies of both Langmuir and Zwikker were carried out using the hot wire modification of the Langmuir method. While this method is capable of yielding excellent precision, major disadvantages are encountered in determining temperatures because an emissivity correction must be used and the method of heating can lead to important thermal gradients in the wire.

2. Experimental Method

The rate of sublimation of tungsten as a function of temperature was determined using a sample of polycrystalline rod fabricated by arc erosion into a right circular cylinder about 1.5 cm long and 0.25 cm in diameter. A hole 0.1 cm in diameter and 1.0 cm long assumed to represent blackbody conditions was drilled along the cylinder axis and a suspension hole 0.025 cm in diameter was drilled along a diameter near the other end of the sample.

According to the supplier, the tungsten was 99.9 percent pure. The results of semiquantitative spectrochemical analyses performed at NBS on the material as supplied and on the sample itself after the sublimation experiments were concluded are given in table 1. The results indicate a maximum metallic impurity content of about 0.02 percent before use, and no appreciable purification or contamination due to the vapor pressure measurements. The density determined by weighing a specimen of known volume was 19.2 g cm^{-3}, close to the reported x-ray density of 19.265 g cm^{-3} at 25 °C [11].

TABLE 1. *Spectrographic analysis of tungsten*

Impurity element	% Before use	% After use
Ag	—	—?
Al	—	—
As	—?	—
B	—	FT
Ba	—	—?
Bi	—	—?
Ca	T	FT
Cu	FT	—?
Fe	T	T
Mg	FT	T
Mo	VW	—
Pb	—	T
Si	VW	VW
Sn	—	—

VW, 0.001—0.01%; T, 0.0001—0.001%; FT, <0.0001%; —, not detected; —?, questionable detection.

Some data were also obtained with an oriented single crystal specimen having an approximately square cross section of about 0.38 cm per edge, a length of 1.9 cm, and blackbody and suspension holes like those in the cylindrical polycrystalline specimen.

It was intended that the faces of this sample be parallel to the (100) crystal planes. Examination of the specimen by an x-ray back reflection technique showed that one of the short and the long sample axes were related to two crystallographic axes by a rotation of approximately 12 deg about the third

[1] This work was supported in part by the National Aeronautics and Space Administration.
[2] Present Address: Department of Materials Science, University of Cincinnati, Cincinnati, Ohio.
[3] Figures in brackets indicate the literature references at the end of this paper.
[4] All temperatures in this paper are based on the 1948 IPTS unless otherwise noted.

780-567—65——3

crystallographic axis, while the other short sample axis differed from the third crystallographic axis by a rotation of approximately 4 deg about one of the other crystallographic axes. A noticeable amount of surface roughening took place during the measurements on this sample. The data obtained agreed with that obtained from polycrystalline tungsten but are not reported in detail in this paper because they were considerably less precise than those obtained using the polycrystalline tungsten. We believe that this was due to a temperature gradient of about 30 °K which was measured across the faces of the sample and that the temperature gradient was a result of the sample geometry.

The measurements were made using the vacuum microbalance apparatus previously described [12]. Samples were heated directly by rf induction at 450 kHz. Vacuum in the ultrahigh vacuum range (10^{-7} to 10^{-9} torr) was maintained by a 90 liter per second ion pump. Weight losses in the microgram range were determined by measuring balance beam displacement with a cathetometer.

The sample was suspended from one arm of an equal-arm quartz beam microbalance at the end of a chain of 0.025 cm diam quartz and sapphire rods by a loop of 0.0075 cm diam tungsten wire which passed through the suspension hole in the sample and over a hook on the lowest rod. The chain of sapphire and quartz rods was connected at each end by V-shaped hooks made by heating and bending the rods.

The arm of the vacuum chamber in which the sample hung was a 16 mm O.D. quartz tube with a graded seal and Pyrex window at the bottom for temperature measurement. The window was protected from vapor deposition during the sublimation experiments by a magnetically operated shutter.

A quartz sleeve of 13 mm O.D. fitted snugly inside the 16 mm O.D. quartz tube of the vacuum system. A thin platinum coating deposited on the inner surface of this sleeve prevented static charge buildup in the vicinity of the sample from interfering with the weighing but did not heat inductively.

An NBS calibrated optical pyrometer with a magnifying objective lens was used to measure temperatures by sighting on the blackbody hole through the calibrated window and mirror. Calibration corrections for the mirror and window were determined in situ, before and after a series of experiments, by sighting the pyrometer on a band lamp located above the vacuum apparatus on a rotatable mount. With the pyrometer and band lamp in one position, readings on the band lamp filament could be made using the same optical path as was used during the vapor pressure measurements except that the source was further away. By rotating the band lamp 90 deg and raising the pyrometer, temperature readings could be made directly on the band lamp filament. The calibration correction was obtained from the difference between reciprocal absolute temperatures with and without the window and mirror in the optical path.

The precision of the temperature measurements, expressed as the standard deviation of the mean temperature of a run, was 8 °K. The uncertainty of the mean temperature 2850 °K is estimated from the precision of the temperature measurements, the uncertainty in window and mirror calibration (±6 °K) and the uncertainty in the pyrometer calibration (±7 °K), to be ±12 °K. This estimate does not include the effects of temperature gradients in the sample or the departure of the blackbody hole from blackbody conditions which were not evaluated with sufficient precision to warrant their inclusion.

The overall uncertainty of the mean third law heat of sublimation is estimated to be 0.8 kcal mol^{-1} based on the uncertainty of ±12 °K in the mean temperature and a value of 70 cal mol^{-1} $°K^{-1}$ for $\Delta H_s^\circ(298)/T$.

In obtaining each datum point the following sequence of operations was performed: (1) The rest point of the microbalance was determined, (2) the sample was slowly heated to a temperature several hundred degrees below the temperature of the experiment, (3) the sample was rapidly heated to the operating temperature and maintained as near constant as possible, (4) the sample was rapidly cooled to a temperature well below the experimental temperature, the power slowly reduced, and the oscillator then turned off, and (5) the rest point of the balance was redetermined. The slow heating and cooling portions of the cycle were necessary to avoid lateral motion of the specimen caused by the rf field while the rapid heating and cooling portions of the cycle made the measurement of the duration of the experiment more accurate. The mass change of the sample was determined from the displacement of the beam of the microbalance and the previously determined sensitivity of the balance which was about 0.5 $\mu g/\mu$.

The change in sensitivity with load was sufficiently small so that the weight change of the sample during a series of experiments had a negligible effect. In general, duplicate rest points agreed to within ±2 μ (±1 μg) so that the corresponding uncertainty in the weight loss would be approximately ±1.4 μg.

3. Data and Thermodynamic Treatment

The experimental results obtained using polycrystalline tungsten are summarized in table 2. The vapor pressure was calculated using the equation; [5]

$$P = \frac{m}{\alpha a t}\left(\frac{2\pi RT}{M}\right)^{1/2} \quad (1)$$

where m is the mass of material sublimed, t is the duration of the experiment, a is the projected surface

[5] Values of constants used in the calculations were: R=1.98717 cal mol^{-1} deg^{-1}, or 8.3143 abs. J $deg^{-1}mol^{-1}$; atomic weight of tungsten=183.85; one standard atmosphere=1,013,250 dyn cm^{-2}.

area of the sample, T is the absolute temperature, R is the gas constant, M is the atomic weight of tungsten, and α is the vaporization coefficient, which was assumed equal to unity. The value of the sample area a, at temperature T was calculated from the area measured at room temperature a_0 by assuming that the equation $a=a_0\,[1+2\beta(T-300)]$ was valid in the temperature range where vapor pressure measurements were carried out. In this equation, β is the coefficient of linear thermal expansion. Literature values [13] for this coefficient show an appreciable spread for the temperature range of interest here. The value, $\beta=6\times10^{-6}$ °K^{-1} was used for the present work.

TABLE 2. *Vapor pressures and heats of sublimation of tungsten* [a] *(present study)*

Temperature	Duration of run	Weight loss [b]	Vapor pressure	$\Delta H_S^\circ(298)$
°K	min	μg	atm x 10^9	kcal mol^{-1}
2786	5.0	25.4	5.42	203.7
2773	5.0	24.5	5.21	202.9
2679	20.0	24.1	1.26	203.5
2574	28.0	6.8	0.250	203.7
2925	5.0	141	30.8	203.9
3034	4.9	434	98.3	204.6
2614	45.0	23.2	0.534	203.0
3068	5.0	881	197	202.7
2934	5.0	183	40.0	203.0
3183	4.0	1910	542	204.0
Mean $\Delta H_S^\circ(298)$ and standard error				203.5±0.2 kcal mol^{-1}
Estimated overall uncertainty				0.8 kcal mol^{-1}

[a] Listed in experimental sequence.
[b] Sample surface area at room temperature=1.332 cm^2.

In general, the heat of sublimation can be computed from vapor pressure data in two ways. In the second law method, one can make use of the experimental data to evaluate both constants in the equation

$$\log P\,(\text{atm})=-\frac{\Delta H^\circ}{R'T}+\frac{\Delta S^\circ}{R'}. \qquad (2)$$

It should be noted that this equation is only approximate since it ignores the temperature dependence of ΔH° and ΔS°. Although a more exact second law treatment can be made by inclusion of the temperature dependence of ΔH° and ΔS°, any error introduced into the second law heat and entropy of sublimation by use of eq (2) in the present case is small in comparison with the error in these quantities resulting from scatter in the vapor pressure data.

In eq (2), ΔH° is the heat of sublimation at an average temperature, ΔS° is the entropy change at the same temperature and R' is equal to $R\ln10$. In the third law method, one makes use of absolute entropies, usually obtained from heat content and spectroscopic data, to calculate the entropy change for the assumed sublimation process at each temperature. These values and the experimental pressures can then be substituted in eq (2) to obtain the experimental values of ΔH° at the specified temperatures. In practice, use is generally made of free energy functions which allow one to calculate a value for the heat of sublimation at a reference temperature, usually 298.15 °K (or 0 °K) according to the equation,

$$\Delta H_S^\circ(298)=T\left[\left(\frac{G_T^\circ-H_{298}^\circ}{T}\right)_c-\left(\frac{G_T^\circ-H_{298}^\circ}{T}\right)_g-R\ln P(\text{atm})\right] \qquad (3)$$

where $\left(\frac{G_T^\circ-H_{298}^\circ}{T}\right)$ is the free energy function. Differences between $\Delta H_S^\circ(298)$ obtained by the second law and the third law methods can give information concerning the consistency of the vapor pressure data obtained, the free energy function data used, the sublimation reaction assumed or the existence of a vaporization coefficient other than unity. Frequently, a lack of trend in the heat of sublimation calculated as a function of the experimental temperature is taken as an indication that no important systematic errors are present in the data. Actually, this method is quite insensitive to systematic error and it is easier to find a discrepancy by comparing second and third law heats of sublimation or the experimental entropy change with that found from heat content and spectroscopic data.

In the present experiments, a mean third law heat of sublimation at 298 °K of 203.5 ±0.2 kcal/mol was obtained [6] using the free energy function data listed in the JANAF Thermochemical Tables [4], while a second law treatment of the data yielded ΔH_S° (2850 °K)=204.4 ±2.7 kcal/mol. The latter was corrected to 298 °K using the JANAF enthalpy functions and the value $\Delta H_S^\circ(298)$=201.6 ±2.7 kcal/mol obtained.

The equation $\log P(\text{atm})=7.790-44680/T$ (2574 to 3183 °K) is the least-squares line through the data obtained in this study. We believe the vapor pressure of tungsten is best represented by the equation $\log P(\text{atm})=7.933-45087/T$ (2574 to 3183 °K), obtained using our experimentally determined mean third law heat of sublimation at 298° of 203.5 kcal/mol, a mean temperature of 2850 °K and the entropy and enthalpy data given by JANAF.

4. Results from Earlier Work

In comparing the values for the heat of sublimation of tungsten listed in several compilations it became apparent that differences in the values were not entirely due to differences in the free energy functions used in these computations. Hence, in view of the date of the original work, it was felt worthwhile to check the conversion of the temperatures reported in the original articles to the 1948 International Practical Temperature Scale. Surprisingly enough, some of the compilations checked had not made any corrections to the temperatures at all.

The corrections to the temperature scale used by Zwikker are easily made. His scale was based on a

[6] Results are given in the form $a\pm b$ where a denotes the arithmetic mean or least squares adjusted value and b is the standard error of a computed from the scatter of the individual determinations about the mean or fitted line.

gold point of 1063 °C and a second radiation constant value of C_2=1.433 cm deg. It should be noted that this differs slightly from the 1927 ITS in the value of C_2 chosen. The original temperatures reported for Zwikker's data, converted to the 1948 IPTS using the methods outlined by Corruccini [14], are given in table 3.

The method of converting Langmuir's reported temperatures [6, 7] to the 1948 IPTS are not so straightforward. Most of the difficulty stems from the fact that the descriptions of the two scales given by Jones et al. [7, 15], are somewhat sketchy and that the equations given for converting from the original scale to the later scale do not give the results reported. The situation with regard to the original and later scales can be summarized as follows.

The original temperature scale was based on the equation,

$$\log C_w = -\frac{11230}{T} + 7.029 \qquad (5)$$

where C_w is the luminance in candelas per cm^2 radiated from a tungsten sample. This equation was based on a temperature scale described by Nernst [16]. The revised data published in 1927 [7] were said to be based on the equation

$$\log C_w = -\frac{10957}{T} + 6.797 \qquad (6)$$

which was claimed to represent the candlepower-temperature relationship derived from the work of Forsythe and Worthing [17]. However, eq (6) actually represents the candlepower data reported by Zwikker [9, 10] multiplied by 0.917, and leads to temperatures varying nonsystematically from 11 to 28 deg below those reported by Jones et al. [7].

We made a least squares treatment of Forsythe and Worthing's candlepower data to obtain an equation similar to (6). This was used with eq (5) to obtain temperatures which should correspond to those reported by Jones et al. The temperatures obtained in this way differed nonsystematically from zero to 6 deg below those reported. We believe that this indicates that the revised temperatures published by Jones et al. are based on the same temperature scale as was used by Forsythe and Worthing which is the same as the scale used by Zwikker. In view of the relatively small differences between the values reported by Jones et al., and those calculated by us, we have accepted their values and converted these to the 1948 IPTS using the method described by Corruccini [14].

Tables 3 and 4 list the vapor pressures of tungsten calculated from the rate of vaporization data obtained by Langmuir and by Zwikker [7], the temperatures as reported in the 1927 work [7], the temperatures based on the 1948 IPTS and third law heats of sublimation obtained using JANAF [4] free energy functions.

TABLE 3. *Vapor pressures and heats of sublimation of tungsten (Zwikker)*

T [a] (Rept.) [7]	T (1948 IPTS)	Rate of sublimation [7]	Vapor pressure	ΔH_s° (298)
°K	°K	$g\ cm^{-2}\ sec^{-1}\times10^9$	$atm\times10^9$	*kcal mol* $^{-1}$
2389	2383	0.000115	0.00934	203.9
2510	2503	.00099	.0824	203.5
2614	2606	.00525	.446	203.3
2637	2628	.00621	.530	204.1
2657	2648	.00969	.829	203.3
2759	2749	.0427	3.72	203.0
2887	2876	.293	26.1	201.4
2889	2878	.275	24.5	201.9
3017	3004	1.28	117	201.5
3108	3094	3.47	321	201.4
3124	3110	3.82	354	201.9
3129	3115	4.69	435	200.9
3132	3118	4.69	436	201.1
3137	3123	4.95	460	201.1

Mean ΔH_s° (298) and standard error ..... 202.3 ±0.3 kcal mol^{-1}

[a] These temperatures are based on a scale defined by C_2=1.433 cm deg, t_{Au} = 1063 °C and Wien's law.

TABLE 4.—*Vapor pressures and heats of sublimation of tungsten (Langmuir)*

T [a] (Rept.) [7]	T (1948 IPTS)	Rate of sublimation	Vapor pressure	ΔH_s° (298)
°K	°K	$g\ cm^{-2}\ sec^{-1}\times10^9$	$atm\times10^9$	*kcal mol* $^{-1}$
2518	2511	0.0020	0.167	200.6
2610	2602	.0059	.501	202.3
2913	2901	.39	34.9	201.5
3300	3283	30.0	2860	199.6
2852	2841	0.151	13.4	202.6
2950	2938	.52	46.9	202.3
2950	2938	.59	53.2	201.6
3000	2987	1.01	91.8	201.8
3000	2987	1.14	104	201.0
3060	3047	1.73	159	202.6
3060	3047	2.33	214	200.8
3066	3053	1.84	169	202.6
3066	3053	2.45	225	200.9

Mean ΔH_s°(298) and standard error ..... 201.6 ±0.3 kcal mol^{-1}

[a] These temperatures are based on a scale defined by C_2=1.433 cm deg, t_{Au} =1063 °C and Wien's law but see discussion of this scale in text.

Table 5 lists the mean third law heats of sublimation at 298 °K, the second law heats of sublimation obtained from least squares treatment of the vapor pressure data and extrapolated to 298 °K using the enthalpy data of JANAF, and the experimental entropy changes at temperature derived from each set of measurements. Least squares analysis of our data yields a standard deviation in the pressure of approximately 10 percent. This is close to the uncertainty in the pressure that would be expected on the basis of the independently estimated precision in temperature measurement. Hence, it appears that imprecision in temperature measurement is the principal source of random error.

5. Discussion and Summary

The heat of sublimation of tungsten obtained in this work is in good agreement with values based on data obtained by Langmuir and by Zwikker. Langmuir's second law heat agrees better with our third law heat than his own, and vice versa, because our experimental entropy change is about as much below the accepted third law entropy change as his

TABLE 5. *Heats and entropies of sublimation of tungsten*

Investigator	$\Delta H_s^\circ(298)$ 2d Law	$\Delta H_s^\circ(298)$ 3d Law	ΔS_s° 2d Law
	kcal mol^{-1}	*kcal mol*$^{-1}$	*cal mol*$^{-1}$ °K^{-1}
Zwikker:			
(Low temp. points)	208.5 ±3.3 (872.4 ±13.8 kJ mol^{-1})	203.5 ±0.2 (851.4 ±0.8 kJ mol^{-1})	38.28 ±1.28 (160.2 ±5.4 J mol^{-1} °K^{-1})
(High temp. points)	206.2 ±3.4 (862.7 ±14.2 kJ mol^{-1})	201.4 ±0.1 (842.7 ±0.4 kJ mol^{-1})	37.83 ±1.13 (158.3 ±4.7 J mol^{-1} °K^{-1})
(All points)	214.1 ±1.3 (895.8 ±5.4 kJ mol^{-1})	202.3 ±0.3 (846.4 ±1.3 kJ mol^{-1})	40.44 ±0.47 (169.2 ±2.0 J mol^{-1} °K^{-1})
Langmuir	203.9 ±3.7 (853.1 ±15.5 kJ mol^{-1})	201.6 ±0.3 (843.5 ±1.3 kJ mol^{-1})	37.04 ±1.28 (155.0 ±5.4 J mol^{-1} °K^{-1})
This work	201.6 ±2.7 (843.5 ±11.3 kJ mol^{-1})	203.5 ±0.2 (851.4 ±0.8 kJ mol^{-1})	35.64 ±0.97 (149.1 ±4.1 J mol^{-1} °K^{-1})

[a] The value of the entropy of sublimation at 2850 °K based on heat content and spectroscopic data is 36.30 cal mol^{-1} °K^{-1} according to JANAF [4] and 35.99 cal mol^{-1} °K^{-1} according to Kirillin et al. [18].

is above it. Recent work [18] on the heat capacity of solid tungsten yields a value for the third law entropy of sublimation in slightly better agreement with that obtained from the present study. However, we prefer to use the JANAF [4] tabulation until the new data have been critically evaluated.

The large difference between the second and third law heats of sublimation obtained from the work of Zwikker is evidence of appreciable systematic error. Considering the way in which his third law heats vary with temperature it appears likely that his vapor pressure data were obtained in two distinct groups and that a systematic difference existed between the groups. Thus, the first six points listed in table 3 form one group which yield third law heats of sublimation larger than the mean value, while the last eight points yield third law heats of sublimation smaller than the mean value. If these groups of points are treated as independent sets, and second law heats of sublimation calculated, the six low temperature points yield a second law heat of sublimation at 298 °K of 208.5 ±3.3 kcal/mol while the eight high temperature points give 206.2 ±3.4 kcal/mol. Hence, the discrepancy between the second and third law heats of sublimation could be partially due to this cause. Similarly, the six low temperature points yield a second law entropy of sublimation of 38.28 ±1.28 cal/mol deg and the eight high temperature points give 37.83 ±1.13 cal/mol deg, compared to 40.44 ±0.47 cal/mol deg for all fourteen points and the JANAF tabulated value at 2850 °K of 36.30 cal/mol deg.

In summary, the results obtained in the present study are in good agreement with those previously obtained. The differences in the mean third law heats of sublimation obtained from this work and from the work of Langmuir correspond to differences in vapor pressures at 3000 °K of about 40 percent, or differences in the observed temperature of about 30°, while the agreement with Zwikker's data is even better.

6. References

[1] R. F. Hampson, Jr. and R. F. Walker, J. Res. NBS **65A** (Phys. and Chem.) No. 4, 289 (1961).
[2] R. F. Hampson, Jr. and R. F. Walker, J. Res. NBS **66A** (Phys. and Chem.) No. 2, 177 (1962).
[3] N. J. Carrera, R. F. Walker, and E. R. Plante, J. Res. NBS **68A** (Phys. and Chem.) No. 3, 325 (1964).
[4] JANAF Thermochemical Tables, Dow Chemical Co., Midland, Michigan, 1961. Tungsten crystal and gas tables dated December 31, 1961.
[5] R. Hultgren, R. L. Orr, P. D. Anderson and K. K. Kelley, Selected Values of Thermodynamic Properties of Metals and Alloys, (John Wiley & Sons, Inc., New York, N.Y., 1963).
[6] I. Langmuir, Phys. Rev. **2,** 329 (1913).
[7] H. A. Jones, I. Langmuir and G. M. J. Mackay, Phys. Rev. **30,** 201 (1927).
[8] An. N. Nesmeyanov, Vapour Pressure of the Elements, Translated and edited by J. I. Carasso (Academic Press, New York, N.Y., 1963).
[9] C. Zwikker, Koninkl. Akad. Wetenschap. Amsterdam, Proc. Sect. Sci. **28,** 466 (1925).
[10] C. Zwikker, Physica **5,** 249 (1925).
[11] H. E. Swanson and E. Tatge, NBS Cir. 539 **1,** 29 (1953),
[12] N. J. Carrera, R. F. Walker, W. Nalley, and C. Steggerda, Vacuum Microbalance Techniques, K. Behrndt, ed. **3,** 153 (Plenum Press, New York, N.Y., 1963).
[13] P. T. B. Shaffer, Materials Index p. 252 (Plenum Press, New York, N.Y., 1964.)
[14] R. J. Corruccini, J. Res. NBS **43,** 133 (1949) RP2014.
[15] H. A. Jones and I. Langmuir, G. E. Review **30,** 310 (1927).
[16] W. Nernst, Physik. Zeit. **7,** 380 (1906).
[17] W. E. Forsythe and A. G. Worthing, Astrophysical Journal **61,** 146 (1925).
[18] V. A. Kirillin, A. E. Sheindlin, V. Ya. Chekhovskoi and V. A. Petrov, Zhur. Fiz. Khim. **37,** 2249 (1963).

(Paper 69A5-363)

JOURNAL OF RESEARCH of the National Bureau of Standards—A. Physics and Chemistry
Vol. 69A, No. 5, September–October 1965

Heat Capacity and Enthalpy Measurements on Aluminum Carbide (Al_4C_3) From 15 to 1173 °K. Thermodynamic Properties From 0 to 2000 °K*

George T. Furukawa, Thomas B. Douglas, William G. Saba, and Andrew C. Victor

(May 18, 1965)

Measurements of the heat capacity and relative enthalpy were made on aluminum carbide (Al_4C_3) from 15 to 1173 °K. The thermodynamic properties were calculated up to 2000 °K from the data by judicious extrapolation above 1173 °K. In conjunction with the heat-of-formation data on Al_4C_3 obtained by King and Armstrong and by Mah, second- and third-law analyses have been made of the thermodynamics of several high-temperature vapor-equilibrium reactions involving Al_4C_3.

1. Introduction

The results of heat-capacity and enthalpy measurements on aluminum carbide, Al_4C_3, in the range 15 to 1173 °K presented in this paper have been obtained in connection with a research program at the National Bureau of Standards to provide accurate thermodynamic and related data on the "light" elements and their compounds. No heat-capacity measurements on Al_4C_3 have been previously published, except for the relative enthalpy measurements in the range 273 to 693 °K by Satoh [1][1] on a sample that contained only 74.74 percent Al_4C_3, the impurities being 23.43 and 1.83 percent Al_2O_3 and SiO_2, respectively. The work reported by Satoh is based on measurements at only three temperatures in the above temperature range.

Aluminum carbide, Al_4C_3, is a yellow rhombohedral crystal of space group D^5_{3d} with $a=8.53$ Å and $\alpha=22°28'$ [2]. Each carbon atom is surrounded by aluminum atoms and the shortest C—C distance is 3.16 Å [2], indicating that the carbon atoms are not bonded to one another. There are two structurally different carbon atoms, and the C—Al distance ranges from 1.90 to 2.22 Å. One of the carbon structures has six aluminum atoms at 2.17 Å, and the other has one aluminum atom at 1.90 Å, three at 1.94 Å, and one at 2.22 Å. On hydrolysis, Al_4C_3 yields methane. Other aluminum carbides that have been reported are $Al_2(C_2)_3$ [3] and Al_3C [4]. The carbide $Al_2(C_2)_3$, made by reacting acetylene with aluminum at 450 to 500 °C, yields acetylene on hydrolysis [3]. The carbide Al_3C, observed in the $Al—Al_2O_3—Al_4C_3$ phase investigations reported by Baur and Brunner [4], should yield CH_4 on hydrolysis.

2. Sample

The measurements of the low-temperature heat capacity and the high-temperature relative enthalpy were made on the same aluminum carbide sample kindly supplied by the Aluminum Company of America, ALCOA Research Laboratories, through the courtesy of George Long. The material had been prepared by heating a stoichiometric mixture of aluminum powder and lampblack in an atmosphere of argon to 1800 °C. Qualitative spectrochemical analyses were made on representative specimens of the sample by the Spectrochemistry Section of the National Bureau of Standards. The results are summarized in table 1.

TABLE 1. *Spectrochemical analysis of the sample of aluminum carbide* (Al_4C_3)

Element	%	Element	%	Element	%
Ag	—(?)	Hf	—	Sb	—
Al	>10	Hg	—	Sc	—
As	—	In	—	Si	0.01 –0.1
Au	—	Ir	—	Sn	—
B	—	La	—	Sr	—
Ba	—	Mg	0.001 –0.01	Ta	—
Be	—	Mn	0.0001–0.001	Te	—
Bi	—	Mo	—	Th	—
Ca	0.0001–0.001	Nb	—	Ti	0.001–0.01
Cd	—	Ni	0.001 –0.01	Tl	—
Ce	—	Os	—	U	—
Co	—	P	—	V	0.01 –0.1
Cr	0.001 –0.01(?)	Pb	—	W	—
Cu	0.001 –0.01	Pd	—	Y	—
Fe	0.1 –1.0	Pt	—	Zn	—
Ga	—	Rh	—	Zr	0.001–0.01
Ge	—	Ru	—		

—: Not detected.

Chemical analyses were performed by Rolf A. Paulson of the Applied Analytical Research Section of the National Bureau of Standards. These results are given in table 2. Specimens 1 and 2 were sampled from the original Al_4C_3 preparation

*This work was sponsored by the Advanced Research Projects Agency, Department of Defense, under ARPA Order No. 20.

[1] Figures in brackets indicate the literature references at the end of this paper.

as received. Specimen 3 was sampled from that portion of the Al_4C_3 preparation on which the low-temperature heat-capacity measurements had been completed. The percentage Al_4C_3 was determined by dissolving a sample in hot sulfuric acid. The evolved gases, taken to be CH_4 and H_2, were burned and the combustion products collected. The amount of CO_2 collected was converted to Al_4C_3 and the excess H_2O over that attributable to CH_4 was reckoned to have been formed from H_2 released from the acid by free aluminum and iron. The insoluble residue from the hot sulfuric acid treatment was taken to be free carbon. Aliquot portions of the sulfuric acid solution were analyzed for total aluminum as Al_2O_3 by precipitating $Al(OH)_3$ with ammonium hydroxide and igniting to Al_2O_3. The excess of aluminum over that attributable to Al_4C_3, free aluminum metal, and AlN was assumed to be Al_2O_3 in the original sample. The iron, determined in specimen 3 only, was analyzed colorimetrically using the thiocyanate-complex method on an aliquot portion of the sulfuric acid solution. The percentage AlN was determined by the Kjeldahl method on separate samples of the Al_4C_3 preparation.

TABLE 2. *Chemical analysis of the sample of aluminum carbide* (Al_4C_3)

Component	Percentage by weight		
	Specimen 1	Specimen 2	Specimen 3
Al_4C_3	94.9	94.8	94.8
Free Al	1.2	1.3	1.0
Free C	0.9	0.7	1.0
AlN	1.4	1.3	1.3
Al_2O_3	2.0	2.0	2.2
Free Fe			0.06
Total	100.4	100.1	100.36

The results of the chemical analysis agree with the usual composition found (of about 95% Al_4C_3) in samples prepared by the same method [5]. The small discrepancies in the analyses can be attributed to either uncertainties in the analytical methods or small inhomogeneities in the sample. The approximate summation of the analyses to 100 percent is an indication of the reliability of the analytical methods used. E. E. Hughes of the Applied Analytical Research Section, National Bureau of Standards, analyzed the gases generated by the action of an acid on the Al_4C_3 sample and found no acetylene or methylacetylene, indicating that $Al_2(C_2)_3$ was not present in the Al_4C_3 preparation. No effort was made to determine whether Al_3C was present.

M. v. Stackelberg et al. [6, 7] reported the conditions for formation and the crystal structure of the compound Al_5C_3N (Al_4C_3·AlN). The results of the heat-capacity measurements presented in this paper were processed assuming that the nitrogen found in the chemical analysis came from AlN mixed with Al_4C_3.

For the analysis of high-temperature relative-enthalpy measurements the average of the chemical analyses obtained in specimens 1 and 2 was normalized to yield 100 percent total analysis. The iron content, the chemical analysis for which was not made in specimens 1 and 2, was considered too small to contribute significantly to the results of the experimental data. In the processing of the heat-capacity data obtained at low temperatures, the chemical analysis obtained on specimen 3 was used, after normalizing to give a total analysis of 100 percent.

The corrections for the impurities were made assuming that the relative enthalpies were additive. The contributions from Al, Al_2O_3, and AlN impurities were adjusted in accordance with the tabular values of thermodynamic functions obtained through the analysis of the literature data in connection with the light element research program [8]. The values for C were based mostly on the measurements of De Sorbo and Tyler [9]. The corrections for Fe were obtained primarily from the heat-capacity data reported by Simon and Swain [10] and by Kelley [11].

3. Low-Temperature Calorimetry

3.1. Apparatus and Method

The low-temperature heat-capacity measurements were made from about 18 to 380 °K in an adiabatic calorimeter similar in design to that described previously [12]. The calorimeter vessel, which was filled with sample as described in section 3.2 and sealed by means of a specially designed gold-gasket closure [13], was suspended within the adiabatic shield system by means of a Nylon string instead of the filling tube shown in the above reference. The adiabatic shield was controlled automatically by means of a combination of electronic and electromechanical equipment. Details of the design of the calorimeter used, its operation, and the automatic adiabatic control system will be described in a later publication.

The platinum resistance thermometer used in the measurements was calibrated in accordance with the International Practical Temperature Scale of 1948 [14]. The temperatures in degrees Kelvin (°K) were obtained by adding 273.15 deg to the temperatures in degrees Celsius (°C). Below 90 °K, the thermometer was calibrated on the NBS–1955 provisional scale which is numerically 0.01 deg lower than the former NBS–1939 provisional scale [15]. The resistance measurements were made by means of a Mueller bridge and a high sensitivity galvanometer to the nearest 0.00001 Ω. The temperatures were calculated from the resistance by inverse interpolation in a table of resistance given as a function of the temperature at closely spaced regular intervals.

The electrical power introduced into the calorimeter heater (100 Ω of constantan wire) was measured by means of a Wenner potentiometer in conjunction with a volt box, standard resistor, and saturated standard cells. A constant-current power supply stable to 10 ppm or better was used to facilitate the power measurements. The duration of each heating

interval was measured by means of a high precision interval timer operated on 60-cycle frequency standard provided at the National Bureau of Standards. The 60-cycle frequency standard is based on a 100 kHz quartz oscillator which is stable to 0.5 ppm. The estimated uncertainty in the readings of the interval timer was not greater than ± 0.01 sec for any heating period, none of which was less than 2 min in these experiments.

3.2. Results

A sample of 153.8063 g mass was poured into the calorimeter vessel in a controlled-atmosphere box filled with argon gas (dew-point of −50 °C). At the same time, samples of the Al_4C_3 were sealed in test tubes under dry argon gas for chemical analysis. The calorimeter vessel plus the sample was evacuated and purged with dry helium gas several times. Finally, helium gas at a pressure of 5.8 cm Hg was sealed in the container with the sample. After completion of the measurements the calorimeter vessel was opened in the controlled-atmosphere box and additional samples taken for chemical analysis. As mentioned earlier, the analysis of the low-temperature heat data was based on the chemical analysis of the sample on which the measurements had been made (chemical analysis of specimen 3).

On the calorimeter vessel plus the sample ("gross"), 14 runs totaling 108 heat-capacity determinations were made and on the empty vessel ("tare"), 11 runs totaling 87 determinations were made. The experimental data of each of these two sets of measurements were fitted to empirical equations over selected, partially overlapping temperature intervals by the method of least squares using a digital computer. (A "set" of measurements consists of the observations of energy increments and the corresponding temperatures from about 18 to 380 °K on the empty vessel or on the vessel with sample. Measurements made during a given condition are classified as a "run" within the "set".) The empirical equations consisted of polynomials, the positive powers of temperature up to 4 being used below the inflection point in the heat capacity and powers from −4 to +4 in the region of the inflection point and above. Details of the computer routines used will be described in a later publication. Briefly, the overlapping equations for each set were joined at temperatures of the most favorable combinations of values of heat capacity and its first and second derivatives. The values of heat capacity obtained at regularly spaced integral temperatures by this process were smoothed by a 9-point cubic smoothing code [16] on the computer. (For the two sets of heat data obtained between 18 and 380 °K, a smooth function is defined and restricted to the following properties: (a) continuous derivatives, (b) monotonic increasing with not more than two inflection points, and (c) sigmoidal configuration of the heat-capacity curve.) The deviations of the observations of each set of measurements from the final smoothed values are shown in figures 1 and 2.

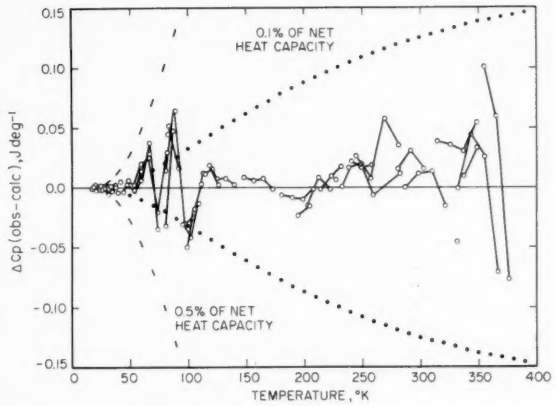

FIGURE 1. *Deviations of the heat-capacity measurements on sample plus calorimeter vessel.*

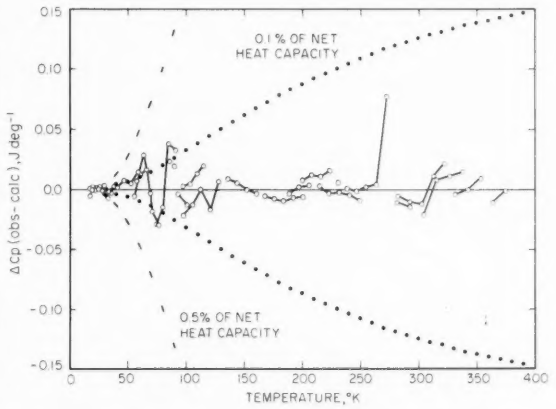

FIGURE 2. *Deviations of the heat-capacity measurements on the empty calorimeter vessel.*

The net values of heat capacity, obtained by differencing the above smoothed gross and tare values at corresponding temperatures, were corrected for the impurities and the helium exchange gas and again smoothed on the computer wherever necessary. These values were then converted to molal units using atomic weights based on carbon-12 [17]. A Debye heat-capacity function, fitted to the smoothed values at the lower temperatures, was used to obtain the values from 0 to 18 °K.

A consideration was given at this point regarding the use of a table of thermodynamic functions. Although the joule is a more fundamental unit of energy and its use is preferred, most scientists who use tables of thermodynamic functions are accustomed to the calorie as an energy unit. The values of heat capacity were converted, therefore, to the unit cal deg^{-1} mol^{-1} using the relation: 1 defined calorie=4.1840 J. These values of heat capacity from 0 to 390 °K were later combined with the high-

temperature heat data (see sec. 5) and the thermodynamic functions from 0 to 1200 °K (table 5) obtained in terms of the defined calorie. The hope is that eventually the joule would be the common energy unit in all scientific work. The thermodynamic functions of table 5 are, therefore, repeated in the appendix in terms of the joule.

TABLE 3. *Observed heat capacity of aluminum carbide* (Al_4C_3)

Gram molecular weight = 143.9594 g, T deg K = t deg C + 273.15

T	C_P	T	C_P
RUN 1		RUN 7	
°K	J deg^{-1} mol^{-1}	°K	J deg^{-1} mol^{-1}
80.9304	19.039	47.9512	4.334
87.5349	22.750	53.8036	6.274
95.5198	27.145	60.2681	8.859
102.6529	31.166	67.1238	11.979
109.1860	34.903	74.4382	15.603
115.2630	38.389	82.5811	20.002
120.9611	41.644		
126.3603	44.702	RUN 8	
RUN 2		53.6690	6.221
		59.9095	8.700
83.3668	20.442	67.0407	11.949
83.7841	20.682	73.8189	15.264
92.0007	25.212	80.9261	19.085
99.2987	29.260	88.8040	23.473
105.9164	33.041	96.7037	27.812
112.1039	36.581	104.9602	32.491
118.3925	40.182	113.3395	37.293
125.2915	44.100		
132.5943	48.216	RUN 9	
140.0859	52.360		
148.2666	56.796	202.6976	83.252
156.8223	61.313	212.7334	87.532
165.0743	65.555	222.8071	91.600
173.0867	69.543	233.1927	95.614
181.1510	73.440	244.9902	99.979
189.9219	77.545	257.7564	104.411
199.0012	81.640	270.1210	108.507
		282.1421	112.178
RUN 3		RUN 10	
208.2596	85.650		
194.8391	79.768	228.2582	93.736
204.7784	84.152	238.8640	97.746
214.3612	88.195	249.4063	101.545
223.6167	91.931	260.0404	105.168
232.5986	95.409	282.9258	112.385
241.3449	98.662		
250.2226	101.831	RUN 11	
259.2433	104.929		
RUN 4		287.5948	113.747
		299.1951	117.040
19.4395	0.154	310.6701	120.112
21.2826	0.214	322.1925	122.999
23.1934	0.298		
26.1223	0.468	RUN 12	
28.9497	0.690		
31.8285	0.978	280.8853	111.785
34.7029	1.356	291.7646	114.978
37.9361	1.897	303.4013	118.188
		314.9180	121.232
RUN 5		326.3407	124.053
		337.6879	126.647
18.3556	0.125	348.8494	129.087
20.5917	0.194		
22.9086	0.286	RUN 13	
25.3911	0.425		
28.2211	0.628	332.8417	125.529
31.0744	0.900	344.3231	128.107
34.2214	1.292	355.7442	130.520
38.0580	1.925	367.1535	132.793
42.2987	2.823		
RUN 6		RUN 14	
32.2736	1.037		
35.9656	1.554	332.3944	125.383
39.9007	2.283	338.2360	126.747
44.3825	3.329	349.3925	129.181
48.7699	4.578	354.7007	130.379
53.7296	6.250	365.6101	132.607
60.1927	8.834	376.3752	134.648
67.1891	12.007		

Heat-capacity determinations usually require two series of measurements, one on the sample plus the calorimeter vessel and the other on the empty vessel. By conducting the two series of measurements under as identical conditions as possible, certain errors that occur equally in both measurements may be canceled in the final processing of the data. The data from both series of measurements are most useful in certain applications, such as in the numerical evaluation of the precision and accuracy of the original observations, in the correlation of the temperature scale, etc. These data are, however, not directly useful where the heat capacity of the substance is needed for the comparison of the precision and accuracy of measurements with other laboratories. The method used in processing the experimental data as outlined above yields the final smoothed values of heat capacity and the relation of these values with the original observations is linked through a somewhat tortuous path.

To meet the requirements for evaluating the precision of the observation and for comparing the results with other laboratories a "compromised" list of experimental data is given in table 3. The values of "observed molal heat capacity" *given in the units of J deg^{-1} mol^{-1}* in table 3 were obtained by subtracting the *smoothed* tare heat capacity from the gross heat capacity at the observed temperatures (midtemperatures of the enthalpy increments). The tare heat capacities at the corresponding temperatures were obtained by interpolation in the table of smoothed tare heat capacities mentioned earlier. Corrections have been made for the impurities and for the helium gas. Curvature corrections were made wherever significant. These observed molal heat capacities are plotted in figure 3.

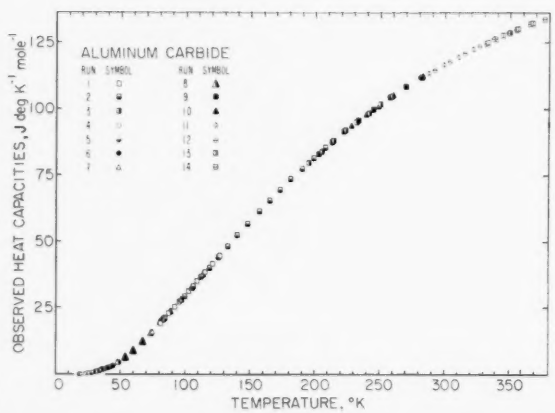

FIGURE 3. *Observed values of the molal heat capacity of aluminum carbide.*

4. High-Temperature Relative Enthalpy Measurements

4.1. Method and Apparatus

The relative enthalpy measurements were made from 273 to 1173 °K (0 to 900 °C) by the "drop" method using a Bunsen ice calorimeter. Details of the method have been described previously [18]. Briefly, the method involved suspending the samples sealed in a container (for the present measurements the container consisted mostly of the alloy Ni(80%)-—Cr(20%)) in a furnace. When a constant, known temperature is attained, the container and its contents are dropped, with nearly free fall, into a Bunsen ice calorimeter in which is determined the heat evolved by the container plus sample in cooling to 273.15 °K. In order to account for the enthalpy of the container and the heat lost during the drop, a similar experiment is made with the empty container at the same furnace temperature. The difference between the two values of heat evolved in the ice calorimeter is a measure of the enthalpy change of the sample between 273.15 °K and the temperature in the furnace.

In the furnace used the sample is surrounded by a silver pipe 25 cm long and of 1.3 cm wall thickness, in order to minimize the temperature gradients around the sample and thus improve the accuracy of measuring its temperatures. Customarily, the temperature of this furnace (and hence that of the sample) is measured by a calibrated platinum resistance thermometer (precision, ±0.002 deg) from 0 to 600 °C and by a calibrated Pt—Pt–10 percent Rh thermocouple (precision, ±0.01 deg) at all temperatures. The routine simultaneous measurement by both instruments at and below 600 °C ensures that the thermocouple readings are consistent with the thermometer readings, which are more accurate. Unfortunately, shortly before the measurements on Al_4C_3 were begun, the thermometer suffered an accident and it was consequently necessary to use the thermocouple alone at all the temperatures.

Just before the measurements of the relative enthalpy of Al_4C_3, similar measurements were carried out on a sample of Calorimetry-Conference standard sample of α-Al_2O_3 in a silver container (six at 400, two at 600, and two at 700 °C), in order to check the overall accuracy. Compared with the smoothed values published earlier by the Bureau and recently slightly corrected [19], the mean enthalpies of the Al_2O_3 found at these three temperatures were respectively +0.02 ±0.06, −0.01 ±0.01, and −0.02 ±0.01 percent higher. (The stated tolerances represent the standard deviations of the means.)

4.2. Results

All the high-temperature heat measurements were made on the same sample of aluminum carbide. The same identical container was used both with and without the sample, in order to preclude possible small differences in the relative enthalpy per unit mass of different specimens of the container alloy. The results of the enthalpy measurements are summarized in table 4. The second and third columns give, in chronological order for each furnace temperature, the heats found in individual measurements on the container with sample and on the empty container, respectively. The values given have been corrected for small unavoidable differences in mass of the various parts of the container, and for the contribution of the impurities to the heats measured. The largest part of the latter correction above 873.15 °K, about −8 cal for the sample measured, was for the heat of fusion of the free aluminum present, and largely eliminated a small hump in a plot against temperature of the uncorrected net enthalpy of the sample near the melting point of this element, 932 °K.

TABLE 4. *High-temperature enthalpy measurements on aluminum carbide* (Al_4C_3)

Furnace temperature	Individual heat measurements [a]		$H_T-H_{273.15}$ of Al_4C_3 [b]	
	Sample + container	Container only	Mean observed	Obs.-calcd., eq (1) [c]
°K	cal	cal	cal mol^{-1}	cal mol^{-1}
373.2	285.0	149.6	2939 [d]	−8
	286.3	150.4		
	287.3	150.6		
	------	151.1		
473.2	600.4	(306.8) [e]	6305	−27
	602.4	310.1		
	601.8	309.8		
	------	311.1		
	------	310.2		
573.2	936.9	475.2	9994	+6
	936.7	475.5		
	938.2	------		
	936.8	------		
	936.7	------		
	936.7	------		
673.2	1289.7	648.0	13877	+49
	1288.9	647.9		
	1288.3	------		
773.2	1648.0	826.8	17794	−8
	1648.6	825.9		
873.2	2021.1	1009.6	21883	+4
	2020.1	1009.9		
973.2	2405.4	1205.9	25980	−56
	2406.0	1205.3		
1073.2	2808.8	1409.1	30289	+29
	2807.7 [f]	1409.1		
	3213.1 [f]	1615.6		
1173.2	3210.4 [f]	1617.4	34543	+5
	------	1614.5		
	------	1616.9		

[a] With all corrections applied, including those for the impurities in the sample. Sample mass = 6.650 g.

[b] Molecular weight of Al_4C_3 = 143.959.

[c] The final values of $(H_T-H_{273.15})$ (table 5) are smaller than those calculated from eq (1) by 11.5 cal mol^{-1} at 373.15 °K and by 10 cal mol^{-1} at each of the other temperatures in table 4.

[d] The value found from the measurements with the adiabatic calorimeter is 2933.0 cal mol^{-1}.

[e] Omitted from the mean because of inferior precision.

[f] In these measurements 0.003 g of the sample had been removed, but these values have been corrected to a basis of the 6.650 g of sample present in the other measurements in this column.

Obviously no individual measurement in the third column of table 4 is uniquely associated with one in the second column. For each furnace temperature the difference between the averages for the two columns gives the mean observed net relative enthalpy of aluminum carbide shown on a mole basis in the fourth column. Using the method of least squares, these values (equally weighted) were used

TABLE 5. *Thermodynamic functions for aluminum carbide* (Al_4C_3) *solid phase*

Gram molecular weight = 143.9594 g, T deg K = t deg C + 273.15

T	C_P°	$(H_T^\circ - H_0^C)$	$(H_T^\circ - H_0^C)/T$	S_T°	$-(G_T^\circ - H_0^C)$	$-(G_T^\circ - H_0^C)/T$
°K	*Cal deg*$^{-1}$ *mol*$^{-1}$	*Cal mol*$^{-1}$	*Cal deg*$^{-1}$ *mol*$^{-1}$	*Cal deg*$^{-1}$ *mol*$^{-1}$	*Cal mol*$^{-1}$	*Cal deg*$^{-1}$ *mol*$^{-1}$
0.00	0.000	0.000	0.000	0.000	0.000	0.000
5.00	.001	.001	.000	.000	.000	.000
10.00	.005	.012	.001	.002	.004	.000
15.00	.017	.062	.004	.006	.021	.001
20.00	.041	.195	.010	.013	.065	.003
25.00	.095	.520	.021	.027	.162	.006
30.00	.188	1.207	.040	.052	.355	.012
35.00	.334	2.486	.071	.091	.707	.020
40.00	.549	4.667	.117	.149	1.299	.032
45.00	.833	8.094	.180	.230	2.236	.050
50.00	1.183	13.106	.262	.335	3.636	.073
55.00	1.603	20.042	.364	.467	5.628	.102
60.00	2.083	29.236	.487	.626	8.350	.139
65.00	2.612	40.956	.630	.814	11.939	.184
70.00	3.191	55.444	.792	1.028	16.532	.236
75.00	3.801	72.910	.972	1.269	22.265	.297
80.00	4.437	93.495	1.169	1.534	29.264	.366
85.00	5.089	117.31	1.380	1.823	37.648	.443
90.00	5.753	144.41	1.605	2.133	47.529	.528
95.00	6.424	174.85	1.841	2.462	59.007	.621
100.00	7.099	208.66	2.087	2.808	72.175	.722
105.00	7.776	245.84	2.341	3.171	87.117	.830
110.00	8.456	286.42	2.604	3.549	103.91	.945
115.00	9.138	330.41	2.873	3.939	122.62	1.066
120.00	9.819	377.80	3.148	4.343	143.32	1.194
125.00	10.499	428.60	3.429	4.757	166.07	1.329
130.00	11.175	482.79	3.714	5.182	190.92	1.469
135.00	11.843	540.34	4.002	5.617	217.91	1.614
140.00	12.503	601.21	4.294	6.059	247.10	1.765
145.00	13.154	665.35	4.589	6.509	278.51	1.921
150.00	13.795	732.73	4.885	6.966	312.20	2.081
155.00	14.427	803.29	5.183	7.429	348.19	2.246
160.00	15.048	876.98	5.481	7.897	386.50	2.416
165.00	15.658	953.75	5.780	8.369	427.16	2.589
170.00	16.258	1033.5	6.080	8.846	470.20	2.766
175.00	16.846	1116.3	6.379	9.325	515.62	2.946
180.00	17.424	1202.0	6.678	9.808	563.46	3.130
185.90	17.991	1290.5	6.976	10.293	613.71	3.317
190.00	18.546	1381.9	7.273	10.780	666.39	3.507
195.00	19.090	1476.0	7.569	11.269	721.51	3.700
200.00	19.622	1572.8	7.864	11.759	779.08	3.895
205.00	20.141	1672.2	8.157	12.250	839.11	4.093
210.00	20.649	1774.2	8.448	12.742	901.59	4.293
215.00	21.144	1878.6	8.738	13.233	966.52	4.495
220.00	21.628	1985.6	9.025	13.725	1033.9	4.700
225.00	22.101	2094.9	9.311	14.216	1103.8	4.906
230.00	22.564	2206.6	9.594	14.707	1176.1	5.113
235.00	23.016	2320.5	9.875	15.197	1250.8	5.323
240.00	23.459	2436.7	10.153	15.687	1328.1	5.534
245.00	23.893	2555.1	10.429	16.175	1407.7	5.746
250.00	24.317	2675.6	10.703	16.662	1489.8	5.959
255.00	24.732	2798.3	10.974	17.147	1574.3	6.174
260.00	25.136	2922.9	11.242	17.632	1661.3	6.389
265.00	25.530	3049.6	11.508	18.114	1750.6	6.606
270.00	25.914	3178.2	11.771	18.595	1842.4	6.824
273.15	26.151	3260.2	11.936	18.897	1901.5	6.961

TABLE 5. *Thermodynamic functions for aluminum carbide* (Al_4C_3) *solid phase*—Continued

Gram molecular weight = 143.9594 g, T deg K = t deg C + 273.15

T	C_P^o	$(H_T^o - H_0^c)$	$(H_T^o - H_0^c)/T$	S_T^o	$-(G_T^o - H_0^c)$	$-(G_T^o - H_0^c)/T$
°K	*Cal deg*$^{-1}$ *mol*$^{-1}$	*Cal mol*$^{-1}$	*Cal deg*$^{-1}$ *mol*$^{-1}$	*Cal deg*$^{-1}$ *mol*$^{-1}$	*Cal mol*$^{-1}$	*Cal deg*$^{-1}$ *mol*$^{-1}$
275.00	26.288	3308.7	12.032	19.074	1936.6	7.042
280.00	26.651	3441.1	12.290	19.551	2033.1	7.261
285.00	27.005	3575.2	12.545	20.026	2132.1	7.481
290.00	27.351	3711.1	12.797	20.498	2233.4	7.701
295.00	27.695	3848.7	13.047	20.969	2337.1	7.922
298.15	27.909	3936.3	13.202	21.264	2403.6	8.062
300.00	28.035	3988.1	13.294	21.437	2443.1	8.144
310.00	28.694	4271.7	13.780	22.367	2662.1	8.587
320.00	29.314	4561.8	14.256	23.288	2890.4	9.032
330.00	29.894	4857.9	14.721	24.199	3127.8	9.478
340.00	30.439	5159.6	15.175	25.100	3374.3	9.925
350.00	30.952	5466.5	15.619	25.990	3629.8	10.371
360.00	31.435	5778.5	16.051	26.868	3894.1	10.817
370.00	31.893	6095.2	16.473	27.736	4167.1	11.262
373.15	32.032	6195.8	16.604	28.007	4254.9	11.403
380.00	32.324	6416.3	16.885	28.592	4448.8	11.707
390.00	32.726	6741.6	17.286	29.437	4738.9	12.151
400.00	33.104	7070.7	17.677	30.270	5037.5	12.594
425.00	33.973	7909.4	18.610	32.304	5819.8	13.694
450.00	34.746	8768.6	19.486	34.268	6652.1	14.782
475.00	35.439	9646.0	20.307	36.166	7532.7	15.858
500.00	36.064	10540.	21.080	38.000	8459.9	16.920
550.00	37.145	12371.	22.493	41.489	10448.	18.996
600.00	38.050	14252.	23.753	44.761	12605.	21.009
650.00	38.818	16174.	24.883	47.838	14921.	22.955
700.00	39.479	18132.	25.902	50.739	17386.	24.837
750.00	40.055	20120.	26.827	53.483	19992.	26.656
800.00	40.561	22136.	27.670	56.085	22732.	28.415
850.00	41.010	24175.	28.442	58.558	25599.	30.116
900.00	41.411	26236.	29.151	60.913	28586.	31.762
950.00	41.772	28316.	29.806	63.162	31688.	33.356
1000.00	42.099	30413.	30.413	65.313	34900.	34.900
1050.00	42.396	32525.	30.976	67.374	38218.	36.398
1100.00	42.669	34652.	31.502	69.353	41636.	37.851
1150.00	42.919	36792.	31.993	71.255	45152.	39.263
1200.00	43.150	38944.	32.453	73.087	48761.	40.634
1250.00	43.364	41106.	32.885	74.853	52460.	41.968
1300.00	43.563	43280.	33.292	76.557	56245.	43.265
1350.00	43.748	45463.	33.675	78.205	60114.	44.529
1400.00	43.922	47654.	34.039	79.799	64065.	45.760
1450.00	44.085	49855.	34.382	81.343	68093.	46.961
1500.00	44.239	52063.	34.708	82.841	72198.	48.132
1550.00	44.384	54278.	35.018	84.294	76377.	49.275
1600.00	44.521	56501.	35.313	85.705	80627.	50.392
1650.00	44.651	58730.	35.594	87.077	84947.	51.483
1700.00	44.774	60966.	35.862	88.412	89334.	52.549
1750.00	44.892	63208.	36.119	89.711	93787.	53.593
1800.00	45.004	65455.	36.364	90.978	98305.	54.614
1850.00	45.111	67708.	36.599	92.212	102884.	55.613
1900.00	45.213	69966.	36.824	93.416	107525.	56.592
1950.00	45.311	72229.	37.041	94.592	112226.	57.552
2000.00	45.406	74497.	37.249	95.741	116984.	58.492

H_0^c is the enthalpy of the solid at 0 °K and 1 atm pressure.

to determine the constants of the following empirical equation for Al_4C_3:

$$H_T - H_{273.15} = 19771.1 + 47.5557T + 1.927(10^{-4})T^2 - 13452.4 \log_{10} T \text{ cal mol}^{-1} \text{ at } T \text{ °K}. \quad (1)$$

(For consistency, the equation has more significant figures than the precision of the observations.) The deviations of the mean observed values from eq (1) are given in the last column. The final values of enthalpy from 373 to 1173 °K, relative to 273 °K (table 5) are consistently lower than eq (1) by 10 cal mol^{-1}, an amount which is within the precision of the high-temperature measurements.

The heat measurements on the empty container were not smoothed separately because their temperature variation possesses an irregularity reflecting a well-known transition in the alloy 80 percent Ni–20 percent Cr in this temperature range.

5. Comparison of the Low- and High-Temperature Heat Data and the Calculation of Thermodynamic Functions

The low-temperature heat-capacity data overlap the high-temperature relative-enthalpy data in the range 273.15 to 380 °K. Numerical integration of the smoothed values of the low-temperature heat-capacity yielded 2933 cal mol^{-1} for the enthalpy change between 273.15 and 373.15 °K. The high-temperature relative enthalpy measurements (see table 4) give an average value of 2939 cal mol^{-1} and the enthalpy equation (eq (1)) gives 2947 cal mol^{-1} for this temperature interval. The smoothed values of heat capacity from the low-temperature measurements were merged with the values of heat capacity calculated from the relative enthalpy equation (eq (1)) in a manner such that the resultant enthalpy change from 273.15 to 373.15 °K would be about the average of the mean values determined by the two methods. After a process of adjusting and smoothing, the final values of heat capacity that were obtained yielded 2936 cal mol^{-1} for the enthalpy change of this temperature interval. In figure 4, the final selected values of heat capacity are compared with those from the low-temperature measurements and from the enthalpy equation (eq (1)) in the interval 270 to 390 °K.

The relative-enthalpy equation (eq (1)) was used to extrapolate the thermodynamic properties up to 2000 °K. The equation is of a form generally used for high-temperature heat capacities and is "well behaved" in terms of the configuration of the heat-capacity curve and the derivatives up to 2000 °K and higher. The various thermodynamic properties between 0 and 2000 °K given in table 5 were calculated from the heat capacities, using the standard thermodynamic relations [18], by numerical methods on the IBM 7094 computer.

Initially the various high-temperature vapor-equilibrium data involving Al_4C_3 were analyzed in order to obtain a guide for extrapolating the calorimetric data above 1200 °K. The entropy of Al_4C_3 was calculated from the $\Delta S°$ of the equilibrium reactions in which the $\Delta C_p°$ of the components was assumed to be zero. After consideration of the uncertainties in the values of $S°$ calculated from the vapor-equilibrium data, the extrapolated values of eq (1) was found to be within the estimated uncertainties. Equation (1) was, therefore, used in the extrapolation. The details of this comparison and the subsequent refinements in the calculation, in which the $\Delta C_p°$ of the components are considered, are discussed in the following section (sec. 6).

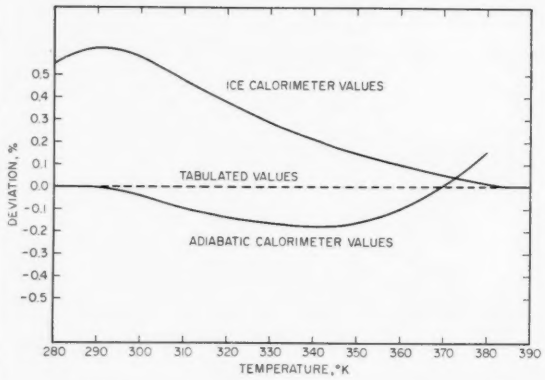

FIGURE 4. *Comparison of the final selected values of heat capacity (table 5) with those of the low-temperature measurements and those derived from the enthalpy equation (eq (1)).*

6. Comparison of the Calorimetric and Vapor-Equilibrium Data

The calorimetric data obtained on Al_4C_3 and the results of extrapolating the thermodynamic properties to 2000 °K have been compared with vapor-equilibrium data on reactions involving Al_4C_3. Intercomparisons were made of the results of thermodynamic analyses by three methods that are ordinarily used, depending upon the thermodynamic data available. The values of $S°$ of Al_4C_3 and $\Delta H°$ and $\Delta S°$ of the various reactions that were obtained are intercompared. Vapor pressures calculated from calorimetric data are compared graphically with the observed values.

In method I the vapor-pressure data only were used, in which $\Delta C_p°=0$ is assumed for the reactions. Whenever the vapor-pressure equation only was given, the $\Delta S°$ of the reaction was calculated from the relations:

$$\Delta G° = -RT \ln p^n \quad (2)$$

and

$$\left(\frac{\partial \Delta G°}{\partial T}\right)_p = -\Delta S°, \quad (3)$$

where n is the net number of moles of gaseous species produced in the reaction as written and R is the molal gas constant. When numerical values of the

vapor pressure were given, the relation

$$\frac{\Delta G^\circ}{T} = -R \ln p^n = \frac{\Delta H^\circ}{T} - \Delta S^\circ \qquad (4)$$

was used and ΔH° and ΔS° obtained by the least squares method. Whenever both equation and numerical values were given, the values obtained through the least-squares analysis were selected for the comparison. The corresponding values of S° of Al_4C_3 were calculated, using the tables of thermodynamic properties recently issued from the National Bureau of Standards [8] containing values for the other substances in the reactions.

In method II, the ΔH° and ΔS° of the vapor equilibrium reactions were calculated taking into consideration the ΔC_p° of the components of the reaction involved. For Al_4C_3 the thermodynamic properties given in table 5 were used and for the other substances several of the appropriate sources of thermodynamic properties were used [8, 20]. The calculations of method II were carried out using a method suggested by Prosen [21] and illustrated by Otto [22]. Margrave [23] reported a similar method. The method involves the relation:

$$\frac{\Delta G_T^\circ}{T} - \Delta\psi = -R \ln K - \Delta\psi = \frac{\Delta H_*^\circ}{T} - \Delta S_*^\circ, \qquad (5)$$

where

$$\Delta\psi = \frac{\Delta[(H_T^\circ - H_*^\circ)}{T} - (S_T^\circ - S_*^\circ)] \qquad (6)$$

and the symbol * indicates the temperature at which the ΔH° and ΔS° are to be determined. For these calculations the temperature * was selected for purposes of the comparison at about the mid-temperature of the range of vapor-equilibrium data (at which the calculations of ΔH° and ΔS° were made assuming $\Delta C_p^\circ = 0$). The equilibrium constant K was taken to be the observed pressures of the gaseous species involved, raised to the appropriate power. The values of ΔH_*° and ΔS_*° were obtained by the least squares method.

In method III, the values of ΔH° and ΔS° of the reaction were calculated using the thermochemical and thermodynamic data on the components of the reactions [8, 20, 24, 25, 26]. For Al_4C_3, Mah [25] reported -53.4 ± 2.0 kcal mol^{-1} for the heat of formation (ΔH_f°) (298 °K) from combustion measurements on Al_4C_3 involving the reaction:

$$Al_4C_3(c) + 6O_2(g) = 2Al_2O_3(\alpha) + 3CO_2(g). \qquad (7)$$

(Henceforth, any thermodynamic property at T °K will be symbolized, for example, by ΔH° (T °K), and 298.15 °K will be abbreviated to 298 °K.) More recently King and Armstrong [26] obtained ΔH_f° (298 °K) $= -49.7 \pm 1.2$ kcal mol^{-1} from combustion measurements on a portion of the same Al_4C_3 preparation on which the present calorimetric results are being reported. Negligible amounts of $\delta - Al_2O_3$ were found in the combustion products by Mah [25], but the experiments of King and Armstrong [26] showed from 50 to 75 percent $\delta - Al_2O_3$ which was corrected for the heat of transition to the α form. The somewhat purer sample used by Mah may be the reason for the negligible amounts of $\delta - Al_2O_3$ found in her experiments [27]. If $\alpha - Al_2O_3$ only were assumed to have been formed in the combustion reaction, the measurements of King and Armstrong [26] would yield ΔH_f° (298 °K) $= -52.6 \pm 1.1$ kcal mol^{-1}. The earlier combustion measurements of Roth and colleagues [28, 29, 30] yield ΔH_f° (298 °K) $= -46.2 \pm 6.2$ kcal mol^{-1} when the recent thermochemical data [8, 24] are applied to their reported heat of reaction (-1036.7 ± 6.2 kcal mol^{-1} for eq (7). The value -49.7 ± 1.2 kcal mol,$^{-1}$ obtained by King and Armstrong [26], was used in the calculations by method III. In the comparison of the vapor pressures of the various equilibrium reactions the value -53.4 ± 2.0 kcal mol^{-1} obtained by Mah [25] was used also.

Table 6 shows the comparison of the calorimetric values of S° of Al_4C_3 with those calculated from the various vapor-equilibrium reactions assuming $\Delta C_p^\circ = 0$ (method I) and when the values of ΔC_p° of the reactions were considered (method II). The comparison of the values of ΔH° and ΔS° of the vapor-equilibrium reaction obtained from vapor-pressure (methods I and II) and calorimetric (method III) data is given in table 7. (Hereafter, the methods of calculation used to obtain the various thermodynamic quantities will be identified by the Roman numerals indicated above.)

The thermochemical and thermodynamic data were used to calculate the vapor pressure of the gaseous species of the vapor-equilibrium data. The activity coefficients of the components were assumed to be unity. The $\log_{10} p$ (observed or vapor-pressure equation obtained from least-square analysis) and $\log_{10} p$ (vapor pressures calculated from calorimetric data) are plotted in figure 5 for comparison.

The simplest vapor-equilibrium reaction analyzed is the dissociation of Al_4C_3:

$$Al_4C_3(c) = 4Al(g) + 3C(c). \qquad (8)$$

Meschi and Searcy [31] measured the vapor pressure of aluminum in the above reaction in the region from 1500 to 1800 °K by means of the Knudsen effusion method and by a torsion method. They reported for the reaction ΔH° (1600 °K) $= 356 \pm 12$ kcal mol^{-1} based on the vapor-pressure equation obtained from two of the runs by the torsion method. The values of ΔH° from each of the above two runs differed by 20 kcal mol^{-1}. The values of ΔH° and ΔS° for the reaction (eq (8)) were evaluated at 1650 °K, the midtemperature of the experimental range, using method I with the numerical data between 1600 and 1700 °K given only for the Knudsen effusion method. The results using method II are based on the same numerical values. (Meschi and Searcy [31] show a large number of observations in their plot but report only seven numerical values.

TABLE 6. *Comparison of the entropy of aluminum carbide (Al_4C_3) obtained from the calorimetric measurements with those calculated from vapor-equilibrium data*

Source	System or reaction	Temperature range	Temperature of $S°$	S^0_T		
				Assuming $\Delta C^0_p=0$	ΔC^0_p from thermal data	Calorimetric data
		°K	°K	e.u.[a]	e.u.[a]	e.u.[a,b]
Meschi and Searcy [31]	$Al_4C_3(c)=4Al(g)+3C(c)$	1500–1800	1650	99.8	99.5	87.1
Prescott and Hincke [36]	$4AlN(c)+3C(c)=Al_4C_3(c)+2N_2(g)$	1774–1909	1850	97.5	97.4	92.2
Prescott and Hincke [37]	$2Al_2O_3(c)+9C(c)=Al_4C_3(c)+6CO(g)$	1967–2293	2150	90.0	84.6	99.0
Brunner [38]	$2Al_2O_3(c)+9C(c)=Al_4C_3(c)+6CO(g)$	1853–2253	2100	58.0	57.3	98.0
Grjotheim et al., [41]	$8MgO(c)+Al_4C_3(c)=2MgAl_2O_4(c)+3C(c)+6Mg(g)$	1324–1452	1400	74.9	74.8	79.8

[a] e.u. = cal $deg^{-1}mol^{-1}$.
[b] Obtained from table 5.

TABLE 7. *Comparison of the thermodynamics of vapor-equilibrium reactions of table 6 calculated by various methods*

Reference	T	Calculations from vapor-equilibrium data				Calculations from calorimetric data		Difference (method II—calorimetric data)		
		Method I assuming $\Delta C_p=0$		Method II ΔC_p from calorimetric data						
		ΔH°_T	ΔS°_T	ΔH°_T	ΔS°_T	ΔH°_T	ΔS°_T	$\delta\Delta H^\circ_T$	$\delta T\Delta S^\circ_T$	$\delta\Delta G^\circ_T$
	°K	*kcal mol*$^{-1}$	*cal deg*$^{-1}$ *mol*$^{-1}$	*kcal mol*$^{-1}$	*cal deg*$^{-1}$*mol*$^{-1}$	*kcal mol*$^{-1}$	*cal deg*$^{-1}$ *mol*$^{-1}$	*kcal mol*$^{-1}$	*kcal mol*$^{-1}$	*kcal mol*$^{-1}$
Meschi and Searcy [31]	1650	345.2±27.3[a]	117.5±16.4[a]	345.6±27.3[a]	117.8±16.4[a]	351.1±2.1[b,c]	130.2±0.3	−5.5	−20.5	+15.0
Prescott and Hincke [36]	1850	257.4±14.9	92.6±8.0	257.2±14.9	92.5±8.0	250.3±1.7	87.3±0.3	+6.9	+9.6	−2.7
Prescott and Hincke [37]	2150	535.6±88.0	239.8±41.5	535.0±87.8	239.6±41.4	566.8±7.2	248.9±0.7	−31.8	−20.0	−11.8
Brunner [38]	2100	467.6±3.4	209.4±1.7	466.1±3.4	208.7±1.6	567.6±7.2	249.3±0.7	−101.5	−85.3	−16.2
Grjotheim et al., [41]	1400	297.2±6.5	172.4±4.7	297.2±6.5	172.3±4.7	301.3±4.7	167.5±0.3	−4.1	+6.7	−10.8

[a] These figures following the ± symbols are standard deviations defined for the values of $\Delta H°$ by:

$$S_b=\left\{\frac{S_v^2}{\Sigma x_i^2-(\Sigma x_i)^2/k}\right\}^{1/2},$$ and of $\Delta S°$ by: $S_a=\left\{\frac{S_v^2\Sigma x_i^2}{k\Sigma x_i^2-(\Sigma x)^2}\right\}^{1/2}$,

where $S_v^2=\Sigma\delta_i^2/(k-2)$, δ_i the deviation of the experimental value from the "least-squared" value, k the number of observations, and $x_i=1/T_i$ [42].
[b] These figures following the ± symbols were obtained from the relation $(\Sigma\epsilon_i^2)^{1/2}$, where ϵ_i is the estimated uncertainty of the calorimetric data used.
[c] These values of $\Delta H°$ are based on the $\Delta H_f°$ (298 °K) for Al_4C_3 reported by King and Armstrong [26].

The analysis is based on these seven values, which are unfortunately closely spaced in temperature and yield a poorer precision figure than that obtained by Meschi and Searcy using a larger number of observations.)

Earlier, Ruff and Jellinek [32] investigated the vapor equilibrium of the Al-C system and found as much as 14 percent of carbon in the gaseous products at 2543 °K. Zeeman [33] reported an analysis of the spectrum of AlC produced at 2423 °K in a graphite resistance furnace containing aluminum. On the other hand, a mass spectrometric analysis of the gaseous products from Al_4C_3 dissociation at 2100 °K by Chupka et al. [34] showed insufficient amounts of gaseous Al-C compounds to account for the large amounts of carbon found by Ruff and Jellinek [32]. Chupka et al. [34] found no molecular species of the formula AlC treated by Zeeman [33]. The measurements of Ruff and Jellinek probably contained CO from oxygen contamination. Therefore, their results are not compared in tables 6 and 7.

The comparison of the vapor pressures of the Al_4C_3 dissociation equilibrium (fig. 5, curves B) shows that the observed values B'' [31] and those calculated from the calorimetric data B, B' are displaced very nearly parallel from each other. The close agreement (about 1.5%) of the values of $\Delta H°$ given in table 7 conforms with the agreement in the "slopes" of the vapor pressures. The displacement of the vapor-pressure curves is related to the deviations in the values of $\Delta S°$. Thus

$$\delta\Delta S°=\frac{\delta\Delta H°}{T}+nR\delta\ln p=-\delta\left(\frac{\partial\Delta G°}{\partial T}\right)_p \qquad (9)$$

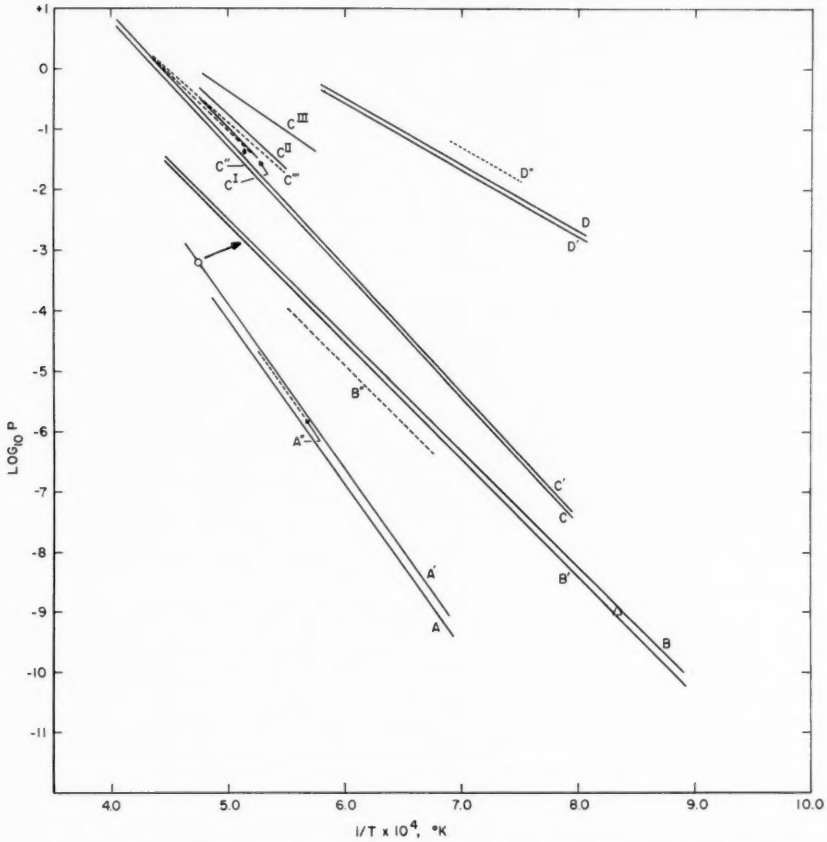

FIGURE 5. *Comparison of vapor pressures (log_{10} p versus 1/T) calculated from heat of formation and thermodynamic data with published values obtained in high-temperature equilibrium measurements.*

(a) $4AlN(c) + 3C(c) \rightarrow Al_4C_3(c) + 2N_2(g)$: A and A′ calculation from thermal data,* A″ = Prescott and Hincke [36].
(b) $Al_4C_3(c) \rightarrow 4Al(g) + 3C(c)$: B and B′ = calculation from thermal data,* B″ = Meschi and Searcy [31], ○ = Chupka et al. [34], Δ = Campbell [35].
(c) $2Al_2O_3(c) + 9C(c) = Al_4C_3(c) + 6CO(g)$: C and C′ calculation from thermal data,*
C″ = Prescott and Hincke [37], C‴ = Brunner [38].
$C^{I} = Al_4O_4C(c) + 6C(c) \rightarrow Al_4C_3(c) + 4CO(g)$: Cox and Pidgeon [40].
$C^{II} = 2Al_2O_3(c) + 3C(c) \rightarrow Al_4O_4C(c) + 2CO(g)$: [40].
$C^{III} = Al_2O_3(c) + 3C(c) \rightarrow Al_2OC(c) + 2CO(g)$: [40].

(d) $8MgO(c) + Al_4C_3(c) \rightarrow 2MgAl_2O_4(c) + 3C(c) + 6Mg(g)$: D and D′ = calculation from thermal data, D″ = Grjotheim et al. [41].

*A, B, C, and D are based on the heat of formation of Al_4C_3 reported by King and Armstrong [26] and A′, B′, C′, and D′ on the value reported by Mah [25.]

and $\delta\Delta G^\circ = -nRT\delta \ln p$, where n is the number of moles of the gas involved in the equilibrium and R is the molal gas constant. If $\delta\Delta H^\circ = 0$, then $\delta\Delta S^\circ = nR\delta \ln p$.

The single vapor-pressure value reported for the Al_4C_3 dissociation by Chupka et al. [34] is shown (fig. 5) to be over an order of magnitude lower than the calculated curve. Campbell [35] reported ΔG° (1193 °K) = 35.8 kcal mol^{-1} for the reaction:

$$Al_4C_3(c) = 4Al(l) + 3C(c), \qquad (10)$$

calculated from the activity coefficient obtained from the measurement of the vapor pressure of aluminum monofluoride over the Al_4C_3-Al-C system and over pure aluminum at 1193 °K (920 °C). The value plotted in figure 5 was obtained after converting to the basis of aluminum vapor [8]. The agreement is fortuitously very close.

Prescott and Hincke [36] investigated the equilibrium reaction between aluminum carbide and nitrogen

$$4AlN(c) + 3C(c) = Al_4C_3(c) + 2N_2(g), \qquad (11)$$

in the region 1774 to 1909 °K. The Al_4C_3 sample was prepared by heating pellets of finely divided aluminum metal and graphite as high as 1880 °K. These pellets were mixed in stoichiometric proportion plus 10 percent excess of graphite. The equilibrium pressures were determined from time-pressure measurements obtained by means of a McLeod gage. M. v. Stackelberg et al. [6, 7] reported an intermediate compound, Al_5C_3N, similar in appearance and properties to Al_4C_3, and pointed out that the equilibrium reaction investigated by Prescott and Hincke [36] possibly involved instead:

$$4Al_5C_3N(c)+3C(c)=5Al_4C_3(c)+2N_2(g) \quad (12)$$

or

$$5AlN(c)+3C(c)=Al_5C_3N(c)+2N_2(g) \quad (13)$$

depending upon the degree of nitridation of Al_4C_3 to AlN. Since no thermodynamic data are available on Al_5C_3N, the comparison is based on the reaction given by eq (11). Methods I and II were applied with the numerical values of vapor pressures reported by Prescott and Hincke [36].

If $\Delta G^\circ < 0$ for the reaction

$$Al_4C_3(c)+AlN(c)=Al_5C_3N(c), \quad (14)$$

then ΔG° (eq (12)) $> \Delta G^\circ$ (eq (11)) and the observed vapor pressures according to eq (12) should be lower than those calculated from the thermal data for eq (11). On the other hand, ΔG° (eq (13)) $< \Delta G^\circ$ (eq (11)) so that the observed vapor pressures according to eq (13) should be higher than the calculated values based on eq (11). The plot of figure 5, curves A, shows that the observed vapor-pressures A'' lie midway between the calculated values A' and A (eq (11)) based on the heat of formation obtained by Mah [25] and by King and Armstrong [26], respectively. The agreement is shown to be reasonably good, so that ΔG° of the reaction represented by eq (14) is probably close to zero or compensating effects exist. (If the compound Al_5C_3N were considered a mixture, the reactions represented by eqs (12) and (13) reduce to eq (11).)

In an earlier investigation, Prescott and Hincke [37] reported vapor-equilibrium measurements on the reaction between aluminum oxide and carbon in the region 1967 to 2293 °K

$$2Al_2O_3(c)+9C(c)=Al_4C_3(c)+6CO(g). \quad (15)$$

Calculations applying methods I and II were made with the numerical values that were reported.

Brunner [38] also investigated the equilibria of the Al_2O_3-C reaction in the region 1853 to 2253 °K. The numerical values reported by Brunner are considerably more precise than those reported by Prescott and Hincke [37] for the reaction. Table 5 was extrapolated slightly above 2000 °K in order to compare the results reported by Prescott and Hincke [37] and by Brunner [38].

The divergent vapor-pressure values reported by various investigators for the Al_2O_3-C reaction (see fig. 5, curves C) may be partially explained, depending upon the equilibrium reaction, on the basis of formation of aluminum oxycarbides. According to the phase diagram investigations reported by Foster, Long, and Hunter [27] and the survey of existing data on the Al-O-C system by Motzfeldt [39], Al_2O_3 and Al_4C_3 can not coexist at equilibrium. The equilibrium investigated by Prescott and Hincke [37] could be

$$Al_4O_4C(c)+3C(c)=2Al_2OC(c)+2CO(g) \quad (16)$$

or

$$2Al_2O_3(c)+3C(c)=Al_4O_4C(c)+2CO(g) \quad (17)$$

instead of the reaction represented by eq (15). At the upper temperatures (above 2100 °K) liquid phases may have been present. If $\Delta G^\circ < 0$ for the formation of the oxycarbides,

$$Al_2O_3(c)+Al_4C_3(c)=3Al_2OC(c) \quad (18)$$

or

$$4Al_2O_3(c)+Al_4C_5(c)=3Al_4O_4C(c), \quad (19)$$

then the equilibrium represented by eq (17) should yield higher vapor pressures than those calculated according to eq (15). For eq (16), the relative values of vapor pressure with respect to eq (15) will depend on the relative values of ΔG_f° of the oxycarbides. Another equilibrium reaction possible, according to the phase diagram [27, 39], is

$$2Al_2OC(c)+3C(c)=Al_4C_3(c)+2CO(g) \quad (20)$$

but for this reaction the observed vapor pressure should be lower than those calculated for eq (15). Prescott and Hincke [37] used an "excess" of Al_2O_3; the reactions given by eqs (16), (17), and (20) are possible depending upon the "excess". Brunner [38], on the other hand, used stoichiometric amounts of Al_2O_3 and C corresponding to eq (15) and his results are even higher than those of Prescott and Hincke [37].

Recently, Cox and Pidgeon [40] using a differential thermal analysis method reported results on the equilibrium reactions represented by eq (17),

$$Al_2O_3(c)+3C(c)=Al_2OC(c)+2CO(g) \quad (21)$$

and

$$Al_4O_4C(c)+6C(c)=Al_4C_3(c)+4CO(g). \quad (22)$$

The measurements were made on each of three samples having Al_2O_3 to C molal ratios of 2:3, 2:6, and 2:9. Vapor-pressure equations of the form given by eq (4) were obtained by fitting the experimental data, corresponding to reactions represented by eqs (17), (21), and (22), respectively, by the method of least squares. (The numerical values, which were absent in the original paper, were kindly supplied by the authors.) These equations, plotted in figure 5, show that the vapor pressures observed by Cox and Pidgeon [40] are considerably higher than those calculated for the reaction given by eq (15). The vapor pressures corresponding to reaction (22) are fairly close to the values reported by Prescott

and Hincke [37]; the values for reaction (17) join at the lower temperatures with those obtained by Brunner [38]. The values for reaction (21) are higher than any of the other vapor pressures plotted for the Al-O-C system. Actually, of the three reactions reported by Cox and Pidgeon [40], only the reaction given by eq (17) is possible according to the phase diagrams [27, 39].

Recently, Grjotheim, Herstad, and Johannessen [41] reported vapor-equilibrium investigations by means of the transpiration method of the reaction:

$$8MgO(c)+Al_4C_3(c)=2MgAl_2O_4(c)+3C(c)+6Mg(g), \quad (23)$$

in the range 1325 to 1450 °K. The observed vapor pressures are higher than the calculated values on the average by a factor of 2 (fig. 5, curves D), which corresponds to $\delta\Delta G°$ (1400 °K) of about 12 kcal for the reaction given in eq (23). The uncertainty in the calorimetric data is considerably lower than 12 kcal and it is unlikely that the vapor-pressure measurements are in error by a factor of 2. The values of $\Delta H°$ (table 7) agree, however, within about 1.3 percent.

The comparisons of the results of thermodynamic analysis of high temperature vapor-equilibrium reactions show that the $\Delta H°$ of the reactions calculated from calorimetric data and by the second-law method using vapor-pressure data can agree within a few percent or better and within about the uncertainty of the calorimetric data. The vapor pressures and, therefore, the $\Delta G°$ of the reactions show systematic differences that are, in some cases, greater than the uncertainties in the calorimetric data or in the vapor-pressure determination. These differences are reflected in the values of $\delta\Delta G°$ of table 7 $\approx \delta \log p$ of figure 5. These differences can be attributed partially to the deviations from unity of the activity coefficients of the components of the equilibrium reaction or the reactions being different from those as written. Also, because of the finite time involved in the experiments, possible kinetic effects can contribute to the deviations. For the second-law values of $\Delta H°$, the standard deviation figures depend on the precision of the measurements and on the temperature distribution of observations. In method I, any departure from linearity of the log p versus $1/T$ relation increases the standard deviation figure. Wide divergences in $\Delta H°$ and $\Delta S°$ were found in the Al–O–C system; the need for further work on the system is indicated.

In the vapor-equilibrium reactions that were analyzed, the results obtained using method I and II were essentially the same, since in method I the $\Delta S°$ and $\Delta H°$ were evaluated at the mean temperature of the range of measurements (as should always be done) and also since the term given by eq (6) is small. In other equilibria or for wider ranges, this term may become important and should be used whenever a value or estimate of $\Delta C_p°$ is available.

The authors are indebted to Willis R. Thurber for all the measurements on the sample with the "drop" calorimeter, and to Rolf A. Paulson of the Analysis and Purification Section of the National Bureau of Standards for the chemical analyses on the samples. The processing of the heat measurements would not have been possible without the chemical analysis. The gift of the Al_4C_3 sample from the Aluminum Company of America, ALCOA Research Laboratories, through the courtesy of George Long, is gratefully acknowledged.

(Continued)

Appendix. Thermodynamic functions for aluminum carbide (Al_4C_3) solid phase

Gram molecular weight = 143.9594 g, T deg K = t deg C + 273.15

T	C_P°	$(H_T^\circ - H_0^\circ)$	$(H_T^\circ - H_0^\circ)/T$	S_T°	$-(G_T^\circ - H_0^\circ)$	$-(G_T^\circ - H_0^\circ)/T$
°K	J deg^{-1} mol^{-1}	J mol^{-1}	J deg^{-1} mol^{-1}	J deg^{-1} mol^{-1}	J mol^{-1}	J deg^{-1} mol^{-1}
0.00	0.000	0.000	0.000	0.000	0.000	0.000
5.00	.003	.003	.001	.001	.001	.000
10.00	.020	.051	.005	.007	.017	.002
15.00	.069	.259	.017	.023	.086	.006
20.00	.170	.817	.041	.054	.272	.014
25.00	.397	2.177	.087	.114	.679	.027
30.00	.786	5.052	.168	.218	1.488	.050
35.00	1.398	10.402	.297	.382	2.958	.085
40.00	2.299	19.525	.488	.624	5.436	.136
45.00	3.484	33.866	.753	.960	9.356	.208
50.00	4.950	54.838	1.097	1.401	15.215	.304
55.00	6.707	83.854	1.525	1.953	23.551	.428
60.00	8.716	122.33	2.039	2.621	34.937	.582
65.00	10.929	171.36	2.636	3.405	49.954	.769
70.00	13.351	231.98	3.314	4.302	69.175	.988
75.00	15.902	305.05	4.067	5.310	93.159	1.242
80.00	18.564	391.18	4.890	6.420	122.44	1.531
85.00	21.294	490.81	5.774	7.627	157.52	1.853
90.00	24.073	604.21	6.713	8.923	198.86	2.210
95.00	26.878	731.57	7.701	10.300	246.89	2.599
100.00	29.702	873.02	8.730	11.750	301.98	3.020
105.00	32.537	1028.6	9.796	13.268	364.50	3.471
110.00	35.381	1198.4	10.895	14.847	434.76	3.952
115.00	38.232	1382.4	12.021	16.483	513.06	4.461
120.00	41.085	1580.7	13.173	18.170	599.67	4.997
125.00	43.929	1793.3	14.346	19.905	694.84	5.559
130.00	46.755	2020.0	15.538	21.683	798.80	6.145
135.00	49.552	2260.8	16.746	23.500	911.74	6.754
140.00	52.314	2515.4	17.967	25.352	1033.9	7.385
145.00	55.037	2783.8	19.199	27.236	1165.3	8.037
150.00	57.719	3065.8	20.438	29.147	1306.3	8.708
155.00	60.361	3361.0	21.684	31.083	1456.8	9.399
160.00	62.959	3669.3	22.933	33.040	1617.1	10.107
165.00	65.513	3990.5	24.185	35.017	1787.3	10.832
170.00	68.022	4324.3	25.437	37.010	1967.3	11.572
175.00	70.485	4670.6	26.689	39.017	2157.4	12.328
180.00	72.902	5029.1	27.940	41.037	2357.5	13.097
185.00	75.273	5399.6	29.187	43.067	2567.8	13.880
190.00	77.598	5781.8	30.430	45.105	2788.2	14.675
195.00	79.873	6175.5	31.669	47.150	3018.8	15.481
200.00	82.098	6580.4	32.902	49.201	3259.7	16.298
205.00	84.271	6996.4	34.129	51.255	3510.8	17.126
210.00	86.394	7423.0	35.348	53.311	3772.2	17.963
215.00	88.466	7860.2	36.559	55.368	4043.9	18.809
220.00	90.492	8307.6	37.762	57.425	4325.9	19.663
225.00	92.471	8765.1	38.956	59.481	4618.2	20.525
230.00	94.407	9232.3	40.140	61.535	4920.7	21.394
235.00	96.300	9709.1	41.315	63.586	5233.5	22.270
240.00	98.154	10195.	42.480	65.632	5556.6	23.152
245.00	99.968	10691.	43.635	67.675	5889.9	24.040
250.00	101.74	11195.	44.779	69.713	6233.3	24.933
255.00	103.48	11708.	45.913	71.745	6587.0	25.831
260.00	105.17	12230.	47.037	73.770	6950.8	26.734
265.00	106.82	12760.	48.149	75.789	7324.7	27.640
270.00	108.42	13298.	49.251	77.801	7708.6	28.551
273.15	109.42	13641.	49.939	79.064	7955.7	29.126

Appendix. Thermodynamic functions for aluminum carbide (Al_4C_3) *solid phase*—Continued

Gram molecular weight = 143.9594 g, T deg K = t deg C + 273.15

T	C_P^0	$(H_T^0 - H_0^C)$	$(H_T^0 - H_0^C)/T$	S_T^0	$-(G_T^0 - H_0^C)$	$-(G_T^0 - H_0^C)/T$
°K	*J deg*$^{-1}$ *mol*$^{-1}$	*J mol*$^{-1}$	*J deg*$^{-1}$ *mol*$^{-1}$	*J deg*$^{-1}$ *mol*$^{-1}$	*J mol*$^{-1}$	*J deg*$^{-1}$ *mol*$^{-1}$
275.00	109.99	13844.	50.341	79.805	8102.7	29.464
280.00	111.51	14397.	51.419	81.800	8506.7	30.381
285.00	112.99	14959.	52.487	83.787	8920.6	31.301
290.00	114.44	15527.	53.542	85.765	9344.5	32.223
295.00	115.87	16103.	54.587	87.733	9778.3	33.147
298.15	116.77	16469.	55.239	88.969	10057.	33.730
300.00	117.30	16686.	55.620	89.693	10222.	34.073
310.00	120.06	17873.	57.655	93.584	11138.	35.930
320.00	122.65	19087.	59.646	97.437	12093.	37.792
330.00	125.08	20325.	61.592	101.25	13087.	39.657
340.00	127.36	21588.	63.493	105.02	14118.	41.524
350.00	129.50	22872.	65.349	108.74	15187.	43.392
360.00	131.53	24177.	67.159	112.42	16293.	45.258
370.00	133.44	25502.	68.925	116.05	17435.	47.122
373.15	134.02	25923.	69.472	117.18	17803.	47.709
380.00	135.24	26846.	70.647	119.63	18614.	48.983
390.00	136.93	28207.	72.325	123.16	19828.	50.840
400.00	138.51	29584.	73.960	126.65	21077.	52.692
425.00	142.14	33093.	77.866	135.16	24350.	57.294
450.00	145.38	36688.	81.528	143.38	27832.	61.850
475.00	148.28	40359.	84.966	151.32	31517.	66.351
500.00	150.89	44099.	88.198	158.99	35396.	70.792
550.00	155.42	51760.	94.110	173.59	43715.	79.481
600.00	159.20	59629.	99.381	187.28	52740.	87.900
650.00	162.42	67671.	104.11	200.15	62429.	96.045
700.00	165.18	75863.	108.38	212.29	72743.	103.92
750.00	167.59	84183.	112.24	223.77	83647.	111.53
800.00	169.71	92617.	115.77	234.66	95111.	118.89
850.00	171.59	101150.	119.00	245.01	107104.	126.01
900.00	173.26	109772.	121.97	254.86	119603.	132.89
950.00	174.77	118474.	124.71	264.27	132583.	139.56
1000.00	176.14	127247.	127.25	273.27	146023.	146.02
1050.00	177.39	136086.	129.61	281.89	159904.	152.29
1100.00	178.53	144984.	131.80	290.17	174207.	158.37
1150.00	179.57	153937.	133.86	298.13	188916.	164.27
1200.00	180.54	162940.	135.78	305.80	204015.	170.01
1250.00	181.43	171989.	137.59	313.18	219491.	175.59
1300.00	182.27	181082.	139.29	320.32	235329.	181.02
1350.00	183.04	190215.	140.90	327.21	251518.	186.31
1400.00	183.77	199386.	142.42	333.88	268047.	191.46
1450.00	184.45	208592.	143.86	340.34	284903.	196.48
1500.00	185.10	217830.	145.22	346.61	302077.	201.38
1550.00	185.70	227101.	146.52	352.68	319560.	206.17
1600.00	186.28	236400.	147.75	358.59	337343.	210.84
1650.00	186.82	245728.	148.93	364.33	355417.	215.40
1700.00	187.34	255082.	150.05	369.91	373773.	219.87
1750.00	187.83	264461.	151.12	375.35	392406.	224.23
1800.00	188.30	273864.	152.15	380.65	411306.	228.50
1850.00	188.74	283290.	153.13	385.82	430468.	232.69
1900.00	189.17	292738.	154.07	390.85	449886.	236.78
1950.00	189.58	302207.	154.98	395.77	469552.	240.80
2000.00	189.98	311696.	155.85	400.58	489461.	244.73

H_0^C is the enthalpy of the solid at 0 °K and 1 atm pressure.

7. References

[1] S. Satoh, Sci Papers Inst. Phys. Chem. Research (Tokyo) **34,** 50 (1938).
[2] M. v. Stackelberg and E. Schnorrenberg, Z. physik. Chem. **B27,** 37 (1934).
[3] J. F. Durand, Bull. Soc. Chim. **35,** 1141 (1924).
[4] E. Baur and R. Brunner, Z. Elektrochem. **40,** 154 (1934).
[5] George Long, private communication, June 21, 1960.
[6] M. v. Stackelberg, E. Schnorrenberg, R. Paulus, and K. F. Spiess, Z. physik. Chem. **A175,** 127 (1935).
[7] M. v. Stackelberg and K. F. Spiess, Z. physik. Chem. **A175,** 140 (1935).
[8] Preliminary Report on the Thermodynamic Properties of Selected Light-Element and Some Related Compounds, National Bureau of Standards Report No. 6928, July 1, 1960.
[9] W. DeSorbo and W. W. Tyler, J. Chem. Phys. **21,** 1660 (1953).
[10] F. Simon and R. C. Swain, Z. physikal. Chem. **28B,** 189 (1935).
[11] K. K. Kelley, J. Chem. Phys. **11,** 16 (1943).
[12] R. B. Scott, C. H. Meyers, R. D. Rands, Jr., F. G. Brickwedde, and N. Bekkedahl, J. Res. NBS **35,** 39 (1945) RP 1661.
[13] G. T. Furukawa, M. L. Reilly, and J. H. Piccirelli, J. Res. NBS **68A** (Phys. and Chem.) No. 4, 381 (1964).
[14] H. F. Stimson, J. Res. NBS **65A** (Phys. and Chem.) No. 3, 139 (1961).
[15] H. J. Hoge and F. G. Brickwedde, J. Res. NBS **22,** 351 (1939) RP1188.
[16] E. T. Whittaker and G. Robinson, The Calculus of Observations. A Treatise on Numerical Mathematics, pp. 285–316, 4th ed. (Blackie and Sons, London, 1944).
[17] IUPAC revises atomic weight values, Chem. Eng. News **39,** 42 (1961).
[18] G. T. Furukawa, T. B. Douglas, R. E. McCoskey, and D. C. Ginnings, J. Res. NBS **57,** 67 (1956) RP2694.
[19] D. C. Ginnings, J. Phys. Chem. **67,** 1917 (1963).
[20] J. Hilsenrath, C. W. Beckett, W. S. Benedict, L. Fano, H. J. Hoge, J. F. Masi, R. L. Nuttall, Y. S. Touloukian, and H. W. Woolley, Tables of thermal properties of gases, NBS Circ. 564, November 1, 1955.
[21] E. J. Prosen, private communication.
[22] E. M. Otto, J. Electrochem. Soc. **111,** 88 (1964).
[23] J. L. Margrave, J. Phys. Chem. **64,** 288 (1960).
[24] JANAF Thermochemical Data, The Dow Chemical Company, Thermal Laboratory, Midland, Mich.
[25] A. D. Mah, Bureau of Mines RI 6415, 1964.
[26] R. C. King and G. T. Armstrong, J. Res. NBS **68A,** (Phys. and Chem.) No. 6, 661 (1964).
[27] L. M. Foster, G. Long, and M. S. Hunter, J. Am. Ceram. Soc. **39,** 1 (1956).
[28] A. Meichsner and W. A. Roth, Z. Elektrochem. **40,** 19 (1934).
[29] W. A. Roth, U. Wolf and O. Fritz, Z. Electrochem. **46,** 42 (1940).
[30] W. A. Roth, Z. Elektrochem. **48,** 267 (1942).
[31] D. J. Meschi and A. W. Searcy, J. Phys. Chem. **63,** 1175 (1959).
[32] O. Ruff and E. Jellinek, Z. anorg. allgem. Chem. **97,** 312 (1916).
[33] P. B. Zeeman, Can. J. Phys. **32,** 9 (1954).
[34] W. A. Chupka, J. Berkowitz, C. F. Giese, and M. G. Inghram, J. Phys. Chem. **62,** 611 (1958).
[35] C. S. Campbell, Met. Soc. Conf. **7,** 412 (1961).
[36] C. H. Prescott, Jr., and W. B. Hincke, J. Am. Chem. Soc. **50,** 3228 (1928).
[37] C. H. Prescott, Jr., and W. B. Hincke, J. Am. Chem. Soc. **49,** 2753 (1927).
[38] R. Brunner, Z. Elektrochem. **38,** 55 (1932).
[39] K. Motzfeldt, Tek. Ukeblad. **109,** 1137 (1962).
[40] J. H. Cox and L. M. Pidgeon, Can. J. Chem. **41,** 671 (1963).
[41] K. Grjotheim, O. Herstad, and K. Stahl-Johannessen, Z. anorg. allgem. Chem. **328,** 267 (1964).
[42] M. G. Natrella, Experimental statistics, (National Bureau of Standards Handbook, No. 91), U.S. Government Printing Office, Washington, D.C., 20402, 1963.

(Paper 69A5–364)

JOURNAL OF RESEARCH of the National Bureau of Standards—A. Physics and Chemistry
Vol. 69A, No. 5, September–October 1965

Properties of Aqueous Mixtures of Pure Salts: Thermodynamics of the Ternary System Water-Potassium Chloride-Barium Chloride at 25 °C

R. A. Robinson and V. E. Bower

(May 17, 1965)

Isopiestic vapor pressure measurements have been made on the system water-potassium chloride-barium chloride. The data have been used to evaluate the activity coefficient of each salt in the presence of the other. Two conditions are considered; in one, the solution is maintained at constant total ionic concentration; in the other, at constant total ionic strength. The excess free energy of mixing is calculated and compared with similar data for the water-hydrochloric acid-barium chloride and water-sodium chloride-barium chloride systems.

1. Introduction

The use of the isopiestic vapor pressure method to determine some thermodynamic properties of the ternary system water-sodium chloride-barium chloride has been described recently [1].[1] This system has several features of simplicity. Thus, the isopiestic ratio (R) of a series of mixed salt solutions is a linear function of the ionic fraction (x); here R is defined as $M_B/(m_B+1.5\ m_c)$ and x as $1.5\ m_c/(m_B+1.5\ m_c)$, where M_B is the molality of the reference solution of sodium chloride and m_B, m_c are the molalities of sodium chloride and barium chloride, respectively, in the mixed solution in isopiestic (vapor-phase) equilibrium with the reference solution.

The ionic fraction, x, defined in this way, is a convenient measure of the solution composition in isopiestic work because, in the limiting case of ideal solutions, all solutions with the same value of $(m_B+1.5\ m_c)$ would have the same aqueous vapor pressure. For example, four solutions, one of 1.5 m sodium chloride only, another of 1.0 m barium chloride only, the third 0.75 m to sodium chloride and 0.5 m to barium chloride, and the fourth 0.3 m to sodium chloride and 0.8 m to barium chloride, would all have the same vapor pressure if they behaved ideally. This would not be true for solutions of the same total ionic strength (m_B+3m_c), even if they were ideal.

The linear relation between isopiestic ratio and ionic fraction for the sodium chloride-barium chloride system enabled us to equate the integral in the McKay-Perring equation [2] to zero and provided a further simplification in the subsequent calculations. Such calculations showed that the equations

$$\log \gamma_B = \log \gamma_B^\circ - \alpha_B m_C \tag{1}$$

$$\log \gamma_c = \log \gamma_c^\circ - \alpha_c m_B \tag{2}$$

described the behavior of the system at constant total ionic concentration, i.e., constant $(m_B+1.5m_c)$; thus the chemical potential of each salt is a linear function of the concentration of the other salt in a system kept at constant total ionic concentration. Similar relations were found to hold for systems of constant total ionic strength (m_B+3m_c), with, of course, different numerical values of the α_B and α_c parameters.

This paper describes similar work on the system water-potassium chloride-barium chloride. The behavior of this system is somewhat more complicated.

2. Definitions

The definitions and symbols of the previous paper [1] will be retained except that D will be used to designate potassium chloride in place of B for sodium chloride. Thus eq (1) becomes

$$\log \gamma_D = \log \gamma_D^\circ - \alpha_D m_c. \tag{3}$$

3. Experimental Procedure

The procedure was as in the previous work [1] except that potassium chloride was used as the reference salt. The potassium chloride was a portion of that used in a study of the system water-potassium chloride-glycine [3].

4. Results

4.1. Isopiestic Data

The experimental results are given in table 1. The second column gives the molality (M_D) of the reference solution of potassium chloride; the third and fourth columns give the molalities of potassium chloride (m_D) and of barium chloride (m_c) in the

[1] Figures in brackets indicate the literature references at the end of this paper.

TABLE 1. *Isopiestic data for the system* H_2O–KCl–$BaCl_2$ *at 25 °C*[a]

Set	M_D	m_D	m_c	x	R	Δ
1	0.7723	0.6309	0.09985	0.1919	0.9892	−0.06
		.4178	.2482	.4712	.9775	−.06
		.1967	.3994	.7528	.9705	+.03
			.5313	1.0	.9691	+.10
	0.7786	0.3099	0.3280	0.6135	0.9709	+0.07
		.2308	.3814	.7125	.9697	−.01
		.1411	.4423	.8246	.9677	+.05
			.5358	1.0	.9688	−.10
	0.7899	0.5789	0.1491	0.2787	0.9842	+0.01
		.4185	.2603	.4827	.9764	+.01
		.2048	.4060	.7483	.9706	+.02
			.5425	1.0	.9706	−.03
	0.7924	0.6644	0.09088	0.1702	0.9864	+0.02
		.5072	.2007	.3725	.9803	+.01
		.3186	.3302	.6086	.9736	−.03
			.5442	1.0	.9707	0
	0.7958	0.7074	0.06345	0.1186	0.9916	+0.13
		.6163	.1269	.2360	.9865	+.04
		.5063	.2028	.3753	.9819	−.07
		.4067	.2712	.5001	.9782	−.10
2	1.0743	0.8081	0.1856	0.2562	0.9889	0
		.5648	.3514	.4827	.9839	+0.07
		.3064	.5228	.7191	.9851	+.04
			.7197	1.0	.9951	−.11
3	1.5519	0.6330	0.6110	0.5915	1.0015	+0.07
		.4063	.7535	.7356	1.0100	+.04
		.2358	.8588	.8453	1.0184	+.04
			.9999	1.0	1.0347	−.13
	1.5837	1.3606	0.1526	0.1440	0.9964	−0.05
		1.1475	.2965	.2786	.9955	−.06
		1.0259	.3772	.3554	.9950	+.05
		0.8270	.5066	.4788	.9978	+.06
4	2.2466	1.9274	0.2142	0.1429	0.9991	−0.01
		1.4671	.5127	.3439	1.0047	+.05
		0.8579	.8894	.6086	1.0249	+.07
		.3443	1.1881	.8381	1.0565	−.09
	2.2611	1.3394	0.6012	0.4024	1.0089	+0.03
		0.6887	.9968	.6846	1.0353	+.07
		.2503	1.2482	.8821	1.0653	−.05
			1.3874	1.0	1.0865	−.05
	2.2788	1.8961	0.2554	0.1681	0.9998	−0.01
		1.1888	.7051	.4708	1.0144	+.01
		0.5955	1.0604	.7276	1.0424	0
			1.3970	1.0	1.0875	−0.01
5	2.4938	1.6329	0.5589	0.3393	1.0091	−0.07
		1.2541	.7931	.4868	1.0205	−.02
		0.3002	1.3455	.8705	1.0756	−.01
			1.5101	1.0	1.1009	+.10
6	2.7188	1.8855	0.5384	0.2999	1.0095	−0.12
		0.5746	1.3145	.7743	1.0677	+.03
		.2539	1.4896	.8980	1.0926	+.04
			1.6244	1.0	1.1159	+.07
	2.7661	2.5365	0.1524	0.0827	1.0004	−0.02
		2.2111	.3630	.1976	1.0038	−.04
		1.7890	.6282	.3450	1.0127	−.01
		1.1054	1.0339	.5850	1.0388	+.06
	2.7763	2.3901	0.2521	0.1366	1.0029	+0.22
		1.5011	.8090	.4470	1.0227	+.06
		0.4287	1.4251	.8330	1.0818	−.09
			1.6547	1.0	1.1185	−.14
	2.8600	2.3016	0.3635	0.1915	1.0046	−0.18
		1.3772	.9332	.5041	1.0299	−.03
		0.9462	1.1832	.6523	1.0511	+.02
			1.6966	1.0	1.1238	+.14

[a] D=KCl, C=$BaCl_2$ x is the "ionic fraction" of $BaCl_2$, $1.5m_c/(m_D+1.5m_c)$
R is the isopiestic ratio, $M_D/(m_D+1.5m_c)$.
Δ is the percentage difference between R calculated by eq (4) with the parameters of table 2 and R (obs), the latter being given in column 6.

mixed solution in isopiestic equilibrium with the reference solution of potassium chloride at molality M_D. The fifth column gives values of the ionic fraction, $x=1.5m_c/(m_D+1.5m_c)$ and the sixth column values of the isopiestic ratio, $R=M_D/(m_D+1.5m_c)$.

Figure 1 is a plot of isopiestic ratio versus ionic fraction for some sets of results recorded in table 1. Unlike the plots for sodium chloride-barium chloride mixtures, where R was found to be linear in x, the

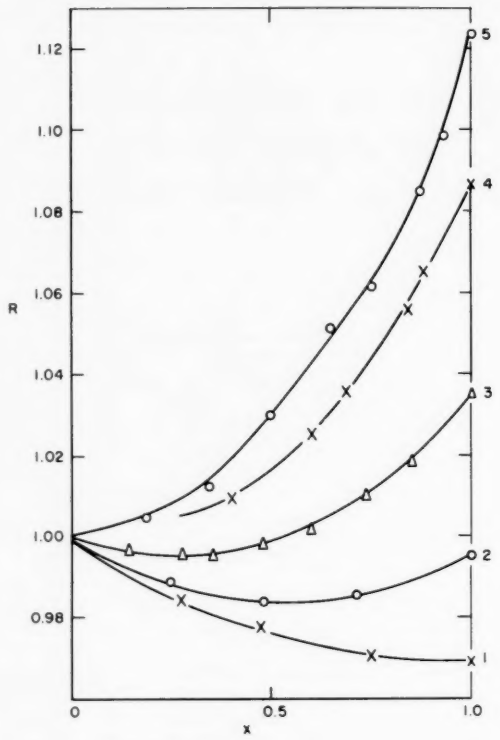

FIGURE 1. *Isopiestic ratio of potassium chloride-barium chloride solutions versus ionic fraction.*

plots for these potassium chloride-barium chloride mixtures show marked curvature. They can, however, be represented adequately by a quadratic equation

$$R=1-ax-bx^2. \quad (4)$$

The last column of table 1 gives the percentage difference between the observed isopiestic ratios and those calculated by eq (4), using the numerical values of a and b given in table 2.

4.2. Activity Coefficients at Constant Total Ionic Concentration

The McKay-Perring equation [2] can be written

$$\ln \gamma_D=\ln \Gamma_D+\ln R+\int_0^{M_D\varphi} f(m, M_D, x)\,d(M_D\varphi) \quad (5)$$

where

$$f(m, M_D, x)=\frac{1}{m^2}\left(\frac{\partial m}{\partial \ln x}\right)_{a_w}+\frac{1}{m}-\frac{1}{M_D}. \quad (6)$$

TABLE 2. *Parameters of eq (4)* $R=1-ax-bx^2$

Set	M_D	a	b
1	0.7723	0.0661	−0.0362
	.7786	.0687	−.0365
	.7899	.0667	−.0370
	.7924	.0665	−.0372
	.7958	.0642	−.0373
2	1.0743	.0563	−.0503
3	1.5519	.0394	−.0728
	1.5837	.0390	−.0743
4	2.2466	.0220	−.1054
	2.2611	.0200	−.1060
	2.2788	.0195	−.1069
5	2.4938	.0151	−.1170
6	2.7188	.0109	−.1275
	2.7661	.0083	−.1297
	2.7763	.0095	−.1302
	2.8600	.0089	−.1341

If the isopiestic ratio is quadratic in x, according to eq (4), then eq (6) becomes

$$f(m, M_D, x)=\frac{bx^2}{M_D} \tag{7}$$

and the integral in eq (5) becomes

$$x^2\int_0^{M_D\varphi}\frac{b}{M_D}\cdot d(M_D\varphi).$$

In the particular case of potassium chloride-barium chloride mixtures, it so happens that b can be represented as a linear function of M_D,

$$b=-0.0469M_D \tag{8}$$

and the integral in eq (5) can be evaluated as

$$-0.0469x^2M_D\varphi$$

or

$$-0.0204x^2M_D\varphi$$

if eq (5) is converted into decadic logarithms.

TABLE 3. *Parameters of eq (3) and eq (2)*

Set	M_D (mean)	α_D	α_c	$(\alpha_D+1.5\alpha_c)$
1	0.7858	0.0484	0.0029	0.0527
2	1.0743	.0301	.0173	.0561
3	1.5678	.0152	.0304	.0608
4	2.2622	.0053	.0403	.0658
5	2.4938	.0035	.0421	.0667
6	2.7803	.0018	.0440	.0678

The activity coefficients of potassium chloride and barium chloride in the mixed solutions have been calculated by eq (5). Then, assuming that eq (3) and eq (2) were valid for this system, as they were for the sodium chloride-barium chloride system, values of α_D and α_c were calculated. For example, at $M_D=1.0743$, $-\log \Gamma_D=0.2217$ [4]; for $m_D=0.3064$, $m_c=0.5228$, $x=0.7191$, it was found that $R=0.9851$ or $\log R=-0.0065$. Moreover, at this value of M_D, $-0.0204\ M_D\varphi=-0.0196$ so that $-0.0204x^2M_D=-0.0101$; this is the contribution of the integral term in eq (5) to $\log \gamma_D$. Thus $\log \gamma_D=-0.2383$. But the total ionic concentration of this mixed solution is $(m_D+1.5m_c)=1.0906$ and a solution of potassium chloride only at this concentration has $\log \gamma_D^\circ=-0.2225$. Hence $\alpha_D m_c=0.0158$ and $\alpha_D=0.0302$. Using all the data in table 1, the values of α_D and α_c given in table 3 were calculated.

It was shown in the appendix to the previous paper [1] that, if eq (3) and eq (2) do indeed describe the behavior of this system, then $(\alpha_D+1.5\alpha_c)$ must be constant at all values of M_D. The last column of table 3 gives values of $(\alpha_D+1.5\alpha_c)$ which are also plotted as the lower curve of figure 2. It is clear that, in the present instance, $(\alpha_D+1.5\alpha_c)$ increases with M_D. This implies that there are terms in higher powers of m_D and m_c in eq (3) and eq (2) such as

$$\log \gamma_D=\log \gamma_D^\circ-\alpha_D m_c-\beta_D m_c^2 \tag{9}$$

$$\log \gamma_c=\log \gamma_c^\circ-\alpha_c m_D-\beta_c m_D^2 \tag{10}$$

where the α and β terms must be related by the equation

$$3(\alpha_D+1.5\alpha_c)=\text{constant}-2(2\beta_D+4.5\beta_c)m \tag{11}$$

where $m=(m_D+1.5m_c)$. From the slope of the plot in figure 3 we calculate

$$(2\beta_D+4.5\beta_c)=-0.0117$$

or

$$\beta_c=-0.0026$$

if $\beta_D=0$.

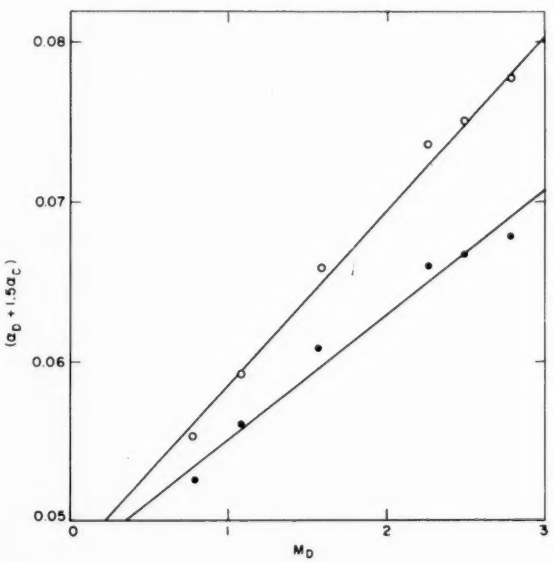

FIGURE 2. $(\alpha_D+1.5\alpha_c)$ *versus* M_D

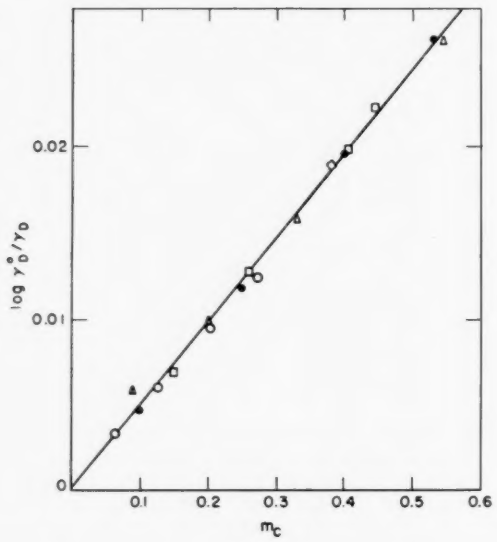

FIGURE 3. *Variation of the activity coefficient of potassium chloride on addition of barium chloride.*

$m \sim 0.8$

We now examine the data for the most concentrated solutions (set 6), because it is here that square terms in eq (9) and eq (10) will be more readily discerned. But in these concentrated solutions, the activity coefficient of potassium chloride is almost constant; log γ_D changes by only 0.0031 at the most and $\alpha_D=0.0018$ gives an adequate description of the change in log γ_D with a change in m_c as demanded by eq (3). It is, therefore, unlikely that there is a significant term in m_c^2 in eq (9).

Moreover, we can use the data for the activity coefficient of potassium chloride derived from the more dilute solutions (set 1); we find that log γ_D changes by a larger amount—as much as 0.0263. These values of log γ_D°/γ_D have been plotted in figure 3; there is no indication of curvature and hence a linear term only is needed as in eq (3).

We return to the data for set 6 and examine the variation of log γ_c with m_D. Figure 4 is a plot of log γ_c°/γ_c against m_D; some curvature is apparent and the best fit to the data is found, by the method least squares, to be log $\gamma_c^\circ/\gamma_c=0.0496\ m_D-0.0025\ m_D^2$. The data for set 4 also show slight curvature when log γ_c°/γ_c is plotted against m_D, the curvature corresponding to $\beta_c=-0.0032$. We now try a value between these two, say $\beta_c=-0.0030$.

Table 4 gives the activity coefficient of barium chloride in the solutions of set 6 calculated from the isopiestic data. The fourth column gives calculated values assuming that eq (2) holds, with only one parameter, $\alpha_c=0.0441$. The last column gives values calculated by the two-parameter equation (10) with $\alpha_c=0.0508$, $\beta_c=-0.0030$. Inspection of the last two columns shows that, in general, the two-parameter equation is superior to the one-parameter equation. The average difference between log γ_D observed and that calculated by the linear equation is 0.0025, between log γ_D observed and that calculated by the quadratic equation is 0.0009. The data for the other five sets of results in table 1 have been recalculated assuming $\beta_c=-0.0030$ throughout. The best values of α_c, together with the α_D values of table 3 and values of $(\alpha_D+1.5\alpha_c)$, are given in table 5. This table also gives average differences between "observed" values of log γ_c and those calculated by the α_c parameters of table 4 and $\beta_c=-0.0030$.

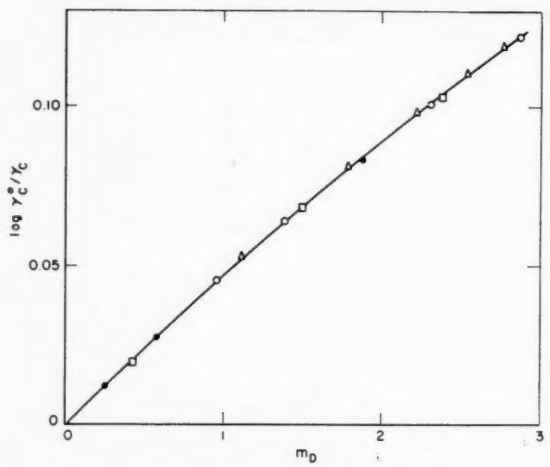

FIGURE 4. *Variation of the activity coefficient of barium chloride on addition of potassium chloride.*

$m \sim 2.8$

These values of $(\alpha_D+1.5\alpha_c)$ are plotted as the upper line in figure 2. The slope of the line, according to eq (11) corresponds to $\beta_c=-0.0036$ if $\beta_D=0$. This is in reasonable but not very good agreement with the value of $\beta_c=-0.0030$ which we used above.

TABLE 4. *Activity coefficient of barium chloride in potassium chloride solutions*

$m \sim 2.8$.

m_D	m_C	log γ_c°/γ_c		
		obs	calc[a]	calc[b]
0.2539	1.4896	0.0124	0.0112	0.0127
.5746	1.3145	.0276	.0254	.0282
1.8855	0.5384	.0829	.0832	.0851
2.7188	--------	.1148	.1199	.1159
1.1054	1.0389	0.0532	0.0487	0.0524
1.7890	0.6282	.0816	.0789	.0813
2.2111	.3630	.0986	.0975	.0976
2.5365	.1524	.1104	.1119	.1096
2.7661	--------	.1189	.1220	.1175
0.4287	1.4251	0.0196	0.0189	0.0213
1.5011	0.8090	.0680	.0662	.0695
2.3901	.2521	.1027	.1054	.1043
2.7763	--------	.1179	.1224	.1179
0.9462	1.1832	0.0456	0.0417	0.0454
1.3772	0.9332	.0644	.0607	.0643
2.3016	.3635	.1013	.1015	.1010
2.8600	--------	.1230	.1261	.1208

[a] Calculated by eq (2) with $\alpha_c=0.0441$.
[b] Calculated by eq (10) with $\alpha_c=0.0508$ and $\beta_c=-0.0030$.

The discrepancy may be due to a small β_D term which would be difficult to detect; it may also be due to a possible variation of β_c with M_D.

Figure 5 illustrates the variation of activity coefficient at constant total ionic concentration. The plots on the left refer to a total ionic concentration of 1, those on the right to a total ionic concentration of 2.5. The data for NaCl-$BaCl_2$ were taken from the previous paper [1].

TABLE 5. *Parameters of eq (9) and eq (10)*

Set	M_D (mean)	α_D	α_c	$(\alpha_B+1.5\alpha_c)$	Δ^a
1	0.7858	0.0484	0.0046	0.0553	0.0006
2	1.0743	.0301	.0194	.0592	.0001
3	1.5678	.0152	.0337	.0658	.0005
4	2.2622	.0053	.0455	.0736	.0004
5	2.4938	.0035	.0477	.0751	.0004
6	2.7803	.0018	.0508	.0777	.0011

$\beta_D=0, \beta_c=-0.0030$

[a] Δ is the average difference between log γ_c (obs.) and that calculated by eq (10), using the recorded values of α_c and $\beta_c=-0.0030$.

At a total ionic concentration of 1 there is not much variation of the activity coefficient of any component when one is replaced by another; for example the top curve at the left shows that $-\log \gamma_{NaCl}=0.1825$ in a solution containing sodium chloride only and 0.1929 when $x=0.5$, $m_B=0.5$, $m_c=0.333$. In the limiting case where the solution contains no sodium chloride and the barium chloride concentration is 0.667, $-\log \gamma_{NaCl}=0.2032$.

It will be seen that the addition of barium chloride to a solution of sodium chloride decreases the activity coefficient of sodium chloride; conversely, the addition of sodium chloride to a solution of barium chloride increases the activity coefficient of barium chloride; in other words, on admixture, the activity coefficients of the two solutes come closer together. This occurs so often that it might be termed the "expected" behavior. One of the few exceptions known occurs in the hydrochloric acid-lithium chloride system [5] at high concentrations where the addition of lithium chloride to a solution of hydrochloric acid "unexpectedly" *increases* the activity coefficient of hydrochloric acid.

In the potassium chloride-barium chloride system at a total ionic concentration of 1, neither salt has much influence on the activity coefficient of the other. But each salt decreases the activity coefficient of the other, and here we see an example of unusual salt interaction.

Turning now to a consideration of the systems at a total ionic concentration of 2.5, in the system sodium chloride-barium chloride, the activity coefficient of sodium chloride is raised on admixture with barium chloride but that of barium chloride is lowered on admixture with sodium chloride. The activity coefficients become more separated on admixture but only by a small amount. The separation effect is much more marked in the potassium chloride-barium chloride system. The effect of barium chloride on the activity coefficient is "normal", lowering the activity coefficient of potassium chloride in its own solution at $2.5m$, $\gamma_{KCl}=0.569$, to $\gamma_{KCl}=0.562$ in the limiting case where the solution contains only barium chloride. But the effect of potassium chloride on the activity coefficient of barium chloride is marked. Thus, $\gamma_c=0.446$ for a solution containing barium chloride only at $m=2.5$, $m_c=1.667$. This is decreased further by the addition of potassium chloride and in the limiting case where the solution contains potassium chloride only at a concentration of 2.5 m, $\gamma_c=0.354$.

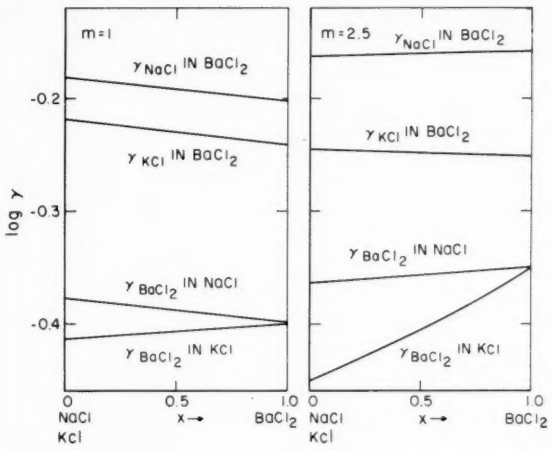

FIGURE 5. *Activity coefficients of the systems* NaCl-$BaCl_2$ *and* KCl-$BaCl_2$.

4.3. Activity Coefficients at Constant Total Ionic Strength

The isopiestic method used in this work is well adapted for a study of systems at constant total ionic concentration and not so suitable for systems at constant total ionic strength. Nevertheless, it is of interest to obtain some description, if only approximate, of such systems. The procedure is as follows. By definition,

$$I=m_D+3m_c \tag{12}$$

and we have defined m as

$$m=m_D+1.5m_c, \tag{13}$$

hence

$$I=m+1.5m_c=m(1+x)$$
$$=\frac{M_D}{R}(1+x)=M_D\frac{1+x}{1-ax-bx^2} \tag{14}$$

or

$$bIx^2+(aI+M_D)x-(I-M_D)=0. \tag{15}$$

Then, for any value of M_D corresponding to an entry in table 1 and for any selected value of I, x

can be calculated using the values of a and b given in table 2. For example, if $M_D=2.4938$, $a=0.0151$, $b=-0.1170$, then the solution of eq (15) for $I=3.5$ is $x=0.4241$. By eq (4), $R=1.0147$ and so $m=2.4577$, $m_D=1.4154$, $m_c=0.6949$. For this value of M_D the integral term of eq (7) is $-0.0204x^2M_D\varphi=-0.0085$. At $M_D=2.4938$, log $\Gamma_D=-0.2448$ [4] and log $R=0.0063$ so that, by eq (5), log $\gamma_D=-0.2470$. But at this total ionic strength, log $\gamma_D^\circ=-0.2427$ and if the equations

$$\log \gamma_D=\log \gamma_D^\circ-\alpha_D I_c \qquad (16)$$

$$\log \gamma_c=\log \gamma_c^\circ-\alpha_c I_B \qquad (17)$$

hold, then $\alpha_D=0.0021$. Note that, in order not to introduce too many symbols, α_D has been used with different meanings in eq (3) and eq (16) and also α_c in eq (2) and eq (17).

In this way, values of α_D and α_c at various values of I have been evaluated and are given in table 6 along with values of $(2\alpha_D+\alpha_c)$. As was shown before [1], if eq (16) and eq (17) hold, which means that there are no terms such as $\beta_D I_c^2$, then $(2\alpha_D+\alpha_c)$ must be independent of I. It is clear from figure 6 that this quantity is not independent of I. The dependence of $(2\alpha_D+\alpha_c)$ on I is given by

$$(2\alpha_D+\alpha_c)=\text{constant}-2(2\beta_D+\beta_c). \qquad (18)$$

TABLE 6. *Parameters of eq (16) and eq (17)*

I	α_D	α_c	$(2\alpha_D+\alpha_c)$
1.0	−0.008	0.033	0.017
1.5	−.003	.025	.019
2.0	−.002	.022	.018
2.5	0	.021	.021
3.0	+0.001	.021	.023
3.5	.002	.020	.024
4.0	.003	.021	.027

The variation of $(2\alpha_D+\alpha_c)$ with I (fig. 6) suggests that $(2\beta_D+\beta_c)$ is about 0.0033. This would be consistent with both β_D and β_c having values about 0.001 but in the absence of more extensive data it is not possible to assign an accurate value to $(2\beta_D+\beta_c)$ or to say how it is divided between β_D and β_c.

The data in figure 6 suggest that α_c may have very large values in dilute solution and α_D large, negative values. This cannot be stated with certitude until more data are available in dilute solutions, but it would not be inconsistent with the behavior found in other systems, for example, hydrochloric acid-cesium chloride [6].

The α_D and α_c parameters are small compared with those found for the hydrochloric acid-barium chloride system [7], but comparable with those for the sodium chloride-barium chloride system [1]. There is one remarkable difference, however, in that α_c has positive values at all values of I accessible to calculation. This means that potassium chloride decreases the activity coefficient of barium chloride in systems at constant total ionic strength.

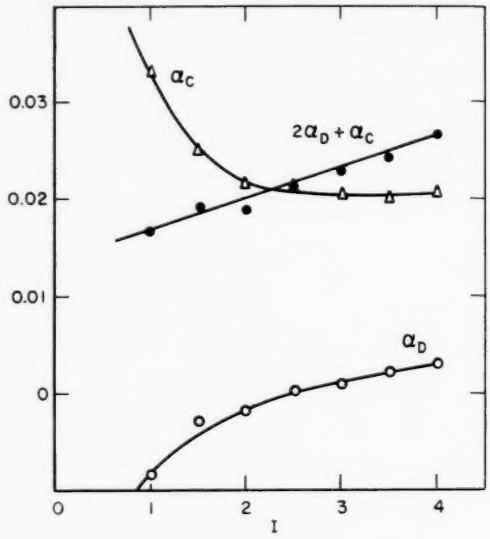

FIGURE 6. *Parameters of eq (16) and eq (17).*

Shonhorn and Gregor [8] have made measurements of the potassium chloride-barium chloride system using as one electrode multilayer membranes of barium stearate. They found $\alpha_D=-0.044$, $\alpha_c=-0.072$ at $I=0.6$ and $\alpha_D=-0.058$, $\alpha_c=-0.081$ at $I=1.5$. These are very different to the values we have found; at this stage we can do little more than note the difference; we might perhaps say that the reversibility of this electrode to barium ions could be questioned and suggest that measurements on this system with a potassium glass electrode would be useful.

5. Excess Free Energy of Mixing

By this we mean the excess free energy when a solution of potassium chloride and another solution of barium chloride are mixed under specified conditions.[2] We are particularly interested in the condition of constant total ionic concentration. This results if a solution of y_D kg of water containing potassium chloride sufficient to give a molality m is mixed with a solution of y_c kg of water containing barium chloride sufficient to give a molality $m/1.5$, $(y_D+y_c=1)$. This gives a solution containing 1 kg of water, y_D m moles of potassium chloride and y_c $m/1.5$ moles of barium chloride. For example, a solution containing 0.5 kg of water and 0.75 mole of potassium chloride (molality 1.5, total ionic concentration 1.5) might be mixed with a solution containing 0.5 kg of water and 0.5 moles of barium chloride (molality 1.0, total ionic concentration 1.5). The result would be a solution containing 1 kg of water, 0.75 m to potassium chloride, 0.5 m to barium chloride, of total ionic concentration 1.50.

[2] The *total* free energy of mixing contains a term which, for 1:1-electrolytes, is $2RT\ m\ [y_B \ln y_B+y_c \ln y]$. This is ignored in calculating the *excess* free energy of mixing (see appendix).

The general equations for the excess free energy of mixing are developed in the appendix to this paper. For the case where potassium chloride and barium chloride solutions are mixed without change in total ionic concentration and the final molalities are such that $m_D=1.5m_c$ and $\beta_D=0$ in eq (9),

$$\frac{\Delta G^E}{2.303RT}=-m_Dm_c(\alpha_D+1.5\alpha_c)-4.5m_Dm_c^2\beta_c$$

$$=-\frac{m^2}{6}(\alpha_D+1.5\alpha_c)-\frac{m^3}{4}\beta_c.$$

Using values of $(\alpha_D+1.5\alpha_c)$ interpolated at round values of m from table 5, values of ΔG^E have been calculated. These are given in table 7. They are remarkable in being comparatively large (and negative). In this respect they contrast with corresponding data for the mixture of solutions of sodium chloride and barium chloride where no free energy of mixing exceeding 1 cal mol^{-1} is found. This is a consequence of the comparatively large values of $(\alpha_D+1.5\alpha_c)$ for the potassium chloride-barium chloride system and the almost negligible values of $(\alpha_D+1.5\alpha_c)$ for the sodium chloride-barium chloride system.

TABLE 7. *Excess free energy of mixing* [a]

Constant total ionic concentration		Constant total ionic strength			
m	KCl-$BaCl_2$	I	KCl-$BaCl_2$	NaCl-$BaCl_2$	HCl-$BaCl_2$
	ΔG^E		ΔG^E	ΔG^E	ΔG^E
0.75	−7	1.0	−3	−2	−10
1.0	−12	1.5	−7	−4	----
1.5	−30	2.0	−12	−7	−33
2.0	−55	2.5	−22	−11	----
2.5	−93	3.0	−35	−17	−72
3.0	−134	3.5	−50	−26	----
		4.0	−73	−35	----

[a] In calories per kg of water, 1 calorie=4.1840 J.

It is also shown in the appendix that for a system with $\beta_D=\beta_c=0$, the excess free energy of mixing at constant total ionic strength with $I/2=I_D=I_c$, is

$$\frac{\Delta G^E}{2.303RT}=-\frac{I^2}{8}(2\alpha_D+\alpha_c).$$

Values of ΔG^E have been calculated using $(2\alpha_D+\alpha_c)$ values from table 6. The results are given in table 7 along with values of ΔG^E for the hydrochloric acid-barium chloride [7] and sodium chloride-barium chloride [1] systems. It will be noted that in the potassium chloride-barium chloride system, the decrease in free energy on mixing is much larger at constant total ionic concentration than at constant total ionic strength. At constant total ionic strength, the values are greatest in the hydrochloric acid-barium chloride system and least in the sodium chloride-barium chloride system. This suggests that, with increasing atomic number of the univalent cation, there is a minimum in the free energy decrease at the sodium chloride-barium system.

These excess free energies of mixing, the one at constant total ionic concentration, the other at constant total ionic strength, are not independent. This can be shown by the following example. Consider an admixture process represented schematically by:

1 | 0.5 kg H_2O
1.333 moles of D

\+

2 | 0.5 kg H_2O
0.889 moles of C

$\longrightarrow$ | 1 kg H_2O
1.333 moles of D
0.889 moles of C

Each of the single salt solutions has a total ionic concentration of $m=2.667$ and so has the solution formed after mixing. The excess free energy of mixing, interpolated from table 7, is −107 cal per kg water.

The same mixed solution could, however, be made by a process at constant total ionic strength:

3 | 0.333 kg H_2O
1.333 moles of D

\+

4 | 0.667 kg H_2O
0.889 moles of C

$\longrightarrow$ | 1 kg H_2O
1.333 moles of D
0.889 moles of C

Each of the single salt solutions has a total ionic strength $I=4$ and so has the solution formed after mixing. The free energy of mixing at $I=4$ is recorded in table 7 as −73 cal per kg of water. This, however, refers to mixing which produces a solution in which potassium chloride and barium chloride are present at equal ionic strength, the concentration of potassium chloride being $2m$ and that of barium chloride $0.667m$. We are now discussing the position when $I_D=m_D=1.333$, $m_c=0.889$, $I_c=2.667$. It is shown in the appendix to this paper that the excess free energy of mixing (if $\beta_D=\beta_c=0$) is given by:

$$\frac{\Delta G^E}{2.303RT}=-\frac{1}{2}I_DI_c(2\alpha_D+\alpha_c)$$

or, using the values of α_D and α_c given in table 6 at $I=4$,

$$\Delta G^E=-65 \text{ cal per kg of water.}$$

The excess free energy of the solutions in boxes 3 and 4 above over that of the solutions in boxes 1 and 2

is given by:

$$\frac{\Delta G}{RT}=\frac{1}{3}[-2m_3\varphi_3+2m_3\ln\gamma_3]+\frac{2}{3}[-3m_4\varphi_4+3m_4\ln\gamma_4]$$

$$-\frac{1}{2}[-2m_1\varphi_1+2m_1\ln\gamma_1]-\frac{1}{2}[-3m_2\varphi_2+2m_2\ln\gamma_2]$$

where the subscripts refer to the values of m, φ, and γ appropriate to the solutions represented by each of the four boxes. Substituting these values of m, φ, and γ [1, 4], we find $\Delta G=-47$ cal per kg of water. Thus we could produce the mixed solution by two routes. The solutions represented by boxes 1 and 2 could be mixed without change in total ionic concentration and with a decrease of free energy of 107 cal per kg of water. Alternatively, they could be converted into the solutions represented by boxes 3 and 4 and then mixed without change in total ionic strength. The decrease in free energy would be $65+47=112$ cal per kg of water. The decrease in free energy should be the same by either route. Exact agreement cannot be expected because of errors due to interpolation and because of the possibility of a β term in eq (17) which would affect the value of -65 cal per kg of water for the free energy of mixing at constant total ionic strength. The agreement is good enough, however, to show that there is internal consistency between the results at constant total ionic strength and those at constant total ionic concentration.

6. Appendix

Equations for the excess free energy of a solution of two electrolytes are derived as follows [6, 9, 10, 11].

Consider a solution of electrolyte B (giving ν_B ions) at molality m_B, and electrolyte C (giving ν_c ions) at molality m_c. Let ζ be a linear combination of the form

$$\zeta=k_Bm_B+k_cm_c$$

and let y_B, y_c be defined by

$$y_B=k_Bm_B/\zeta,\ y_c=k_cm_c/\zeta,\ y_B+y_c=1.$$

Let the activity coefficients of B and C be given by

$$\ln\gamma_B=\ln\gamma_B^0+A_Bm_c+B_Bm_c^2$$

$$\ln\gamma_c=\ln\gamma_c^0+A_cm_B+B_cm_B^2$$

subject to the condition that ζ is constant; here A_B, A_c are functions of ζ but not of m_B, m_c independently and B_B, B_c are parameters independent of ζ, m_B, and m_c. If both electrolytes are of the 1:1 type, $\nu_B=\nu_c=2$, it is convenient to put $k_B=k_c=1$ and $\zeta=m=m_B+m_c$. The change in free energy on mixing is that for a process which can be represented schematically:

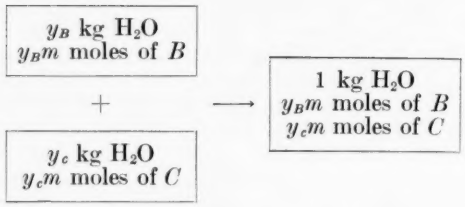

With respect to B the increment in free energy is $2RTm_B\ln(m_B\gamma_B/m\gamma_B^\circ)$ and with respect to m_c it is $2RTm_c\ln(m_c\gamma_c/m\gamma_c^\circ)$. Thus the increment due to B and C can be written

$$2RTm[y_B\ln y_B+y_c\ln y_c]$$

$$+2RT[m_B\ln\gamma_B/\gamma_B^\circ+m_c\ln\gamma_c/\gamma_c^\circ].$$

The first of these terms will occur in the expression for the free energy increment on mixing even ideal solutions and is not considered part of the *excess* free energy of mixing. An analogous term is found in the expression for the *total* entropy of mixing but not in the expression for the enthalpy of mixing.

The second term,

$$2RT[m_B\ln\gamma_B/\gamma_B^\circ+m_c\ln\gamma_c/\gamma_c^\circ]$$

$$=2RT[m_B(A_Bm_c+B_Bm_c^2)+m_c(A_cm_B+B_cm_B^2)],$$

is part of the free energy change resulting from departures from ideality. This, together with changes in the solvent free energy, constitutes the *excess* free energy of mixing.

In the more complicated case of two electrolytes of different valence type, we can represent the mixing process as:

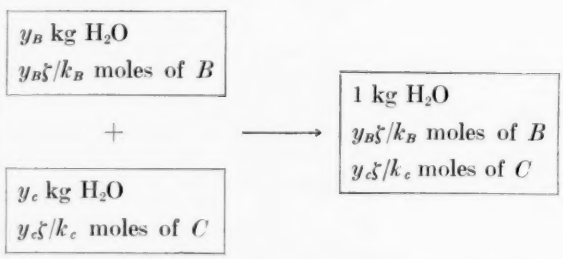

where all three solutions have the same value of ζ. With respect to B the excess free energy is

$$\nu_BRTm_B\ln\gamma_B/\gamma_B^0=\nu_BRTm_B(A_Bm_c+B_Bm_c^2)$$

and with respect to C the excess free energy is

$$\nu_cRTm_c\ln\gamma_c/\gamma_c^0=\nu_cRTm_c(A_cm_B+B_cm_B^2).$$

As before, the free energy increment of the solvent remains to be computed.

The solvent effect can be evaluated as follows.

The Gibbs-Duhem equation can be written:

$$-55.51d\ln a_w=\nu_B m_B d\ln m_B+\nu_c m_c d\ln m_c$$
$$+\nu_B m_B d\ln\gamma_B+\nu_c m_c d\ln\gamma_c.$$

The first two terms on the right can be written

$$\zeta\left(\frac{\nu_B}{k_B}-\frac{\nu_c}{k_c}\right)dy_B.$$

The third term is

$$-\frac{\nu_B y_B}{k_B k_c}\zeta^2\left(A_B+\frac{2B_B y_c}{k_c}\zeta\right)dy_B$$

and the fourth term

$$\frac{\nu_c y_c}{k_B k_c}\zeta^2\left(A_c+\frac{2B_c y_B}{k_B}\zeta\right)dy_B.$$

Consequently

$$-55.51d\ln a_w=\zeta\left(\frac{\nu_B}{k_B}-\frac{\nu_c}{k_c}+\frac{\nu_c\zeta}{k_B k_c}A_c\right)dy_B$$
$$-\frac{\zeta^2}{k_B k_c}(\nu_B A_B+\nu_c A_c)y_B dy_B$$
$$-\frac{2\zeta^3}{k_B k_c}\left(\frac{\nu_B B_B}{k_c}-\frac{\nu_c B_c}{k_B}\right)y_B y_c dy_B.$$

On integration from $y_B=0$ to y_B,

$$-55.51\ln\frac{a_w}{a_{w(c)}}=\zeta\left(\frac{\nu_B}{k_B}-\frac{\nu_c}{k_c}+\frac{\nu_c\zeta}{k_B k_c}A_c\right)y_B$$
$$-\frac{\zeta^2}{2k_B k_c}(\nu_B A_B+\nu_c A_c)y_B^2$$
$$-\frac{\zeta^3}{k_B k_c}\left(\frac{\nu_B B_B}{k_c}-\frac{\nu_c B_c}{k_B}\right)\left(y_B^2-\frac{2y_B^3}{3}\right)$$

where a_w is the water activity of the mixed solution and $a_{w(c)}$ that of the solution containing C only. On integration from $y_B=1$ to y_B,

$$-55.51\ln\frac{a_w}{a_{w(B)}}=\zeta\left(\frac{\nu_c}{k_c}-\frac{\nu_B}{k_B}+\frac{\nu_B}{k_B k_C}\zeta A_B\right)y_c$$
$$-\frac{\zeta^2}{2k_B k_c}(\nu_B A_B+\nu_c A_c)y_c^2+\frac{\zeta^3}{k_B k_c}\left(\frac{\nu_B B_B}{k_c}-\frac{\nu_c B_c}{k_B}\right)\left(y_c^2-\frac{2y_c^3}{3}\right)$$

where $a_{w(B)}$ is the water activity of the solution containing B only.

The total excess free energy is

$$\frac{\Delta G^E}{RT}=\nu_B m_B\ln\frac{\gamma_B}{\gamma_B^0}+\nu_c m_c\ln\frac{\gamma_c}{\gamma_0^c}$$
$$+55.51y_B\ln\frac{a_w}{a_{w(B)}}+55.51y_c\ln\frac{a_w}{a_{w(c)}}$$

which reduces to

$$\frac{\Delta G^E}{RT}=\frac{\zeta^2}{2k_B k_c}y_B y_c(\nu_B A_B+\nu_c A_c)$$
$$+\frac{\zeta^3}{k_B k_c}y_B y_c\left\{\left(\frac{\nu_B}{k_c}y_B B_B+\frac{\nu_c}{k_B}y_c B_c\right)\right.$$
$$\left.-\frac{2}{3}\left(\frac{\nu_B B_B}{k_c}-\frac{\nu_c B_c}{k_B}\right)(y_B-y_c)\right\}.$$

Putting $\nu_B=\nu_c=2$, $k_B=k_c=1$,

$$\zeta=m_B+m_c,$$

$$\frac{\Delta G^E}{RT}=m_B m_c\left[(A_B+A_c)+2\left\{(m_B B_B+m_c B_c)\right.\right.$$
$$\left.\left.-\frac{2}{3}(B_B-B_c)(m_B-m_c)\right\}\right]$$

and when $y_B=y_c=0.5$, $A_B=-2.303\alpha_B$, $A_c=-2.303\alpha_c$, $B_B=-2.303\beta_B$, $B_c=-2.303\beta_c$,

$$\log\gamma_B=\log\gamma_B^0-\alpha_B m_c-\beta_B m_c^2$$
$$\log\gamma_c=\log\gamma_c^0-\alpha_c m_B-\beta_c m_B^2$$
$$\frac{\Delta G^E}{2.303RT}=-\frac{m^2}{4}[(\alpha_B+\alpha_c)+m(\beta_B+\beta_c)].$$

For a mixture of sodium chloride and barium chloride at constant total ionic strength, we put $\nu_B=2$, $\nu_c=3$, $k_B=1$, $k_c=3$, $A_B=-3\times2.303\alpha_B$, $A_c=-2.303\alpha_c$, $B_B=-9\times2.303\beta_B$, $B_c=-2.303\beta_c$, $\zeta=I=I_B+I_c=m_B+3m_c$,

$$\log\gamma_B=\log\gamma_B^0-\alpha_B I_c-\beta_B I_c^2$$
$$\log\gamma_c=\log\gamma_c^0-\alpha_c I_B-\beta_c I_B^2$$
$$\frac{\Delta G^E}{2.303RT}=-\frac{1}{2}I_B I_c(2\alpha_B+\alpha_c)$$
$$-I_B I_c\left\{2\beta_B I_B+\beta_c I_c-\frac{2}{3}(2\beta_B-\beta_c)(I_B-I_c)\right\}$$

and when $I_B=I_c$, $I/2=I_B=I_c$,

$$\frac{\Delta G^E}{2.303RT}=-\frac{I^2}{8}\{(2\alpha_B+\alpha_c)+I(2\beta_B+\beta_c)\}$$

and when $\beta_B=\beta_c=0$

$$\frac{\Delta G^E}{RT}=-\frac{I^2}{8}(2\alpha_B+\alpha_c).$$

For the condition of constant total ionic concentration, we put $\nu_B=2$, $\nu_c=3$, $k_B=1$, $k_c=1.5$,

$$\zeta = m_B + 1.5m_c = m,$$

$$A_B = -2.303\alpha_B,\ A_c = -2.303\alpha_c,$$

$$B_B = -2.303\beta_B,\ B_c = -2.303\beta_c,$$

$$\log \gamma_B = \log \gamma_B^0 - \alpha_B m_c - \beta_B m_c^2$$

$$\log \gamma_c = \log \gamma_c^0 - \alpha_c m_B - \beta_c m_B^2$$

$$\frac{\Delta G^E}{2.303RT} = -m_B m_c(\alpha_B + 1.5\alpha_c) - m_B m_c\left\{\frac{2}{1.5}m_B\beta_B + 4.5m_c\beta_c - \frac{2}{3}\left(\frac{2\beta_B}{1.5} - 3\beta_c\right)(m_B - 1.5m_c)\right\}$$

and if $m_B = 1.5m_c$, $m = 2m_B = 3m_c$, $\beta_B = 0$,

$$\frac{\Delta G^E}{2.303RT} = -\frac{m^2}{6}(\alpha_B + 1.5\alpha_c) - \frac{m^3}{4}\beta_c.$$

Grateful acknowledgment is made to the Office of Saline Water for a grant in partial support of this work.

7. References

[1] R. A. Robinson and V. E. Bower, J. Res. NBS 69A (Phys. and Chem.) No. 1, 19 (1965).
[2] H. A. C. McKay and J. K. Perring, Trans. Faraday Soc. **49,** 163 (1953).
[3] V. E. Bower and R. A. Robinson, J. Res. NBS 69A (Phys. and Chem.) p. 131 (1965).
[4] R. A. Robinson and R. H. Stokes, Electrolyte solutions, Appendix 8.3, 2d. ed., (Butterworths Scientific Publications, London, 1959).
[5] J. E. Hawkins, J. Am. Chem. Soc. **54,** 4480 (1932).
[6] H. S. Harned and B. B. Owen, The physical chemistry of electrolytic solutions, ch. 14, 3d. ed. p. 610, (Reinhold Publ. Corp., New York, N.Y., (1958).
[7] H. S. Harned and R. Gary, J. Am. Chem. Soc. **76,** 5924 (1954).
[8] H. Schonhorn and H. P. Gregor, J. Am. Chem. Soc. **83,** 3576 (1961).
[9] H. S. Harned, J. Phys. Chem. **63,** 1299 (1959).
[10] H. S. Harned, J. Phys. Chem. **64,** 112 (1960).
[11] H. A. C. McKay, Disc. Faraday Soc. **24,** 76 (1957).

(Paper 69A5-365)

JOURNAL OF RESEARCH of the National Bureau of Standards—A. Physics and Chemistry
Vol. 69A, No. 5, September–October 1965

A Wide-Range (up to 10^{10} P) Rotating Cylinder Viscometer

Albert Napolitano, Pedro B. Macedo, and Earl G. Hawkins

(May 17, 1965)

The range of a high temperature rotating cylinder viscometer has been extended so that viscosity measurements can be made between 10^0 to 10^{10} poises to within 2-percent accuracy. This involves three different techniques. After a calibration constant has been determined for the apparatus in the standard oil range, the other two constants for the higher viscosities were self-determined. In making measurements at the low viscosities, 10^0 to 10^5 poises, the outer cylinder is rotated at constant speed and the torque measured on the inner cylinder; from $10^{4.5}$ to $10^{7.5}$ poises the inner cylinder is rotated through an angle and timed as it returns to its zero position, and from $10^{5.5}$ to 10^{10} poises the inner cylinder is driven through an angle at constant torque and timed as it traverses this angle. The Fulcher equation viscosity values obtained from previous measurements on Standard Glasses No. 710 and No. 711 by the fiber elongation and rotating cylinder methods have been compared with the present results.

1. Introduction

In 1924, English [1] [1] reviewed methods for measuring viscosity of glasses and concluded that the Margules [2] rotating cylinder technique was readily adaptable to this work and gave much more reliable and repeatable results than the previous techniques. His apparatus consisted of a fixed cup and an inner rotating cylinder driven by the torque produced from a counter-weight and pulley system. With this equipment English was able to make viscosity measurements from 10^1 to 10^7 poises [2] on soda-lime-silica glasses. Later Parks et al., [3,4] using the same technique, made viscosity measurements on B_2O_3 glass from 10^5 to 10^{11} P.

About this time Field [5] and Lillie [6], working with molten glasses, improved the rotating cylinder viscometer by eliminating the disadvantages inherent in the counter-weight and pulley system. They rotated the cup at a constant angular velocity and measured the force on the inner cylinder by means of the angle of deflection of a torsion wire. This not only allowed Lillie to measure absolute viscosities but also gave him a higher degree of accuracy. This method was useful in the range 10 to 10^5 P.

Lillie went still further and extended the range of his viscometer by developing the aperiodic method of measuring viscosities. In this method the inner cylinder was deflected and allowed to decay to equilibrium as the outer cylinder remained at rest. This extended the range of his viscometer up to 10^7 P.

In later years, other glass investigators such as Babcock [7], and Robinson and Peterson [8], have used equipment similar to Lillie's because of the comparatively high accuracy. A further improvement to Lillie's apparatus was made by Bockris and Lowe [9], who inserted in the suspension system of the inner cylinder a coil and magnet for electromagnetically measuring the torque on the inner cylinder. Their apparatus was used to make viscosity measurements on molten silicates in the range $10^{-1.3}$ to $10^{+4.2}$ P and up to 1800 °C.

The rotating cylinder apparatus has become, over the years, a standard method for measuring viscosities of glasses at high temperatures, but other techniques had to be developed to determine viscosities above 10^7 P. Above 10^9 P the fiber elongation method of measuring viscosities has proven to be both reliable and accurate. In the gap between these two methods there has been relatively little work.

Hampton [10] measured viscosities from 10^8 to 10^{13} P observing the rate of deflection of a beam held in cantilever fashion. Recently, Hagy [11] developed a method of determining the viscosity in the range 10^8 to 10^{15} P by the viscous bending of a simple beam under load. Kelley [12] et al., have developed a penetrometer to measure viscosity of glasses from $10^{5.7}$ to 10^9 P by measuring the rate of penetration of a solid cylinder under load into the glass.

Even though measurements can now be made continuously over the whole viscosity range of glasses by various techniques, it seems desirable to make measurements with the rotation viscometer over as wide a range as possible since it has proven to be the most reliable and accurate apparatus that has been used in this work.

2. Apparatus

The geometry of this apparatus, see figure 1, is similar to that of Lillie [6], Bockris and Lowe [9]. This equipment has been previously described in more detail by Napolitano and Hawkins [13].

The outer cylinder consisted of a platinum crucible 5 cm in diam and 10 cm high. The bob was 1.25 cm in diam 3.75 cm long with 45° tapered ends and was suspended by a hollow platinum spindle extending into the center of the bob to accommodate a thermocouple for measuring the temperature of the glass

[1] Figures in brackets indicate the literature references at the end of this paper.
[2] One poise is 1 g/cm sec which is equal to 0.1 kg/m sec.

780-567—65——5

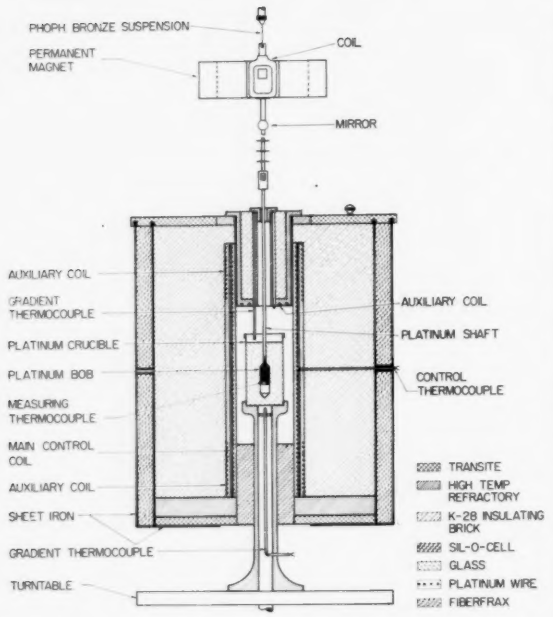

FIGURE 1. *Wide-range high temperature rotating cylinder viscometer.*

before and after viscosity measurements. The crucible was mounted on a mullite pedestal which extended out through the bottom of the furnace and was attached to the rotating mechanism. The rotating mechanism provided a range of crucible speeds from 0.03029 rpm to 1.3493 rpm.

An electromagnetic torque balance [9] based on the principle of a large moving coil galvanometer was used to measure the torque by a null detection method. The galvanometer was made up of a permanent magnet with a 1650 G gap field strength and a coil which was an integral part of the suspension apparatus. The coil consisted of a rectangular aluminum frame with about 25 m of No. 34 insulated copper wire, wound around it. The resistance of the coil was 222 Ω. In series with the coil were several resistors which allowed continuous adjustment between 2 kΩ and 5 MΩ and four L and N Standard Fixed Resistors 10, 25, 100, and 1000 Ω. The source of power consisted of 12–2 V cells. The balance was observed through a telescope on a 1 m radius scale located 1 m distant from a reflecting mirror set on the axis of the suspension shaft just below the coil. The amount of current through the coil was found by measuring the voltage across a standard resistor with a Type K potentiometer. Polarity in the coil would be reversed to accommodate reversal of rotation.

3. Operation and Calibration

The extension of the viscosity range of this apparatus was accomplished by operating it in three different modes. A careful examination of its equation of motion is very important before describing each mode of operation. The general equation of motion for the viscometer is

$$I\frac{d^2\theta}{dt^2}+\eta K_1\frac{d\theta}{dt}+K_2\theta=K_3 i \tag{1}$$

I—moment of inertia;
θ—angular displacement;
t—time;
η—dynamic viscosity;
K_1, K_2, and K_3 are constants of the apparatus; and
i—current through coil.

Thus the first term of the equation represents the resistance to acceleration due to inertia. The second term is the viscous drag. The third term represents an elastic torque due to an angular deflection of the suspension, and the last term represents the magnetic torque applied to the system. The limitations of eq (1) are discussed in the appendix.

Method 1. Over the lowest viscosity range[3] log $\eta=0$ to log $\eta=5$ the outer cylinder is rotated at a fixed angular velocity. The viscous drag of the liquid produced a torque on the inner cylinder. A measure of this torque is made by applying an appropriate current to the coil such that the resulting magnetic torque will bring the inner cylinder back to its rest position at $\theta=0$.

Therefore the first term of the eq (1) is zero, because there is no angular acceleration in the system when measurements are being made. The second term is present and significant. It is retained in the equation of motion for Mode I, but since the inner cylinder is held at rest, it is the angular velocity of the outer cylinder that is used in this term. The third term is zero when the system is balanced, since the angle across the suspension is zero. Even so, it controls the sensitivity. By changing suspensions the value of K_2 can be changed and with it the sensitivity. Since the fourth term is significant, it is kept. Thus the equation of motion for Mode I is

$$\eta K_1\frac{d\theta}{dt}=K_3 i \tag{2}$$

or

$$\eta=C_1 i/\omega \tag{3}$$

where $C_1=\dfrac{K_3}{K_1}$ and $\omega=\dfrac{d\theta}{dt}$ (angular velocity).

To obtain C_1 in eq (3) the viscometer was calibrated at 25 and 40 °C with NBS Standard oils. These oils ranged in viscosity from 1 to 500 P. Some of Dow Corning's silicons have also proven to be a valuable check on the calibration constant at the higher viscosities. Thermal expansion corrections on C_1, known for room temperatures, have to be made for accurate viscosity measurements at temperatures, T,

[3] During calibrations (at room temperature) measurements were made for viscosities below 1 P. At elevated temperatures the lower viscosity limit was 10^2 P because of the characteristics of the NBS Standard Glasses and the temperature limit of the furnace.

up to 1400 °C according to the following equation

$$C_1(T)=C_{1_{25\,^\circ C}}(1+\alpha[T-25])^{-3} \tag{4}$$

where α is the linear expansion coefficient of platinum.

TABLE 1. *Typical series of viscosity measurements made on Standard Glass No. 711 by Method I*

Standard resistor 100Ω; 0.030 cm diam. suspension

Rotation	i	ω	N
	μA	rpm	$\mu A/rpm$
Clockwise	149.706	1.3493	
Counter-clockwise	149.605	1.3493	110.91
Clockwise	87.026	.7845	
Counter-clockwise	86.655	.7845	110.70
Clockwise	49.991	.4513	
Counter-clockwise	49.905	.4513	110.68
Clockwise	36.892	.3332	
Counter-clockwise	36.630	.3332	110.34
Clockwise	149.010	1.3493	
Counter-clockwise	148.505	1.3493	110.25
Average			110.58

Temperature before start of measurements was 1050.7 °C and after measurements was 1051.3 °C; the average being 1051.0 °C.

A typical series of viscosity measurements made by this mode of operation is shown in table 1. In making these measurements four different speeds are used with readings taken in the clockwise and counterclockwise rotation for each speed. The first speed selected is always repeated at the end of the series to determine whether the glass viscosity and, therefore, the temperature, has remained essentially constant. Note the slight change in N which reflects the increase in temperature. From these measurements the viscosity is

$$\eta=N\times C_{1_{(1050\,^\circ C)}}=110.6\times10^{-6}\times11.99\times10^{+6}=1326\text{ P}$$

or

$$\log\eta=3.123\text{ at }T=1051\,^\circ C.$$

Method 2. For viscosities from about log $\eta=4.5$ to log $\eta=7.5$ the aperiodic method developed by Lillie is used. In this decay mode of operation the outer cylinder remains at rest while the inner cylinder is displaced by an angle θ and allowed to return to its zero position under the force of the torsion wire. Since the system is an over-damped harmonic oscillator one observes an exponentially decaying angular velocity as the inner cylinder approaches its equilibrium position. The term involving the moment of inertia in eq (1) is extremely small and can be neglected, giving rise to the following equation:

$$\eta\frac{d\theta}{dt}=-C_2\theta \tag{5}$$

where

$$C_2=\frac{K_2}{K_1}.$$

Integrating

$$\int_{\theta_1}^{\theta_2}\eta\frac{d\theta}{\theta}=-\int_{t_1}^{t_2}C_2dt$$

we have

$$\eta=\frac{C_2(t_2-t_1)}{\ln\ \theta_1/\theta_2}. \tag{6}$$

The calibration constant (C_2) for Method II can be calculated once the viscometer has been calibrated by Method I. First an independent measurement of the current required for a given angular deflection of the inner cylinder is made. This gives us:

$$\theta=\frac{K_3}{K_2}i=C_4i. \tag{7}$$

If the current, i, is given in amperes, and the angle, θ, in units of 17′ of arc which correspond to a deflection of 1 cm in a circular scale 1 m distant from the central axis of the spindle; one has

$$C_4=\frac{\theta}{i}=\frac{25}{5.094\times10^{-3}}=4907.7.$$

From eq (3), (5), and (7) one may obtain C_2 from C_1 and C_4, according to the following:

$$C_2=\frac{C_1}{C_4}u \tag{8}$$

where u changes units from revolutions per minute to centimeters per second. The rates in centimeters per second were read on the circular scale.

$$u=\frac{\text{cm}}{\text{sec}}\frac{\text{min}}{\text{revolution}}=\frac{1}{60}\times\frac{2\pi\times100\times2}{1}=20.95.$$

Thus

$$C_2=\frac{20.95\times1.212\times10^6}{4907.7}=5{,}174.$$

TABLE 2. *Typical series of viscosity measurements made on Standard Glass No. 711 by Method II*

0.063 cm diam suspension

Readings	θ_1	θ_2	t_2-t_1
	cm	cm	sec
1	25	2.5	557.31
2	25	2.5	545.40
3	25	2.5	548.49
Average	25	2.5	550.40

Temperature before start of measurements was 704.2 °C and after measurements was 704.4 °C, the average being 704.3 °C.

A typical series of viscosity measurements made by this mode of operation is shown in table 2. A phosphor bronze suspension wire of 0.063 cm diam was used. Before starting, the zero was checked and properly adjusted. The current was applied to the coil so that the inner cylinder was rotated from

its equilibrium position to an angle corresponding to about 30 cm on the telescope scale. The current was turned off and time was measured for the displacement to decay from 25 to 2.5 cm. Thus the viscosity is

$$\eta=\frac{C_{2T}(t_2-t_1)}{\ln \theta_1/\theta_2}=\frac{5174\times 550.4}{2.303}=1.236\times 10^6 P$$

or

$$\log \eta=6.092 \text{ at } T=704.3\ ^\circ\text{C}.$$

Method 3. For viscosities from about log $\eta=5.5$ to log $\eta=10$ this method was used. The outer cylinder again remains at rest, while a torque is applied to the inner cylinder by means of the magnetic field interaction, and the angular velocity is measured about $\theta=0$. Thus the term $K_2\theta$ is negligible and can be omitted. Since measurements are made in a steady state the acceleration is zero, and we have the following:

$$\eta\frac{d\theta}{dt}=\frac{K_3 i}{K_1}=C_3 i \tag{9}$$

integrating

$$\int_{\theta_1}^{\theta_2}\eta d\theta=\int_{t_1}^{t_2} C_3 i dt$$

we have

$$\eta=C_3 i\,\frac{t_2-t_1}{\theta_2-\theta_1}. \tag{10}$$

C_3 and C_1 are equal, but expressed in different units:

$$C_3=uC_1=20.95\times 1.212\times 10^6=2.539\times 10^7, \tag{11}$$

where u is the same conversion factor used in calculating C_2.

TABLE 3. *Typical series of viscosity measurements made on Standard Glass No. 710 by Method III*

Standard resistor 10Ω; 0.063 cm diam suspension

Rotation	$\theta_2-\theta_1$	t_2-t_1	i A×10⁻⁴
	cm	*sec*	
Clockwise	1	197.58	196.13
Counter clockwise	1	195.48	196.13
Clockwise	1	193.62	196.13
Counter clockwise	1	191.42	196.13
Average	1	194.52	196.13

Temperature before start of measurements was 706.0 °C and after measurements was 707.6 °C: the average being 706.8.

A typical series of viscosity measurements made by this mode of operation is shown in table 3. A measured amount of current is applied to the coil, which rotates the inner cylinder at a constant angular velocity. The time required to traverse 1 cm about the equilibrium position ($\theta=0$) on the scale is measured. By appropriately selecting the current, measurements can be made up to log $\eta=10$ P within reasonable waiting periods.

From these measurements the viscosity is

$$\eta=\frac{C_{3T}(t_2-t_1)}{\theta_2-\theta_1}i=2539\times 10^4\times 194.52\times 10\times 196.13\times 10^{-4}$$

$=9.6866\times 10^7$ or log $\eta=7.986$ at $T=706.8$ °C.

4. Discussion of Results

Measurements were made on NBS Standard Viscosity Glasses Nos. 710 and 711. These results are given in tables 4 and 5. Only the measurements made by Methods II and III are listed here, since Method I and the fiber elongation methods of measuring viscosities have been covered in previous work [13, 14].

TABLE 4. *Viscosity values of Standard Glass No. 710 by Methods II and III compared with values calculated from Method I and fiber elongation method**

Temp. °C	log η_{obs}		log η_{calc} Fulcher equation
	Method II	Method III	
951.7	4.581	.....	4.553
902.3	5.028	.....	5.033
851.2	5.629	.....	5.614
810.3	6.169	.....	6.158
774.7	.....	6.718	6.702
773.4	.....	6.734	6.723
757.5	6.999	.....	6.993
757.1	.....	7.013	7.000
725.9	.....	7.608	7.585
706.8	.....	7.986	7.984
693.2	.....	8.298	8.290
677.8	.....	8.675	8.660
657.9	.....	9.178	9.182
636.0	.....	9.827	9.821

*Fulcher equation constants taken from Napolitano and Hawkins (Lab. A) [13

TABLE 5. *Viscosity values of Standard Glass No. 711 by Methods II and III compared with values calculated from Method I and fiber elongation method**

Temp. °C	log η_{obs}		log η_{calc} Fulcher equation
	Method II	Method III	
774.2	5.220	.....	5.229
770.5	5.255	.....	5.270
755.0	5.438	5.436	5.446
734.4	5.696	5.690	5.695
732.0	5.722	5.713	5.725
725.0	5.831	5.813	5.815
704.3	6.092	6.082	6.092
677.6	6.488	6.480	6.482
651.7	.....	6.909	6.900
631.5	.....	7.281	7.256
607.4	.....	7.752	7.723
574.7	.....	8.423	8.454
554.9	.....	8.904	8.924
528.1	.....	9.653	9.674

*Fulcher equation constants from Napolitano and Hawkins (Lab. A) [14].

The viscosity values obtained by the rotation method (Method I) and the fiber elongation method were fitted by a least square calculation to the Fulcher [15] equation. Fulcher stated that an empirical equation of the form

$$\log \eta=A+B/(T-T_0) \tag{12}$$

accurately relates viscosity to temperature in many glasses. These equations become:

$$\log \eta = -1.626 + 4239/(T - 265.7)$$

for St'd. Glass No. 710; (13)

$$\log \eta = -1.654 + 4317/(T - 147.0)$$

for St'd Glass No. 711. (14)

These are shown in figure 2 as the line curves in order to illustrate the viscosity values obtained in this study, and to compare the results from Methods II and III with previous measurements. The viscosity values obtained by these methods for the two standard glasses fall so close to the curves obtained from the previous measurements, that no deviation can be seen. In order to inspect these deviations more closely, the observed viscosity values were compared with the values calculated from eqs (13) and (14), for each temperature. These deviations are plotted in figure 3 as well as those from Method I and from the fiber elongation method. The gap in rotation and fiber elongation measurements has been bridged. Using all four techniques one can make measurements over a continuous viscosity range from 10^1 to 10^{12} P. The scatter of the viscosity values obtained by the driving technique is less than that obtained from the fiber elongation technique.

In figure 3, the zero lines represent the Fulcher equation as calculated from Methods I and IV. Thus the agreement between the data from Modes II and III and this line is a test not only of the precision but also of the accuracy of these measurements. Since the errors fluctuate to both sides of the zero line, any systematic deviation should be small. In fact the systematic deviations were calculated for each mode

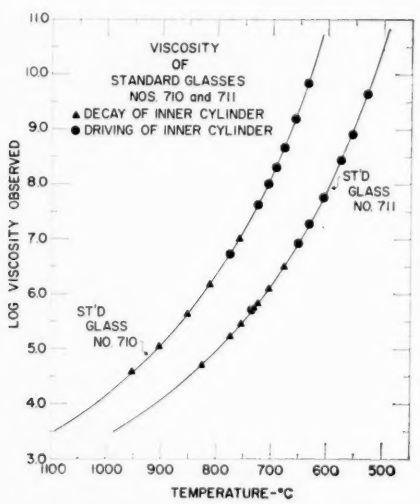

FIGURE 2. *Plot of log viscosity versus temperature of NBS Standard Glasses No. 710 and 711.*

Circles represent data taken by driving inner cylinder while triangles represent data taken with the decay mode of operation. The line curves represent calculated values from Napolitano and Hawkins (Lab. A) [13,14].

using all the measurements taken in both standard glasses. Their values were 0.30 percent for Mode II and 0.45 percent for Mode III. The standard deviations were calculated similarly. They were 0.010 log viscosity (2.3%) for Mode II, and 0.013 log viscosity (3.1%) for Method III.

Thus the equation of motion of the apparatus (eq (1)) has been proven correct as well as the calculated relations between the various calibration constants. This has been indicated in the appendix. The relatively little loss in accuracy due to the extension of the viscometer is probably due to the larger temperature dependence of the viscosity at lower temperatures.

5. Summary

The range of the rotating cylinder high temperature viscometer was extended up to 10^{10} P without loss of accuracy. Measurement at the higher viscosities could be made within reasonable time periods.

This extension was accomplished by operating the viscometer in three different modes: (1), rotating the outer cylinder at uniform angular velocity and measuring the torque in the inner cylinder; (2), the outer cylinder remains at rest while the inner cylinder is displaced by an angle and allowed to return to its zero position under the force of a torsion wire; and (3), the outer cylinder again remains at rest while a torque is applied to the inner cylinder by means of the magnetic field interaction and the angular velocity is measured about $\theta = 0$. The viscometer was calibrated by Method I, and from this the constants for the other two methods were calculated. This calibration was checked with NBS Standard Samples Nos. 710 and 711, and found to be within 0.5 percent, well inside the statistical fluctuation, whose standard deviation was 0.010 log viscosity (2%) for Methods I and II and 0.013 log viscosity (3%) for Method III. This is considerably better than that obtained for the fiber elongation data 0.034 log viscosity (8%).

6. Appendix

The second term of eq (1) assumes perfect laminar flow, which is not always obtainable in a rotation viscometer. Three other flow patterns are possible in such a system—Taylor vortices [16], convection currents and turbulence.

Taylor has made an extensive study of nonlaminar flow of viscous liquids between rotating cylinders and some of his conclusions can be applied to the geometry of the present apparatus. Taylor found that his vortices appeared above a critical value of ω/η.

The largest value of $\frac{\omega}{\eta}$ for Mode I in the present investigation was 0.52. This compares with Taylor's experimental critical value much greater than 1000 and calculated at infinite speeds. For Mode II they can also be neglected since its highest ω is 0.1 rad/sec and lowest η is equal to 5×10^4 giving $\frac{\omega}{\eta} = 5 \times 10^{-5}$

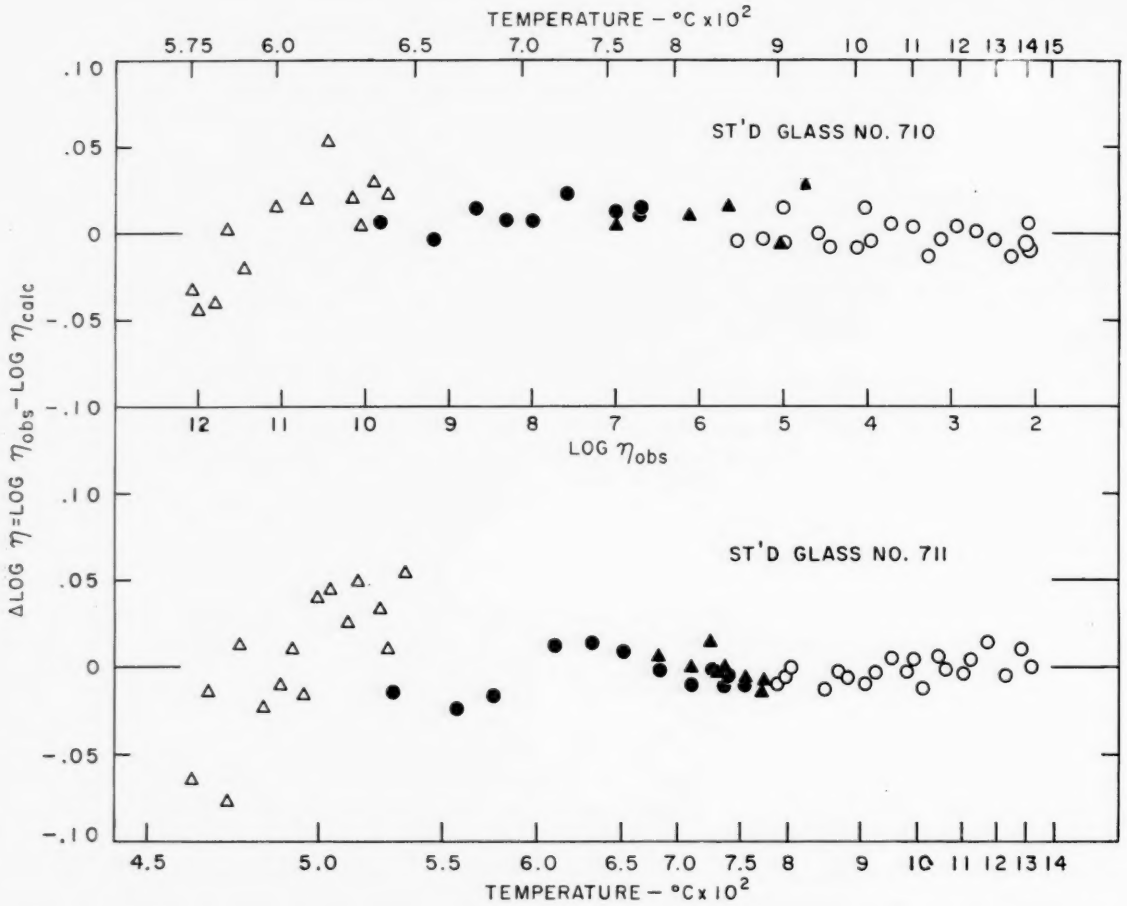
TEMPERATURE – °C x 10²
5.75 6.0 6.5 7.0 7.5 8 9 10 11 12 13 14 15
ST'D GLASS NO. 710
ΔLOG η=LOG η_obs – LOG η_calc
LOG η_obs
ST'D GLASS NO. 711
4.5 5.0 5.5 6.0 6.5 7.0 7.5 8 9 10 11 12 13 14
TEMPERATURE – °C x 10²

FIGURE 3. *Discrepancies between the observed log viscosity values and those calculated from the Fulcher equation for NBS Standard Glasses No. 710 and No. 711 are plotted versus log viscosity.*

Open triangles—fiber elongation; closed circles—driving inner cylinder; closed triangles—driving outer cylinder; and open circles—rotating outer cylinder.

compared with Taylor's experimental value of 30. Similarly, they are absent for Mode III. One should note that the ratio of diameters of the present apparatus is considerably larger than that of Taylor's and also that the center cylinder is very much shorter. However, since the values of $\frac{\omega}{\eta}$ used in this work are many orders of magnitude smaller than Taylor's critical values above which vortices appear, one is justified in assuming the absence of said vortices in this apparatus.

Following similar reasoning one can rule out the effects of convection currents in molten glasses when the cup has a temperature gradient of less than 5 deg. In a previous paper [13] it has been shown that the temperature gradients in the cup are much less than this. Since turbulence requires an even higher value of $\frac{\omega}{\eta}$, it definitely is not present.

The expectation that nonlaminar flow does not exist under the experimental conditions used was checked experimentally by plotting the torque versus angular velocity for both Modes I and III. The relationship was found to be linear. In Mode II a plot of displacement versus time was found to be exponential. This is direct experimental evidence that these nonlaminar effects are negligible, in agreement with the analysis given above.

Two other possible sources of error exist in our apparatus. They are (1), any effects due to the bob and cup not being perfectly centered; and (2), the dependence of end effects on the depth of immersion and clearance from the bottom of the cup.

Due to the large ratio of cup-to-bob diameters, precise centering is difficult to achieve. However, this difficulty is more than compensated for by the fact that slight departures from centering are not critical. After reasonable care is taken to center

the cup and bob, a quantitative but sensitive measure of the alinement obtained can be determined from the stability of the null position in making viscosity measurements according to Mode I. The results thus obtained are applicable to Modes II and III.

Lillie [17] and Rait [18] have shown that by having conical ends on the bob the dependence of end effects due to bob clearance is considerably reduced. This has been confirmed by the authors, who raised and lowered the cup 3 mm during viscosity measurements with negligible effects.

In conclusion it has been shown that eq (1) is valid for viscosities between 10^0 and 10^{10} P.

7. References

[1] S. English, J. of Glass Tech. **8,**, 205 (1924).
[2] M. Margules, Sitz. Weiner Akad **83,** 588 (1881).
[3] G. S. Parks, L. E. Barton, M. E. Spaght, and J. W. Richardson, Physics **5,** 193 (1934).
[4] G. S. Parks, and M. E. Spaght, Physics **6,** 69 (1935).
[5] A. L. Field, Trans, Faraday Soc. **13,** 3 (1917–18).
[6] H. R. Lillie, J. Am. Ceram. Soc. **12,** No. 8, 505 (1929); J. Am. Ceram. Soc. **12,** No. 8, 516 (1929).
[7] C. L. Babcock, J. Am. Ceram. Soc. **17,** No. 11, 329 (1934).
[8] H. A. Robinson and C. A. Peterson, J. Am. Ceram. Soc. **27,** No. 5, 129 (1944).
[9] J. O'M. Bockris and D. C. Lowe, J. Sci. Instr. **30,** 403 (1953).
[10] W. H. Hampton, Trans. Opt. Soc. (London) **27,** 171 (1925–26).
[11] H. E. Hagy, J. Am. Ceram. Soc. **46,** No. 2, 93 (1963).
[12] J. E. Kelley, T. D. Roberts and H. M. Harris, U.S. Bur. of Mines RI 6358 (1964).
[13] A. Napolitano and E. G. Hawkins, NBS J. Res. **68A** (Phys. and Chem.) No. 5, 439 (1964).
[14] A. Napolitano and E. G. Hawkins, to be published.
[15] G. S. Fulcher, J. Am. Ceram. Soc. **8,** No. 6, 339 (1925).
[16] G. I. Taylor, Phil. Trans. Royal Soc. (London) **A223,** 289 (1923).
[17] H. R. Lillie, Phys. Rev. **36,** 2d Series, 347 (1930).
[18] J. R. Rait, Trans. Brit. Ceram. Soc., **40,** 151 (1941).

(Paper 69A5–366)

JOURNAL OF RESEARCH of the National Bureau of Standards—A. Physics and Chemistry
Vol. 69A, No. 5, September-October 1965

Internal Friction in ZrO_2 Containing CaO

J. B. Wachtman, Jr., and W. C. Corwin*

(May 27, 1965)

Internal friction was measured on polycrystalline ZrO_2 containing 4, 7, 10, 13, 16, and 20 mole percent CaO. In the range 10 to 20 percent a symmetrical internal friction peak occurs with its maximum at about 300 °C at 1 kHz; below 10 percent a nonsymmetrical peak occurs at somewhat higher temperature which may be associated with the presence of two phases. The symmetrical peak in as-sintered specimens has the same dependence on CaO content as that reported for electrical resistivity at 1000 °C and is probably caused by motion of oxygen vacancies. Annealing at 1000 °C for 1000 hours causes reduction of the peak height but with a different composition dependence from that reported for annealing of electrical resistivity. The results suggest that oxygen vacancies in calcia stabilized zirconia exist in several states of binding but that detailed models are likely to be complex.

1. Introduction

Ceramics high in ZrO_2 are of considerable technological importance; an extensive bibliography on structural and physical properties of zirconia has recently been published [1].[1] Many applications of zirconia rely upon the presence of additives to produce partial or complete stabilization in the cubic phase and so avoid difficulties caused in pure ZrO_2 by the transformation which occurs in the range 1200 to 1000 °C from the high temperature tetragonal phase to a low temperature monoclinic phase. Various additives have been tried, but CaO appears to be the most successful and widely studied. The phase diagram of the ZrO_2–CaO system remains a subject of discussion; it is generally agreed that a cubic phase exists for compositions neighboring 15 percent CaO (mole percent rather than weight percent is used throughout this paper). The reported limits of the one phase region vary considerably; Carter and Roth [2] take them to be 10 and 20 percent. Below the lower limit a mixture of two phases exists.

The cubic phase is usually regarded as a fluorite structure with Zr^{4+} and Ca^{2+} distributed at random over the cation sites and with enough oxygen vacancies to provide charge compensation distributed at random over the oxygen sites. This model is in accord with x-ray diffraction evidence and the high diffusion rate for oxygen but is generally thought to be oversimplified in not allowing for the association or ordering of defects or even the possibility of additional phases not yet detected. The variation of electrical resistivity with composition and heat treatment has been interpreted as indicating ordering of vacancies [3, 2]. Neutron diffraction patterns [2] are consistent with this interpretation.

Homogeneous stress or electric field acting upon a point defect can, under certain conditions, cause reorientation of the defect and produce a corresponding mechanical or electrical relaxation. Measurements of the internal friction peak or dielectric loss peak can then be used to study the variation of point defect concentration with composition and heat treatment.

An internal friction peak was found by Dew [4] in commercial zirconia partially stabilized with CaO and its existence was confirmed in two subsequent investigations [5, 6]. All workers used polycrystalline specimens. Interpretation of this peak is difficult because the specimens probably contained some of the tetragonal phase as well as the cubic phase. Dew suggested plastic deformation as a possible cause; Chang suggested the motion of twin boundaries; and Wachtman et al., suggested the motion of oxygen vacancies.

A dielectric relaxation process which occurs in the same frequency and temperature range as the internal friction peak has been found by Carter [7] in both single crystal and polycrystalline zirconia stabilized with 14.2 percent CaO. This relaxation process appears to involve motion of oxygen vacancies because its dependence on heat treatment parallels that of the electrical conductivity at 1000 °C which is known to take place by oxygen vacancy motion. The observed dielectric relaxation probably arises from the series combination of two regions with different oxygen mobility either on an atomic scale (such as a vacancy constrained to the sites neighboring a relatively immobile point defect) or on a somewhat larger scale (such as a small region of a second phase or a surface layer under the electrode). The composition of Carter's specimen places it within the single, cubic phase area of conventional phase diagrams, but Carter and Roth present neutron diffraction and x-ray diffraction evidence that annealing at 1000 °C results in the formations of small ordered regions of a preprecipitate which are epitaxially related to the host lattice.

*Present address: Physics Department, Iowa State University, Ames, Iowa
[1] Figures in brackets indicate the literature references at the end of this paper.

780-567—65——6

Investigation of the composition and heat treatment dependence of the internal friction peak has been undertaken to test the similarity of its behavior with the electrical conductivity and dielectric relaxation.

2. Specimens

Single crystals suitable for internal friction measurements were not available. Polycrystalline specimens were prepared from ZrO_2 powder containing 0.15 percent SiO_2, 0.02 percent HfO_2, and 0.03 percent MgO as the major impurities: mixtures were made up using CaO powder produced by calcining "chemically pure" calcium carbonate at 1000 °C. Specimens were cold pressed in a steel bar-mold, isostatically pressed, and sintered for 1 hr at 1800 °C in a gas fired furnace. The porosity and grain size of the resulting bars are given in table 1; the dimensions were about 6 by 0.5 by 0.25 in.

TABLE 1

Additive	Porosity	Grain size	Frequency at peak	Temperature at peak	Peak height, Q^{-1}	Apparent activation energy
% CaO		*Microns*	*c/sec*	°C	10^{-2}	*kcal/mole* [b]
4		19	1115	455	1.7	
4[a]			397			
7		29	1362	427	1.8	
7[a]			366		1.8	
10	0.18	28	1983	315	1.2	42±7
10[a]			628	297	1.0	
13	.28	22	1883	319	2.2	29±7
13[a]			486	290	2.1	
16	.24	32	1913	305	1.5	43±9
16[a]			582	290	1.6	
20	.27	24			1.1	

[a] Specimen thinned to reduce resonance frequency.
[b] kcal=4184 joules. Standard errors are based on peak temperatures obtained by curve fitting through twenty points.

3. Experimental Procedure

The variation of internal friction with temperature was determined by Forster's method in which a bar is suspended horizontally from two fiberglass threads tied near the nodes of flexural vibration. One thread was driven by a magnetic record-cutting head and the other was attached to a piezoelectric pickup. The driving frequency was varied until the resonance frequency, f_1, was found and measured on a crystal controlled counter. The frequencies f_2 and f_3 (on either side of f_1) at which the amplitude of vibration is half that at resonance were also measured. The internal friction was calculated from [8]

$$Q^{-1}=0.5773(f_3-f_2)/f_1. \tag{1}$$

Measurements of Q^{-1} as a function of temperature up to 650 °C were first made on as-sintered specimens of all the compositions made (ZrO_2 containing 4, 7, 10, 13, 16, and 20% CaO). All of the specimens were then thinned over the central third of their length by diamond grinding to lower the resonance frequency and all were then remeasured except for the 20 percent CaO specimen which was broken in grinding. The activation energy, E, was calculated from [8]

$$E=\frac{RT_{p1}T_{p2}\ln f_{p1}/f_{p2}}{T_{p1}-T_{p2}} \tag{2}$$

where T_{p1} is the absolute temperature at which the quantity TQ^{-1} was largest and f_{p1} is the corrresponding resonance frequency; T_{p2} and f_{p2} are the corresponding quantities for the same specimen after thinning.

Three additional unthinned specimens (containing 10, 13, and 16 percent CaO) were then held at 1000 °C in air for 1000 hr and subsequently measured: we refer to these as annealed specimens.

4. Results

The curves of internal friction as a function of temperature are shown in figure 1; for each composition the lower solid curve (shown dashed for the 4% specimen because of scatter) refers to the thinned specimen. Results obtained on the annealed specimens after the 1000 hr heat treatment are shown by dot-dash curves. A marked contrast is evident between the results for the 4 and 7 percent specimens, on the one hand, and the specimens completely stabilized in the cubic phase, on the other hand.

The partially stabilized specimens show an unsymmetrical peak with a shoulder on the high temperature side. Grinding these specimens apparently produced internal cracking leading to wide scatter in results, particularly for the 4 percent specimen.

The peaks for specimens in the 10 through 20 percent range of compositions are symmetrical, but are much too broad to result from a relaxation process with a single relaxation time. For comparison, the curve calculated for a single relaxation time process (Debye type process) has been drawn under the lower curve for the specimen containing 13 percent CaO. The height of the Debye peak was chosen equal to the experimental peak and the activation energy calculated from eq (2) was used. The experimental curve is about three times as wide as the Debye curve. The variation of peak height with composition for the as-sintered specimens (greatest at 13%, decreasing toward 10% or toward 20%) parallels the variation of electrical conductivity found for comparable specimens [2, 3]. The heat treatment at 1000 °C has somewhat similar results on electrical conductivity at 1000 °C and on internal friction in that both properties decrease for certain compositions and remain unchanged for others. The composition dependence is different, however. Carter and Roth report that the electrical conductivity of ZrO_2 containing 14 percent CaO remains unchanged with time at 1000 °C but the conductivity of compositions less than 13 or more than 16 percent decreases. In contrast, the internal friction peak

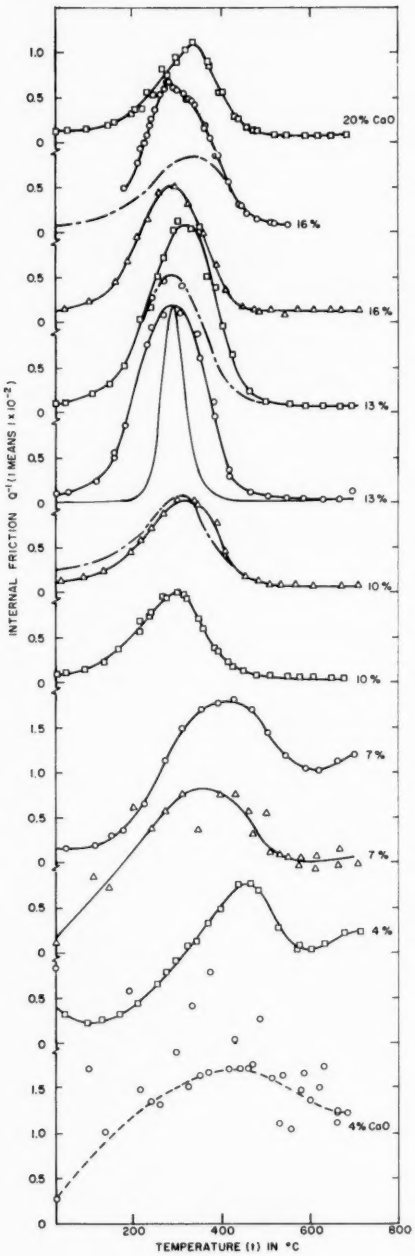

FIGURE 1. *Internal friction of* ZrO_2 *containing stated amounts of* CaO.

The dot-dash curves were determined after 1000 hr at 1000 °C in air. The other curves were obtained on as-sintered specimens; where more than one such curve is given the lower one was obtained after machining the specimen to lower its resonance frequency.

height for the specimen containing 10 percent CaO was not changed but the peak for the specimen with 13 percent CaO was decreased and that for the specimen with 16 percent CaO was reduced even more.

5. Discussion

The unsymmetrical peak occurring in partially stabilized ZrO_2 might be associated with Chang's mechanicism of twin boundary motion in tetragonal grains, but the symmetrical peak occurring in the range of 10 to 20 percent CaO can not be associated with tetragonal grains. The similarity of peak height dependence and electrical conductivity dependence on CaO content suggests that the symmetrical peak is associated with oxygen vacancy motion.

The concentration of oxygen vacancies and of Ca^{2+} ions is so high that many complex groupings probably occur. We discuss three defect models that might be appropriate at very low concentrations in order to illustrate certain qualitative features which may be valid even at high concentrations.

First, consider a single oxygen vacancy in an otherwise perfect fluorite structure (see fig. 2). This vacancy would move under electric field but not under homogeneous stress [9]. It would contribute to the frequency independent part of the electrical conductivity but would not contribute to internal friction or dielectric relaxation.

Second, consider an oxygen vacancy neighboring a Ca^{2+} ion at (0, 0, 0) and constrained by electrostatic attraction to the eight nearest neighbor oxygen sites at $(\pm\frac{1}{4}, \pm\frac{1}{4}, \pm\frac{1}{4})$. Either homogeneous stress or electric field will cause a preferred distribution so that this oxygen vacancy will make no contribution to the frequency independent electrical conductivity but will contribute both to

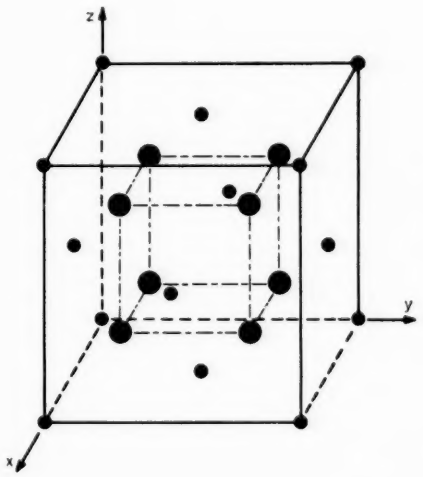

FIGURE 2. *The fluorite structure.*

internal friction and to dielectric relaxation. Each should be characterized by a single relaxation time. This type of defect is thought to be responsible for a dielectric relaxation process and internal friction peak observed in ThO_2 containing small amounts of CaO [10].

Third, consider two oxygen vacancies at (¼, ¼, ¼) and (¼, ¼, −¼) neighboring two Ca^{2+} ions at (0, 0, 0) and (½, ½, 0). Two defects of the second type should have electrostatic attraction of the dipole-dipole type tending to cause this defect to form. The oxygen vacancies in this defect will make no contribution to the frequency independent part of the electrical conductivity, to dielectric relaxation, or to internal friction.

It is tempting to interpret the as-sintered specimens as having defects of all three types with quenched in concentrations corresponding to thermal equilibrium at some temperature above 1000 °C at which the Ca^{2+} ion motion was frozen out during furnace cooling. Subsequent long time heat treatment at 1000 °C would cause slow diffusion of Ca^{2+} and produce a slow increase in the concentration of defects of the third type accompanied by a decrease in the concentrations of the first and second type. This would account for the observed decrease of measured properties for some concentrations with 1000 °C heat treatment. We can hardly expect, however, to take such a model literally at concentrations so high that one cation in five is Ca^{2+} and the model cannot account for several features of the data. This model predicts a single relaxation time for the internal friction peak in contrast to the broad peak observed. The model gives no indication why some compositions (10% CaO for the internal friction peak and 14% CaO for the electrical conductivity) are unaffected by heat treatment at 1000 °C. Nevertheless, the model is probably correct in attributing the 1000 °C annealing effect to Ca^{2+} diffusion and the accompanying changes in the binding of oxygen vacancies. The model is also probably correct in assuming some defect similar to type three in which the oxygen vacancies are too tightly bound to move, but some features of defects of the first and second type might be combined. An oxygen vacancy making successive jumps in the same direction may encounter several sites with an equal number of Ca^{2+} neighbors before coming to one which has fewer Ca^{2+} neighbors and so requires some energy of dissociation. The jump involving dissociation would be rate limiting for the electrical conductivity while motion back and forth along the equally favored sites would correspond to dielectric relaxation. The initially equally favored sites may become inequivalent under stress if permitted by symmetry [9] and so cause an internal friction peak. Various arrangements of Ca^{2+} ions can be visualized which fit these conditions so that the existence of a distribution of relaxation times is not surprising.

It does not appear fruitful to attempt more detailed interpretation. Measurements of orientation dependence of internal friction might be helpful if suitable single crystals become available, but progress in understanding probably depends primarily on diffraction studies of single crystals of various compositions.

6. References

[1] B. C. Weber, An annotated bibliography of research on the structural and physical properties of zirconia, Aerospace Research Laboratories Report 64–205 (1964); Available from Office of Technical Services, U.S. Department of Commerce, Washington 25, D.C.

[2] R. E. Carter and W. L. Roth, Ionic conductivity and vacancy ordering in calcia stabilized zirconia, General Electric Research Laboratory Report 63–RL–3479 (1963).

[3] D. W. Strickler and W. G. Carlson, Ionic conductivity of cubic solid solutions in the CaO-Y_2O_3-ZrO_2 System, J. Am. Ceram. Soc. **47,** 122 (1964).

[4] R. J. Dew, Jr., Damping capacity of refractory oxides under various stress and temperature conditions, Sc. D. Thesis, Mass. Inst. of Technology (1950) unpublished.

[5] J. B. Wachtman, Jr., W. E. Tefft, D. G. Lam, Jr., and R. P. Stinchfield, Factors controlling resistance to deformation and mechanical failure in polycrystalline (glass-free) ceramics, Wright Air Development Center Technical Report 59–278 (1959)

[6] Roger Chang, The elastic and anelastic properties of refractory oxides, pp 209–219 in Mechanical Properties of Engineering Ceramics, edited by W. W. Kriegel and H. Palmour III (Interscience Publishers, New York, (1961)).

[7] R. E. Carter, private communication with the authors.

[8] C. Zener, Elasticity and anelasticity of metals, Univ. of Chicago Press (1948).

[9] J. B. Wachtman, Jr., H. S. Peiser, and E. P. Levine, Symmetry splitting of equivalent sites in oxide crystals and related mechanical effects, J. Res. NBS **67A** (Phys. and Chem.) No. 4, 281 (1963).

[10] J. B. Wachtman, Jr., Mechanical and electrical relaxation in ThO_2 containing CaO, Phys. Rev. **131**, 517 (1963).

(Paper 69A5–367)

JOURNAL OF RESEARCH of the National Bureau of Standards—A. Physics and Chemistry
Vol. 69A, No. 5, September–October 1965

Splitting of Equivalent Points in Noncentrosymmetric Space Groups Into Subsets Under Homogeneous Stress

H. S. Peiser, J. B. Wachtman, Jr., F. A. Munley, and L. C. McCleary

(March 29, 1965)

Splitting of general positions in crystals into subsets of equivalent sites under homogeneous stress has previously been given for all centrosymmetric space groups; the tabulation is here completed for all space groups by listing the results for noncentrosymmetric space groups.

1. Introduction

The present paper presents results analogous to those previously submitted for centrosymmetric space groups [1][1] and for point groups [2]; these previous papers should be consulted for detailed discussion.

It is assumed that the symmetry elements possessed by a homogeneously stressed crystal will be those common to the crystal and to the macroscopic state of stress. Application of stress either leaves a space group unaltered or lowers it to a subgroup. Such lowering can always be considered to take place in successive steps each of which leaves no group which is both a stress-induced subgroup of the initial group and a supergroup of the final group, and which is distinct from both. Each such step can be accomplished by a uniaxial stress; for the noncentrosymmetric space groups all but two of the symmetry reductions consisting of two or more successive steps can also be accomplished by uniaxial stress. These two require biaxial stress [2]. More general stress states are, however, consistent with many of the steps of symmetry lowering; we list the most general state of stress (in terms of the modified stress ellipsoid [1]) consistent with each step. The same stress is appropriate for all space-group-to-space-group transformations associated with a given point-group-to-point-group transformation. There are 25 of the latter which are minimum steps of symmetry lowering for noncentrosymmetric point groups so that the results for the noncentrosymmetric space groups are collected into 25 corresponding tables.

A set of points all of which are equivalent in the unstressed crystal frequently splits into two or more subsets under stress. For each space group all possibilities are taken into account by considering the behavior of the general position because the behavior of each special position can be derived by specializing the general position. This process of specialization in space groups has been discussed and a technique for visualizing it in terms of stereograms of point groups has been described [2].

2. Results

2.1. Behavior of General Position

The splitting of the general position (set of equivalent sites having no symmetry) into subsets is listed in tables 1 through 25. Each table is headed by a point-group transformation which is a minimum step of symmetry lowering. Each of the space groups associated with the initial point group is listed in the table together with the coordinates of a set of sites making up a general position. The latter are collected into subsets; all of the sites in a subset remain equivalent after symmetry reduction to the final space group which is also listed. For some of the point-group reductions the final point group can occur in two or three non-equivalent orientations. These may correspond to different final space groups; in table 12, for example, one orientation corresponds to the caption at the top of the table and the other to the caption at the bottom. The stress is described by giving conditions on the axes X, Y, Z of the stress ellipsoid [1] to the crystal axes x, y, z; the stress described is the most general (i.e., least restricted) consistent with the symmetry reduction. In many of the tables a single stress specification suffices for all space groups, but in some (table 10, for example) the stress must be specified for each space group because it is customary to choose the axes in different orientations with respect to the point group.

2.2. Stress Table

The most general stress consistent with each possible step of stress-induced symmetry lowering, minimum or compound, is listed in table 26 for all of the noncentrosymmetric point groups. The stress conditions for the minimum steps of stress-induced symmetry lowering are equivalent, though not always identical, to those given in tables 1–25.

Figures in brackets indicate the literature references on page 462.

TABLE 1. *Reduction from $\bar{4}3m$ to $\bar{4}2m$*

Space group of unstrained crystal, order 24 per lattice point		If stressed so that $X=Y$; $z\|\|Z$			Space group of strained crystal, order 8 per lattice point	
		Coordinates referred to axes of unstrained crystal				
No.	Symbol	1st Subset	2d Subset	3d Subset	No.	Symbol
215	$P\bar{4}3m$	(x, y, z) (y, x, z) $(\bar{y}, x, \bar{z})$ $(\bar{x}, y, \bar{z})$ $(\bar{x}, \bar{y}, z)$ $(\bar{y}, \bar{x}, z)$ $(y, \bar{x}, \bar{z})$ $(x, \bar{y}, \bar{z})$	(y, z, x) (z, y, x) $(\bar{z}, y, \bar{x})$ $(\bar{y}, z, \bar{x})$ $(\bar{y}, \bar{z}, x)$ $(\bar{z}, \bar{y}, x)$ $(z, \bar{y}, \bar{x})$ $(y, \bar{z}, \bar{x})$	(z, x, y) (x, z, y) $(\bar{z}, x, \bar{y})$ $(\bar{x}, z, \bar{y})$ $(\bar{z}, \bar{x}, y)$ $(\bar{x}, \bar{z}, y)$ $(x, \bar{z}, \bar{y})$ $(z, \bar{x}, \bar{y})$	111	$P\bar{4}2m$
216	$F\bar{4}3m$	(x, y, z) $(\quad, \quad, z)$ $(\bar{y}, x, \bar{z})$ $(\bar{x}, y, \bar{z})$ $(\bar{x}, \bar{y}, z)$ $(\bar{y}, \bar{x}, z)$ $(y, \bar{x}, \bar{z})$ $(x, \bar{y}, \bar{z})$	(y, z, x) (z, y, x) $(\bar{z}, y, \bar{x})$ $(\bar{y}, z, \bar{x})$ $(\bar{y}, \bar{z}, x)$ $(\bar{z}, \bar{y}, x)$ 5 $z, \bar{y}, \bar{x})$ $(y, \bar{z}, \bar{x})$	(z, x, y) (x, z, y) $(\bar{z}, x, \bar{y})$ $(\bar{x}, z, \bar{y})$ $(\bar{z}, \bar{x}, y)$ $(\bar{x}, \bar{z}, y)$ $(x, \bar{z}, \bar{y})$ $(z, \bar{x}, \bar{y})$	119	$I\bar{4}m2$
217	$I\bar{4}3m$	(x, y, z) (y, x, z) $(\bar{y}, x, \bar{z})$ $(\bar{x}, y, \bar{z})$ $(\bar{x}, \bar{y}, z)$ $(\bar{y}, \bar{x}, z)$ $(y, \bar{x}, \bar{z})$ $(x, \bar{y}, \bar{z})$	(y, z, x) (z, y, x) $(\bar{z}, y, \bar{x})$ $(\bar{y}, z, \bar{x})$ $(\bar{y}, \bar{z}, x)$ $(\bar{z}, \bar{y}, x)$ $(z, \bar{y}, \bar{x})$ $(y, \bar{z}, \bar{x})$	(z, x, y) (x, z, y) $(\bar{z}, x, \bar{y})$ $(\bar{x}, z, \bar{y})$ $(\bar{z}, \bar{x}, y)$ $(\bar{x}, \bar{z}, y)$ $(x, \bar{z}, \bar{y})$ $(z, \bar{x}, \bar{y})$	121	$I\bar{4}2m$
218	$P\bar{4}3n$	(x, y, z) $(\frac{1}{2}+y, \frac{1}{2}+x, \frac{1}{2}+z)$ $(\frac{1}{2}-y, \frac{1}{2}+x, \frac{1}{2}-z)$ $(\bar{x}, y, \bar{z})$ $(\bar{x}, \bar{y}, z)$ $(\frac{1}{2}-y, \frac{1}{2}-x, \frac{1}{2}+z)$ $(\frac{1}{2}+y, \frac{1}{2}-x, \frac{1}{2}-z)$ $(x, \bar{y}, \bar{z})$	(y, z, x) $(\frac{1}{2}+z, \frac{1}{2}+y, \frac{1}{2}+x)$ $(\frac{1}{2}-z, \frac{1}{2}+y, \frac{1}{2}-x)$ $(\bar{y}, z, \bar{x})$ $(\bar{y}, \bar{z}, x)$ $(\frac{1}{2}-z, \frac{1}{2}-y, \frac{1}{2}+x)$ $(\frac{1}{2}+z, \frac{1}{2}-y, \frac{1}{2}-x)$ $(y, \bar{z}, \bar{x})$	(z, x, y) $(\frac{1}{2}+x, \frac{1}{2}+z, \frac{1}{2}+y)$ $(\frac{1}{2}-x, \frac{1}{2}+z, \frac{1}{2}-y)$ $(\bar{z}, x, \bar{y})$ $(\bar{z}, \bar{x}, y)$ $(\frac{1}{2}-x, \frac{1}{2}-z, \frac{1}{2}+y)$ $(\frac{1}{2}+x, \frac{1}{2}-z, \frac{1}{2}-y)$ $(z, \bar{x}, \bar{y})$	112	$P\bar{4}2c$
219	$F\bar{4}3c$	(x, y, z) $(y, x, \frac{1}{2}+z)$ $(\bar{y}, x, \frac{1}{2}-z)$ $(\bar{x}, y, \bar{z})$ $(\bar{x}, \bar{y}, z)$ $(\bar{y}, \bar{x}, \frac{1}{2}+z)$ $(y, \bar{x}, \frac{1}{2}-z)$ $(x, \bar{y}, \bar{z})$	(y, z, x) $(z, y, \frac{1}{2}+x)$ $(\bar{z}, y, \frac{1}{2}-x)$ $(\bar{y}, z, \bar{x})$ $(\bar{y}, \bar{z}, x)$ $(\bar{z}, \bar{y}, \frac{1}{2}+x)$ $(z, \bar{y}, \frac{1}{2}-x)$ $(y, \bar{z}, \bar{x})$	(z, x, y) $(x, z, \frac{1}{2}+y)$ $(\bar{z}, x, \frac{1}{2}-y)$ $(\bar{x}, z, \bar{y})$ $(\bar{z}, \bar{x}, y)$ $(\bar{x}, \bar{z}, \frac{1}{2}+y)$ $(x, \bar{z}, \frac{1}{2}-y)$ $(z, \bar{x}, \bar{y})$	120	$I\bar{4}c2$
220	$I\bar{4}3d$	(x, y, z) $(\frac{1}{4}+y, \frac{1}{4}+x, \frac{1}{4}+z)$ $(\frac{3}{4}-y, \frac{3}{4}+x, \frac{1}{4}-z)$ $(\bar{x}, \frac{1}{2}+y, \frac{1}{2}-z)$ $(\frac{1}{2}-x, \bar{y}, \frac{1}{2}+z)$ $(\frac{1}{4}-y, \frac{3}{4}-x, \frac{3}{4}+z)$ $(\frac{3}{4}+y, \frac{1}{4}-x, \frac{3}{4}-z)$ $(\frac{1}{2}+x, \frac{1}{2}-y, \bar{z})$	(y, z, x) $(\frac{1}{4}+z, \frac{1}{4}+y, \frac{1}{4}+x)$ $(\frac{3}{4}-z, \frac{3}{4}+y, \frac{1}{4}-x)$ $(\bar{y}, \frac{1}{2}+z, \frac{1}{2}-x)$ $(\frac{1}{2}-y, \bar{z}, \frac{1}{2}+x)$ $(\frac{1}{4}-z, \frac{3}{4}-y, \frac{3}{4}+x)$ $(\frac{3}{4}+z, \frac{1}{4}-y, \frac{3}{4}-x)$ $(\frac{1}{2}+y, \frac{1}{2}-z, \bar{x})$	(z, x, y) $(\frac{1}{4}+x, \frac{1}{4}+z, \frac{1}{4}+y)$ $(\frac{3}{4}-x, \frac{3}{4}+z, \frac{1}{4}-y)$ $(\bar{z}, \frac{1}{2}+x, \frac{1}{2}-y)$ $(\frac{1}{2}-z, \bar{x}, \frac{1}{2}+y)$ $(\frac{1}{4}-x, \frac{3}{4}-z, \frac{3}{4}+y)$ $(\frac{3}{4}+x, \frac{1}{4}-z, \frac{3}{4}-y)$ $(\frac{1}{2}+z, \frac{1}{2}-x, \bar{y})$	122	$I\bar{4}2d$

3. References

[1] J. B. Wachtman, Jr., and H. S. Peiser, Splitting of a set of equivalent sites in centrosymmetric space groups into subsets under homogeneous stress, J. Res. NBS **69A** (Phys. and Chem.) No. 2, 193–207 (1965).

[2] H. S. Peiser and J. B. Wachtman, Jr., Reduction of crystallographic point groups to subgroups by homogeneous stress, J. Res. NBS**69A** (Phys. and Chem.) No. 4, 309–324 (1965).

TABLE 2. *Reduction from $\bar{4}3m$ to 3m*

Space group of unstrained crystal, order 24 per lattice point		If stressed so that $X=Y$; $[111]\parallel Z$				Space group of strained crystal, order 6 per lattice point	
		Coordinates referred to axes of unstrained crystal					
No.	Symbol	1st Subset	2d Subset	3d Subset	4th Subset	No.	Symbol
215	$P\bar{4}3m$	(x, y, z) (y, z, x) (z, x, y) (y, x, z) (z, y, x) (x, z, y)	$(x, \bar{y}, \bar{z})$ $(\bar{y}, \bar{z}, x)$ $(\bar{z}, x, \bar{y})$ $(\bar{y}, x, \bar{z})$ $(\bar{z}, \bar{y}, x)$ $(x, \bar{z}, \bar{y})$	$(\bar{x}, y, \bar{z})$ $(y, \bar{z}, \bar{x})$ $(\bar{z}, \bar{x}, y)$ $(y, \bar{x}, \bar{z})$ $(\bar{z}, y, \bar{x})$ $(\bar{x}, \bar{z}, y)$	$(\bar{x}, \bar{y}, z)$ $(\bar{y}, z, \bar{x})$ $(z, \bar{x}, \bar{y})$ $(\bar{y}, \bar{x}, z)$ $(z, \bar{y}, \bar{x})$ $(\bar{x}, z, \bar{y})$	160	R3m
216	$F\bar{4}3m$	(x, y, z) (y, z, x) (z, x, y) (y, x, z) (z, y, x) (x, z, y)	$(x, \bar{y}, \bar{z})$ $(\bar{y}, \bar{z}, x)$ $(\bar{z}, x, \bar{y})$ $(\bar{y}, x, \bar{z})$ $(\bar{z}, \bar{y}, x)$ $(x, \bar{z}, \bar{y})$	$(\bar{x}, y, \bar{z})$ $(y, \bar{z}, \bar{x})$ $(\bar{z}, \bar{x}, y)$ $(y, \bar{x}, \bar{z})$ $(\bar{z}, y, \bar{x})$ $(\bar{x}, \bar{z}, y)$	$(\bar{x}, \bar{y}, z)$ $(\bar{y}, z, \bar{x})$ $(z, \bar{x}, \bar{y})$ $(\bar{y}, \bar{x}, z)$ $(z, \bar{y}, \bar{x})$ $(\bar{x}, z, \bar{y})$	160	R3m
217	$I\bar{4}3m$	(x, y, z) (y, z, x) (z, x, y) (y, x, z) (z, y, x) (x, z, y)	$(x, \bar{y}, \bar{z})$ $(\bar{y}, \bar{z}, x)$ $(\bar{z}, x, \bar{y})$ $(\bar{y}, x, \bar{z})$ $(\bar{z}, \bar{y}, x)$ $(x, \bar{z}, \bar{y})$	$(\bar{x}, y, \bar{z})$ $(y, \bar{z}, \bar{x})$ $(\bar{z}, \bar{x}, y)$ $(y, \bar{x}, \bar{z})$ $(\bar{z}, y, \bar{x})$ $(\bar{x}, \bar{z}, y)$	$(\bar{x}, \bar{y}, z)$ $(\bar{y}, z, \bar{x})$ $(z, \bar{x}, \bar{y})$ $(\bar{y}, \bar{x}, z)$ $(z, \bar{y}, \bar{x})$ $(\bar{x}, z, \bar{y})$	160	R3m
218	$P\bar{4}3n$	(x, y, z) (y, z, x) (z, x, y) $(\frac{1}{2}+y, \frac{1}{2}+x, \frac{1}{2}+z)$ $(\frac{1}{2}+z, \frac{1}{2}+y, \frac{1}{2}+x)$ $(\frac{1}{2}+x, \frac{1}{2}+z, \frac{1}{2}+y)$	$(x, \bar{y}, \bar{z})$ $(\bar{y}, \bar{z}, x)$ $(\bar{z}, x, \bar{y})$ $(\frac{1}{2}-y, \frac{1}{2}+x, \frac{1}{2}-z)$ $(\frac{1}{2}-z, \frac{1}{2}-y, \frac{1}{2}+x)$ $(\frac{1}{2}+x, \frac{1}{2}-z, \frac{1}{2}-y)$	$(\bar{x}, y, \bar{z})$ $(y, \bar{z}, \bar{x})$ $(\bar{z}, \bar{x}, y)$ $(\frac{1}{2}+y, \frac{1}{2}-x, \frac{1}{2}-z)$ $(\frac{1}{2}-z, \frac{1}{2}+y, \frac{1}{2}-x)$ $(\frac{1}{2}-x, \frac{1}{2}-z, \frac{1}{2}+y)$	$(\bar{x}, \bar{y}, z)$ $(\bar{y}, z, \bar{x})$ $(z, \bar{x}, \bar{y})$ $(\frac{1}{2}-y, \frac{1}{2}-x, \frac{1}{2}+z)$ $(\frac{1}{2}+z, \frac{1}{2}-y, \frac{1}{2}-x)$ $(\frac{1}{2}-x, \frac{1}{2}+z, \frac{1}{2}-y)$	161	R3c
219	$F\bar{4}3c$	(x, y, z) (y, z, x) (z, x, y) $(y, x, \frac{1}{2}+z)$ $(z, y, \frac{1}{2}+x)$ $(x, z, \frac{1}{2}+y)$	$(x, \bar{y}, \bar{z})$ $(\bar{y}, \bar{z}, x)$ $(\bar{z}, x, \bar{y})$ $(\bar{y}, x, \frac{1}{2}-z)$ $(\bar{z}, \bar{y}, \frac{1}{2}+x)$ $(x, \bar{z}, \frac{1}{2}-y)$	$(\bar{x}, y, \bar{z})$ $(y, \bar{z}, \bar{x})$ $(\bar{z}, \bar{x}, y)$ $(y, \bar{x}, \frac{1}{2}-z)$ $(\bar{z}, y, \frac{1}{2}-x)$ $(\bar{x}, \bar{z}, \frac{1}{2}+y)$	$(\bar{x}, \bar{y}, z)$ $(\bar{y}, z, \bar{x})$ $(z, \bar{x}, \bar{y})$ $(\bar{y}, \bar{x}, \frac{1}{2}+z)$ $(z, \bar{y}, \frac{1}{2}-x)$ $(\bar{x}, z, \frac{1}{2}-y)$	161	R3c
220	$I\bar{4}3d$	(x, y, z) (y, z, x) (z, x, y) $(\frac{1}{4}+y, \frac{1}{4}+x, \frac{1}{4}+z)$ $(\frac{1}{4}+z, \frac{1}{4}+y, \frac{1}{4}+x)$ $(\frac{1}{4}+x, \frac{1}{4}+z, \frac{1}{4}+y)$	$(\frac{1}{2}+x, \frac{1}{2}-y, \bar{z})$ $(\frac{1}{2}-y, \bar{z}, \frac{1}{2}+x)$ $(\bar{z}, \frac{1}{2}+x, \frac{1}{2}-y)$ $(\frac{3}{4}-y, \frac{3}{4}+x, \frac{1}{4}-z)$ $(\frac{1}{4}-z, \frac{3}{4}-y, \frac{3}{4}+x)$ $(\frac{3}{4}+x, \frac{1}{4}-z, \frac{3}{4}-y)$	$(\bar{x}, \frac{1}{2}+y, \frac{1}{2}-z)$ $(\frac{1}{2}+y, \frac{1}{2}-z, \bar{x})$ $(\frac{1}{2}-z, \bar{x}, \frac{1}{2}+y)$ $(\frac{3}{4}+y, \frac{1}{4}-x, \frac{3}{4}-z)$ $(\frac{3}{4}-z, \frac{3}{4}+y, \frac{1}{4}-x)$ $(\frac{1}{4}-x, \frac{3}{4}-z, \frac{3}{4}+y)$	$(\frac{1}{2}-x, \bar{y}, \frac{1}{2}+z)$ $(\bar{y}, \frac{1}{2}+z, \frac{1}{2}-x)$ $(\frac{1}{2}+z, \frac{1}{2}-x, \bar{y})$ $(\frac{1}{4}-y, \frac{3}{4}-x, \frac{3}{4}+z)$ $(\frac{3}{4}+z, \frac{1}{4}-y, \frac{3}{4}-x)$ $(\frac{3}{4}-x, \frac{3}{4}+z, \frac{1}{4}-y)$	161	R3c

TABLE 3. *Reduction from 432 to 422*

Space group of unstrained crystal, order 24 per lattice point		If stressed so that $X=Y$, $z\|\|Z$			Space group of strained crystal, order 8 per lattice point	
		Coordinates referred to axes of unstrained crysta				
No.	Symbol	1st Subset	2d Subset	3d Subset	No.	Symbol
207	P432	(x, y, z) $(y, x, \bar{z})$ $(\bar{y}, x, z)$ $(\bar{x}, y, \bar{z})$ $(\bar{x}, \bar{y}, z)$ $(\bar{y}, \bar{x}, \bar{z})$ $(y, \bar{x}, z)$ $(x, \bar{y}, \bar{z})$	(y, z, x) $(z, y, \bar{x})$ $(\bar{z}, y, x)$ $(\bar{y}, z, \bar{x})$ $(\bar{y}, \bar{z}, x)$ $(\bar{z}, \bar{y}, \bar{x})$ $(z, \bar{y}, x)$ $(y, \bar{z}, \bar{x})$	(z, x, y) $(x, z, \bar{y})$ $(\bar{x}, z, y)$ $(\bar{z}, x, \bar{y})$ $(\bar{z}, \bar{x}, y)$ $(\bar{x}, \bar{z}, \bar{y})$ $(x, \bar{z}, y)$ $(z, \bar{x}, \bar{y})$	89	P422
208	$P4_232$	(x, y, z) $(\frac{1}{2}+y, \frac{1}{2}+x, \frac{1}{2}-z)$ $(\frac{1}{2}-y, \frac{1}{2}+x, \frac{1}{2}+z)$ $(\bar{x}, y, \bar{z})$ $(\bar{x}, \bar{y}, z)$ $(\frac{1}{2}-y, \frac{1}{2}-x, \frac{1}{2}-z)$ $(\frac{1}{2}+y, \frac{1}{2}-x, \frac{1}{2}+z)$ $(x, \bar{y}, \bar{z})$	(y, z, x) $(\frac{1}{2}+z, \frac{1}{2}+y, \frac{1}{2}-x)$ $(\frac{1}{2}-z, \frac{1}{2}+y, \frac{1}{2}+x)$ $(\bar{y}, z, \bar{x})$ $(\bar{y}, \bar{z}, x)$ $(\frac{1}{2}-z, \frac{1}{2}-y, \frac{1}{2}-x)$ $(\frac{1}{2}+z, \frac{1}{2}-y, \frac{1}{2}+x)$ $(y, \bar{z}, \bar{x})$	(z, x, y) $(\frac{1}{2}+x, \frac{1}{2}+z, \frac{1}{2}-y)$ $(\frac{1}{2}-x, \frac{1}{2}+z, \frac{1}{2}+y)$ $(\bar{z}, x, \bar{y})$ $(\bar{z}, \bar{x}, y)$ $(\frac{1}{2}-x, \frac{1}{2}-z, \frac{1}{2}-y)$ $(\frac{1}{2}+x, \frac{1}{2}-z, \frac{1}{2}+y)$ $(z, \bar{x}, \bar{y})$	93	$P4_222$
209	F432	(x, y, z) $(y, x, \bar{z})$ $(\bar{y}, x, z)$ $(\bar{x}, y, \bar{z})$ $(\bar{x}, \bar{y}, z)$ $(\bar{y}, \bar{x}, \bar{z})$ $(y, \bar{x}, z)$ $(x, \bar{y}, \bar{z})$	(y, z, x) $(z, y, \bar{x})$ $(\bar{z}, y, x)$ $(\bar{y}, z, \bar{x})$ $(\bar{y}, \bar{z}, x)$ $(\bar{z}, \bar{y}, \bar{x})$ $(z, \bar{y}, x)$ $(y, \bar{z}, \bar{x})$	(z, x, y) $(x, z, \bar{y})$ $(\bar{x}, z, y)$ $(\bar{z}, x, \bar{y})$ $(\bar{z}, \bar{x}, y)$ $(\bar{x}, \bar{z}, \bar{y})$ $(x, \bar{z}, y)$ $(z, \bar{x}, \bar{y})$	97	I422
210	$F4_132$	(x, y, z) $(\frac{3}{4}+y, \frac{1}{4}+x, \frac{1}{4}-z)$ $(\frac{3}{4}-y, \frac{1}{4}+x, \frac{1}{4}+z)$ $(\bar{x}, y, \bar{z})$ $(\bar{x}, \bar{y}, z)$ $(\frac{3}{4}-y, \frac{1}{4}-x, \frac{1}{4}-z)$ $(\frac{3}{4}+y, \frac{1}{4}-x, \frac{1}{4}+z)$ $(x, \bar{y}, \bar{z})$	(y, z, x) $(\frac{3}{4}+z, \frac{1}{4}+y, \frac{1}{4}-x)$ $(\frac{3}{4}-z, \frac{1}{4}+y, \frac{1}{4}+x)$ $(\bar{y}, z, \bar{x})$ $(\bar{y}, \bar{z}, x)$ $(\frac{3}{4}-z, \frac{1}{4}-y, \frac{1}{4}-x)$ $(\frac{3}{4}+z, \frac{1}{4}-y, \frac{1}{4}+x)$ $(y, \bar{z}, \bar{x})$	(z, x, y) $(\frac{3}{4}+x, \frac{1}{4}+z, \frac{1}{4}-y)$ $(\frac{1}{4}-x, \frac{1}{4}+z, \frac{1}{4}+y)$ $(\bar{z}, x, \bar{y})$ $(\bar{z}, \bar{x}, y)$ $(\frac{3}{4}-x, \frac{1}{4}-z, \frac{1}{4}-y)$ $(\frac{1}{4}+x, \frac{1}{4}-z, \frac{1}{4}+y)$ $(z, \bar{x}, \bar{y})$	98	$I4_122$
211	I432	(x, y, z) $(y, x, \bar{z})$ $(\bar{y}, x, z)$ $(\bar{x}, y, \bar{z})$ $(\bar{x}, \bar{y}, z)$ $(\bar{y}, \bar{x}, \bar{z})$ $(y, \bar{x}, z)$ $(x, \bar{y}, \bar{z})$	(y, z, x) $(z, y, \bar{x})$ $(\bar{z}, y, x)$ $(\bar{y}, z, \bar{x})$ $(\bar{y}, \bar{z}, x)$ $(\bar{z}, \bar{y}, \bar{x})$ $(z, \bar{y}, x)$ $(y, \bar{z}, \bar{x})$	(z, x, y) $(x, z, \bar{y})$ $(\bar{x}, z, y)$ $(\bar{z}, x, \bar{y})$ $(\bar{z}, \bar{x}, y)$ $(\bar{x}, \bar{z}, \bar{y})$ $(x, \bar{z}, y)$ $(z, \bar{x}, \bar{y})$	97	I422
212	$P4_332$	(x, y, z) $(\frac{3}{4}+y, \frac{3}{4}+x, \frac{3}{4}-z)$ $(\frac{3}{4}-y, \frac{1}{4}+x, \frac{3}{4}+z)$ $(\bar{x}, \frac{1}{2}+y, \frac{1}{2}-z)$ $(\frac{1}{2}-x, \bar{y}, \frac{1}{2}+z)$ $(\frac{3}{4}-y, \frac{1}{4}-x, \frac{1}{4}-z)$ $(\frac{3}{4}+y, \frac{3}{4}-x, \frac{1}{4}+z)$ $(\frac{1}{2}+x, \frac{1}{2}-y, \bar{z})$	(y, z, x) $(\frac{3}{4}+z, \frac{3}{4}+y, \frac{3}{4}-x)$ $(\frac{3}{4}-z, \frac{1}{4}+y, \frac{3}{4}+x)$ $(\bar{y}, \frac{1}{2}+z, \frac{1}{2}-x)$ $(\frac{1}{2}-y, \bar{z}, \frac{1}{2}+x)$ $(\frac{3}{4}-z, \frac{1}{4}-y, \frac{1}{4}-x)$ $(\frac{3}{4}+z, \frac{3}{4}-y, \frac{1}{4}+x)$ $(\frac{1}{2}+y, \frac{1}{2}-z, \bar{x})$	(z, x, y) $(\frac{3}{4}+x, \frac{3}{4}+z, \frac{3}{4}-y)$ $(\frac{3}{4}-x, \frac{1}{4}+z, \frac{3}{4}+y)$ $(\bar{z}, \frac{1}{2}+x, \frac{1}{2}-y)$ $(\frac{1}{2}-z, \bar{x}, \frac{1}{2}+y)$ $(\frac{3}{4}-x, \frac{1}{4}-z, \frac{1}{4}-y)$ $(\frac{3}{4}+x, \frac{3}{4}-z, \frac{1}{4}+y)$ $(\frac{1}{2}+z, \frac{1}{2}-x, \bar{y})$	96	$P4_232$
213	$P4_132$	(x, y, z) $(\frac{3}{4}+y, \frac{3}{4}+x, \frac{1}{4}-z)$ $(\frac{3}{4}-y, \frac{3}{4}+x, \frac{1}{4}+z)$ $(\bar{x}, \frac{1}{2}+y, \frac{1}{2}-z)$ $(\frac{1}{2}-x, \bar{y}, \frac{1}{2}+z)$ $(\frac{3}{4}-y, \frac{3}{4}-x, \frac{3}{4}-z)$ $(\frac{1}{4}+y, \frac{1}{4}-x, \frac{3}{4}+z)$ $(\frac{1}{2}+x, \frac{1}{2}-y, \bar{z})$	(y, z, x) $(\frac{3}{4}+z, \frac{1}{4}+y, \frac{1}{4}-x)$ $(\frac{1}{4}-z, \frac{3}{4}+y, \frac{1}{4}+x)$ $(\bar{y}, \frac{1}{2}+z, \frac{1}{2}-x)$ $(\frac{1}{2}-y, \bar{z}, \frac{1}{2}+x)$ $(\frac{3}{4}-z, \frac{3}{4}-y, \frac{3}{4}-x)$ $(\frac{1}{4}+z, \frac{1}{4}-y, \frac{3}{4}+x)$ $(\frac{1}{2}+y, \frac{1}{2}-z, \bar{x})$	(z, x, y) $(\frac{3}{4}+x, \frac{1}{4}+z, \frac{1}{4}-y)$ $(\frac{1}{4}-x, \frac{3}{4}+z, \frac{1}{4}+y)$ $(\bar{z}, \frac{1}{2}+x, \frac{1}{2}-y)$ $(\frac{1}{2}-z, \bar{x}, \frac{1}{2}+y)$ $(\frac{3}{4}-x, \frac{3}{4}-z, \frac{3}{4}-y)$ $(\frac{1}{4}+x, \frac{1}{4}-z, \frac{3}{4}+y)$ $(\frac{1}{2}+z, \frac{1}{2}-x, \bar{y})$	92	$P4_122$
214	$I4_132$	(x, y, z) $(\frac{3}{4}+y, \frac{3}{4}+x, \frac{3}{4}-z)$ $(\frac{3}{4}-y, \frac{1}{4}+x, \frac{3}{4}+z)$ $(\bar{x}, \frac{1}{2}+y, \frac{1}{2}-z)$ $(\frac{1}{2}-x, \bar{y}, \frac{1}{2}+z)$ $(\frac{3}{4}-y, \frac{1}{4}-x, \frac{1}{4}-z)$ $(\frac{3}{4}+y, \frac{3}{4}-x, \frac{1}{4}+z)$ $(\frac{1}{2}+x, \frac{1}{2}-y, \bar{z})$	(y, z, x) $(\frac{3}{4}+z, \frac{3}{4}+y, \frac{3}{4}-x)$ $(\frac{3}{4}-z, \frac{1}{4}+y, \frac{3}{4}+x)$ $(\bar{y}, \frac{1}{2}+z, \frac{1}{2}-x)$ $(\frac{1}{2}-y, \bar{z}, \frac{1}{2}+x)$ $(\frac{3}{4}-z, \frac{3}{4}-y, \frac{1}{4}-x)$ $(\frac{3}{4}+z, \frac{3}{4}-y, \frac{1}{4}+x)$ $(\frac{1}{2}+y, \frac{1}{2}-z, \bar{x})$	(z, x, y) $(\frac{3}{4}+x, \frac{3}{4}+z, \frac{3}{4}-y)$ $(\frac{3}{4}-x, \frac{1}{4}+z, \frac{3}{4}+y)$ $(\bar{z}, \frac{1}{2}+x, \frac{1}{2}-y)$ $(\frac{1}{2}-z, \bar{x}, \frac{1}{2}+y)$ $(\frac{3}{4}-x, \frac{3}{4}-z, \frac{1}{4}-y)$ $(\frac{3}{4}+x, \frac{3}{4}-z, \frac{1}{4}+y)$ $(\frac{1}{2}+z, \frac{1}{2}-x, \bar{y})$	98	$I4_122$

TABLE 4. *Reduction from 432 to 32*

Space group of unstrained crystal order 24 per lattice point		If stressed so that $X=Y$; $[111]\parallel Z$				Space group of strained crystal order 6 per lattice point	
		Coordinates referred to axes of unstrained crystal					
No.	Symbol	1st Subset	2d Subset	3d Subset	4th Subset	No.	Symbol
207	P432	(x, y, z) (y, z, x) (z, x, y) $(\bar{y}, \bar{x}, \bar{z})$ $(\bar{z}, \bar{y}, \bar{x})$ $(\bar{x}, \bar{z}, \bar{y})$	$(x, \bar{y}, \bar{z})$ $(\bar{y}, \bar{z}, x)$ $(\bar{z}, x, \bar{y})$ $(y, \bar{x}, z)$ $(z, y, \bar{x})$ $(\bar{x}, z, y)$	$(\bar{x}, y, \bar{z})$ $(y, \bar{z}, \bar{x})$ $(\bar{z}, \bar{x}, y)$ $(\bar{y}, x, z)$ $(z, \bar{y}, x)$ $(x, z, \bar{y})$	$(\bar{x}, \bar{y}, z)$ $(\bar{y}, z, \bar{x})$ $(z, \bar{x}, \bar{y})$ $(y, x, \bar{z})$ $(\bar{z}, y, x)$ $(x, \bar{z}, y)$	155	R32
208	$P4_232$	(x, y, z) (y, z, x) (z, x, y) $(\frac{1}{2}-y, \frac{1}{2}-x, \frac{1}{2}-z)$ $(\frac{1}{2}-z, \frac{1}{2}-y, \frac{1}{2}-x)$ $(\frac{1}{2}-x, \frac{1}{2}-z, \frac{1}{2}-y)$	$(x, \bar{y}, \bar{z})$ $(\bar{y}, \bar{z}, x)$ $(\bar{z}, x, \bar{y})$ $(\frac{1}{2}+y, \frac{1}{2}-x, \frac{1}{2}+z)$ $(\frac{1}{2}+z, \frac{1}{2}+y, \frac{1}{2}-x)$ $(\frac{1}{2}-x, \frac{1}{2}+z, \frac{1}{2}+y)$	$(\bar{x}, y, \bar{z})$ $(y, \bar{z}, \bar{x})$ $(\bar{z}, \bar{x}, y)$ $(\frac{1}{2}-y, \frac{1}{2}+x, \frac{1}{2}+z)$ $(\frac{1}{2}+z, \frac{1}{2}-y, \frac{1}{2}+x)$ $(\frac{1}{2}+x, \frac{1}{2}+z, \frac{1}{2}-y)$	$(\bar{x}, \bar{y}, z)$ $(\bar{y}, z, \bar{x})$ $(z, \bar{x}, \bar{y})$ $(\frac{1}{2}+y, \frac{1}{2}+x, \frac{1}{2}-z)$ $(\frac{1}{2}-z, \frac{1}{2}+y, \frac{1}{2}+x)$ $(\frac{1}{2}+x, \frac{1}{2}-z, \frac{1}{2}+y)$	155	R32
209	F432	(x, y, z) (y, z, x) (z, x, y) $(\bar{y}, \bar{x}, \bar{z})$ $(\bar{z}, \bar{y}, \bar{x})$ $(\bar{x}, \bar{z}, \bar{y})$	$(x, \bar{y}, \bar{z})$ $(\bar{y}, \bar{z}, x)$ $(\bar{z}, x, \bar{y})$ $(y, \bar{x}, z)$ $(z, y, \bar{x})$ $(\bar{x}, z, y)$	$(\bar{x}, y, \bar{z})$ $(y, \bar{z}, \bar{x})$ $(\bar{z}, \bar{x}, y)$ $(\bar{y}, x, z)$ $(z, \bar{y}, x)$ $(x, z, \bar{y})$	$(\bar{x}, \bar{y}, z)$ $(\bar{y}, z, \bar{x})$ $(z, \bar{x}, \bar{y})$ $(y, x, \bar{z})$ $(\bar{z}, y, x)$ $(x, \bar{z}, y)$	155	R32
210	$F4_132$	(x, y, z) (y, z, x) (z, x, y) $(\frac{1}{4}-y, \frac{1}{4}-x, \frac{1}{4}-z)$ $(\frac{1}{4}-z, \frac{1}{4}-y, \frac{1}{4}-x)$ $(\frac{1}{4}-x, \frac{1}{4}-z, \frac{1}{4}-y)$	$(x, \bar{y}, \bar{z})$ $(\bar{y}, \bar{z}, x)$ $(\bar{z}, x, \bar{y})$ $(\frac{1}{4}+y, \frac{1}{4}-x, \frac{1}{4}+z)$ $(\frac{1}{4}+z, \frac{1}{4}+y, \frac{1}{4}-x)$ $(\frac{1}{4}-x, \frac{1}{4}+z, \frac{1}{4}+y)$	$(\bar{x}, y, \bar{z})$ $(y, \bar{z}, \bar{x})$ $(\bar{z}, \bar{x}, y)$ $(\frac{1}{4}-y, \frac{1}{4}+x, \frac{1}{4}+z)$ $(\frac{1}{4}+z, \frac{1}{4}-y, \frac{1}{4}+x)$ $(\frac{1}{4}+x, \frac{1}{4}+z, \frac{1}{4}-y)$	$(\bar{x}, \bar{y}, z)$ $(\bar{y}, z, \bar{x})$ $(z, \bar{x}, \bar{y})$ $(\frac{1}{4}+y, \frac{1}{4}+x, \frac{1}{4}-z)$ $(\frac{1}{4}-z, \frac{1}{4}+y, \frac{1}{4}+x)$ $(\frac{1}{4}+x, \frac{1}{4}-z, \frac{1}{4}+y)$	155	R32
211	I432	(x, y, z) (y, z, x) (z, x, y) $(\bar{y}, \bar{x}, \bar{z})$ $(\bar{z}, \bar{y}, \bar{x})$ $(\bar{x}, \bar{z}, \bar{y})$	$(x, \bar{y}, \bar{z})$ $(\bar{y}, \bar{z}, x)$ $(\bar{z}, x, \bar{y})$ $(y, \bar{x}, z)$ $(z, y, \bar{x})$ $(\bar{x}, z, y)$	$(\bar{x}, y, \bar{z})$ $(y, \bar{z}, \bar{x})$ $(\bar{z}, \bar{x}, y)$ $(\bar{y}, x, z)$ $(z, \bar{y}, x)$ $(x, z, \bar{y})$	$(\bar{x}, \bar{y}, z)$ $(\bar{y}, z, \bar{x})$ $(z, \bar{x}, \bar{y})$ $(y, x, \bar{z})$ $(\bar{z}, y, x)$ $(x, \bar{z}, y)$	155	R32
212	$P4_232$	(x, y, z) (y, z, x) (z, x, y) $(\frac{1}{4}-y, \frac{1}{4}-x, \frac{1}{4}-z)$ $(\frac{1}{4}-z, \frac{1}{4}-y, \frac{1}{4}-x)$ $(\frac{1}{4}-x, \frac{1}{4}-z, \frac{1}{4}-y)$	$(\frac{1}{2}+x, \frac{1}{2}-y, \bar{z})$ $(\frac{1}{2}-y, \bar{z}, \frac{1}{2}+x)$ $(\bar{z}, \frac{1}{2}+x, \frac{1}{2}-y)$ $(\frac{3}{4}+y, \frac{3}{4}-x, \frac{1}{4}+z)$ $(\frac{1}{4}+z, \frac{3}{4}+y, \frac{3}{4}-x)$ $(\frac{3}{4}-x, \frac{1}{4}+z, \frac{3}{4}+y)$	$(\bar{x}, \frac{1}{2}+y, \frac{1}{2}-z)$ $(\frac{1}{2}+y, \frac{1}{2}-z, \bar{x})$ $(\frac{1}{2}-z, \bar{x}, \frac{1}{2}+y)$ $(\frac{3}{4}-y, \frac{1}{4}+x, \frac{3}{4}+z)$ $(\frac{3}{4}+z, \frac{3}{4}-y, \frac{1}{4}+x)$ $(\frac{1}{4}+x, \frac{3}{4}+z, \frac{3}{4}-y)$	$(\frac{1}{2}-x, \bar{y}, \frac{1}{2}+z)$ $(\bar{y}, \frac{1}{2}+z, \frac{1}{2}-x)$ $(\frac{1}{2}+z, \frac{1}{2}-x, \bar{y})$ $(\frac{1}{4}+y, \frac{3}{4}+x, \frac{3}{4}-z)$ $(\frac{3}{4}-z, \frac{1}{4}+y, \frac{3}{4}+x)$ $(\frac{3}{4}+x, \frac{3}{4}-z, \frac{1}{4}+y)$	155	R32
213	$P4_232$	(x, y, z) (y, z, x) (z, x, y) $(\frac{3}{4}-y, \frac{3}{4}-x, \frac{3}{4}-z)$ $(\frac{3}{4}-z, \frac{3}{4}-y, \frac{3}{4}-x)$ $(\frac{3}{4}-x, \frac{3}{4}-z, \frac{3}{4}-y)$	$(\frac{1}{2}+x, \frac{1}{2}-y, \bar{z})$ $(\frac{1}{2}-y, \bar{z}, \frac{1}{2}+x)$ $(\bar{z}, \frac{1}{2}+x, \frac{1}{2}-y)$ $(\frac{1}{4}+y, \frac{1}{4}-x, \frac{3}{4}+z)$ $(\frac{3}{4}+z, \frac{1}{4}+y, \frac{1}{4}-x)$ $(\frac{1}{4}-x, \frac{3}{4}+z, \frac{1}{4}+y)$	$(\bar{x}, \frac{1}{2}+y, \frac{1}{2}-z)$ $(\frac{1}{2}+y, \frac{1}{2}-z, \bar{x})$ $(\frac{1}{2}-z, \bar{x}, \frac{1}{2}+y)$ $(\frac{1}{4}-y, \frac{3}{4}+x, \frac{1}{4}+z)$ $(\frac{1}{4}+z, \frac{1}{4}-y, \frac{3}{4}+x)$ $(\frac{3}{4}+x, \frac{1}{4}+z, \frac{1}{4}-y)$	$(\frac{1}{2}-x, \bar{y}, \frac{1}{2}+z)$ $(\bar{y}, \frac{1}{2}+z, \frac{1}{2}-x)$ $(\frac{1}{2}+z, \frac{1}{2}-x, \bar{y})$ $(\frac{3}{4}+y, \frac{1}{4}+x, \frac{1}{4}-z)$ $(\frac{1}{4}-z, \frac{3}{4}+y, \frac{1}{4}+x)$ $(\frac{1}{4}+x, \frac{1}{4}-z, \frac{3}{4}+y)$	155	K32
214	$I4_132$	(x, y, z) (y, z, x) (z, x, y) $(\frac{1}{4}-y, \frac{1}{4}-x, \frac{1}{4}-z)$ $(\frac{1}{4}-z, \frac{1}{4}-y, \frac{1}{4}-x)$ $(\frac{1}{4}-x, \frac{1}{4}-z, \frac{1}{4}-y)$	$(\frac{1}{2}+x, \frac{1}{2}-y, \bar{z})$ $(\frac{1}{2}-y, \bar{z}, \frac{1}{2}+x)$ $(\bar{z}, \frac{1}{2}+x, \frac{1}{2}-y)$ $(\frac{3}{4}+y, \frac{3}{4}-x, \frac{1}{4}+z)$ $(\frac{1}{4}+z, \frac{3}{4}+y, \frac{3}{4}-x)$ $(\frac{3}{4}-x, \frac{1}{4}+z, \frac{3}{4}+y)$	$(\bar{x}, \frac{1}{2}+y, \frac{1}{2}-z)$ $(\frac{1}{2}+y, \frac{1}{2}-z, \bar{x})$ $(\frac{1}{2}-z, \bar{x}, \frac{1}{2}+y)$ $(\frac{3}{4}-y, \frac{1}{4}+x, \frac{3}{4}+z)$ $(\frac{3}{4}+z, \frac{3}{4}-y, \frac{1}{4}+x)$ $(\frac{1}{4}+x, \frac{3}{4}+z, \frac{3}{4}-y)$	$(\frac{1}{2}-x, \bar{y}, \frac{1}{2}+z)$ $(\bar{y}, \frac{1}{2}+z, \frac{1}{2}-x)$ $(\frac{1}{2}+z, \frac{1}{2}-x, \bar{y})$ $(\frac{1}{4}+y, \frac{3}{4}+x, \frac{3}{4}-z)$ $(\frac{3}{4}-z, \frac{1}{4}+y, \frac{3}{4}+x)$ $(\frac{3}{4}+x, \frac{3}{4}-z, \frac{1}{4}+y)$	155	R32

TABLE 5. *Reduction from 23 to 222*

Space group of unstrained crystal, order 12 per lattice point		If stressed so that $x, y, z \parallel X, Y, Z$, any permutation			Space group of strained crystal, order 4 per lattice point	
		Coordinates referred to axes of unstrained crystal				
No.	Symbol	1st Subset	2d Subset	3d Subset	No.	Symbol
195	P23	(x, y, z) $(x, \bar{y}, \bar{z})$ $(\bar{x}, y, \bar{z})$ $(\bar{x}, \bar{y}, z)$	(y, z, x) $(y, \bar{z}, \bar{x})$ $(\bar{y}, z, \bar{x})$ $(\bar{y}, \bar{z}, x)$	(z, x, y) $(z, \bar{x}, \bar{y})$ $(\bar{z}, x, \bar{y})$ $(\bar{z}, \bar{x}, y)$	16	P222
196	F23	(x, y, z) $(x, \bar{y}, \bar{z})$ $(\bar{x}, y, \bar{z})$ $(\bar{x}, \bar{y}, z)$	(y, z, x) $(y, \bar{z}, \bar{x})$ $(\bar{y}, z, \bar{x})$ $(\bar{y}, \bar{z}, x)$	(z, x, y) $(z, \bar{x}, \bar{y})$ $(\bar{z}, x, \bar{y})$ $(\bar{z}, \bar{x}, y)$	22	F222
197	I23	(x, y, z) $(x, \bar{y}, \bar{z})$ $(\bar{x}, y, \bar{z})$ $(\bar{x}, \bar{y}, z)$	(y, z, x) $(y, \bar{z}, \bar{x})$ $(\bar{y}, z \bar{x})$ $(\bar{y}, \bar{z}, x)$	(z, x, y) $(z, \bar{x}, \bar{y})$ $(\bar{z}, x, \bar{y})$ $(\bar{z}, \bar{x}, y)$	23	I222
198	$P2_13$	(x, y, z) $(\frac{1}{2}+x, \frac{1}{2}-y, \bar{z})$ $(\bar{x}, \frac{1}{2}+y, \frac{1}{2}-z)$ $(\frac{1}{2}-x, \bar{y}, \frac{1}{2}+z)$	(y, z, x) $(\frac{1}{2}+y, \frac{1}{2}-z, \bar{x})$ $(\bar{y}, \frac{1}{2}+z, \frac{1}{2}-x)$ $(\frac{1}{2}-y, \bar{z}, \frac{1}{2}+x)$	(z, x, y) $(\frac{1}{2}+z, \frac{1}{2}-x, \bar{y})$ $(\bar{z}, \frac{1}{2}+x, \frac{1}{2}-y)$ $(\frac{1}{2}-z, \bar{x}, \frac{1}{2}+y)$	19	$P2_12_12_1$
199	$I2_13$	(x, y, z) $(\frac{1}{2}+x, \frac{1}{2}-y, \bar{z})$ $(\bar{x}, \frac{1}{2}+y, \frac{1}{2}-z)$ $(\frac{1}{2}-x, \bar{y}, \frac{1}{2}+z)$	(y, z, x) $(\frac{1}{2}+y, \frac{1}{2}-z, \bar{x})$ $(\bar{y}, \frac{1}{2}+z, \frac{1}{2}-x)$ $(\frac{1}{2}-y, \bar{z}, \frac{1}{2}+x)$	(z, x, y) $(\frac{1}{2}+z, \frac{1}{2}-x, \bar{y})$ $(\bar{z}, \frac{1}{2}+x, \frac{1}{2}-y)$ $(\frac{1}{2}-z, \bar{x}, \frac{1}{2}+y)$	24	$I2_12_12_1$

TABLE 6. *Reduction from 23 to 3*

Space group of unstrained crystal, order 12 per lattice point		If stressed so that $X=Y$; $[111] \parallel Z$				Space group of strained crystal, order 3 per lattice point	
		Coordinates referred to axes of unstrained crystal					
No.	Symbol	1st Subset	2d Subset	3d Subset	4th Subset	No.	Symbol
195	P23	(x, y, z) (y, z, x) (z, x, y)	$(x, \bar{y}, \bar{z})$ $(\bar{y}, \bar{z}, x)$ $(\bar{z}, x, \bar{y})$	$(\bar{x}, y, \bar{z})$ $(y, \bar{z}, \bar{x})$ $(\bar{z}, \bar{x}, y)$	$(\bar{x}, \bar{y}, z)$ $(\bar{y}, z, \bar{x})$ $(z, \bar{x}, \bar{y})$	146	R3
196	F23	(x, y, z) (y, z, x) (z, x, y)	$(x, \bar{y}, \bar{z})$ $(\bar{y}, \bar{z}, x)$ $(\bar{z}, x, \bar{y})$	$(\bar{x}, y, \bar{z})$ $(y, \bar{z}, \bar{x})$ $(\bar{z}, \bar{x}, y)$	$(\bar{x}, \bar{y}, z)$ $(\bar{y}, z, \bar{x})$ $(z, \bar{x}, \bar{y})$	146	R3
197	I23	(x, y, z) (y, z, x) (z, x, y)	$(x, \bar{y}, \bar{z})$ $(\bar{y}, \bar{z}, x)$ $(\bar{z}, x, \bar{y})$	$(\bar{x}, y, \bar{z})$ $(y, \bar{z}, \bar{x})$ $(\bar{z}, \bar{x}, y)$	$(\bar{x}, \bar{y}, z)$ $(\bar{y}, z, \bar{x})$ $(z, \bar{x}, \bar{y})$	146	R3
198	$P2_13$	(x, y, z) (y, z, x) (z, x, y)	$(\frac{1}{2}+x, \frac{1}{2}-y, \bar{z})$ $(\frac{1}{2}-y, \bar{z}, \frac{1}{2}+x)$ $(\bar{z}, \frac{1}{2}+x, \frac{1}{2}-y)$	$(\bar{x}, \frac{1}{2}+y, \frac{1}{2}-z)$ $(\frac{1}{2}+y, \frac{1}{2}-z, \bar{x})$ $(\frac{1}{2}-z, \bar{x}, \frac{1}{2}+y)$	$(\frac{1}{2}-x, \bar{y}, \frac{1}{2}+z)$ $(\bar{y}, \frac{1}{2}+z, \frac{1}{2}-x)$ $(\frac{1}{2}+z, \frac{1}{2}-x, \bar{y})$	146	R3
199	$I2_13$	(x, y, z) (y, z, x) (z, x, y)	$(\frac{1}{2}+x, \frac{1}{2}-y, \bar{z})$ $(\frac{1}{2}-y, \bar{z}, \frac{1}{2}+x)$ $(\bar{z}, \frac{1}{2}+x, \frac{1}{2}-y)$	$(\bar{x}, \frac{1}{2}+y, \frac{1}{2}-z)$ $(\frac{1}{2}+y, \frac{1}{2}-z, \bar{x})$ $(\frac{1}{2}-z, \bar{x}, \frac{1}{2}+y)$	$(\frac{1}{2}-x, \bar{y}, \frac{1}{2}+z)$ $(\bar{y}, \frac{1}{2}+z, \frac{1}{2}-x)$ $(\frac{1}{2}+z, \frac{1}{2}-x, \bar{y})$	146	R3

TABLE 7. *Reduction from $\bar{6}m2$ to mm2*

Space group of unstrained crystal, order 12 per lattice point		If stressed so that y and $z \parallel$ any two of X, Y, and Z			Space group of strained crystal, order 4 per lattice point	
		Coordinates referred to axes of unstrained crystal				
No.	Symbol	1st Subset	2d Subset	3d Subset	No.	Symbol
187	$P\bar{6}m2$	(x, y, z) $(x, x-y, z)$ $(x, y, \bar{z})$ $(x, x-y, \bar{z})$	$(\bar{y}, x-y, z)$ $(\bar{y}, \bar{x}, z)$ $(\bar{y}, x-y, \bar{z})$ $(\bar{y}, \bar{x}, \bar{z})$	$(y-x, \bar{x}, z)$ $(y-x, y, z)$ $(y-x, \bar{x}, \bar{z})$ $(y-x, y, \bar{z})$	38	Amm2
188	$P\bar{6}c2$	(x, y, z) $(x, x-y, \frac{1}{2}+z)$ $(x, y, \frac{1}{2}-z)$ $(x, x-y, \bar{z})$	$(\bar{y}, x-y, z)$ $(\bar{y}, \bar{x}, \frac{1}{2}+z)$ $(\bar{y}, x-y, \frac{1}{2}-z)$ $(\bar{y}, \bar{x}, \bar{z})$	$(y-x, \bar{x}, z)$ $(y-x, y, \frac{1}{2}+z)$ $(y-x, \bar{x}, \frac{1}{2}-z)$ $(y-x, y, \bar{z})$	40	Ama2
189	$P\bar{6}2m$	(x, y, z) $(\bar{x}, y-x, z)$ $(x, y, \bar{z})$ $(\bar{x}, y-x, \bar{z})$	$(\bar{y}, x-y, z)$ (y, x, z) $(\bar{y}, x-y, \bar{z})$ $(y, x, \bar{z})$	$(y-x, \bar{x}, z)$ $(x-y, \bar{y}, z)$ $(y-x, \bar{x}, \bar{z})$ $(x-y, \bar{y}, \bar{z})$	38	Amm2
190	$P\bar{6}2c$	(x, y, z) $(\bar{x}, y-x, \frac{1}{2}+z)$ $(x, y, \frac{1}{2}-z)$ $(\bar{x}, y-x, \bar{z})$	$(\bar{y}, x-y, z)$ $(y, x, \frac{1}{2}+z)$ $(\bar{y}, x-y, \frac{1}{2}-z)$ $(y, x, \bar{z})$	$(y-x, \bar{x}, z)$ $(x-y, \bar{y}, \frac{1}{2}+z)$ $(y-x, \bar{x}, \frac{1}{2}-z)$ $(x-y, \bar{y}, \bar{z})$	40	Ama2

TABLE 8. *Reduction from 6mm to mm2*

Space group of unstrained crystal, order 12 per lattice point		If stressed so that y and $z \parallel$ any two of X, Y, and Z			Space group of strained crystal, order 4 per lattice point	
		Coordinates referred to axes of unstrained crystal				
No.	Symbol	1st Subset	2d Subset	3d Subset	No.	Symbol
183	P6mm	(x, y, z) $(x, x-y, z)$ $(\bar{x}, \bar{y}, z)$ $(\bar{x}, y-x, z)$	$(\bar{y}, x-y, z)$ $(\bar{y}, \bar{x}, z)$ $(y, y-x, z)$ (y, x, z)	$(y-x, \bar{x}, z)$ $(y-x, y, z)$ $(x-y, x, z)$ $(x-y, \bar{y}, z)$	35	Cmm2
184	P6cc	(x, y, z) $(x, x-y, \frac{1}{2}+z)$ $(\bar{x}, \bar{y}, z)$ $(\bar{x}, y-x, \frac{1}{2}+z)$	$(\bar{y}, x-y, z)$ $(\bar{y}, \bar{x}, \frac{1}{2}+z)$ $(y, y-x, z)$ $(y, x, \frac{1}{2}+z)$	$(y-x, \bar{x}, z)$ $(y-x, y, \frac{1}{2}+z)$ $(x-y, x, z)$ $(x-y, \bar{y}, \frac{1}{2}+z)$	37	Ccc2
185	$P6_3cm$	(x, y, z) $(x, x-y, \frac{1}{2}+z)$ $(\bar{x}, \bar{y}, \frac{1}{2}+z)$ $(\bar{x}, y-x, z)$	$(\bar{y}, x-y, z)$ $(\bar{y}, \bar{x}, \frac{1}{2}+z)$ $(y, y-x, \frac{1}{2}+z)$ (y, x, z)	$(y-x, \bar{x}, z)$ $(y-x, y, \frac{1}{2}+z)$ $(x-y, x, \frac{1}{2}+z)$ $(x-y, \bar{y}, z)$	36	$Cmc2_1$
186	$P6_3mc$	(x, y, z) $(x, x-y, z)$ $(\bar{x}, \bar{y}, \frac{1}{2}+z)$ $(\bar{x}, y-x, \frac{1}{2}+z)$	$(\bar{y}, x-y, z)$ $(\bar{y}, \bar{x}, z)$ $(y, y-x, \frac{1}{2}+z)$ $(y, x, \frac{1}{2}+z)$	$(y-x, \bar{x}, z)$ $(y-x, y, z)$ $(x-y, x, \frac{1}{2}+z)$ $(x-y, \bar{y}, \frac{1}{2}+z)$	36	$Cmc2_1$

TABLE 9. *Reduction from 622 to 222*

Space group of unstrained crystal, order 12 per lattice point		If stressed so that y and $z \parallel$ any two of X, Y, and Z			Space group of strained crystal, order 4 per lattice point	
		Coordinates referred to axes of unstrained crysta				
No.	Symbol	1st Subset	2d Subset	3d Subset	No.	Symbol
177	P622	(x, y, z) $(x, x-y, \bar{z})$ $(\bar{x}, \bar{y}, z)$ $(\bar{x}, y-x, \bar{z})$	$(\bar{y}, x-y, z)$ $(\bar{y}, \bar{x}, \bar{z})$ $(y, y-x, z)$ $(y, x, \bar{z})$	$(y-x, \bar{x}, z)$ $(y-x, y, \bar{z})$ $(x-y, x, z)$ $(x-y, \bar{y}, \bar{z})$	21	C222
178	$P6_122$	(x, y, z) $(x, x-y, \frac{1}{6}-z)$ $(\bar{x}, \bar{y}, \frac{1}{2}+z)$ $(\bar{x}, y-x, \frac{2}{3}-z)$	$(\bar{y}, x-y, \frac{1}{3}+z)$ $(\bar{y}, \bar{x}, \frac{5}{6}-z)$ $(y, y-x, \frac{1}{6}+z)$ $(y, x, \frac{1}{2}-z)$	$(y-x, \bar{x}, \frac{2}{3}+z)$ $(y-x, y, \frac{1}{2}-z)$ $(x-y, x, \frac{1}{6}+z)$ $(x-y, \bar{y}, \bar{z})$	20	$C222_1$
179	$P6_522$	(x, y, z) $(x, x-y, \frac{5}{6}-z)$ $(\bar{x}, \bar{y}, \frac{1}{2}+z)$ $(\bar{x}, y-x, \frac{1}{3}-z)$	$(\bar{y}, x-y, \frac{2}{3}+z)$ $(\bar{y}, \bar{x}, \frac{1}{6}-z)$ $(y, y-x, \frac{1}{6}+z)$ $(y, x, \frac{2}{3}-z)$	$(y-x, \bar{x}, \frac{1}{3}+z)$ $(y-x, y, \frac{1}{2}-z)$ $(x-y, x, \frac{5}{6}+z)$ $(x-y, \bar{y}, \bar{z})$	20	$C222_1$
180	$P6_222$	(x, y, z) $(x, x-y, \frac{1}{3}-z)$ $(\bar{x}, \bar{y}, z)$ $(\bar{x}, y-x, \frac{1}{3}-z)$	$(\bar{y}, x-y, \frac{2}{3}+z)$ $(\bar{y}, \bar{x}, \frac{2}{3}-z)$ $(y, y-x, \frac{2}{3}+z)$ $(y, x, \frac{2}{3}-z)$	$(y-x, \bar{x}, \frac{1}{3}+z)$ $(y-x, y, \bar{z})$ $(x-y, x, \frac{1}{3}+z)$ $(x-y, \bar{y}, \bar{z})$	21	C222
181	$P6_422$	(x, y, z) $(x, x-y, \frac{2}{3}-z)$ $(\bar{x}, \bar{y}, z)$ $(\bar{x}, y-x, \frac{2}{3}-z)$	$(\bar{y}, x-y, \frac{1}{3}+z)$ $(\bar{y}, \bar{x}, \frac{1}{3}-z)$ $(y, y-x, \frac{1}{3}+z)$ $(y, x, \frac{1}{3}-z)$	$(y-x, \bar{x}, \frac{2}{3}+z)$ $(y-x, y, \bar{z})$ $(x-y, x, \frac{2}{3}+z)$ $(x-y, \bar{y}, \bar{z})$	21	C222
182	$P6_322$	(x, y, z) $(x, x-y, \frac{1}{2}-z)$ $(\bar{x}, \bar{y}, \frac{1}{2}+z)$ $(\bar{x}, y-x, \bar{z})$	$(\bar{y}, x-y, z)$ $(\bar{y}, \bar{x}, \frac{1}{2}-z)$ $(y, y-x, \frac{1}{2}+z)$ $(y, x, \bar{z})$	$(y-x, \bar{x}, z)$ $(y-x, y, \frac{1}{2}-z)$ $(x-y, x, \frac{1}{2}+z)$ $(x-y, \bar{y}, \bar{z})$	20	$C222_1$

TABLE 10. *Reduction from $\bar{4}2m$ to mm2*

Space group of unstrained crystal, order 8 per lattice point		If stressed so that	Coordinates referred to axes of unstrained crystal				Space group of strained crystal, order 4 per lattice point	
			1st Subset		2d Subset			
No.	Symbol						No.	Symbol
111	$P\bar{4}2m$	$[1\bar{1}0]$, $[110]$, $z \parallel X, Y, Z$, any permutation.	(x, y, z) $(\bar{x}, \bar{y}, z)$	(y, x, z) $(\bar{y}, \bar{x}, z)$	$(x, \bar{y}, \bar{z})$ $(\bar{x}, y, \bar{z})$	$(y, \bar{x}, \bar{z})$ $(\bar{y}, x, \bar{z})$	35	Cmm2
112	$P\bar{4}2c$	Do.	(x, y, z) $(\bar{x}, \bar{y}, z)$	$(y, x, \frac{1}{2}+z)$ $(\bar{y}, \bar{x}, \frac{1}{2}+z)$	$(x, \bar{y}, \frac{1}{2}-z)$ $(\bar{x}, y, \frac{1}{2}-z)$	$(y, \bar{x}, \bar{z})$ $(\bar{y}, x, \bar{z})$	37	Ccc2
113	$P\bar{4}2_1m$	Do.	(x, y, z) $(\bar{x}, \bar{y}, z)$	$(\frac{1}{2}+y, \frac{1}{2}+x, z)$ $(\frac{1}{2}-y, \frac{1}{2}-x, z)$	$(\frac{1}{2}+x, \frac{1}{2}-y, \bar{z})$ $(\frac{1}{2}-x, \frac{1}{2}+y, \bar{z})$	$(y, \bar{x}, \bar{z})$ $(\bar{y}, x, \bar{z})$	35	Cmm2
114	$P\bar{4}2_1c$	Do.	(x, y, z) $(\bar{x}, \bar{y}, z)$	$(\frac{1}{2}+y, \frac{1}{2}+x, \frac{1}{2}+z)$ $(\frac{1}{2}-y, \frac{1}{2}-x, \frac{1}{2}+z)$	$(\frac{1}{2}+x, \frac{1}{2}-y, \frac{1}{2}-z)$ $(\frac{1}{2}-x, \frac{1}{2}+y, \frac{1}{2}-z)$	$(y, \bar{x}, \bar{z})$ $(\bar{y}, x, \bar{z})$	37	Ccc2
115	$P\bar{4}m2$	$x, y, z \parallel X, Y, Z$, any permutation.	(x, y, z) $(\bar{x}, \bar{y}, z)$	$(x, \bar{y}, z)$ $(\bar{x}, y, z)$	$(y, x, \bar{z})$ $(\bar{y}, \bar{x}, \bar{z})$	$(y, \bar{x}, \bar{z})$ $(\bar{y}, x, \bar{z})$	25	Pmm2
116	$P\bar{4}c2$	Do.	(x, y, z) $(\bar{x}, \bar{y}, z)$	$(x, \bar{y}, \frac{1}{2}+z)$ $(\bar{x}, y, \frac{1}{2}+z)$	$(y, x, \frac{1}{2}-z)$ $(\bar{y}, \bar{x}, \frac{1}{2}-z)$	$(y, \bar{x}, \bar{z})$ $(\bar{y}, x, \bar{z})$	27	Pcc2
117	$P\bar{4}b2$	Do.	(x, y, z) $(\bar{x}, \bar{y}, z)$	$(\frac{1}{2}+x, \frac{1}{2}-y, z)$ $(\frac{1}{2}-x, \frac{1}{2}+y, z)$	$(\frac{1}{2}+y, \frac{1}{2}+x, \bar{z})$ $(\frac{1}{2}-y, \frac{1}{2}-x, \bar{z})$	$(y, \bar{x}, \bar{z})$ $(\bar{y}, x, \bar{z})$	32	Pba2
118	$P\bar{4}n2$	Do.	(x, y, z) $(\bar{x}, \bar{y}, z)$	$(\frac{1}{2}+x, \frac{1}{2}-y, \frac{1}{2}+z)$ $(\frac{1}{2}-x, \frac{1}{2}+y, \frac{1}{2}+z)$	$(\frac{1}{2}+y, \frac{1}{2}+x, \frac{1}{2}-z)$ $(\frac{1}{2}-y, \frac{1}{2}-x, \frac{1}{2}-z)$	$(y, \bar{x}, \bar{z})$ $(\bar{y}, x, \bar{z})$	34	Pnn2
119	$I\bar{4}m2$	Do.	(x, y, z) $(\bar{x}, \bar{y}, z)$	$(x, \bar{y}, z)$ $(\bar{x}, y, z)$	$(y, x, \bar{z})$ $(\bar{y}, \bar{x}, \bar{z})$	$(y, \bar{x}, \bar{z})$ $(\bar{y}, x, \bar{z})$	44	Imm2
120	$I\bar{4}c2$	Do.	(x, y, z) $(\bar{x}, \bar{y}, z)$	$(x, \bar{y}, \frac{1}{2}+z)$ $(\bar{x}, y, \frac{1}{2}+z)$	$(y, x, \frac{1}{2}-z)$ $(\bar{y}, \bar{x}, \frac{1}{2}-z)$	$(y, \bar{x}, \bar{z})$ $(\bar{y}, x, \bar{z})$	45	Iba2
121	$I\bar{4}2m$	$[1\bar{1}0]$, $[110]$, $z \parallel X, Y, Z$, any permutation.	(x, y, z) $(\bar{x}, \bar{y}, z)$	(y, x, z) $(\bar{y}, \bar{x}, z)$	$(x, \bar{y}, \bar{z})$ $(\bar{x}, y, \bar{z})$	$(y, \bar{x}, \bar{z})$ $(\bar{y}, x, \bar{z})$	42	Fmm2
122	$I\bar{4}2d$	Do.	(x, y, z) $(\bar{x}, \bar{y}, z)$	$(y, \frac{1}{2}+x, \frac{1}{4}+z)$ $(\bar{y}, \frac{1}{2}-x, \frac{1}{4}+z)$	$(x, \frac{1}{2}-y, \frac{1}{4}-z)$ $(\bar{x}, \frac{1}{2}+y, \frac{1}{4}-z)$	$(y, \bar{x}, \bar{z})$ $(\bar{y}, x, \bar{z})$	43	Fdd2

TABLE 11. *Reduction from $4\bar{2}m$ to 222*

Space group of unstrained crystal, order 8 per lattice point		If stressed so that	Coordinates referred to axes of unstrained crystal				Space group of strained crystal, order 4 per lattice point	
			1st Subset		2d Subset			
No.	Symbol						No.	Symbol
111	$P\bar{4}2m$	$x, y, z \parallel X, Y, Z$, any permutation.	(x, y, z)	$(\bar{x}, \bar{y}, z)$	(y, x, z)	$(\bar{y}, \bar{x}, z)$	16	P222
			$(\bar{x}, \bar{y}, z)$	(x, y, z)	$(\bar{y}, \bar{x}, z)$	(y, x, z)		
112	$P\bar{4}2c$	Do.	(x, y, z)	$(\bar{x}, \bar{y}, \frac{1}{2}-z)$	$(y, x, \frac{1}{2}+z)$	$(\bar{y}, \bar{x}, \frac{1}{2}+z)$	16	P222
			$(\bar{x}, \bar{y}, z)$	$(x, y, \frac{1}{2}-z)$	$(\bar{y}, \bar{x}, \frac{1}{2}+z)$	$(y, x, \frac{1}{2}+z)$		
113	$P\bar{4}2_1m$	Do.	(x, y, z)	$(\frac{1}{2}+x, \frac{1}{2}-y, \bar{z})$	$(\frac{1}{2}+y, \frac{1}{2}+x, z)$	$(y, \bar{x}, \bar{z})$	18	$P2_12_12$
			$(\bar{x}, \bar{y}, z)$	$(\frac{1}{2}-x, \frac{1}{2}+y, \bar{z})$	$(\frac{1}{2}-y, \frac{1}{2}-x, z)$	$(\bar{y}, x, \bar{z})$		
114	$P\bar{4}2_1c$	Do.	(x, y, z)	$(\frac{1}{2}+x, \frac{1}{2}-y, \frac{1}{2}-z)$	$(\frac{1}{2}+y, \frac{1}{2}+x, \frac{1}{2}+z)$	$(y, \bar{x}, \bar{z})$	18	$P2_12_12$
			$(\bar{x}, \bar{y}, z)$	$(\frac{1}{2}-x, \frac{1}{2}+y, \frac{1}{2}-z)$	$(\frac{1}{2}-y, \frac{1}{2}-x, \frac{1}{2}+z)$	$(\bar{y}, x, \bar{z})$		
115	$P\bar{4}m2$	$[1\bar{1}0], [110], z \parallel X, Y, Z$, any permutation.	(x, y, z)	$(\bar{y}, \bar{x}, \bar{z})$	$(x, \bar{y}, z)$	$(y, \bar{x}, \bar{z})$	21	C222
			$(\bar{x}, \bar{y}, z)$	$(y, x, \bar{z})$	$(\bar{x}, y, z)$	$(\bar{y}, x, \bar{z})$		
116	$P\bar{4}c2$	Do.	(x, y, z)	$(\bar{y}, \bar{x}, \frac{1}{2}-z)$	$(x, \bar{y}, \frac{1}{2}+z)$	$(y, \bar{x}, \bar{z})$	21	C222
			$(\bar{x}, \bar{y}, z)$	$(y, x, \frac{1}{2}-z)$	$(\bar{x}, y, \frac{1}{2}+z)$	$(\bar{y}, x, \bar{z})$		
117	$P\bar{4}b2$	Do.	(x, y, z)	$(\frac{1}{2}+y, \frac{1}{2}+x, \bar{z})$	$(\frac{1}{2}+x, \frac{1}{2}-y, z)$	$(y, \bar{x}, \bar{z})$	21	C222
			$(\bar{x}, \bar{y}, z)$	$(\frac{1}{2}-y, \frac{1}{2}-x, \bar{z})$	$(\frac{1}{2}-x, \frac{1}{2}+y, z)$	$(\bar{y}, x, \bar{z})$		
118	$P\bar{4}n2$	Do.	(x, y, z)	$(\frac{1}{2}+y, \frac{1}{2}+x, \frac{1}{2}-z)$	$(\frac{1}{2}+x, \frac{1}{2}-y, \frac{1}{2}+z)$	$(y, \bar{x}, \bar{z})$	21	C222
			$(\bar{x}, \bar{y}, z)$	$(\frac{1}{2}-y, \frac{1}{2}-x, \frac{1}{2}-z)$	$(\frac{1}{2}-x, \frac{1}{2}+y, \frac{1}{2}+z)$	$(\bar{y}, x, \bar{z})$		
119	$I\bar{4}m2$	Do.	(x, y, z)	$(\bar{y}, \bar{x}, \bar{z})$	$(x, \bar{y}, z)$	$(y, \bar{x}, \bar{z})$	22	F222
			$(\bar{x}, \bar{y}, z)$	$(y, x, \bar{z})$	$(\bar{x}, y, z)$	$(\bar{y}, x, \bar{z})$		
120	$I\bar{4}c2$	Do.	(x, y, z)	$(\bar{y}, \bar{x}, \frac{1}{2}-z)$	$(x, \bar{y}, \frac{1}{2}+z)$	$(y, \bar{x}, \bar{z})$	22	F222
			$(\bar{x}, \bar{y}, z)$	$(y, x, \frac{1}{2}-z)$	$(\bar{x}, y, \frac{1}{2}+z)$	$(\bar{y}, x, \bar{z})$		
121	$I\bar{4}2m$	$x, y, z \parallel X, Y, Z$, any permutation.	(x, y, z)	$(\bar{x}, \bar{y}, \bar{z})$	(y, x, z)	$(\bar{y}, \bar{x}, \bar{z})$	23	I222
			$(\bar{x}, \bar{y}, z)$	$(x, y, \bar{z})$	$(\bar{y}, \bar{x}, z)$	$(y, x, \bar{z})$		
122	$I\bar{4}2d$	Do.	(x, y, z)	$(\bar{x}, \frac{1}{2}-y, \frac{1}{4}-z)$	$(y, \frac{1}{2}+x, \frac{1}{4}+z)$	$(\bar{y}, \bar{x}, \bar{z})$	24	$I2_12_12_1$
			$(\bar{x}, \bar{y}, z)$	$(x, \frac{1}{2}+y, \frac{1}{4}-z)$	$(\bar{y}, \frac{1}{2}-x, \frac{1}{4}+z)$	$(y, x, \bar{z})$		

TABLE 12. *Reduction from 4mm to mm2*

Space group of unstrained crystal, order 8 per lattice point		If stressed so that $x, y, z \parallel X, Y, Z$, any permutation				Space group of strained crystal, order 4 per lattice point			
		Coordinates referred to axes of unstrained crystal							
No.	Symbol	1st Subset		2d Subset		No.	Symbol		
99	P4mm	(x, y, z) $(\bar{x}, \bar{y}, z)$	$(\ x,\ \bar{y},\ z)$ $(\ \bar{x},\ y,\ z)$	$(\ y,\ x,\ z)$ $(\ \bar{y},\ \bar{x},\ z)$	$(\ y,\ \bar{x},\ z)$ $(\ \bar{y},\ x,\ z)$	25	Pmm2	35	Cmm2
100	P4bm	(x, y, z) $(\bar{x}, \bar{y}, z)$	$(\frac{1}{2}+x, \frac{1}{2}-y,\ z)$ $(\frac{1}{2}-x, \frac{1}{2}+y,\ z)$	$(\frac{1}{2}+y, \frac{1}{2}+x,\ z)$ $(\frac{1}{2}-y, \frac{1}{2}-x,\ z)$	$(\ y,\ \bar{x},\ z)$ $(\ \bar{y},\ x,\ z)$	32	Pba2	35	Cmm2
101	$P4_2cm$	(x, y, z) $(\bar{x}, \bar{y}, z)$	$(\ x,\ \bar{y}, \frac{1}{2}+z)$ $(\ \bar{x},\ y, \frac{1}{2}+z)$	$(\ y,\ x,\ z)$ $(\ \bar{y},\ \bar{x},\ z)$	$(\ y,\ \bar{x}, \frac{1}{2}+z)$ $(\ \bar{y},\ x, \frac{1}{2}+z)$	27	Pcc2	35	Cmm2
102	$P4_2nm$	(x, y, z) $(\bar{x}, \bar{y}, z)$	$(\frac{1}{2}+x, \frac{1}{2}-y, \frac{1}{2}+z)$ $(\frac{1}{2}-x, \frac{1}{2}+y, \frac{1}{2}+z)$	$(\ y,\ x,\ z)$ $(\ \bar{y},\ \bar{x},\ z)$	$(\frac{1}{2}+y, \frac{1}{2}-x, \frac{1}{2}+z)$ $(\frac{1}{2}-y, \frac{1}{2}+x, \frac{1}{2}+z)$	34	Pnn2	35	Cmm2
103	P4cc	(x, y, z) $(\bar{x}, \bar{y}, z)$	$(\ x,\ \bar{y}, \frac{1}{2}+z)$ $(\ \bar{x},\ y, \frac{1}{2}+z)$	$(\ y,\ x, \frac{1}{2}+z)$ $(\ \bar{y},\ \bar{x}, \frac{1}{2}+z)$	$(\ y,\ \bar{x},\ z)$ $(\ \bar{y},\ x,\ z)$	27	Pcc2	37	Ccc2
104	P4nc	(x, y, z) $(\bar{x}, \bar{y}, z)$	$(\frac{1}{2}+x, \frac{1}{2}-y, \frac{1}{2}+z)$ $(\frac{1}{2}-x, \frac{1}{2}+y, \frac{1}{2}+z)$	$(\frac{1}{2}+y, \frac{1}{2}+x, \frac{1}{2}+z)$ $(\frac{1}{2}-y, \frac{1}{2}-x, \frac{1}{2}+z)$	$(\ y,\ \bar{x},\ z)$ $(\ \bar{y},\ x,\ z)$	34	Pnn2	37	Ccc2
105	$P4_2mc$	(x, y, z) $(\bar{x}, \bar{y}, z)$	$(\ x,\ \bar{y},\ z)$ $(\bar{x},\ y,\ z)$	$(\ y,\ x, \frac{1}{2}+z)$ $(\ \bar{y},\ \bar{x}, \frac{1}{2}+z)$	$(\ y,\ \bar{x}, \frac{1}{2}+z)$ $(\ \bar{y},\ x, \frac{1}{2}+z)$	25	Pmm2	37	Ccc2
106	$P4_2bc$	(x, y, z) $(\bar{x}, \bar{y}, z)$	$(\frac{1}{2}+x, \frac{1}{2}-y,\ z)$ $(\frac{1}{2}-x, \frac{1}{2}+y,\ z)$	$(\frac{1}{2}+y, \frac{1}{2}+x, \frac{1}{2}+z)$ $(\frac{1}{2}-y, \frac{1}{2}-x, \frac{1}{2}+z)$	$(\ y,\ \bar{x}, \frac{1}{2}+z)$ $(\ \bar{y},\ x, \frac{1}{2}+z)$	32	Pba2	37	Ccc2
107	I4mm	(x, y, z) $(\bar{x}, \bar{y}, z)$	$(\ x,\ \bar{y},\ z)$ $(\ \bar{x},\ y,\ z)$	$(\ y,\ x,\ z)$ $(\ \bar{y},\ \bar{x},\ z)$	$(\ y,\ \bar{x},\ z)$ $(\ \bar{y},\ x,\ z)$	44	Imm2	42	Fmm2
108	I4cm	(x, y, z) $(\bar{x}, \bar{y}, z)$	$(\frac{1}{2}+x, \frac{1}{2}-y,\ z)$ $(\frac{1}{2}-x, \frac{1}{2}+y,\ z)$	$(\frac{1}{2}+y, \frac{1}{2}+x,\ z)$ $(\frac{1}{2}-y, \frac{1}{2}-x,\ z)$	$(\ y,\ \bar{x},\ z)$ $(\ \bar{y},\ x,\ z)$	45	Iba2	42	Fmm2
109	$I4_1md$	(x, y, z) $(\bar{x}, \bar{y}, z)$	$(\ x,\ \bar{y},\ z)$ $(\ \bar{x},\ y,\ z)$	$(\ y, \frac{1}{2}+x, \frac{1}{4}+z)$ $(\ \bar{y}, \frac{1}{2}-x, \frac{1}{4}+z)$	$(\ y, \frac{1}{2}-x, \frac{1}{4}+z)$ $(\ \bar{y}, \frac{1}{2}+x, \frac{1}{4}+z)$	44	Imm2	43	Fdd2
110	$I4_1cd$	(x, y, z) $(\bar{x}, \bar{y}, z)$	$(\ x,\ \bar{y}, \frac{1}{2}+z)$ $(\ \bar{x},\ y, \frac{1}{2}+z)$	$(\ y, \frac{1}{2}+x, \frac{3}{4}+z)$ $(\ \bar{y}, \frac{1}{2}-x, \frac{3}{4}+z)$	$(\ y, \frac{1}{2}-x, \frac{1}{4}+z)$ $(\ \bar{y}, \frac{1}{2}+x, \frac{1}{4}+z)$	45	Iba2	43	Fdd2
No.	Symbol	1st Subset	2d Subset	1st Subset	2d Subset	----------	----------	No.	Symbol
Space group of unstrained crystal, order 8 per lattice point		Coordinates referred to axes of unstrained crystal				----------	----------	Space group of strained crystal, order 4 per lattice point	
		If stressed so that $[1\bar{1}0]$, $[110]$, $z \parallel X, Y, Z$, any permutation							

TABLE 13. *Reduction from 422 to 222*

Space group of unstrained crystal, order 8 per lattice point		If stressed so that $x, y, z \parallel X, Y, Z$, any permutation				Space group of strained crystal, order 4 per lattice point			
		Coordinates referred to axes of unstrained crystal							
No.	Symbol	1st Subset		2d Subset		No.	Symbol		
89	P422	(x, y, z) $(\bar{x}, \bar{y}, z)$	$(x, \bar{y}, \bar{z})$ $(\bar{x}, y, \bar{z})$	$(y, x, \bar{z})$ $(\bar{y}, \bar{x}, \bar{z})$	$(y, \bar{x}, z)$ $(\bar{y}, x, z)$	16	P222	21	C222
90	P42$_1$2	(x, y, z) $(\bar{x}, \bar{y}, z)$	$(\frac{1}{2}+x, \frac{1}{2}-y, \bar{z})$ $(\frac{1}{2}-x, \frac{1}{2}+y, \bar{z})$	$(y, x, \bar{z})$ $(\bar{y}, \bar{x}, \bar{z})$	$(\frac{1}{2}+y, \frac{1}{2}-x, z)$ $(\frac{1}{2}-y, \frac{1}{2}+x, z)$	18	P2$_1$2$_1$2	21	C222
91	P4$_1$22	(x, y, z) $(\bar{x}, \bar{y}, \frac{1}{2}+z)$	$(x, \bar{y}, \frac{1}{2}-z)$ $(\bar{x}, y, \bar{z})$	$(y, x, \frac{3}{4}-z)$ $(\bar{y}, \bar{x}, \frac{1}{4}-z)$	$(y, \bar{x}, \frac{3}{4}+z)$ $(\bar{y}, x, \frac{1}{4}+z)$	17	P222$_1$	20	C222$_1$
92	P4$_1$2$_1$2	(x, y, z) $(\bar{x}, \bar{y}, \frac{1}{2}+z)$	$(\frac{1}{2}+x, \frac{1}{2}-y, \frac{3}{4}-z)$ $(\frac{1}{2}-x, \frac{1}{2}+y, \frac{1}{4}-z)$	$(y, x, \bar{z})$ $(\bar{y}, \bar{x}, \frac{1}{2}-z)$	$(\frac{1}{2}+y, \frac{1}{2}-x, \frac{3}{4}+z)$ $(\frac{1}{2}-y, \frac{1}{2}+x, \frac{1}{4}+z)$	19	P2$_1$2$_1$2$_1$	20	C222$_1$
93	P4$_2$22	(x, y, z) $(\bar{x}, \bar{y}, z)$	$(x, \bar{y}, \bar{z})$ $(\bar{x}, y, \bar{z})$	$(y, x, \frac{1}{2}-z)$ $(\bar{y}, \bar{x}, \frac{1}{2}-z)$	$(y, \bar{x}, \frac{1}{2}+z)$ $(\bar{y}, x, \frac{1}{2}+z)$	16	P222	21	C222
94	P4$_2$2$_1$2	(x, y, z) $(\bar{x}, \bar{y}, z)$	$(\frac{1}{2}+x, \frac{1}{2}-y, \frac{1}{2}-z)$ $(\frac{1}{2}-x, \frac{1}{2}+y, \frac{1}{2}-z)$	$(y, x, \bar{z})$ $(\bar{y}, \bar{x}, \bar{z})$	$(\frac{1}{2}+y, \frac{1}{2}-x, \frac{1}{2}+z)$ $(\frac{1}{2}-y, \frac{1}{2}+x, \frac{1}{2}+z)$	18	P2$_1$2$_1$2	21	C222
95	P4$_3$22	(x, y, z) $(\bar{x}, \bar{y}, \frac{1}{2}+z)$	$(x, \bar{y}, \frac{1}{2}-z)$ $(\bar{x}, y, \bar{z})$	$(y, x, \frac{1}{4}-z)$ $(\bar{y}, \bar{x}, \frac{3}{4}-z)$	$(y, \bar{x}, \frac{1}{4}+z)$ $(\bar{y}, x, \frac{3}{4}+z)$	17	P222$_1$	20	C222$_1$
96	P4$_3$2$_1$2	(x, y, z) $(\bar{x}, \bar{y}, \frac{1}{2}+z)$	$(\frac{1}{2}+x, \frac{1}{2}-y, \frac{1}{4}-z)$ $(\frac{1}{2}-x, \frac{1}{2}+y, \frac{3}{4}-z)$	$(y, x, \bar{z})$ $(\bar{y}, \bar{x}, \frac{1}{2}-z)$	$(\frac{1}{2}+y, \frac{1}{2}-x, \frac{1}{4}+z)$ $(\frac{1}{2}-y, \frac{1}{2}+x, \frac{3}{4}+z)$	19	P2$_1$2$_1$2$_1$	20	C222$_1$
97	I422	(x, y, z) $(\bar{x}, \bar{y}, z)$	$(x, \bar{y}, \bar{z})$ $(\bar{x}, y, \bar{z})$	$(y, x, \bar{z})$ $(\bar{y}, \bar{x}, \bar{z})$	$(y, \bar{x}, z)$ $(\bar{y}, x, z)$	23	I222	22	F222
98	I4$_1$22	(x, y, z) $(\bar{x}, \bar{y}, z)$	$(x, \frac{1}{2}-y, \frac{1}{4}-z)$ $(\bar{x}, \frac{1}{2}+y, \frac{1}{4}-z)$	$(y, x, \bar{z})$ $(\bar{y}, \bar{x}, \bar{z})$	$(y, \frac{1}{2}-x, \frac{1}{4}+z)$ $(\bar{y}, \frac{1}{2}+x, \frac{1}{4}+z)$	24	I2$_1$2$_1$2$_1$	22	F222
No.	Symbol	1st Subset	2d Subset	1st Subset	2d Subset			No.	Symbol
Space group of unstrained crystal, order 8 per lattice point		Coordinates referred to axes of unstrained crystal If stressed so that $[1\bar{1}0]$, $[110]$, $z \parallel X, Y, Z$, any permutation						Space group of strained crystal, order 4 per lattice point	

TABLE 14. *Reduction from 6 to 2*

Space group of unstrained crystal, order 6 per lattice point		If stressed so that $z \parallel X$, Y, or Z			Space group of strained crystal, order 2 per lattice point	
		Coordinates referred to axes of unstrained crystal				
No.	Symbol	1st Subset	2d Subset	3d Subset	No.	Symbol
168	P6	(x, y, z) $(\bar{x}, \bar{y}, z)$	$(\bar{y}, x-y, z)$ $(y, y-x, z)$	$(y-x, \bar{x}, z)$ $(x-y, x, z)$	3	P2
169	P6$_1$	(x, y, z) $(\bar{x}, \bar{y}, \frac{1}{2}+z)$	$(\bar{y}, x-y, \frac{1}{3}+z)$ $(y, y-x, \frac{5}{6}+z)$	$(y-x, \bar{x}, \frac{2}{3}+z)$ $(x-y, x, \frac{1}{6}+z)$	4	P2$_1$
170	P6$_5$	(x, y, z) $(\bar{x}, \bar{y}, \frac{1}{2}+z)$	$(\bar{y}, x-y, \frac{2}{3}+z)$ $(y, y-x, \frac{1}{6}+z)$	$(y-x, \bar{x}, \frac{1}{3}+z)$ $(x-y, x, \frac{5}{6}+z)$	4	P2$_1$
171	P6$_2$	(x, y, z) $(\bar{x}, \bar{y}, z)$	$(\bar{y}, x-y, \frac{2}{3}+z)$ $(y, y-x, \frac{2}{3}+z)$	$(y-x, \bar{x}, \frac{1}{3}+z)$ $(x-y, x, \frac{1}{3}+z)$	3	P2
172	P6$_4$	(x, y, z) $(\bar{x}, \bar{y}, z)$	$(\bar{y}, x-y, \frac{1}{3}+z)$ $(y, y-x, \frac{1}{3}+z)$	$(y-x, \bar{x}, \frac{2}{3}+z)$ $(x-y, x, \frac{2}{3}+z)$	3	P2
173	P6$_3$	(x, y, z) $(\bar{x}, \bar{y}, \frac{1}{2}+z)$	$(\bar{y}, x-y, z)$ $(y, y-x, \frac{1}{2}+z)$	$(y-x, \bar{x}, z)$ $(x-y, x, \frac{1}{2}+z)$	4	P2$_1$

TABLE 15. *Reduction from* $\bar{6}$ *to m*

Space group of unstrained crystal, order 6 per lattice point		If stressed so that $z \parallel X$, Y, or Z			Space group of strained crystal, order 2 per lattice point	
		Coordinates referred to axes of unstrained crystal				
No.	Symbol	1st Subset	2d Subset	3d Subset	No.	Symbol
174	$P\bar{6}$	(x, y, z) $(x, y, \bar{z})$	$(\bar{y}, x-y, z)$ $(\bar{y}, x-y, \bar{z})$	$(y-x, \bar{x}, z)$ $(y-x, \bar{x}, \bar{z})$	6	Pm

TABLE 16. *Reduction from 3m to m*

Space group of unstrained crystal, order 6 per lattice point		If stressed so that	Coordinates referred to axes of unstrained crystal			Space group of strained crystal, order 2 per lattice point	
No.	Symbol		1st Subset	2d Subset	3d Subset	No.	Symbol
156	P3m1	[110] $\parallel$ *X*, *Y*, or *Z*	(x, y, z) $(\bar{y}, \bar{x}, z)$	$(y-x, \bar{x}, z)$ $(x, x-y, z)$	$(\bar{y}, x-y, z)$ $(y-x, y, z)$	8	Cm
157	P31m	[1$\bar{1}$0] $\parallel$ *X*, *Y*, or *Z*	(x, y, z) (y, x, z)	$(y-x, \bar{x}, z)$ $(\bar{x}, y-x, z)$	$(\bar{y}, x-y, z)$ $(x-y, \bar{y}, z)$	8	Cm
158	P3c1	[110] $\parallel$ *X*, *Y*, or *Z*	(x, y, z) $(\bar{y}, \bar{x}, \frac{1}{2}+z)$	$(y-x, \bar{x}, z)$ $(x, x-y, \frac{1}{2}+z)$	$(\bar{y}, x-y, z)$ $(y-x, y, \frac{1}{2}+z)$	9	Cc
159	P31c	[1$\bar{1}$0] $\parallel$ *X*, *Y*, or *Z*	(x, y, z) $(y, x, \frac{1}{2}+z)$	$(y-x, \bar{x}, z)$ $(\bar{x}, y-x, \frac{1}{2}+z)$	$(\bar{y}, x-y, z)$ $(x-y, \bar{y}, \frac{1}{2}+z)$	9	Cc
160	R3m hex. axes	[110] $\parallel$ *X*, *Y*, or *Z*	(x, y, z) $(\bar{y}, \bar{x}, z)$	$(y-x, \bar{x}, z)$ $(x, x-y, z)$	$(\bar{y}, x-y, z)$ $(y-x, y, z)$	8	Cm
161	R3c hex. axes	[110] $\parallel$ *X*, *Y*, or *Z*	(x, y, z) $(\bar{y}, \bar{x}, \frac{1}{2}+z)$	$(y-x, \bar{x}, z)$ $(x, x-y, \frac{1}{2}+z)$	$(\bar{y}, x-y, z)$ $(y-x, y, \frac{1}{2}+z)$	9	Cc

TABLE 17. *Reduction from 32 to 2*

Space group of unstrained crystal, order 6 per lattice point		If stressed so that	Coordinates referred to axes of unstrained crystal			Space group of strained crystal, order 2 per lattice point	
No.	Symbol		1st Subset	2d Subset	3d Subset	No.	Symbol
149	P312	[1$\bar{1}$0] $\parallel$ *X*, *Y*, or *Z*	(x, y, z) $(\bar{y}, \bar{x}, \bar{z})$	$(\bar{y}, x-y, z)$ $(y-x, y, \bar{z})$	$(y-x, \bar{x}, z)$ $(x, x-y, \bar{z})$	5	C2
150	P321	[110] $\parallel$ *X*, *Y*, or *Z*	(x, y, z) $(y, x, \bar{z})$	$(\bar{y}, x-y, z)$ $(x-y, \bar{y}, \bar{z})$	$(y-x, \bar{x}, z)$ $(\bar{x}, y-x, \bar{z})$	5	C2
151	$P3_112$	[1$\bar{1}$0] $\parallel$ *X*, *Y*, or *Z*	(x, y, z) $(\bar{y}, \bar{x}, \frac{2}{3}-z)$	$(\bar{y}, x-y, \frac{1}{3}+z)$ $(y-x, y, \frac{1}{3}-z)$	$(y-x, \bar{x}, \frac{2}{3}+z)$ $(x, x-y, \bar{z})$	5	C2
152	$P3_121$	[110] $\parallel$ *X*, *Y*, or *Z*	(x, y, z) $(y, x, \bar{z})$	$(\bar{y}, x-y, \frac{1}{3}+z)$ $(x-y, \bar{y}, \frac{2}{3}-z)$	$(y-x, \bar{x}, \frac{2}{3}+z)$ $(\bar{x}, y-x, \frac{1}{3}-z)$	5	C2
153	$P3_212$	[1$\bar{1}$0 $\parallel$ *X*, *Y*, or *Z*	(x, y, z) $(\bar{y}, \bar{x}, \frac{1}{3}-z)$	$(\bar{y}, x-y, \frac{2}{3}+z)$ $(y-x, y, \frac{2}{3}-z)$	$(y-x, \bar{x}, \frac{1}{3}+z)$ $(x, x-y, \bar{z})$	5	C2
154	$P3_221$	[110] $\parallel$ *X*, *Y*, or *Z*	(x, y, z) $(y, x, \bar{z})$	$(\bar{y}, x-y, \frac{2}{3}+z)$ $(x-y, \bar{y}, \frac{1}{3}-z)$	$(y-x, \bar{x}, \frac{1}{3}+z)$ $(\bar{x}, y-x, \frac{2}{3}-z)$	5	C2
155 hex.	R32 axes	[110] $\parallel$ *X*, *Y*, or *Z*	(x, y, z) $(y, x, \bar{z})$	$(\bar{y}, x-y, z)$ $(x-y, \bar{y}, \bar{z})$	$(y-x, \bar{x}, z)$ $(\bar{x}, y-x, \bar{z})$	5	C2

TABLE 18. *Reduction from 4 to 2*

Space group of unstrained crystal, order 4 per lattice point		If stressed so that $z \parallel X$, Y, or Z		Space group of strained crystal, order 2 per lattice point	
		Coordinates referred to axes of unstrained crystal			
No.	Symbol	1st Subset	2d Subset	No.	Symbol
75	P4	(x, y, z) $(\bar{x}, \bar{y}, z)$	$(\bar{y}, x, z)$ $(y, \bar{x}, z)$	3	P2
76	$P4_1$	(x, y, z) $(\bar{x}, \bar{y}, \frac{1}{4}+z)$	$(\bar{y}, x, \frac{1}{4}+z)$ $(y, \bar{x}, \frac{3}{4}+z)$	4	$P2_1$
77	$P4_2$	(x, y, z) $(\bar{x}, \bar{y}, z)$	$(\bar{y}, x, \frac{1}{2}+z)$ $(y, \bar{x}, \frac{1}{2}+z)$	3	P2
78	$P4_3$	(x, y, z) $(\bar{x}, \bar{y}, \frac{1}{2}+z)$	$(\bar{y}, x, \frac{3}{4}+z)$ $(y, \bar{x}, \frac{1}{4}+z)$	4	$P2_1$
79	I4	(x, y, z) $(\bar{x}, \bar{y}, z)$	$(\bar{y}, x, z)$ $(y, \bar{x}, z)$	5	C2
80	$I4_1$	(x, y, z) $(\bar{x}, \bar{y}, z)$	$(\bar{y}, \frac{1}{2}+x, \frac{1}{4}+z)$ $(y, \frac{1}{2}-x, \frac{1}{4}+z)$	5	C2

TABLE 19. *Reduction from $\bar{4}$ to 2*

Space group of unstrained crystal, order 4 per lattice point		If stressed so that $z \parallel X$, Y, or Z		Space group of strained crystal, order 2 per lattice point	
		Coordinates referred to axes of unstrained crystal			
No.	Symbol	1st Subset	2d Subset	No.	Symbol
81	$P\bar{4}$	(x, y, z) $(\bar{x}, \bar{y}, z)$	$(\bar{y}, x, \bar{z})$ $(y, \bar{x}, \bar{z})$	3	P2
82	$I\bar{4}$	(x, y, z) $(\bar{x}, \bar{y}, z)$	$(\bar{y}, x, \bar{z})$ $(y, \bar{x}, \bar{z})$	5	C2

TABLE 20. *Reduction from mm2 to m*

Space group of unstrained crystal, order 4 per lattice point		If stressed so that $x \parallel X$, Y, or Z		Space group of strained crystal, order 2 per lattice point		If stressed so that $y \parallel X$, Y, or Z		Space group of strained crystal, order 2 per lattice point	
		Coordinates referred to axes of unstrained crystal				Coordinates referred to axes of unstrained crystal			
No.	Symbol	1st Subset	2d Subset	No.	Symbol	1st Subset	2d Subset	No.	Symbol
25	$Pmm2$	(x, y, z) $(\bar{x}, y, z)$	$(x, \bar{y}, z)$ $(\bar{x}, \bar{y}, z)$	6	Pm	(x, y, z) $(x, \bar{y}, z)$	$(\bar{x}, y, z)$ $(\bar{x}, \bar{y}, z)$	6	Pm
26	$Pmc2_1$	(x, y, z) $(\bar{x}, y, z)$	$(x, \bar{y}, \frac{1}{2}+z)$ $(\bar{x}, \bar{y}, \frac{1}{2}+z)$	6	Pm	(x, y, z) $(x, \bar{y}, \frac{1}{2}+z)$	$(\bar{x}, y, z)$ $(\bar{x}, \bar{y}, \frac{1}{2}+z)$	7	Pc
27	$Pcc2$	(x, y, z) $(\bar{x}, y, \frac{1}{2}+z)$	$(x, \bar{y}, \frac{1}{2}+z)$ $(\bar{x}, \bar{y}, z)$	7	Pc	(x, y, z) $(x, \bar{y}, \frac{1}{2}+z)$	$(\bar{x}, y, \frac{1}{2}+z)$ $(\bar{x}, \bar{y}, z)$	7	Pc
28	$Pma2$	(x, y, z) $(\frac{1}{2}-x, y, z)$	$(\frac{1}{2}+x, \bar{y}, z)$ $(\bar{x}, \bar{y}, z)$	6	Pm	(x, y, z) $(\frac{1}{2}+x, \bar{y}, z)$	$(\frac{1}{2}-x, y, z)$ $(\bar{x}, \bar{y}, z)$	7	Pc
29	$Pca2_1$	(x, y, z) $(\frac{1}{2}-x, y, \frac{1}{2}+z)$	$(\frac{1}{2}+x, \bar{y}, z)$ $(\bar{x}, \bar{y}, \frac{1}{2}+z)$	7	Pc	(x, y, z) $(\frac{1}{2}+x, \bar{y}, z)$	$(\frac{1}{2}-x, y, \frac{1}{2}+z)$ $(\bar{x}, \bar{y}, \frac{1}{2}+z)$	7	Pc
30	$Pnc2$	(x, y, z) $(\bar{x}, \frac{1}{2}+y, \frac{1}{2}+z)$	$(x, \frac{1}{2}-y, \frac{1}{2}+z)$ $(\bar{x}, \bar{y}, z)$	7	Pc	(x, y, z) $(x, \frac{1}{2}-y, \frac{1}{2}+z)$	$(\bar{x}, \frac{1}{2}+y, \frac{1}{2}+z)$ $(\bar{x}, \bar{y}, z)$	7	Pc
31	$Pmn2_1$	(x, y, z) $(\bar{x}, y, z)$	$(\frac{1}{2}+x, \bar{y}, \frac{1}{2}+z)$ $(\frac{1}{2}-x, \bar{y}, \frac{1}{2}+z)$	6	Pm	(x, y, z) $(\frac{1}{2}+x, \bar{y}, \frac{1}{2}+z)$	$(\bar{x}, y, z)$ $(\frac{1}{2}-x, \bar{y}, \frac{1}{2}+z)$	7	Pc
32	$Pba2$	(x, y, z) $(\frac{1}{2}-x, \frac{1}{2}+y, z)$	$(\frac{1}{2}+x, \frac{1}{2}-y, z)$ $(\bar{x}, \bar{y}, z)$	7	Pc	(x, y, z) $(\frac{1}{2}+x, \frac{1}{2}-y, z)$	$(\frac{1}{2}-x, \frac{1}{2}+y, z)$ $(\bar{x}, \bar{y}, z)$	7	Pc
33	$Pna2_1$	(x, y, z) $(\frac{1}{2}-x, \frac{1}{2}+y, \frac{1}{2}+z)$	$(\frac{1}{2}+x, \frac{1}{2}-y, z)$ $(\bar{x}, \bar{y}, \frac{1}{2}+z)$	7	Pc	(x, y, z) $(\frac{1}{2}+x, \frac{1}{2}-y, z)$	$(\frac{1}{2}-x, \frac{1}{2}+y, \frac{1}{2}+z)$ $(\bar{x}, \bar{y}, \frac{1}{2}+z)$	7	Pc
34	$Pnn2$	(x, y, z) $(\frac{1}{2}-x, \frac{1}{2}+y, \frac{1}{2}+z)$	$(\frac{1}{2}+x, \frac{1}{2}-y, \frac{1}{2}+z)$ $(\bar{x}, \bar{y}, z)$	7	Pc	(x, y, z) $(\frac{1}{2}+x, \frac{1}{2}-y, \frac{1}{2}+z)$	$(\frac{1}{2}-x, \frac{1}{2}+y, \frac{1}{2}+z)$ $(\bar{x}, \bar{y}, z)$	7	Pc
35	$Cmm2$	(x, y, z) $(\bar{x}, y, z)$	$(x, \bar{y}, z)$ $(\bar{x}, \bar{y}, z)$	8	Cm	(x, y, z) $(x, \bar{y}, z)$	$(\bar{x}, y, z)$ $(\bar{x}, \bar{y}, z)$	8	Cm
36	$Cmc2_1$	(x, y, z) $(\bar{x}, y, z)$	$(x, \bar{y}, \frac{1}{2}+z)$ $(\bar{x}, \bar{y}, \frac{1}{2}+z)$	8	Cm	(x, y, z) $(x, \bar{y}, \frac{1}{2}+z)$	$(\bar{x}, y, z)$ $(\bar{x}, \bar{y}, \frac{1}{2}+z)$	9	Cc
37	$Ccc2$	(x, y, z) $(\bar{x}, y, \frac{1}{2}+z)$	$(x, \bar{y}, \frac{1}{2}+z)$ $(\bar{x}, \bar{y}, z)$	9	Cc	(x, y, z) $(x, \bar{y}, \frac{1}{2}+z)$	$(\bar{x}, y, \frac{1}{2}+z)$ $(\bar{x}, \bar{y}, z)$	9	Cc
38	$Amm2$	(x, y, z) $(\bar{x}, y, z)$	$(x, \bar{y}, z)$ $(\bar{x}, \bar{y}, z)$	6	Pm	(x, y, z) $(x, \bar{y}, z)$	$(\bar{x}, y, z)$ $(\bar{x}, \bar{y}, z)$	8	Cm
39	$Abm2$	(x, y, z) $(\bar{x}, \frac{1}{2}+y, z)$	$(x, \frac{1}{2}-y, z)$ $(\bar{x}, \bar{y}, z)$	7	Pc	(x, y, z) $(x, \frac{1}{2}-y, z)$	$(\bar{x}, \frac{1}{2}+y, z)$ $(\bar{x}, \bar{y}, z)$	8	Cm
40	$Ama2$	(x, y, z) $(\frac{1}{2}-x, y, z)$	$(\frac{1}{2}+x, \bar{y}, z)$ $(\bar{x}, \bar{y}, z)$	6	Pm	(x, y, z) $(\frac{1}{2}+x, \bar{y}, z)$	$(\frac{1}{2}-x, y, z)$ $(\bar{x}, \bar{y}, z)$	9	Cc
41	$Aba2$	(x, y, z) $(\frac{1}{2}-x, \frac{1}{2}+y, z)$	$(\frac{1}{2}+x, \frac{1}{2}-y, z)$ $(\bar{x}, \bar{y}, z)$	7	Pc	(x, y, z) $(\frac{1}{2}+x, \frac{1}{2}-y, z)$	$(\frac{1}{2}-x, \frac{1}{2}+y, z)$ $(\bar{x}, \bar{y}, z)$	9	Cc
42	$Fmm2$	(x, y, z) $(\bar{x}, y, z)$	$(x, \bar{y}, z)$ $(\bar{x}, \bar{y}, z)$	8	Cm	(x, y, z) $(x, \bar{y}, z)$	$(\bar{x}, y, z)$ $(\bar{x}, \bar{y}, z)$	8	Cm
43	$Fdd2$	(x, y, z) $(\frac{1}{4}-x, \frac{1}{4}+y, \frac{1}{4}+z)$	$(\frac{1}{4}+x, \frac{1}{4}-y, \frac{1}{4}+z)$ $(\bar{x}, \bar{y}, z)$	9	Cc	(x, y, z) $(\frac{1}{4}+x, \frac{1}{4}-y, \frac{1}{4}+z)$	$(\frac{1}{4}-x, \frac{1}{4}+y, \frac{1}{4}+z)$ $(\bar{x}, \bar{y}, z)$	9	Cc
44	$Imm2$	(x, y, z) $(\bar{x}, y, z)$	$(x, \bar{y}, z)$ $(\bar{x}, \bar{y}, z)$	8	Cm	(x, y, z) $(x, \bar{y}, z)$	$(\bar{x}, y, z)$ $(\bar{x}, \bar{y}, z)$	8	Cm
45	$Iba2$	(x, y, z) $(\bar{x}, y, \frac{1}{2}+z)$	$(x, \bar{y}, \frac{1}{2}+z)$ $(\bar{x}, \bar{y}, z)$	9	Cc	(x, y, z) $(x, \bar{y}, \frac{1}{2}+z)$	$(\bar{x}, y, \frac{1}{2}+z)$ $(\bar{x}, \bar{y}, z)$	9	Cc
46	$Ima2$	(x, y, z) $(\frac{1}{2}-x, y, z)$	$(\frac{1}{2}+x, \bar{y}, z)$ $(\bar{x}, \bar{y}, z)$	8	Cm	(x, y, z) $(\frac{1}{2}+x, \bar{y}, z)$	$(\frac{1}{2}-x, y, z)$ $(\bar{x}, \bar{y}, z)$	9	Cc

TABLE 21. *Reduction from mm2 to 2*

Space group of unstrained crystal, order 4 per lattice point		If stressed so that $z \parallel X$, Y, or Z		Space group of strained crystal, order 2 per lattice point	
		Coordinates referred to axes of unstrained crystal			
No.	Symbol	1st Subset	2d Subset	No.	Symbol
25	Pmm2	(x, y, z) $(\bar{x}, \bar{y}, z)$	$(x, \bar{y}, z)$ $(\bar{x}, y, z)$	3	P2
26	Pmc2_1	(x, y, z) $(\bar{x}, \bar{y}, \frac{1}{2}+z)$	$(x, \bar{y}, \frac{1}{2}+z)$ $(\bar{x}, y, z)$	4	P2_1
27	Pcc2	(x, y, z) $(\bar{x}, \bar{y}, z)$	$(x, \bar{y}, \frac{1}{2}+z)$ $(\bar{x}, y, \frac{1}{2}+z)$	3	P2
28	Pma2	(x, y, z) $(\bar{x}, \bar{y}, z)$	$(\frac{1}{2}+x, \bar{y}, z)$ $(\frac{1}{2}-x, y, z)$	3	P2
29	Pca2_1	(x, y, z) $(\bar{x}, \bar{y}, \frac{1}{2}+z)$	$(\frac{1}{2}+x, \bar{y}, z)$ $(\frac{1}{2}-x, y, \frac{1}{2}+z)$	4	P2_1
30	Pnc2	(x, y, z) $(\bar{x}, \bar{y}, z)$	$(x, \frac{1}{2}-y, \frac{1}{2}+z)$ $(\bar{x}, \frac{1}{2}+y, \frac{1}{2}+z)$	3	P2
31	Pmn2_1	(x, y, z) $(\frac{1}{2}-x, \bar{y}, \frac{1}{2}+z)$	$(\frac{1}{2}+x, \bar{y}, \frac{1}{2}+z)$ $(\bar{x}, y, z)$	4	P2_1
32	Pba2	(x, y, z) $(\bar{x}, \bar{y}, z)$	$(\frac{1}{2}+x, \frac{1}{2}-y, z)$ $(\frac{1}{2}-x, \frac{1}{2}+y, z)$	3	P2
33	Pna2_1	(x, y, z) $(\bar{x}, \bar{y}, \frac{1}{2}+z)$	$(\frac{1}{2}+x, \frac{1}{2}-y, z)$ $(\frac{1}{2}-x, \frac{1}{2}+y, \frac{1}{2}+z)$	4	P2_1
34	Pnn2	(x, y, z) $(\bar{x}, \bar{y}, z)$	$(\frac{1}{2}+x, \frac{1}{2}-y, \frac{1}{2}+z)$ $(\frac{1}{2}-x, \frac{1}{2}+y, \frac{1}{2}+z)$	3	P2
35	Cmm2	(x, y, z) $(\bar{x}, \bar{y}, z)$	$(x, \bar{y}, z)$ $(\bar{x}, y, z)$	3	P2
36	Cmc2_1	(x, y, z) $(\bar{x}, \bar{y}, \frac{1}{2}+z)$	$(x, \bar{y}, \frac{1}{2}+z)$ $(\bar{x}, y, z)$	4	P2_1
37	Ccc2	(x, y, z) $(\bar{x}, \bar{y}, z)$	$(x, \bar{y}, \frac{1}{2}+z)$ $(\bar{x}, y, \frac{1}{2}+z)$	3	P2
38	Amm2	(x, y, z) $(\bar{x}, \bar{y}, z)$	$(x, \bar{y}, z)$ $(\bar{x}, y, z)$	5	C2
39	Abm2	(x, y, z) $(\bar{x}, \bar{y}, z)$	$(x, \frac{1}{2}-y, z)$ $(\bar{x}, \frac{1}{2}+y, z)$	5	C2
40	Ama2	(x, y, z) $(\bar{x}, \bar{y}, z)$	$(\frac{1}{2}+x, \bar{y}, z)$ $(\frac{1}{2}-x, y, z)$	5	C2
41	Aba2	(x, y, z) $(\bar{x}, \bar{y}, z)$	$(\frac{1}{2}+x, \frac{1}{2}-y, z)$ $(\frac{1}{2}-x, \frac{1}{2}+y, z)$	5	C2
42	Fmm2	(x, y, z) $(\bar{x}, \bar{y}, z)$	$(x, \bar{y}, z)$ $(\bar{x}, y, z)$	5	C2
43	Fdd2	(x, y, z) $(\bar{x}, \bar{y}, z)$	$(\frac{1}{4}+x, \frac{1}{4}-y, \frac{1}{4}+z)$ $(\frac{1}{4}-x, \frac{1}{4}+y, \frac{1}{4}+z)$	5	C2
44	Imm2	(x, y, z) $(\bar{x}, \bar{y}, z)$	$(x, \bar{y}, z)$ $(\bar{x}, y, z)$	5	C2
45	Iba2	(x, y, z) $(\bar{x}, \bar{y}, z)$	$(x, \bar{y}, \frac{1}{2}+z)$ $(\bar{x}, y, \frac{1}{2}+z)$	5	C2
46	Ima2	(x, y, z) $(\bar{x}, \bar{y}, z)$	$(\frac{1}{2}+x, \bar{y}, z)$ $(\frac{1}{2}-x, y, z)$	5	C2

TABLE 22. *Reauction from 222 to 2*

Space group of unstrained crystal, order 4 per lattice point		If stressed so that $x \parallel X$, Y, or Z		Space group of strained crystal, order 2 per lattice point		If stressed so that $y \parallel X$, Y, or Z		Space group of strained crystal, order 2 per lattice point		If stressed so that $z \parallel X$, Y, or Z		Space group of strained crystal, order 2 per lattice point	
		Coordinates referred to axes of unstrained crystal				Coordinates referred to axes of unstrained crystal				Coordinates referred to axes of unstrained crystal			
No.	Symbol	1st Subset	2d Subset	No.	Symbol	1st Subset	2d Subset	No.	Symbol	1st Subset	2d Subset	No.	Symbol
16	P222	(x, y, z) $(x, \bar{y}, \bar{z})$	$(\bar{x}, y, \bar{z})$ $(\bar{x}, \bar{y}, z)$	3	P2	(x, y, z) $(\bar{x}, y, \bar{z})$	$(x, \bar{y}, \bar{z})$ $(\bar{x}, \bar{y}, z)$	3	P2	(x, y, z) $(\bar{x}, \bar{y}, z)$	$(x, \bar{y}, \bar{z})$ $(\bar{x}, y, \bar{z})$	3	P2
17	$P222_1$	(x, y, z) $(x, \bar{y}, \bar{z})$	$(\bar{x}, y, \frac{1}{2}-z)$ $(\bar{x}, \bar{y}, \frac{1}{2}+z)$	3	P2	(x, y, z) $(\bar{x}, y, \frac{1}{2}-z)$	$(x, \bar{y}, \bar{z})$ $(\bar{x}, \bar{y}, \frac{1}{2}+z)$	3	P2	(x, y, z) $(\bar{x}, \bar{y}, \frac{1}{2}+z)$	$(x, \bar{y}, \bar{z})$ $(\bar{x}, y, \frac{1}{2}-z)$	4	$P2_1$
18	$P2_12_12$	(x, y, z) $(\frac{1}{2}+x, \frac{1}{2}-y, \bar{z})$	$(\frac{1}{2}-x, \frac{1}{2}+y, \bar{z})$ $(\bar{x}, \bar{y}, z)$	4	$P2_1$	(x, y, z) $(\frac{1}{2}-x, \frac{1}{2}+y, \bar{z})$	$(\frac{1}{2}+x, \frac{1}{2}-y, \bar{z})$ $(\bar{x}, \bar{y}, z)$	4	$P2_1$	(x, y, z) $(\bar{x}, \bar{y}, z)$	$(\frac{1}{2}+x, \frac{1}{2}-y, \bar{z})$ $(\frac{1}{2}-x, \frac{1}{2}+y, \bar{z})$	3	P2
19	$P2_12_12_1$	(x, y, z) $(\frac{1}{2}+x, \frac{1}{2}-y, \bar{z})$	$(\bar{x}, \frac{1}{2}+y, \frac{1}{2}-z)$ $(\frac{1}{2}-x, \bar{y}, \frac{1}{2}+z)$	4	$P2_1$	(x, y, z) $(\bar{x}, \frac{1}{2}+y, \frac{1}{2}-z)$	$(\frac{1}{2}+x, \frac{1}{2}-y, \bar{z})$ $(\frac{1}{2}-x, \bar{y}, \frac{1}{2}+z)$	4	$P2_1$	(x, y, z) $(\frac{1}{2}-x, \bar{y}, \frac{1}{2}+z)$	$(\frac{1}{2}+x, \frac{1}{2}-y, \bar{z})$ $(\bar{x}, \frac{1}{2}+y, \frac{1}{2}-z)$	4	$P2_1$
20	$C222_1$	(x, y, z) $(x, \bar{y}, \bar{z})$	$(\bar{x}, y, \frac{1}{2}-z)$ $(\bar{x}, \bar{y}, \frac{1}{2}+z)$	5	C2	(x, y, z) $(\bar{x}, y, \frac{1}{2}-z)$	$(x, \bar{y}, \bar{z})$ $(\bar{x}, \bar{y}, \frac{1}{2}+z)$	5	C2	(x, y, z) $(\bar{x}, \bar{y}, \frac{1}{2}+z)$	$(x, \bar{y}, \bar{z})$ $(\bar{x}, y, \frac{1}{2}-z)$	4	$P2_1$
21	C222	(x, y, z) $(x, \bar{y}, \bar{z})$	$(\bar{x}, y, \bar{z})$ $(\bar{x}, \bar{y}, z)$	5	C2	(x, y, z) $(\bar{x}, y, \bar{z})$	$(x, \bar{y}, \bar{z})$ $(\bar{x}, \bar{y}, z)$	5	C2	(x, y, z) $(\bar{x}, \bar{y}, z)$	$(x, \bar{y}, \bar{z})$ $(\bar{x}, y, \bar{z})$	3	P2
22	F222	(x, y, z) $(x, \bar{y}, \bar{z})$	$(\bar{x}, y, \bar{z})$ $(\bar{x}, \bar{y}, z)$	5	C2	(x, y, z) $(\bar{x}, y, \bar{z})$	$(x, \bar{y}, \bar{z})$ $(\bar{x}, \bar{y}, z)$	5	C2	(x, y, z) $(\bar{x}, \bar{y}, z)$	$(x, \bar{y}, \bar{z})$ $(\bar{x}, y, \bar{z})$	5	C2
23	I222	(x, y, z) $(x, \bar{y}, \bar{z})$	$(\bar{x}, y, \bar{z})$ $(\bar{x}, \bar{y}, z)$	5	C2	(x, y, z) $(\bar{x}, y, \bar{z})$	$(x, \bar{y}, \bar{z})$ $(\bar{x}, \bar{y}, z)$	5	C2	(x, y, z) $(\bar{x}, \bar{y}, z)$	$(x, \bar{y}, \bar{z})$ $(\bar{x}, y, \bar{z})$	5	C2
24	$I2_12_12_1$	(x, y, z) $(\frac{1}{2}+x, \frac{1}{2}-y, \bar{z})$	$(\bar{x}, \frac{1}{2}+y, \frac{1}{2}-z)$ $(\frac{1}{2}-x, \bar{y}, \frac{1}{2}+z)$	5	C2	(x, y, z) $(\bar{x}, \frac{1}{2}+y, \frac{1}{2}+z)$	$(\frac{1}{2}+x, \frac{1}{2}-y, \bar{z})$ $(\frac{1}{2}-x, \bar{y}, \frac{1}{2}+z)$	5	C2	(x, y, z) $(\frac{1}{2}-x, \bar{y}, \frac{1}{2}+z)$	$(\frac{1}{2}+x, \frac{1}{2}-y, \bar{z})$ $(\bar{x}, \frac{1}{2}+y, \frac{1}{2}-z)$	5	C2

TABLE 23. *Reduction from 3 to 1*

Space group of unstrained crystal, order 3 per lattice point		No specialization of stress			Space group of strained crystal, order 1 per lattice point	
		Coordinates referred to axes of unstrained crystal				
No.	Symbol	1st Subset	2d Subset	3d Subset	No.	Symbol
143	P3	(x, y, z)	$(\bar{y}, x-y, z)$	$(y-x, \bar{x}, z)$	1	P1
144	$P3_1$	(x, y, z)	$(\bar{y}, x-y, \frac{1}{3}+z)$	$(y-x, \bar{x}, \frac{2}{3}+z)$	1	P1
145	$P3_2$	(x, y, z)	$(\bar{y}, x-y, \frac{2}{3}+z)$	$(y-x, \bar{x}, \frac{1}{3}+z)$	1	P1
146	R3 hex. axes	(x, y, z)	$(\bar{y}, x-y, z)$	$(y-x, \bar{x}, z)$	1	P1

TABLE 24. *Reduction from m to 1*

Space group of unstrained crystal, order 2 per lattice point		No specialization of stress		Space group of strained crystal, order 1 per lattice point	
		Coordinates referred to axes of unstrained crystal ($m \perp y$)			
No.	Symbol	1st Subset	2d Subset	No.	Symbol
6	Pm	(x, y, z)	$(x, \bar{y}, z)$	1	P1
7	Pc	(x, y, z)	$(x, \bar{y}, \frac{1}{2}+z)$	1	P1
8	Cm	(x, y, z)	$(x, \bar{y}, z)$	1	P1
9	Cc	(x, y, z)	$(x, \bar{y}, \frac{1}{2}+z)$	1	P1

TABLE 25. *Reduction from 2 to 1*

Space group of unstrained crystal, order 2 per lattice point		No specialization of stress		Space group of strained crystal, order 1 per lattice point	
		Coordinates referred to axes of unstrained crystal ($2 \parallel y$)			
No.	Symbol	1st Subset	2d Subset	No.	Symbol
3	P2	(x, y, z)	$(\bar{x}, y, \bar{z})$	1	P1
4	$P2_1$	(x, y, z)	$(\bar{x}x, \frac{1}{2}+y, \bar{z})$	1	P1
5	C2	(x, y, z)	$(\bar{x}, y, \bar{z})$	1	P1

TABLE 26. *Most general stress consistent with a reduction of a noncentrosymmetric point group to any one of its stress-induced subgroups*

Initial group	Subgroup										
						Minimum←		→Compound			
	Self subgroup	$\bar{4}2m$	422	3m	32	3	mm2	222	m	2	1
$\bar{4}3m$	$X=Y=Z$	$X=Y$; z ∥ Z	.....	$X=Y$; [111] ∥ Z	.....	.....	[1$\bar{1}$0], [110], z ∥ X, Y, Z, any permutation	x, y, z ∥ X, Y, Z, any permutation	[110] ∥ X, Y, or Z	x ∥ X, Y, or Z	Any
432	$X=Y=Z$	.....	$X=Y$; z ∥ Z	.....	$X=Y$; [111] ∥ Z	.....	.....	x, y, z or [1$\bar{1}$0], [110], z ∥ X, Y, Z, any permutation	.....	x or [110] ∥ X, Y, or Z	Any
23	$X=Y=Z$	.....	.....	.....	.....	$X=Y=Z$; [111] ∥ Z	.....	x, y, z ∥ X, Y, Z, any permutation	.....	x ∥ X, Y, or Z	Any

TABLE—Continued

Initial group	Subgroup					
	Self subgroup	mm2	222	m	2	1
$\bar{6}$m2 (hex. axes)	$X=Y$, $z \parallel Z$	[1$\bar{1}$0], [110], $z \parallel$ X, Y, Z, any permutation	----------	$z \parallel X$, Y, or Z or [For $\bar{6}$m2: [110]; for $\bar{6}$2m: [1$\bar{1}$0] $\parallel X$, Y, or Z]	[For $\bar{6}$m2: [1$\bar{1}$0]; for $\bar{6}$2m: [110] $\parallel X$, Y, or Z]	Any
6mm (hex. axes)	$X=Y$, $z \parallel Z$	z, $y \parallel$ any two of X, Y, Z	----------	[110] or [1$\bar{1}$0] $\parallel X$, Y, or Z	$z \parallel$ X, Y, or Z	Any
622 (hex. axes)	$X=Y$, $z \parallel Z$	----------	z, $y \parallel$ any two of X, Y, Z	----------	[110], [1$\bar{1}$0], or $z \parallel X$, Y, or Z	Any
6 (hex. axes)	$X=Y$, $z \parallel Z$	----------	----------	----------	$z \parallel$ X, Y, or Z	Any
$\bar{6}$ (hex. axes)	$X=Y$, $z \parallel Z$	----------	----------	$z \parallel$ X, Y, or Z	----------	Any
$\bar{4}$2m	$X=Y$, $z \parallel Z$	[For $\bar{4}$2m: [1$\bar{1}$0], [110], z; for $\bar{4}$m2: x, y, $z \parallel X$, Y, Z, any permutation]	[For $\bar{4}$2m: x, y, z; for $\bar{4}$m2: [1$\bar{1}$0], [110], $z \parallel$ X, Y, Z, any permutation]	[For $\bar{4}$2m: [110]; for $\bar{4}$m2: $x \parallel$ X, Y, or Z]	[For $\bar{4}$2m: x; for $\bar{4}$m2: [110] $\parallel$ X, Y, or Z or $z \parallel X$, Y, or Z]	Any
4mm	$X=Y$, $z \parallel Z$	x, y, z or [1$\bar{1}$0], [110], $z \parallel X$, Y, Z, any permutation	----------	x or [110] $\parallel X$, Y, or Z	$z \parallel$ X, Y, or Z	Any
422	$X=Y$, $z \parallel Z$	----------	x, y, z or [1$\bar{1}$0], [110], $z \parallel X$, Y, Z, any permutation	----------	x, [110], or $z \parallel X$, Y, or Z	Any
4	$X=Y$, $z \parallel Z$	----------	----------	----------	$z \parallel$ X, Y, or Z	Any
$\bar{4}$	$X=Y$, $z \parallel Z$	----------	----------	----------	$z \parallel$ X, Y, or Z	Any
3m (hex. axes)	$X=Y$, $z \parallel Z$	----------	----------	[For 3m1: [110]; for 31m: [1$\bar{1}$0] $\parallel X$, Y, or Z]	----------	Any
32 (hex. axes)	$X=Y$, $z \parallel Z$	----------	----------	----------	[For 321: [110]; for 312: [1$\bar{1}$0] $\parallel X$, Y, or Z]	Any
3 (hex. axes)	$X=Y$, $z \parallel Z$	----------	----------	----------	----------	Any
mm2	x, y, $z \parallel$ X, Y, Z, any perm.			x or $y \parallel X$, Y, or Z	$z \parallel X$, Y, or Z	Any
222	x, y, $z \parallel$ X, Y, Z, any perm.			----------	x, y, or $z \parallel X$, Y, or Z	Any
m($\perp$y)	$y \parallel$ X, Y, or Z					Any
2($\parallel$y)	$y \parallel$ X, Y, or Z					Any
1	Any					

Large square brackets indicate same subgroup in equivalent setting.

(Paper 69A5–368)

JOURNAL OF RESEARCH of the National Bureau of Standards—A. Physics and Chemistry
Vol. 69A, No. 5, September–October 1965

Inclusion of Perfluoromethyl Groups in the Crystals of Copolymers of Tetrafluoroethylene and Hexafluoropropylene*

L. H. Bolz and R. K. Eby

(June 21, 1965)

X-ray diffraction has been used to measure the separation of the molecular axes as a function of temperature, lamella thickness, and comonomer concentration in copolymers of tetrafluoroethylene and hexafluoropropylene. These data show that the increase of separation with increasing concentration of perfluoromethyl groups is a consequence of inclusion of the groups in the crystals and not an artifact associated with lamella thickness or crystal transition temperature. This conclusion is supported by the fact that diffuseness of some of the x-ray reflections in the copolymers indicates the presence of molecular disorder which might be expected from inclusion of the perfluoromethyl groups in the crystals. The lamellas in the copolymers are thinner than those in the typical homopolymer and this aspect of the structure is the primary cause of the lower density in the copolymers. Analysis of the available data indicates that this is also the situation in copolymers of ethylene and propylene. For both copolymer series, the density of the lamellas is apparently increased by the inclusion of the methyl groups in the crystals as defects.

1. Introduction

In an earlier article [1],[1] evidence was presented that copolymers of tetrafluoroethylene and hexafluoropropylene form lamellar crystals with the perfluoromethyl groups within the crystals as point defects. Part of this evidence was the fact that the copolymer exhibited a larger separation of the molecular axes than did polytetrafluoroethylene. This result, which disagrees with a report of no change of separation [2], is subject to a question arising from the fact that polytetrafluoroethylene undergoes first-order, crystal-crystal transitions at about 290 and 305 °K [3, 4]. These transitions, at which both the lattice parameters and the thermal coefficients of expansion increase [3, 5] occur at lower temperatures in the copolymers. Thus, it can be asked whether the lattice of the copolymer is larger than that of polytetrafluoroethylene at 296 °K merely because the copolymer is at a temperature which is further removed from the phase transition.

Another question arises from the fact that the lamella thickness was observed to decrease with increasing concentration of perfluoromethyl groups [1][1] (the same effect has also been observed in ethylene-propylene copolymers [6, 7]). It might be argued that at the lamella surface there is strain and an increase of the unit cell size. Then it can be asked whether the lattice of the copolymer is larger not because of inclusion of perfluoromethyl groups but because the lamella surfaces are more numerous and therefore exert a stronger influence on cell size.

This article presents data and analyses as evidence that the larger separation of the axes in the copolymer is a result of inclusion of the perfluoromethyl groups in the crystals and not an artifact associated with transition temperature or lamella thickness. Also presented are data and analyses concerning the density, lamella thickness, and unit cell dimension of tetrafluoroethylene-hexafluoropropylene and ethylene-propylene copolymers. These indicate that the thinner lamellas of the copolymers rather than "amorphous defects" of reduced density around the methyl [8] or perfluoromethyl groups are primarily responsible for the reduction in density from that of the homopolymer.

2. Experimental Procedures

Wide angle x-ray diffraction measurements were made as a function of temperature using Cu radiation filtered by Ni and a cryostat that provided temperature control in the range 4 to 300 °K [9, 10]. The present measurements for polytetrafluoroethylene and a copolymer similar to the intermediate one of reference [1] were made above to 80 °K only, since this temperature was found to be well below the transition temperature. Measurements were made at approximately 10 deg intervals with increasing temperature and a wait of about 50 min at each temperature. In the temperature range of the transition, the temperature intervals were shortened to 5 deg with a wait of 40 min. Temperatures were measured with a Au-2.1 percent Co versus Cu thermocouple [9] and are subject to an uncertainty of about 1 deg.

Since the polymers, especially the copolymer, did not yield suitable diffraction at large angles, they could not be used to aline the goniometer [11]. Therefore, silicon which had been measured previously [11] was pressed into asperities on the front surface of the polymer and diffraction from the {111}, {220}, {311}, {400}, {331}, {511}, and {440} planes

*Abstract in Bull. Am. Phys. Soc. **10**, 354 (1965); NBS Tech. Note 236, 56 (1963); and NBS Tech. Note 260, 47 (1965).

[1] Figures in brackets indicate the literature references at the end of this paper.

780-567—65——7

was used to aline that surface.[2] Because the surface responded to contraction of both the sample, which was about 1 mm thick, and the apparatus, alinement was carried out at the lowest temperature after 2 hr were allowed for the attainment of thermal equilibrium. Subsequently, the alinement was checked at each temperature using diffraction from only the first planes above, and more were used only if realinement was necessary. Over the present temperature range, the expansion of silicon is very small, corresponding to a total change of less than 2×10^{-3} A in the dimension of the unit cell [12].

Because of beam penetration into the sample, alinement of the front surface yields a small error in the determined spacings and a very small correction was made for this effect. However, comparison of the spacings determined for the two samples is not altered significantly by omission of this correction for the following reasons: the effect is small, measurements for the two samples were made in the same angular range, the difference in density of the two samples is about 5 percent only, and the variation of density over the temperature range of interest is about 5 percent only [13]. There are other sources of possible error, and the determined spacings are subject to an estimated uncertainty of about 0.02Å. Most of this uncertainty is the result of systematic errors and because of similarity of the samples and the experimental procedures for each, is also not relevant to a comparison of the results for each. In order to minimize unwanted surface orientation effects [14], the samples were cooled slowly from the melt. Orientation in the surface layers of the samples was examined by x-ray diffraction with a Norelco micro camera and a 100-μ beam of Cu radiation filtered by Ni. Transverse sections were cut from the samples and diffraction patterns were obtained with the beam parallel to the surface and incident upon the top 50 to 100μ of surface.

Wide-angle x-ray diffraction measurements were made at about 296 °K as a function of comonomer concentration and lamella thickness with a Norelco diffractometer and Cu radiation filtered by Ni. Samples about 0.3 mm thick were carefully placed at the same position in the same sample holder and at the same position in the diffractometer. With the slowest speed of the diffractometer and four recordings for each of the one to three positionings of each sample, this procedure yields average angles of the diffraction maxima which are subject to standard deviations corresponding to less than 2×10^{-3}Å in the unit cell dimension. This value is small enough that, together with the small differences in densities and in angles of the diffraction maxima of the different samples, it permits comparative measurements for the samples without use of an internal standard. The validity of this technique is supported by the fact that for two of the samples, the difference between the cell dimensions was reproduced with a powder camera. Similarly, the difference between cell dimensions of two other samples did not differ significantly from that measured by the technique described in the previous paragraph.

Samples with comonomer concentrations of approximately 0, 3, 4, 5.75, 6.2, 7, 7.6, and 8 CF_3 units per 100 main chain carbon atoms were used. Lamella thickness was varied by isothermal crystallization for about one week at different supercoolings followed by slow cooling. Thinner lamellas were produced by quenching thin films of melt in ice water. Lamella thickness was measured with Cu radiation and a small-angle diffractometer.

3. Results and Discussion

A number of papers have discussed various aspects of the crystal structure of polytetrafluoroethylene [3, 5, 15–19]. With the present sample, diffraction from more than five ($hk0$) planes could be observed in addition to that from several other planes at all temperatures. When the separation of the molecular axes (cell dimension a) was determined from each of the various $hk0$ reflections at 327 °K, there were small variations which were probably contributed to by variations in both the background of the scattering curve and the beam penetration of the sample with angle. These variations were not large enough to hamper comparisons with the copolymer and the 100 reflection was selected for comparison since it was the strongest of the $hk0$ reflections that could be observed readily in the copolymer. At temperatures below the transition temperature, the lateral packing of the molecules is not quite hexagonal [19] and an average of the nearest neighbor distances is given.

Data for intermolecular distance, which are presented in figure 1, show a transition to occur at about 225 °K in the copolymer. The scatter of the data gives a measure of the reproducibility and may be sufficient to mask the small [19] transition that occurs near 305 °K in polytetrafluoroethylene. Below 225 °K, as well as above, the spacing of the molecular axes in the copolymer is larger than in polytetrafluoroethylene.[3] The difference increases slightly at 225 °K and above but the increase is only a small portion of the total difference for two reasons. First, the increase in spacing at the transition is not too great. Second, the difference between the average values of the expansion above and below the transition is only about 1.2×10^{-4} Å/°K. Thus, it seems reasonable to conclude that the larger separation of the molecular axes in the copolymer is real and that the answer to the first question raised in the introduction is negative. That is, at 296 °K, the greater part of the increase of separation of the axes in the copolymer is not an anomaly associated with transition temperature.

Variation of intermolecular distance with comonomer concentration is shown in more detail in figure 2.

[2] The silicon had initially been placed on the front surface with a silicone grease. The pressing technique was used after it was observed that the grease crystallized at about 230 °K.

[3] Only a few data were taken with polytetrafluoroethylene for purposes of comparison here since precise measurements have been published [19]. The present results for 298 °K do agree with these but there does not seem to be any reason to expect exact agreement in the range of the transitions which varies with rate of heating, polymer sample, etc. [4, 13].

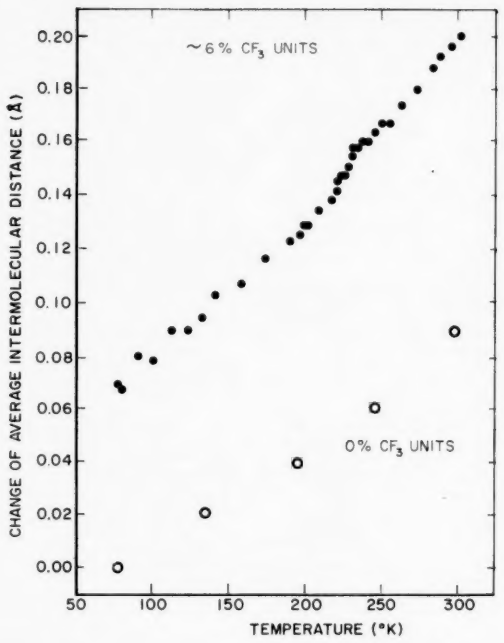

FIGURE 1. *Temperature dependence of the change of average intermolecular distance with respect to an arbitrary reference.*

The solid points represent a copolymer of tetrafluoroethylene and hexafluoropropylene with about six perfluoromethyl groups per 100 main-chain carbon atoms. The copolymer exhibits a phase change near 225 °K. Open points represent polytetrafluoroethylene.

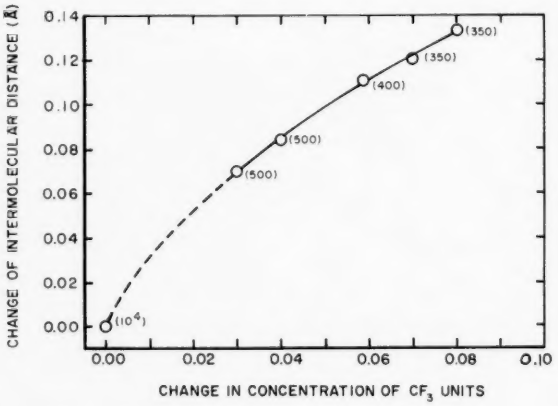

FIGURE 2. *Change of intermolecular distance with the ratio of perfluoromethyl groups to main-chain carbon atoms (concentration).*

The reference point is polytetrafluoroethylene at about 296 °K. The numbers in brackets give the approximate lamella thickness for each sample.

Between the samples with 0 and 3 perfluoromethyl units per hundred main chain atoms, there is a dotted line which is intended to guide the eye rather than represent the detailed variation of intermolecular distance. As noted above, part of this variation (~0.013 Å) is a consequence of the fact that at about 296 °K, polytetrafluoroethylene is not completely above the transitions [19] whereas the copolymer is. In the range of perfluoromethyl concentration between 3 and 8 percent, the intermolecular distance increases approximately uniformly with concentration at an average rate of about 1.4×10^{-2} Å per 1 percent change in concentration. The intermolecular distance in the copolymer is evidently not the same as that in the homopolymer as has been reported [2].

On figure 2 the approximate lamella thickness is given next to each point. These show the basis of the possibility that the variation of intermolecular distance with concentration might be caused by the variation of lamella thickness. However, as figure 3 shows for two concentrations of perfluoromethyl groups, when thickness is varied at constant concentration, there is little discernible variation of intermolecular distance for a thickness variation of about 200 Å. (The latter is greater than the variation of thickness when concentration varies from 0.03 to 0.08, cf. fig. 2.) This conclusion is supported by statistical analysis which yields a rate of change of intermolecular distance with thickness of -2×10^{-6}Å/Å with a standard deviation of 1.2×10^{-5}Å/Å. Therefore, it is concluded that the answer to the second question in the introduction is negative. That is, the greater part of the change of intermolecular distance with comonomer concentration is not a consequence of the change of lamella thickness.[4]

On the basis of the results in the last two paragraphs, it is concluded that the increase of intermolecular distance with concentration of perfluoromethyl groups is primarily the consequence of inclusion of the groups within the crystals. This concept is supported by an aspect of the data other than the increase of cell dimension; that is, the diffuse nature of the diffraction from certain planes. The 107, 108, 1, 0, 15, and 0, 0, 15 reflections could be

[4] Although 99 percent confidence limits on the change of intermolecular distance with lamella thickness are somewhat larger, they are too small to invalidate the conclusion just made. We wish to note also that for both copolymers the three samples with thickest lamellas exhibited a trend toward increasing spacing with decreasing lamella thickness. Although this trend is too small to be considered significant in our data, it tends to be reproducible. Also, it is always vitiated by the data for the quenched (thinnest lamellas) samples. Such a trend could result from a number of possible causes ranging from artifact to real physical effect and they have not been pursued.

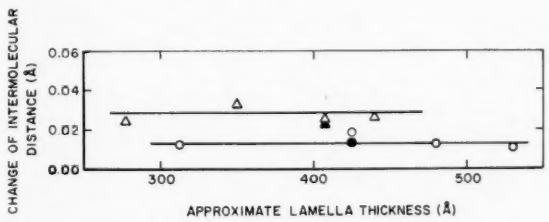

FIGURE 3. *Change of intermolecular distance with approximate lamella thickness for samples with two different concentrations of perfluoromethyl groups (upper curve 0.076, lower curve 0.062).*

The reference is 0.10 Å on fig. 2 and the data were obtained at 296 °K. Data represented by open points were obtained with a diffractometer and the data represented by the solid points were obtained with a powder camera.

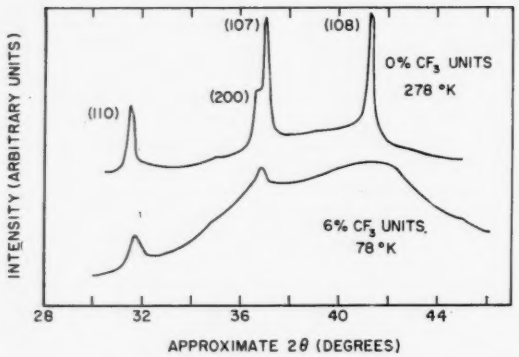

FIGURE 4. *Intensity in arbitrary units as a function of approximate diffraction angle (2θ) for polytetrafluoroethylene at 278 °K and for a copolymer at 78 °K.*

These are the same samples as in figure 1. The curve for polytetrafluoroethylene has been arbitrarily displaced to higher intensities.

observed readily in polytetrafluoroethylene at room temperature but the corresponding ones were very broad and diffuse in the copolymer. Even at the lowest experimental temperatures, these reflections (or the corresponding ones below the transition temperature) remain diffuse as shown in figure 4. While this effect can be the consequence of surface orientation in quenched samples [14], wide angle x-ray diffraction shows that this is probably not the case in the present, slowly cooled sample. As shown in figure 5, patterns obtained with the beam parallel to the surface and intercepting the top 50 to 100μ of surface show little preferential orientation. While the absence of orientation is difficult to confirm positively, patterns similar to figure 5 were

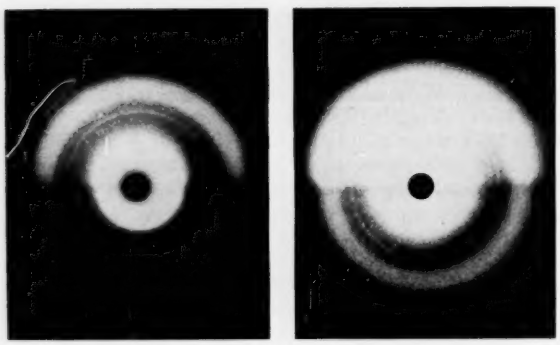

FIGURE 5. *Diffraction pattern obtained with the x-ray beam parallel to the surface and incident upon the top 50 to 100 μ of surface of the copolymer sample in figure 1.*

The beam of CuK_α radiation is 100-μ in diameter. Because the beam is near the horizontal surface, radiation diffracted upward encounters a different pathlength (and absorption) than that diffracted downward. Therefore, one-half of the film is more strongly exposed than the other and two prints are presented in order to show the equivalence of the essential details in each half.

obtained with several geometries of beam and sample. Also, one long exposure did not show orientation in the diffuse 0, 0, 15 reflection.

Another possible cause of the effect is disorder. Although a certain amount of caution must be exercised in interpreting the present limited number of reflections (especially those with $l=15$ since they are intrinsically weak [19]), some observations can be made. For example, for $l=15$ (or 13 at low temperature) the reflections are governed by a zero-order Bessel function and therefore diffuseness would not result from rotational disorder about the chain axis but would result from disorder along the axis [17, 19]. Longitudinal disorder would probably be the cause of diffuseness for $l=7$ and 8 (or 6 and 7) but since these reflections are governed by a first-order Bessel function, diffuseness could result from rotational disorder. Thus, subject to the caution above, the diffuse nature of the reflections suggests longitudinal disorder along and possibly rotational disorder about the chain axis. Small disordering in rotation and translation might be expected from inclusion of the perfluoromethyl groups within the crystals.[5]

The density of the copolymers in figure 2 ranged from 2.155 to 2.133 g/cm^3 at 296 °K. These are smaller than typical homopolymer values which can be greater than 2.22 g/cm^3. However, it would be incorrect to assume that lamella thickness is largely independent of copolymer concentration and then to attribute lowering of the density directly to reduced density [8] around the comonomer units without first considering the known tendency for lamella thickness to decrease with increasing comonomer content [1, 6, 7]. Since mispacking of the folds of adjacent lamellas lowers the gross density [20, 21], copolymers should be less dense than the homopolymer simply because lamellas of the latter are often an order of magnitude thicker than the 350 to 500 Å lamellas of the copolymers in figure 2 [22]. However, greater supercooling of the polytetrafluoroethylene melt produces samples with thinner lamellas. Data obtained by electron microscopy indicate that such samples with densities somewhat less than 2.18 g/cm^3 would have lamellas less than 500 Å thick [23]. Also, light scattering yielded a structural dimension of 260 Å for a sample with density of 2.13 g/cm^3 [24].

These densities are in the range of those for copolymers with similar lamella thickness. Therefore, to provide a more direct comparison and avoid systematic differences in thickness and density as determined by different techniques, a quenched sample of polytetrafluoroethylene was prepared and measured by the present techniques. This yielded a sample with lamella thickness of 550 to 600 Å and density of 2.139 g/cm^3 which is less than the values of 2.151 and 2.155 for the copolymer samples with

[5] This type of disordering cannot be adequately described by the word amorphous which implies liquid-like disorder.

the 500 Å lamellas. Reduced lamella thickness of the copolymer apparently accounts for the usual reduction of density. In fact, the data indicate that for copolymer and homopolymer samples with lamellas of equal thickness, the copolymer would be more dense.

Consideration of the increase of mass associated with the comonomer units together with the increase of cell volume suggests that the density of the lamellas is increased slightly by the comonomer units.[6] This type of analysis is based upon results from calculations for point and slightly larger centers of dilation in an elastic continuum [25–27] After introduction of the defects, the fractional dilations of the macroscopic and cell volumes are equal if no new substitutional sites are introduced. Experimental verification of the effect has been obtained for a number of examples in atomic solids [26, 28, 29]. While the present analysis may be subject to errors, the increase of lamella density would remove almost completely the discrepancy noted above for the density of copolymer and homopolymer samples with similar lamella thickness.

It can be argued that each case must be considered separately and therefore it is of interest that the available data indicate that the same effects occur in copolymers of ethylene and propylene. For slowly cooled samples, the measured density decreases ca. 8×10^{-3} g/cm^3 for each methyl group per 100 main chain atoms [8]. Slowly cooled copolymers with methyl group concentrations between 0 and 1.5 percent exhibit a decrease of lamella thickness of about 55 Å for each percent of methyl groups [6].[7] Together with the variation of density of the homopolymer with lamella thickness [20] these data yield a calculated decrease of ca. 10×10^{-3} g/cm^3 for each percent of methyl groups. While all these data were not available for a coherent set of samples as were the data presented above for the fluorocarbons, the density decrease calculated from lamella thickness again appears to be greater than that actually observed. However, taking the data for cell dimension and comonomer concentration given in reference [8] and calculating the density of the lamellas again removes most of the discrepancy.

The decrease of density of both copolymer series is apparently a result primarily of decreasing lamella thickness and not of reduced density around the comonomer units. Indeed, lamella density based on comonomer concentration and cell size is increased by the comonomer units and this result tends to agree with the experimental data. However, this latter fact cannot be established unambiguously without a rather formidable set of very accurate measurements of density, unit cell, and lamella thickness on a series of copolymer samples which have accurately known, different comonomer concentrations and which have been isothermally crystallized at different supercoolings. In any event, there are no data for small scale techniques which unambiguously indicate extensive amorphous disorder around the methyl groups and so gross a measurement as density is a poor one to use in the resolution of small scale structural details such as the nature of the disorder around the groups.

[6] The concentration of perfluoromethyl groups in the lamellas is taken as that in the whole polymer.

[7] Although data over a wider range of concentration are available, they have been obtained on samples which were not slowly cooled. These show the same general trend in lamella thickness with the rate of decrease becoming smaller at higher concentrations.

4. Conclusions

Measurements of the separation of molecular axes have been made as a function of comonomer concentration, temperature and lamella thickness in copolymers of tetrafluoroethylene and hexafluoropropylene. These give evidence that the increase of separation with concentration is primarily the consequence of inclusion of the perfluoromethyl groups in the crystals. This conclusion is supported by the fact that the diffuseness of some of the x-ray reflections in the copolymers indicates the presence of molecular disorder which might be expected from inclusion of the perfluoromethyl groups in the crystals. The density of the copolymers is lower than that of the homopolymer primarily because the former have thinner lamellas and not because of "amorphous defects" of lower density around the perfluoromethyl groups. The same statement applies to copolymers of ethylene and propylene at low methyl group concentrations. For both copolymer series, the density of the lamellas is apparently increased by the inclusion of the methyl groups in the crystals as defects.

The authors express their thanks to W. A. Zisman and Marianne K. Bernett of the U.S. Naval Research Laboratory for providing samples of copolymers. Also, they want to thank E. S. Clark of the DuPont Experimental Station and J. P. Colson and their other colleagues at the National Bureau of Standards for helpful discussions and encouragement. Helpful discussions with Professor R. W. Balluffi are gratefully acknowledged.

5. References

[1] R. K. Eby, J. Res. NBS **68A** (Phys. and Chem.) No. 3, 269 (1964).
[2] H. G. Killian, Kolloid-Z. **176,** 49 (1961).
[3] C. W. Bunn and E. R. Howells, Nature **174,** 549 (1954).
[4] F. A. Quinn, D. E. Roberts, and R. N. Work, J. Appl. Phys. **22,** 1084 (1951).
[5] H. A. Rigby and C. W. Bunn, Nature **164,** 583 (1949).
[6] H. Hendus, Ergeb. Exakt. Naturw. **31,** 331 (1959).
[7] C. Sella, Compt. Rend. **248,** 1819 (1959).
[8] B. Wunderlich and D. Poland, J. Polymer Sci. **1A,** 357 (1963).
[9] A. Black, L. H. Bolz, F. P. Brooks, F. A. Mauer, and H. S. Peiser, J. Res. NBS **61,** No. 5, 367 (1958) Rp2907.
[10] F. A. Mauer and L. H. Bolz, J. Res. NBS **65C** (Engr. and Instr.) No. 4, 225 (1961).
[11] F. A. Mauer and L. H. Bolz, WADC Technical Report 55–473, December 1955.
[12] S. I. Novikova and P. G. Strelkov, Soviet Phys.—Solid State **1,** 1687 (1959).
[13] R. K. Kirby, J. Research NBS **57,** 91 (1956) Rp2696· also I. E. Leksina and S. I. Novikova, Soviet Phys.—Solid State **1,** 453 (1959).

[14] E. S. Clark and H. W. Starkweather, Jr., J. Appl. Polymer Sci. **6,** 541 (1962).
[15] R. H. H. Pierce, Jr., E. S. Clark, J. F. Whitney, and W. M. D. Bryant, presented at the 130th meeting of the American Chemical Society, Atlantic City, N.J., September 1956.
[16] G. Butenuth, Verhandlungsberichte der Kolloid Gesellschaft **18,** 168 (1958).
[17] E. S. Clark and L. T. Muus, Z. f. Kristallographie **117,** 2/3, 109 (1962).
[18] A review is presented by C. A. Sperati and H. W. Starkweather, Jr., Fortschr. Hochpolymer. Forsch. **2,** 465 (1961).
[19] E. S. Clark and L. T. Muus, Z. f. Kristallographie **117,** 2/3, 119 (1962).
[20] R. G. Brown and R. K. Eby, J. Appl. Phys. **35,** 1156 (1964).
[21] E. W. Fischer and G. F. Schmidt, Angew. Chem. Intern. Ed. Engl. **1,** 488 (1962).
[22] C. W. Bunn, A. J. Cobbold, and R. P. Palmer, J. Polymer Sci. **28,** (1958).
[23] H. W. Starkweather, Jr., SPE Transactions **3,** 57 (1963).
[24] H. W Starkweather, Jr., J. Polymer Sci. **2B,** 499 (1964).
[25] J. D. Eshelby, J. Appl. Phys. **25,** 255 (1954); Proc. Royal Soc. London, **142A,** 376 (1957); and Solid State Physics **3,** 79 (1956). See also, K. Huang, Proc. Roy. Soc. (London) **A190,** 102 (1947).
[26] R. O. Simmons and R. W. Balluffi, J. Appl. Phys. **30,** 1249 (1959).
[27] R. W. Balluffi and R. O. Simmons, J. Appl. Phys. **31,** 2284 (1960).
[28] J.A. Bearden, Phys. Rev. **137,** B181 (1965).
[29] Francisco Eiichi Fujita and Ulrich Gonser, J. Phys. Soc. Japan **13,** 1068 (1958).

(Paper 69A5–369)

JOURNAL OF RESEARCH of the National Bureau of Standards—A. Physics and Chemistry
Vol. 69A, No. 5, September-October 1965

Publications of the National Bureau of Standards*

Selected Abstracts

Improved ten-picofarad fused silica dielectric capacitor, R. D. Cutkosky and L. H. Lee, *J. Res. NBS* **69C** (*Engr. and Instr.*), *No. 3, 173–179 (July–Sept. 1965). $0.75*
Some defects in a set of fused silica dielectric capacitors constructed in 1961 are listed, and methods for their reduction or elimination are described. The construction of a new set of capacitors completed in 1964 is described in detail. Preliminary stability data presented indicates that the typical drift of the 1964 capacitors with respect to their mean was less than two parts in 10^7 in five months.

Equipment for single-crystal growth from the melt suitable for substances with a low melting point, A. T. Horton and A. R. Glasgow, *J. Res. NBS* **69C** (*Engr. and instr.*), *No. 3, 195–198 (July–Sept. 1965). $0.75*
Glass apparatus is described for the purification and growth of crystals with melting points up to about 130 °C by a modified Bridgman technique. The temperatures of the melt and the solid are maintained by two immiscible liquids at whose interface a sharp temperature drop exists. A sealed Pyrex tube containing the specimen is slowly lowered throuth the interface. The specimen is maintained under its own vapor pressure in contact only with the glass container. Provision is made for the removal of the last portions of the specimen to solidify from each of several successive recrystallizations.
The equipment has been found effective for the purification of trans-stilbene, dimethyl oxalate, benzoic acid and benzene. It could also be used for careful studies of thermal and radiation stability of pure substances.

Cartesian diver as a density comparator, H. A. Bowman and R. M. Schoonover, *J. Res NBS* **69C** (*Engr. and Instr.*), *No. 3, 217–223 (July–Sept. 1965). $0.75*
This report describes a hydrostatic weighing system which provides values of apparent mass in water reproducible (standard deviation) between independent measurements of about 0.2 microgram. The definition of "independent" used here, includes the requirement that the sample under observation be removed from the water, dried, and recleaned between measurements. This precision is between one and two orders better than existing hydrostatic balances, and permits high quality density measurements without recourse to large sample sizes. The system is used as a comparator, hence the absolute accuracy of results can be no better than that of the standards used. Typical data are presented which were taken during experiments on 2-gram pieces of single crystal silicon, and the standard deviation in density of an independent observation was computed to be $2{:}10^7$.
The system is particularly well suited to detection of slight density changes in small size samples. In this service, it is not subject to the requirement for high accuracy standards. Data are reported on density changes of about $5{:}10^5$ which occurred in a 250 milligram ceramic crystal. Two independent observations reported this change to agreement of about 7½ percent.

Cryogenic behavior of selected magnetic materials, J. J. Gniewek and E. Ploge, *J. Res. NBS* **69C** (*Engr. and Instr.*), *No. 3, 225–236 (July–Sept. 1965). $0.75*
Measurements of a-c core loss and d-c magnetic properties including coercive force, remanence and hysteresis loss are reported at temperatures of 273, 195, 76, and 4 °K for a variety of commercial magnetic Fe-Si and Fe-48 percent Ni alloys. Of the materials tested the high silicon content (3–4.45% Si) Fe-Si alloys were found to be the least temperature sensitive. Hysteresis loss increases between 273 and 4 °K of up to 100 percent were measured for the iron-nickel materials.

Effects of rocket outgassing on rf experiments, W. Pfister and J. C. Ulwick, *Radio Sci. J. Res. NBS/USNC–URSI* **69D,** *No. 9, 1219–1225 (September 1965). $1.00*
Peculiarities in the results of electron density measurements with rockets were noticed on several occasions. They were found to be effects of rocket outgassing. When the fuel valves of Aerobee rockets are not shut after burnout, residual fuel leaks out and diffuses into the atmosphere. Electrons attach to the fuel and decrease in concentration while the positive ions are not affected. Outgassing effects were observed on probe experiments flown in rockets as well as on propagation experiments between rocket and ground. Quantitative estimates indicate that the leaking fuel is a very effective attaching agent. Some solid fuel rockets also show similar effects.

Magneto-ionic propagation in inhomogeneous media. Part I. Transverse propagation, B. K. Banerjea, *Radio Sci. J. Res. NBS/USNC-URSI 69D, No. 9,* 1285–1295 (*September 1965*). *$1.00*
Propagation of electromagnetic waves in an inhomogeneous magneto-ionic medium has been discussed with special reference to ionospheric propagation. This involves the study of two coupled linear second-order differential equations with coefficients having one essential and more than one regular singularity. The problem has been tackled in two stages divided into Parts I and II of this paper.
In Part I, dealing with the transverse propagation in a parabolic electron-layer, the wave-equation, belonging to a class higher than the confluent hypergeometric or Mathieu equations, has been investigated. In Part II, dealing with the oblique propagation, the effect of the coupling function for the above class of equations has been studied, and relevant asymptotic solutions for the coupled equations derived.
Mathematical expressions for the physical observables in ionospheric investigations have been derived from the solutions of the wave-equations inside a parabolic electron-layer.

Magneto-ionic propagation in inhomogeneous media. Part II. Oblique propagation, B. K. Banerjea, *Radio Sci. J. Res. NBS/USNC-URSI, 69D, No. 9,* 1297–1306 (*September 1965*). *$1.00*
Oblique propagation of electromagnetic waves in an inhomogeneous magneto-ionic medium is described by a pair of coupled, linear, second-order differential equations, with coefficient functions having one essential singularity and more than one pole. An analytic method to study this general type of propagation has been developed in this paper.
Mathematical expressions for all the physical observables in the inospheric investigations have been derived for a parabolic electron-layer. The expressions for the phase-retardation and the tilt of the polarization ellipse differ radically from those derived from the ray-optics of Appleton and Hartree.

Automatic indexing: A state-of-the-art report, M. E. Stevens, *NBS Mono. 91 (Mar. 30, 1965), $1.50.*
A state-of-the-art survey of automatic indexing systems and experiments has been conducted by the Research Information Center and Advisory Service on Information Processing, Information Technology Division, Institute for Applied Technology, National Bureau of Standards. Consideration is first given to indexes compiled by or with the aid of machines, including citation indexes. Automatic derivative indexing is exemplified by key-word-in-context (KWIC) and other word-in-context techniques. Advantages, disadvantages, and possibilities for modification and improvement are discussed. Experiments in automatic assignment indexing are summarized. Related research efforts in such areas as automatic classification and categorization, computer use of thesauri, statistical association techniques, and linguistic data processing are described. A major question is that of evaluation,

particularly in view of evidence of human inter-indexer inconsistency. It is concluded that indexes based on words extracted from text are practical for many purposes today, and that automatic assignment indexing and classification experiments show promise for future progress.

The examination of weighing equipment, M. W. Jensen and R. W. Smith, *NBS Handbook 94* (*Mar. 1, 1965*), *$3.00.* (*Supersedes H37*).
This Handbook is primarily directed to the presentation of a coordinated series of step-by-step Examination Procedure Outlines (EPO's) for weighing equipment, recommended for adoption and use, as minimal requirements, by weights and measures agencies, commercial service agencies, weighing equipment owners and operators, and manufacturers of weighing devices. Supporting information embraces discussions on related topics such as reference and field standards report forms, tolerances, weighing principles, and elements of scale construction and performance. Extensive weights and measures tables—basic, interrelation of units, and equivalents—and a list of references for further study are appended. An alphabetical index is supplied.

Standard Reference Materials: Accuracy of solution x-ray spectrometric analysis of copper-base alloys, R. Alvarez and R. Flitsch, *NBS Misc. Publ. 260–5* (*Mar. 15, 1965*), *25 cents.*
X-ray fluorescence spectrometry has been investigated as an independent method for the analysis of certain major constituents in NBS standard reference materials. The determination of copper and zinc in cartridge and aluminum brass samples which were to be certified as standard materials, was selected for study. After a preliminary analysis, a solution of the unknown and a closely-matched synthetic standard were compared without the use of an internal standard or added control element. To achieve reliable results, close control of the type and concentration of acid was found necessary, and, for cells employing films as windows, the position of the film was critical. The temperature rise of the cell during irradiation was 0.1 °C, which did not contribute significantly to error. Typical coefficients of variation obtained for individual results in a group of 8 runs were 0.3% for copper and 0.4% for zinc. The agreement between chemical and x-ray results was within 0.3% of the amount present for both elements.

Thermal properties of aqueous uni-univalent electrolytes, V. B. Parker, *NSRDS–NBS2*, (*Apr. 1, 1965*), *45 cents.*
The available specific heat, heat of dilution, and heat of solution data for aqueous solutions of uni-univalent electrolytes have been critically reviewed and tables of selected "best" values at 25 °C prepared. In addition, the neutralization data have been critically reviewed in order to obtain the "best" value, 13,345 cal/mole, for the heat of ionization of water at 25 °C.
The electrolytes reviewed include the hydroxides, halides and oxyhalides, nitrates and nitrites, formates and acetates, cyanides, cyanates and thiocyanates, and permanganates of hydrogen, ammonium and the methyl ammonium derivatives, silver, and the alkali metals.

Optical scintillation; a survey of the literature, J. R. Meyer-Arendt and C. B. Emmanuel, *NBS Tech. Note 225* (*Apr. 5, 1965*), *70 cents.*
In this Technical Note, main emphasis is placed on providing the rader with an exhaustive survey of the literature, covering the field of effects of atmospheric refraction on the propagation of electromagnetic radiation at optical frequencies.
One may distinguish systematic, regular, or normal refraction on the one side from random refraction on the other. The former can be predicted theoretically, using various types of atmospheric models; the latter requires analysis by statistical methods.
Numerous observational, experimental, and theoretical aspects of random refraction, that is, of scintillation in its widest sense, are discussed. The following topics are dealt with: refraction in plane and in spherically stratified media, refractive index variations, radio refraction, scintillation as a function of aperture size, zenith distance, site location, dispersion, and meteorolcgical conditions, the frequency spectrum of scintillation, terrestrial scintillation, image distortion and contrast reduction, refraction and diffraction theories of scintillation, autocorrelation analyses, radio star scintillation, and coherence problems. Questions of atmospheric scattering, absorption, and depolarization are excluded. Finally, a brief review is given concerning newer experimental methods for the observation, recording, and analysis of optical scintillation, including suggestions as to what further theoretical and experimental efforts should be undertaken.

A calorimetric determination of the enthalpy of graphite from 1200 to 2600 °K, E. D. West and S. Ishihara, (*Proc. 3rd Symp. Thermal Physical Properties, Purdue Univ., Lafayette, Ind., Mar. 22-26, 1965*), *Book, Advances in Thermophysical Properties at Extreme Temperatures and Pressures, pp. 146–151* (*American Society of Mechanical Engineers, New York, N.Y., 1965*).
Measurements are reported of the increase in the enthalpy of high-purity graphite between room temperature and 1200 to 2600 °K. A new apparatus is described briefly. Methods of operation are developed which eliminate some systematic and random errors and are especially advantageous at high temperatures. The enthalpy data fit the equation

$$H_T - H_{298.15} = 28.9004T - 1.045\times10^{-4}\,T^2 - 16{,}126.2\log_{10} T/313.15 - 8907.3$$

where H is in absolute joules per gram atomic weights and T in degrees Kelvin.

A high-speed (milliseconds) method for the simultaneous measurement of enthalpy, specific heat, and resistivity of electrical conductors at high temperatures, A. Cezairliyan (*Proc. 3rd Symp. Thermophysical Properties, 1965*), *Book, Advances in Thermophysical Properties at Extreme Temperatures and Pressures, pp. 253–262* (*American Society of Mechanical Engineers, New York, N.Y., 1965*).
A method for the simultaneous measurement of enthalpy, specific heat, and electrical resistivity of electrical conductors at high temperatures (1000 °K to the melting point of the sample) in experiments of short duration (milliseconds) is described. The rapid direct joulean heating is achieved by a single energy pulse obtained from a battery unit. The average heating rate was approximately 6600 °K sec^{-1}. The sample is tubular in form with a small hole drilled through the call at the middle of its length to approximate black body conditions, thus allowing the measurement of transient true temperatures by photoelectric methods. Results on molybdenum (from approximately 1300 to 1600 °K) are obtained and compared with available literature values.

Absolute measurement of *W* for polonium-210 alpha particles in nitrogen, argon, and argon-methane mixture, Z. Bay and F. D. McLernon, *Radiation Res.* **24,** *No. 1, 1–8* (*Jan. 1965*).
Absolute values of W_a at the Po^{210} alpha energy have been measured by both the slow and fast charge collection methods in nitrogen, argon, and in a mixture of argon and ten percent methane. The full alpha energy was expended in a gridded ionization chamber. The ionization chamber's collection plate was directly connected to a vibrating reed electrometer and was capacitively connected to a fast pulse height measuring system. Pulse height calibration was achieved by charges from a pulser collected and measured in the same electrometer. The W_a values obtained in the fast measurements agree with previous values measured with the slow method. From the difference between the charges measured in the slow and fast methods an estimate of the recoil ionization could be made.

Atomic lifetimes in neon I, J. Z. Klose, *Astrophys. J.* **141,** *No. 2, 814–818* (*Feb. 15, 1965*).
Mean lives of several atomic levels in Neon I have been determined using a method of electronic excitation and delayed coincidence. Lifetimes of the following levels given in the Paschen notation are: $2p_1$, 15.3 ± 0.4 nanoseconds; $2p_2$, 16.3 ± 0.6 ns; $2p_5$, 40.7 ± 1.8 ns; and $4d'_5$, 476 ± 33 ns. The errors given are probable errors in the measurement. The systematic errors assigned to the $2p_1$ and $2p_2$ levels are each 5% with the corresponding errors for the $2p_5$ and $4d'_5$ levels 50% each.

Description and analysis of the third spectrum of cerium (Ce III), J. Sugar, *J. Opt. Soc. Am.* **55,** *No. 1, 33–58 (Jan. 1965).*

New observations of the Ce III spectrum from 757 Å to 11091 Å are given, including 1700 lines not previously reported. The ground level of the ion is established as the $^3H_4$ state of the $4f^2$ electron configuration. One hundred twenty-six newly discovered energy levels are given. The ionization limit, at 161955 cm^{-1}, is calculated from the three member $4fnd$ series.

Effect of temperature on the vacuum ultraviolet transmittance of lithium fluoride, calcium floride, barium fluoride, and sapphire, A. H. Laufer, J. A. Pirog, and J. R. McNesby, *J. Opt. Soc. Am.* **55,** *No. 1, 64–66 (Jan. 1965).*

The effect of temperature on the vacuum ultraviolet transmission of LiF, CaF_2, BaF_2, and sapphire has been measured. It is found that, at the short wave edge, the transmission curves shift to higher wavelengths as the temperature is raised. Thus, near the short wave cutoff, windows are rendered opaque with relatively modest increases in temperature. The importance of these observations to vacuum ultraviolet photochemistry and spectroscopy at elevated temperatures is discussed.

Elastic constant of single crystal ThO_2 at 25 °C, P. B. Macedo, W. Capps, and J. B. Wachtman, Jr., *J. Am. Ceram. Soc.* **47,** *No. 12, 651 (Dec. 1964).*

The elastic constants of single crystal ThO_2 at 25 °C were determined to be $c_{11}=3.67\pm.04$, $c_{12}=1.06\pm.02$, and $c_{44}=0.797\pm.008$ in units of 10^{12} d/cm^2.

Electron density measurements in the magnetically confined arc, C. K. McLane, S. Takeda, W. E. Thomas, Jr., and R. C. Thompson, *J. Appl. Phys.* **36,** *No. 2, 327–341 (Feb. 1965).*

Three methods were used to obtain electron density as a function of radius in a magnetically confined, low pressure argon arc. The first utilized the phase shift of a reflected 35 GHz microwave, and the second determined density from the ion saturation current to a Langmuir probe. The third determination utilized the broadening of the Hβ line emitted by a small quantity of added hydrogen. Agreement among the three methods is satisfactory; the electron density at the axis of this discharge is of order 10^{14} cm^{-3} in agreement with results obtained by others for discharges of similar type.

Observation of the products of ionic collision processes and ion decomposition in a linear, pulsed time-of-flight mass spectrometer, R. E. Ferguson, K. E. McCulloh, and H. M. Rosenstock, *J. Chem. Phys.* **42,** *No. 1, 100–106 (Jan. 1, 1965).*

A retarding potential technique has been investigated which permits study of secondary processes occurring after ion acceleration in a time-of-flight mass spectrometer. By application of a retarding field near the end of the flight path, peaks due to neutral species and fragment ions formed after acceleration are separated from their parent ion peaks and displayed in the same panoramic mass spectrum. Charge exchange, collision-induced dissociation, and spontaneous (metastable) ion decomposition are easily observed. The identities of initial ions and fragment ions involved in secondary processes can be determined unambiguously without complications of peak overlap.

Oscillator strengths for lines of Fe I between 2500 and 3200 A, R. B. King, K. H. Olsen, and C. H. Corliss, *Astrophys. J.* **141,** *No. 2, 354–363 (Feb. 15, 1965).*

Measurements of total absorption have been made for lines of Fe I excited in a graphite tube furnace operated at various temperatures between 1600 and 3000 °K. Oscillator strengths derived from them are reported for 300 lines between 2500 and 3200 A.

Direct and inert-gas-sensitized radiolysis and photolysis of methane in the solid phase, P. Ausloos, R. E. Rebbert, and S. G. Lias, *J. Chem. Phys.* **42,** *No. 2, 540–548 (Jan. 15, 1965).*

The photolysis of CH_4–CD_4 mixtures has been briefly investigated at 20 °K using the xenon and krypton resonance lines. From the isotopic composition of the hydrogen and ethane fractions, it was shown that, in the solid phase, the excited methane molecule decomposes according to the following two modes:

$$1.\ CH_4^* \rightarrow CH_3 + H$$
$$2.\ CH_4^* \rightarrow CH_2 + H_2$$

The methylene radical inserts into methane to form ethane $-d_6$, $-d_4$, $-d_2$, and $-d_0$. In the direct radiolysis of methane at 20 °K and 77 °K, the same processes may occur as in the photolysis. But, in addition, other bimolecular reactions, probably of the type

$$CH_4^+ + CH_4 \rightarrow CH_5^+ + CH_3$$

have to be involved. When methane is irradiated in an argon matrix, however, elimination of a hydrogen molecule from methane becomes the major process. This is in strong contrast to the xenon-sensitized radiolysis in which case mainly hydrogen atoms and methyl radicals are formed. In the argon-, krypton-, and xenon-sensitized radiolysis, there is a gradual decrease in the efficiency of the energy transfer with increasing dilution. Radiolysis of CD_4–C_2H_4 (1:0.01) mixtures indicated that, at 77 °K, hydrogen atoms react with ethylene and propylene to form higher saturated hydrocarbons while, at 20 °K, hydrogen atoms disappeared mainly by recombination with other free radicals.

Vapor phase growth kinetics of potassium and mercury crystals, R. L. Parker and S. C. Hardy, *Book, Condensation and Evaporation of Solids, Proc. Symp. Condensation and Evaporation of Solids, pp. 649–664 (Gordon and Breech, New York, N.Y., Nov. 1964).*

Results are presented regarding two types of experiment on the growth rates of single crystals of potassium and of mercury from supersaturated vapor; and some preliminary results on the evaporation of potassium crystals. In the first growth experiment, direct optical measurements of the growth rates of (110) faces of an equiaxed potassium crystal of 1 mm size, for low vapor supersaturations between 3.0 and 0.11 have given unit condensation coefficients. Comparison of this result with the Burton, Cabrera, and Frank theory is made. In the second type of growth experiment, results are presented on the growth kinetics of mercury and of potassium whiskers using Gomer's electron field emission technique. Many of the results on Hg whiskers agree with those obtained earlier by Gomer, including positive exponential length growth, orientation, terminal lengths, and surface diffusion coefficients. Some similar and some new features are observed on K whiskers; these represent the first use of an alkali metal as a field emitter, to the best of our knowledge. Finally, the evaporation of potassium whiskers at saturation ratios near unity is found to occur from the tip only, in rather the reverse process of growth; this result is of interest in connection with the role of crystal edges in evaporation.

Effect of electrical fields and density in the radiolysis of ethane, H. H. Carmichael, R. Gorden, Jr., and P. Ausloos, *J. Chem. Phys.* **42** *No. 1, 343–351 (Jan. 1, 1965).*

The gamma-ray radiolysis of $C_2H_6-C_2D_6-NO$ and CH_3CD_3-NO mixtures has been investigated as a function of applied electrical field. In the saturation current region, a number of products resulting from the decomposition of neutral excited molecules increase about fivefold before the onset of secondary ionization while several other products, which can be ascribed to ion molecule reactions, remain essentially unchanged. The modes of decomposition of the excited ethane molecules formed by electron impact, as derived from the applied field experiments, are the same as those observed in the vacuum ultraviolet photolysis at 1470 A and at 1236 A. From the isotopic composition of the products it could be deduced that the average energy transferred to ethane by electron impact is greater than 10 eV. A value of 0.5 was derived for the number of neutral excited molecule decompositions per ion pair.

A change in density has a pronounced effect on the product distribution, both in the photolysis at 1236 A and the radiolysis. In the radiolysis, several of the changes can be ascribed

to the diminishing fragmentation of the parent ion with an increase in density. However, products resulting from the fragmentation of the neutral excited ethane molecules formed in the radiolysis also show a strong dependence on density because of collisional stabilization of the primary fragments and of the products formed in secondary reactions. For instance, the propane which could be entirely ascribed to the insertion reaction:

$$CH_2 + C_2H_6 + M \rightarrow C_3H_8 + M$$

increases with an increase in density in the photolysis as well as in the radiolysis.

Equilibrium pressures of oxygen over MnO_2-Mn_2O_3 at various temperatures, E. M. Otto, *J. Electrochem. Soc.* **112,** *No. 4, 367–370 (Apr. 1965).*

Oxygen pressures of the pyrolusite form of MnO_2 have been determined in a temperature range of 441° to 642 °C. The dissociation reaction $4\,MnO_2(c) = 2Mn_2O_3(c) + O_2\,(g)$ has been found to reach a steady state in the forward direction; reaction in the reverse direction was exceedingly slow and did not reach a steady state.

$\triangle H°$ and $\triangle S°$ for the reaction at 813 °K are 37.87 kcal* and 51.28 cal/deg, respectively. With little error these values can be used in the equation

$$-4.5758 \log pO_2(atm) = 37{,}870/T - 51.28$$

to calculate the pressure for any temperature in the above mentioned range. Conversion to 298.15 °K resulted in $\triangle H°_{298} = 38.8$ kcal and $\triangle S°_{298} = 52.8$ cal/deg for the dissociation. The limits of uncertainties are not given here because equilibria were not attained by recombination.

Direct observation of the optical anisotropy of the holmium nucleus, E. Ambler, E. G. Fuller, and H. Marshak, *Phys Rev.* **138,** *No. 1B, B117–B126 (Apr. 12, 1965).*

The optical anisotropy of the holmium nucleus in the giant resonance energy region has been shown to exist by measuring the yield of photoneutrons as a function of the orientation of the nucleus with respect to a bremsstrahlung beam direction. The nuclei were aligned by the Bleaney method using a continuously operating He^3 refrigerator to cool a single crystal of holmium ethyl sulfate to 0.29 °K. The orientation effects observed could be explained if the absorption cross section for holmium was made up primarily of a component given by the dynamic collective theory but which also included a small scalar component (about 15% of the total) which had no orientation effects associated with it. In fitting the data, a reanalysis of previous data on the holmium absorption cross section was made.

Interference patterns in reverberant sound fields. II, R. V. Waterhouse and R. K. Cook, *J. Acouts. Soc. Am.* **37,** *No. 3, 424-428 (Mar. 1965).*

Contour charts are given of the sound fields near one, two, or three reflecting surfaces at right angles, for random sound incidence. The charts show contours of the mean-squared-pressure in decibels as a function of position in the region within 2 wavelengths of the boundary surfaces. The boundary conditions at the reflecting planes are pressure reflecting (normal velocity equal to zero) or pressure release (pressure equal to zero). By reciprocity, the charts also give the radiation resistance of a point source as a function of position near such reflectors. The formulas used are tabulated; they extend and in some places correct formulas given in an earlier paper (Journ. Acous. Soc. Am. **27,** 247–258, March 1955). The features of the sound fields near the reflectors are discussed, and some applications to accoustics measurements in reverberant sound fields are considered.

Line profiles in the far-uv absorption spectra of the rare gases, U. Fano and J. W. Cooper, *Phys. Rev.* **137,** *No. 5A, A1364–A1379 (Mar. 1, 1965).*

The line profiles of a dozen series of widely different appearance, observed recently in the rare gas optical absorption spectra between 20 and 100 ev, are analyzed by adapting and extending previously developed theory. Theory characterizes each profile by its line width, q-index and correlation coefficient ρ and relates these parameters to matrix elements of the energy and of the electric dipole moment. Because the profiles result from interference effects, the signs of these matrix elements are highly relevant. Crude estimates of such, hitherto hardly accessible, matrix elements are obtained from experimental evidence and from atomic theory, are intercompared and found to be in general agreement. Similarities and differences among the line profiles are thereby tentatively explained. The connection of Rydberg series and absorption edges is discussed and the occurrence of downward jumps at some edges is explained. This exploratory investigation demonstrates how one can treat experimental data and surveys the kind and volume of information on the dynamics of highly and multiply excited atoms made accessible by recent experimental techniques.

Low temperature magnetic transitions in some rare-earth trichlorides, J. C. Eisenstein, R. P. Hudson, and B. W. Mangum, *Phys. Rev.* **137,** *No. 6A, A1886–A1895 (Mar. 15, 1965).*

The magnetic susceptibilities of $CeCl_3$, $PrCl_3$, and $NdCl_3$ single crystals and of polycrystalline $SmCl_3$ have been measured in the temperature region between 0.2 and 4.2°K. Each of these compounds exhibits somewhat anomalous behavior. $NdCl_3$ has two sharp spikes in its susceptibility vs. T curve at 1.035°K and 1.74°K. These spikes are strongly affected by a weak external field and also depend on the amplitude and frequency of the ac measuring field. $CeCl_3$ has a single sharp spike in its susceptibility at 0.345°K. $PrCl_3$ and $SmCl_3$ have rather broad maxima in their susceptibilities at about 0.7 and 0.4°K, respectively.

It is shown, on the basis of a simple molecular field model, that the superexchange coupling between nearest neighbors is ferromagnetic while that between next nearest neighbors is antiferromagnetic. The two spikes in the $NdCl_3$ susceptibility curve are ascribed to two successive cooperative magnetic transitions. An attempt is made to correlate in a quantitative way the temperatures of the transitions in $CeCl_3$ and $NdCl_3$, and to explain why no similar transitions were observed in $PrCl_3$ and $SmCl_3$.

Nonlinear ambipolar diffusion of an isothermal plasma across a magnetic field, E. R. Mosburg, Jr., and K. B. Persson, *Phys. Fluids* **7,** *No. 11, 1829–1833 (Nov. 1964).*

Solutions are presented of the first two moment equations, including nonlinear terms, for the ambipolar diffusion of an isothermal plasma across a magnetic field. The two geometries considered are the plane parallel case and the infinite cylinder with axial symmetry. The Bohm criterion is automatically satisfied by the solutions. It is shown that the singularity in the space derivative of the ambipolar drift velocity at the plasma boundary cannot be removed by an axial magnetic field of any strength. Thus the plasma drift velocity and the plasma density remain monotonic functions of the position coordinate. It is also shown under the assumptions of this theory, that the ambipolar space charge field is always directed outward and does not reverse direction in this isothermal approximation even for extremely high magnetic fields. One is forced to conclude that a realistic theory of ambipolar diffusion requires the consideration of the thermal gradients within the plasma.

Other NBS Publications

J. Res. NBS 69C (Engr. and Instr.), No. 3 (July–Sept. 1965), $0.75.

Two-terminal dielectric measurements up to 6×10^8 Hz. M. G. Broadhurst and A. J. Bur.

Improved ten-picofarad fused silica dielectric capacitor. R. D. Cutkosky and L. H. Lee. (See above abstracts).

Errors in the series-parallel buildup of four-terminal resistors. C. H. Page.

*One thermochemical calorie = 4.1840 joules.

Centerable rotator for measuring properties of crystals. C. P. Saylor and H. B. Lowey.
Equipment for single-crystal growth from the melt suitable for substances with a low melting point. A. T. Horton and A. R. Glasgow. (See above abstracts).
Phase and amplitude contrast microscopy in partially coherent light. M. De and P. K. Mondal.
Exposure time relations for Kossel microdiffraction photographs. H. Yakowitz and D. L. Vieth.
Cartesian diver as a density comparator. H. A. Bowman and R. M. Schoonover. (See above abstracts).
Cryogenic behavior of selected magnetic materials. J. J. Gniewek and E. Ploge. (See above abstracts).

Radio Sci. J. Res. NBS/USNC–URSI, 69D, No. 8 (Aug. 1965), $1.00.

"Ultra Low Frequency Electromagnetic Fields" Papers

Preface to "Ultra Low Frequency Electromagnetic Fields" Papers. W. H. Campbell and S. Matsushita.
Solar wind and its interaction with the magnetosphere. C. P. Sonett.
Schumann resonances. J. Galejs.
Earth-ionosphere cavity resonances and the propagation of ELF radio waves. J. R. Wait.
Resonances of the earth-ionosphere cavity observed at Cambridge, England. M. J. Rycroft.
Experimental results on the dynamics of the *F* region. W. Becker, R. Rüster, and J. Klostermeyer.
Regular oscillations near 1 c/s observed at middle and low latitudes. L. Tepley.
Preliminary results of a micropulsation experiment at conjugate points. R. E. Gendrin and V. A. Troitskaya.
Some characteristics of geomagnetic pulsations at frequencies near 1 c/s. W. H. Campbell and E. C. Stiltner.
Propagation of hydromagnetic waves in the magnetosphere. M. Sugiura.
Ionospheric perturbation (the roles played by the ionosphere in geomagnetic pulsations). S. Matsushita.
Effects of induced earth currents on low-frequency electromagnetic oscillations. A. T. Price.
Equatorial effects. R. Hutton.
Interpretation of early magnetic transients caused by high-altitude nuclear detonations. S. L. Kahalas and P. Newman.
Abstracts of ULF Conference papers not published in this issue.

Regular Contributions

A note on the application of pulse compression techniques to ionospheric sounding. D. C. Coll and J. R. Storey.
Comments on a paper "Measurement of the phase velocity of VLF propagation in the earth ionosphere waveguide" by F. K. Steele and C. J. Chilton. H. F. Bates.
Reply to H. F. Bates' Comments on "Measurement of the phase velocity of VLF propagation in the earth ionosphere waveguide" by F. K. Steele and C. J. Chilton. F. K. Steele and C. J. Chilton.

Radio Sci. J. Res. NBS/USNC–URSI, 69D, No. 9 (Sept. 1965), $1.00.

Ground-based passive probing using the microwave spectrum of oxygen. E. R. Westwater.
Response of NBS microwave refractometer cavities to atmospheric variations. R. O. Gilmer, R. E. McGavin, and B. R. Bean.
Effects of rocket outgassing on rf experiments. W. Pfister and J. C. Ulwick. (See above abstracts).
Further analysis of propagation of plasma waves in a "spoke-wheel" magnetic field. R. R. Gold.
Measurement of group velocity of 17.8-kHz VLF radio waves. W. D. Westfall.
On the radio noise level at low and very low frequencies in polar regions. T. Stockfleth Jørgensen.
Experimental study on the circular loop antenna immersed shallowly in a conducting medium. K. Iizuka.
Directivity of uniformly spaced optimum endfire arrays with equal sidelobes. M. T. Ma.
Extension of Fock theory for currents in the penumbra region. V. H. Weston.
Isometric-circle interpretation of bilinear transformation and its application to VSWR minimization. J. G. Rudolph and D. K. Cheng.
Magneto-ionic propagation in inhomogeneous media. Part I. Transverse propagation. B. K. Banerjea. (See above abstracts).
Magneto-ionic propagation in inhomogeneous media. Part II. Oblique propagation. B. K. Banerjea. (See above abstracts).
Editorial comment on the scientific papers of Lord Rayleigh (John William Strutt). J. R. Wait.

Radio Sci. J. Res. NBS/USNC–URSI, 69D10 (Oct. 1965), $1.00.

Irreversible power and radiation resistance of antennas in anisotropic ionized gases. K. S. H. Lee and C. H. Papas.
Scattering resonances of a cylindrical plasma. W. M. Leavens.
Radiation patterns from plasma enclosed cylindrical hypersonic vehicles. J. H. Harris, A. T. Villeneuve, and L. A. Broca.
The Schumann resonances. R. K. Cole, Jr.
Atmospheric radio noise bursts in the LF band at Bangalore. S. V. C. Aiya and K. N. Lakshminarayan.
Influence of finite ground conductivity on the propagation of VLF radio waves. J. R. Wait and K. P. Spies.
Model experiments on propagation of groundwaves across an abrupt boundary at perpendicular incidence. R. J. King and S. W. Maley.
Reviews and selected abstracts in radio science.

Ionospheric radio propagation, K. L. Davies, NBS Mono. 80 (Apr. 1965), $2.75.
Effects of thermal shrinkage on built-up roofing, W. C. Cullen, NBS Mono. 89 (Mar. 4, 1965), 10 cents.
Examination of liquefied petroleum gas liquid-measuring devices, M. W. Jensen, NBS Handb. 99 (Apr. 23, 1965), 35 cents.
Systems engineering in ceramics. Proceedings of a symposium April 19, 1964, NBS Misc. Publ. 267 (May 1, 1965), $2.00.
Builder's template hinges, CS9–65 (Jan. 15, 1965), 10 cents. (Supersedes CS9–33).
Aluminum alloy chain link fencing, CS269–65 (Mar. 1, 1965), 10 cents.
Steel medicine cabinets, NBS CS267–65 (Mar. 1, 1965), 10 cents.
Hide trim pattern for domestic cattlehides, NBS CS268–65 (Apr. 4, 1965) 10 cents.
Microwave reflection techniques for dense plasma diagnostics, S. Takeda and T. Tsukishima, NBS Tech. Note 256 (Mar. 10, 1965), 25 cents.
Practical aspects of the use of AC–DC transfer instruments, E. S. Williams, NBS Tech. Note 257 (Mar. 9, 1965), 15 cents.
Research on crystal growth and characterization at the National Bureau of Standards July to December 1964, Ed. H. F. McMurdie, NBS Tech. Note 260 (May 8, 1965), 50 cents.
Summary of current research on archival microfilm, C. S. McCamy and C. I. Pope, NBS Tech. Note 261 (Apr. 16, 1965), 25 cents.
Bibliography of fading on microwave line of sight tropospheric propagation paths and associated subjects, H. T. Dogherty, NBS Tech. Note 302 (Aug. 31, 1964), 60 cents.
Bibliography on tropospheric propagation of radio waves, W. Nupen, NBS Tech. Note 304 (Apr. 1, 1965), $2.00.
Atlas of Fourier coefficients of diurnal variation of foF_2 Part II. Distribution of amplitude and phase, W. B. Jones and R. M. Gallet, NBS Tech. Note 305 (Feb. 14, 1965), 60 cents.
Studies of solar flare effects and other ionospheric disturbances with a high frequency Doppler technique, V. Agy, D. M. Baker, and R. M. Jones, NBS Tech. Note 306, (Apr. 28, 1965), 75 cents.

Phase and amplitude diversity in over-water transmissions at two microwave frequencies, H. B. Janes, A. W. Kirkpatrick, D. M. Waters, and D. Smith, NBS Tech. Note 307 (Apr. 12, 1965), 40 cents.

Data reduction for stable auroral red arcs observed at Rapid City, South Dakota, J. E. Cruz, R. Davies, L. K. Droppleman, E. Marovich, L. R. Megill, M. H. Rees, L. Reisbeck, and F. E. Roach, NBS Tech. Note 308 (May 3, 1965), 50 cents.

A bibliography of experimental saturation properties of the cryogenic fluids, N. A. Olien and L. A. Hall, NBS Tech. Note 309 (Apr. 9, 1965), 60 cents.

Attenuation of the ground wave of a low-frequency electromagnetic pulse, J. C. Morgenstern and J. R. Johler, NBS Tech. Note 310 (Apr. 1965). 30 cents.

Blood: Bone equilibrium in calcium homoeostasis, J. MacGregor and W. E. Brown, Nature **205,** No. 4969, 359–361 (Jan. 23, 1965).

Carbon monoxide on niobium, R. Klein and J. W. Little, Surface Science **2,** 167–176 (North-Holland Publ. Co., Amsterdam, The Netherlands, 1964).

Fracture in corrosive media, H. L. Logan, Book, Fracture of Engineering Materials, ch. 8, pp. 143–161 (American Society for Metals, Metals Park, Ohio, Nov. 1964).

Gas-phase radiolysis of *n*-pentane. A study of the decompositions of the parent ion and neutral exicted pentane molecule, P. Ausloos and S. G. Lias, J. Chem. Phys. **41,** No. 12, 3962–3970 (Dec. 15, 1964).

Impedance of sealed nickel-cadmium dry cells, R. J. Brodd and H. J. DeWane, Electrochem. Tech. **3,** No. 1–2, 12–17 (Jan.–Feb. 1965).

Moderation in instrumentation, J. K. Taylor, Science Teacher **32,** No. 3, 18–19 (Mar. 1965).

Pressure-indicator-paste patterns in duplicate dentures made by different processing technics for the same patients, J. B. Woelfel and G. C. Paffenbarger, J. Am. Dental Assoc. **70,** 339–343 (Feb. 1965).

Radioisotope dilution and its application to the radioassay of Ce^{144}, L. A. Currie, G. M. France, III, and H. L. Steinberg, Intern. J. Appl. Radiation Isotopes **16,** No. 1, 1–8 (Jan. 1965).

Reference buffer solutions for *p*H measurements in 50% methanol. Dissociation constants of acetic acid and dihydrogen phosphate ion from 10 to 40°, M. Paabo, R. A. Robinson, and R. G. Bates, J. Am. Chem. Soc. **87,** 415–418 (1965).

Resins and technics used in constructing dentures, G. C. Paffenbarger, J. B. Woelfel, and W. T. Sweeney, Dental Clinics of North America, pp. 51–262 (W. B. Saunders Co., Philadelphia, Pa., 1965).

Spectra of matrix-isolated NiF_2 and $NiCl_2$, D. E. Milligan, M. E. Jacox, and J. D. McKinley, J. Chem. Phys. **42,** No. 3, 902–905 (Feb. 1965).

The polarographic analysis of titanium (IV)—EDTA complex: Application to paint pigments, H. W. Berger and B. C. Cadoff, Offic. Digest Paint Tech. **37,** No. 480, 28–34 (Jan. 1965).

The structures of anhydrous sodium trimetaphosphate, $Na_3P_3O_9$, and the monohydrate, $Na_3P_3O_9{\cdot}H_2O$, H. M. Ondik, Acta. Cryst. **18,** Part 2, 226–232 (Feb. 1965).

Vacuum ultraviolet photochemistry. VIII. Propylene, D. A. Becker, H. Ikabe, and J. R. McNesby, J. Phys. Chem. **69,** No. 2, 538–542 (Feb. 1965).

A magnetic amplifier for use with diode logic, E. W. Hogue, IEEE Trans. Commun. Electron. **83,** No. 75, 803–808 (Nov. 1964).

A study of the variation of the surface electrical resistance of lead iodide films with relative humidity at room temperature, F. E. Jones (Proc. 1963 Intern. Symp. Humidity and Moisture, Washington, D.C.), Book, Humidity and Moisture. Measurement and Control in Science and Industry. Vol. **1,** Principles and Methods of Measuring Humidity in Gases, Sec. III, Paper 37, pp. 361–365 (Reinhold Publ. Corp., New York, N.Y., 1965).

An investigation of psychrometric measurement techniques in air-conditioning calorimetry, J. C. Davis and P. R. Achenbach (Proc. 1963 Intern. Symp. Humidity and Moisture, Washington, D.C.), Book, Humidity and Moisture. Measurement and Control in Science and Industry. Vol. **2,** Applications, Sec. IV, Paper 37, pp. 303–313 (Reinhold Publ. Corp., New York, N.Y., 1965).

Application of cooled air detector in an optical system, S. Abramowitz, A. M. Bass, and A. E. Ledford, Jr., Appl. Opt. **4,** No. 2, p. 255 (Feb. 1965).

Calculation of the temperature of a flat-plate wet surface under adiabatic conditions with respect to the Lewis relation, T. Kusuda (Proc. 1963 Intern. Symp. Humidity and Moisture, Washington, D.C.), Book, Humidity and Moisture. Measurement and Control in Science and Industry. Vol. **1,** Principles and Methods of Measuring Humidity in Gases, Sec. I, Paper 2, pp. 16–32 (Reinhold Publ. Corp., New York, N.Y., 1965).

Clinical behavior of *o*-ethoxybenzoic acid-eugenol-zinc oxide cements, S. Civjan and G. M. Brauer, J. Dental Res. **44,** No. 1, 80–83 (Jan.–Feb. 1965).

Control of relative humidity and temperature in rubber laboratory of National Bureau of Standards, F. L. Roth and R. D. Stiehler (Proc. 1963 Intern. Sypm. Humidity and Moisture. Washington, D.C.), Book, Humidity and Moisture. Measurement and Control in Science and Industry. Vol. **2,** Applications, Sec. III, Paper 35, pp. 287–292 (Reinhold Publ. Corp., New York, N.Y., 1965).

Measurement of radiation dose distributions with photochromic materials, W. E. McLaughlin and L. Chalkley, Radiology **84,** No. 1, 124–125 (Jan. 1965).

Soil corrosion, W. J. Schwerdtfeger, Encyclopedia of Electrochemistry, pp. 1068–1071 (Reinhold Publ. Corp., New York, N.Y., Mar. 1965).

A theorem on the automorphs of a skew-symmetric matrix, M. Newman, Mich. Math. J. **12,** 61–63 (1965).

On the location of the zeros of some infrapolynomials with prescribed coefficients, J. L. Walsh and O. Shisha, Pacific J. Math. **14,** No. 3, 1103–1109 (1964).

On the structure of infrapolynomials with prescribed coefficients, O. Shisha, Pacific J. Math. **14,** No. 3, 1039–1051 (1964).

Continuous-absorption hygrometry with a pneumatic bridge utilizing critical flow, W. A. Wildhack, T. A. Perls, C. W. Kissinger, and J. W. Haves (Proc. 1963 Intern. Symp. Humidity and Moisture, Washington, D.C.), Book, Humidity and Moisture. Measurement and Control in Science and Industry. Vol. **1.** Principles and Methods of Measuring Humidity in Gases, Sec. VI, Paper 53, pp. 552–570 (Reinhold Publ. Corp., New York, N.Y., 1965).

Comment on the difference between a non-LTE and a pure absorption model for the line-blanketing effect, R. N. Thomas, Astrophys. J. **141,** 333–335 (Jan. 1, 1965).

Displacement of dislocation images formed in transmission electron microscopy, R. DeWit, J. Appl. Phys. **36,** No. 1, 329–330 (Jan. 1965).

On the relative roles of free volume and activation energy in the viscosity of liquids, P. B. Macedo and T. A. Litovitz, J. Chem. Phys. **42,** No. 1, 245–256 (Jan. 1, 1965).

On trapped trajectories in Brownian motion, J. L. Jackson and S. R. Coriell, J. Math. Phys. **5,** No. 8, 1075–1078 (Aug. 1964)

Reaction $^{59}Co(p,\alpha)^{56}Fe$, M. Barloutaud, R. S. Caswell, J. Gasteblis, A. G. de Pinho, and J. Quidort (Proc. Intern. Congress Nuclear Physics, Paris, France, July 2–8, 1964), Compt. Rend. Cong. Intern. Phys. Nucleaire II, 717–719 (Centre National de la Recherche Scientifique, Paris, France, 1964).

Screening effects in elastic electron scattering, E. Zeithler and H. Olsen, Phys. Rev. **136,** No. 6A, A1546–A1552 (Dec. 14, 1964).

Stability of the shape of a solid cylinder growing in a diffusion field, R. L. Parker and S. R. Coriell, J. Appl. Phys. **36,** No. 2, 632–637 (Feb. 1965).

The intensity and spectral distribution of scattered radiation from Co^{60} sources, B. Petree and J. C. Humphreys, Radiology **84,** No. 1, 129–130 (Jan. 1965).

The interaction of 350 keV polarized neutrons with oriented Ho^{165} nuclei, R. Wagner, P. D. Miller, T. Tamura, and H. Marshak, Phys. Letters **10,** No. 3, 316–318 (June 15, 1964).

Zeeman filter, D. G. Dessler and W. G. Schweitzer, Jr., J. Opt. Soc. Am. **55,** No. 3, 284–288 (Mar. 1965).

Cosmic noise absorption events at geomagnetically conjugate stations, C. G. Little, E. R. Schiffmacher, H. J. A. Chivers and K. W. Sullivan, J. Geophys. Res. **70,** No. 3, 639–648 (Feb. 1, 1965).

Fluctuations in a laser beam over 9- and 90-mile paths, W. R. Hinchman and A. L. Buck, Proc. IEEE **52,** No. 3, 305–306 (Mar. 1964).

On the effect of solar disturbances on the low-radiofrequency ionosphere reflection process, J. R. Johler and J. D. Harper, Jr. (North Atlantic Treaty Organization Advisory Group for Aeronautical Research and Development. Avionics Panel. 6th Symp. Ionospheric Research Committee, AGARD., Naples, Italy, 1961), Book, The Effect of Disturbances of Solar Origin on Communications, ed. G. J. Gassman, pp. 303–304 (Pergamon Press, Inc., New York, N.Y., 1963).

A line-formula notation system for coordination compounds, P.M. McDonnell and R. F. Pasternack, J. Chem. Documentation **5**, No. 1, 56–60 (Feb. 1965). Decyclization of cyclohexene, 4-methylcyclohexene, and 4-vinylcyclohexene in a single-pulse shock tube, W. Tsang, J. Chem. Phys. **42**, No. 5, 1805–1809 (Mar. 1, 1965).

Hydrogen atom addition to olefins: Relative rates at the two carbon positions and derived heats of formation of several alkyl radicals, R. D. Kelley, R. Klein, and M. D. Scheer, J. Phys. Chem. **69**, No. 3, 905–908 (Mar. 1965).

Isotopic mixing in CO chemisorbed on tungsten. A kinetic study, T. E. Madey, J. T. Yates, Jr., and R. C. Stern, J. Chem. Phys. **42**, No. 1, 1372–1378 (Feb. 15, 1965).

Some new co-ordination compounds of copper (II) chloride, C. Reimann and G. Gordon, Nature **205**, No. 4974, 902–903 (Feb. 27, 1965).

Standardization of analytical data obtained with silver-silver chloride electrodes in methanol-water solvents, M. Paabo, R. G. Bates, and R. A. Robinson, Anal. Chem. **37**, 462–464 (1965).

Watermarks for papermaking by electroforming, J. P. Young, Tappi **48**, No. 1, 36A–37A (Jan. 1965); Metal Finishing **63**, No. 4, 79–82 (Apr. 1965).

Latensification in radiographic emulsions, W. L. McLaughlin, J. Photo. Sci. **13**, 1–11 (1965)

On the information in a microphotograph, C. S. McCamy, Appl. Opt. **4**, No. 4, 405–411 (Apr. 1965).

Results of National Bureau of Standards corrosion investigation in disturbed and undisturbed soils, M. Romanoff, Proc. Appalachian Underground Short Course, Tech. Bull. **72**, p. 566–589 (West Virginia Univ., Morgantown, West Va., 1965).

Statistical design of experiments, W. J. Youden, Handbook on Metals Engineering-Design, American Society of Mechanical Engineers, ch. 3, pt. 5, pp. 583–585 (McGraw-Hill Publ. Corp., New York, N.Y., 1965).

Technique for determining spin-lattice relaxation times, G. A. Candela and R. E. Mundy, Rev. Sci. Instr. **36**, No. 3, 338–342 (Mar. 1965).

Two cases of stress corrosion cracking in copper tubing, H. L. Logan and G. M. Uginsky, Materials Protection **4**, No. 3, 79–80 (May 1965).

A uniqueness theorem for entire functions, R. F. DeMar, Proc. Am. Math. Soc. **16**, No. 1, 59–71 (Feb. 1965).

Nomograms for computing real, imaginary, and absolute values of vector ratios, H. S. Bowman, Acoust. Soc. Am. **37,** No. 4, 751 (Apr. 1965).

On a theorem concerning existence of interpolating functions, R. F. DeMar, Trans. Am. Math. Soc. **114,** No. 1, 23–29 (Jan. 1965).

A study of errors in the measurement of microscopic spheres, C. P. Saylor, Appl. Opt. **4,** No. 4, 477–486 (Apr. 1965).

Definition of "ampere" and "magnetic constant," C. H. Page, Proc. IEEE **53,** No. 1, 100–101 (Jan. 1965).

Electromagnetic measurement, H. W. Lance, SPACE/AERONAUTICS Res. Develop. Handb. **42,** No. 4, 199–202 (1964–1965).

A proper accounting of conformation of a polymer near a surface, E. A. DiMarzio, J. Chem. Phys. **42,** No. 6, 2101–2106 (Mar. 1965).

A test of analytical expressions for the thermal emissivity of shallow cylindrical cavities, F. J. Kelly and D. G. Moore, Appl. Opt. **4,** No. 1, 31–40 (Jan. 1965).

A universal color language, K. L. Kelly, Color Eng. **3,** No. 2, 16–21 (Mar.–Apr. 1965).

Characteristics of the "synchrotron light" from the NBS–180 MeV machine, K. Codling and R. P. Madden, J. Appl. Phys. **36,** No. 2, 380–387 (Feb. 1965).

Dependence of the superconducting transition temperature on carrier concentration in semiconducting $SrTiO_3$, J. F. Schooley, W. R. Hosler, E. Ambler, J. H. Becker, M. L. Cohen, and C. S. Koonce, Phys. Rev. Letters **14,** No. 9, 305–307 (Mar. 1, 1965).

Growth layers on ammonium dihydrogen phosphate, J. L. Torgesen and R. W. Jackson, Science **148,** No. 3672, 952–954 (May 14, 1965).

High silica glass, quartz, and vitreous silica, J. S. Laufer, J. Opt. Soc. Am. **55,** No. 4, 458–460 (Apr. 1965).

Influence of paramagnetic resonance on the static susceptibility. Spin-lattice relaxation time of cupric sulfate pentahydrate, G. A. Candela, J. Chem. Phys. **42,** No. 1, 113–117 (Jan. 1, 1965).

Multichannel resonances in the forward scattering of electrons by helium, G. E. Chamberlain, Phys. Rev. Letters **14,** No. 15, 581–582 (Apr. 12, 1965).

Polymorphism in hydrogen iodide, F. A. Mauer, C. J. Keffer, R. B. Reeves, and D. W. Robinson, J. Chem. Phys. **42,** No. 4, 1465–1466 (Feb. 15, 1965).

Stability of traveling waves in lasers, J. A. White, Phys. Rev. **137**, No. 6A, A1651–A1654 (Mar. 15, 1965).

Temperature and mean free path dependence of the Ginzburg-Landau parameter, S. Gygax and R. H. Kropschot, Phys. Letters **12,** No. 1, 7–9 (Sept. 1, 1964).

The measurement of water vapor boundary layers in biological systems with a radio refractometer, D. M. Gates (Proc. 1963 Intern. Symp. Humidity and Moisture, Washington, D.C.), Book, Humidity and Moisture. Measurement and Control in Science and Industry. Vol. **2**. Applications, Sec. I, Paper 5, pp. 33–38 (Reinhold Publ. Corp., New York, N.Y., 1965).

The use of terahertz photobeats for precise velocity-of-light measurement, Z. Bay and H. S. Boyne, Proc. Enrico Fermi International School of Physics: Course No. XXXI Quantum Electronics and Coherent Light 1963, 352–371 (1964).

Two-electron excitation states in helium, R. P. Madden and K. Codling, Astrophys. J. **141,** No. 2, 362–375 (Feb. 15, 1965).

Cavity resonances for spherical earth with a concentric anisotropic shell, J. R. Wait, J. Atmos. Terres. Phys. **27,** 81–89 (1965).

Potential use of passive probing of atmospheric structure by thermal emissions at radio frequencies, B. R. Bean, E. R. Westwater, and R. L. Abbott (Proc. 1963 Intern. Symp. Humidity and Moisture, Washington, D.C.), Book, Humidity and Moisture. Measurement and Control in Science and Industry. Vol. **2,** Applications, Sec. VII, Paper 71, pp. 595–608 (Reinhold Publ. Corp., New York, N. Y., 1965).

Radio refractometry and its potential for humidity studies, R. E. McGavin and M. J. Vetter (Proc. 1963 Intern. Symp. Humidity and Moisture, Washington, D.C.), Book, Humidity and Moisture. Measurement and Control in Science and Industry. Vol. **2**. Applications, Sec. VII, Paper 66, pp. 553–560 (Reinhold Publ. Corp., New York, N.Y., 1965).

The use of the radio refractometer to measure water vapor turbulence, B. R. Bean and R. E. McGavin (Proc. 1963 Intern. Symp. Humidity and Moisture, Washington, D.C.), Book, Humidity and Moisture. Measurement and Control in Science and Industry. Vol. **2**. Applications, Sec. VII, Paper 67, pp. 561–568 (Reinhold Publ. Corp., New York, N.Y., 1965).

**Publications for which a price is indicated are available by purchase from the Superintendent of Documents, U.S. Government Printing Office, Washington, D.C., 20402 (foreign postage, one-fourth additional). Reprints from outside journals and the NBS Journal of Research may often be obtained directly from the authors.*

UNIVERSITY MICROFILMS
313 NORTH FIRST STREET
ANN ARBOR, MICHIGAN
SJR-A-OCT

UNITED ST
GOVERNMENT PRINTING OFFICE
DIVISION OF PUBLIC DOCUMENTS
WASHINGTON, D.C. 20402
OFFICIAL BUSINESS

POSTAGE AND FEES PAID
U.S. GOVERNMENT PRINTING OFFICE

JOURNAL OF RESEARCH of the National Bureau of Standards Vol. 69A, No. 5 September–October 1965
A. Physics and Chemistry

Contents

	Page
Current research on preservation of archival records on silver-gelatin type microfilm in roll form. C. S. McCamy and C. I. Pope.	385
Franck-Condon factors to high quantum numbers VI: C_2 band systems. R. W. Nicholls.	397
Matrices of spin-orbit interaction in the electron configurations $p^3 d$ and $p^4 d$. Jack L. Tech and Roy H. Garstang.	401
Heat of formation of calcium aluminate tricarbonate at 25 °C. H. A. Berman.	407
Vapor pressure and heat of sublimation of tungsten. R. Szwarc, E. R. Plante, and J. J. Diamond.	417
Heat capacity and enthalpy measurements on aluminum carbide (Al_4C_3) from 15 to 1173 °K. Thermodynamic properties from 0 to 2000 °K. George T. Furukawa, Thomas B. Douglas, William G. Saba, and Andrew C. Victor.	423
Properties of aqueous mixtures of pure salts: thermodynamics of the ternary system water-potassium chloride-barium chloride at 25 °C. R. A. Robinson and V. E. Bower.	439
A wide-range (up to 10^{19} P) rotating cylinder viscometer. Albert Napolitano, Pedro B. Macedo, and Earl G. Hawkins.	449
Internal friction in ZrO_2 containing CaO. J. B. Wachtman, Jr., and W. C. Corwin.	457
Splitting of equivalent points in noncentrosymmetric space groups into subsets under homogeneous stress. H. S. Peiser, J. B. Wachtman, Jr., F. A. Munley, and L. C. McCleary.	461
Inclusion of perfluoromethyl groups in the crystals of copolymers of tetrafluoroethylene and hexafluoropropylene. L. H. Bolz and R. K. Eby.	481
Publications of the National Bureau of Standards.	487

Library of Congress Catalog Card Number: 62-37059

For sale by the Superintendent of Documents, U.S. Government Printing Office, Washington, D.C., 20402. Price 70 cents (single copy)
Subscription price: $4 a year; 75 cents additional for foreign mailing.
UNITED STATES GOVERNMENT PRINTING OFFICE, WASHINGTON : 1965